

Nuclear Fuel Characterization Studies Using Mass Spectrometry

By

SAJIMOL. R

(Enrolment No: CHEM 02201004010)

Indira Gandhi Centre for Atomic Research, Kalpakkam

*A thesis submitted to the
Board of Studies in Chemical Sciences*

*In partial fulfillment of requirements
for the Degree of*

DOCTOR OF PHILOSOPHY

of

HOMI BHABHA NATIONAL INSTITUTE



August 2017

Homi Bhabha National Institute

Recommendations of the Viva Voce Committee

As members of the Viva Voce Committee, we certify that we have read the dissertation prepared by **Sajimol. R** entitled “**Nuclear Fuel Characterization Studies Using Mass Spectrometry**” and recommend that it may be accepted as fulfilling the thesis requirement for the award of Degree of Doctor of Philosophy.

Chairman – Dr. S. Anthonysamy	Date:
Guide / Convener – Dr. M. Joseph	Date:
Examiner - Prof. Ravi Bhushan	Date:
Member 1- Dr. N. Sivaraman	Date:
Member 2- Dr. B. S. Panigrahi	Date:
Member 3- Dr. K. I. Gnanasekaran	Date:

Final approval and acceptance of this thesis is contingent upon the candidate’s submission of the final copies of the thesis to HBNI.

I/We hereby certify that I/we have read this thesis prepared under my/our direction and recommend that it may be accepted as fulfilling the thesis requirement.

Date:

Place:

Dr. M. Joseph

Guide

STATEMENT BY AUTHOR

This dissertation has been submitted in partial fulfillment of requirements for an advanced degree at Homi Bhabha National Institute (HBNI) and is deposited in the Library to be made available to borrowers under rules of the HBNI.

Brief quotations from this dissertation are allowable without special permission, provided that accurate acknowledgement of source is made. Requests for permission for extended quotation from or reproduction of this manuscript in whole or in part may be granted by the Competent Authority of HBNI when in his or her judgment the proposed use of the material is in the interests of scholarship. In all other instances, however, permission must be obtained from the author.

Sajimol. R

DECLARATION

I, hereby declare that the investigation presented in the thesis has been carried out by me.

The work is original and has not been submitted earlier as a whole or in part for a degree / diploma at this or any other Institution / University.

Sajimol. R

List of publications arising from the thesis

Journals

1. Effect of laser parameters on the measurement of U/Nd ratio using Pulsed Laser Deposition followed by Isotopic Dilution Mass Spectrometry.
R. Sajimol, P. Manoravi, S. Bera, M. Joseph, International Journal of Mass Spectrometry, 2015, 387, 51-55.
2. Preferential Removal of Sm by Evaporation from Nd- Sm Mixture and its Application in Direct Burn-up Determination of Spent Nuclear Fuel.
R. Sajimol, S. Bera, S. Nalini, N. Sivaraman, M. Joseph, T. Kumar, , Journal of Radioanalytical and Nuclear Chemistry, 2016, 309, 563–573.
3. Direct burn-up determination of fast reactor mixed oxide (MOX) fuel by preferential evaporation of interfering elements.
R. Sajimol, S. Bera, N. Sivaraman, M. Joseph, , Journal of Radioanalytical and Nuclear Chemistry, 2017, 311, 1593–1603.
4. Laser-Mass spectrometric studies on measurement of isotopic ratios of Li- A comparative study using ps and ns pulsed lasers.
P. Manoravi, **R. Sajimol**, M. Joseph, N. Sivakumar, , International Journal of Mass Spectrometry, 2014, 367, 16-20.

Other Publications

1. S. Burn- up measurements on dissolver solution of Mixed Oxide fuel using HPLC-Mass spectrometric method.
S. Bera, R. Balasubramanian, Arpita Datta, **R. Sajimol**, S. Nalini, T. S. Lakshmi Narasimhan, M. P. Antony, N. Sivaraman, K. Nagarajan and P. R. Vasudeva Rao, International Journal of Analytical Mass Spectrometry and Chromatography, 2013, 1, 55-60.

Conferences/Symposia

1. Mass spectrometric studies of dissolution products of uranium carbide in nitric acid.
R. Sajimol, P. Manoravi, N. Sivakumar, M. Joseph, Chemistry Research Scholars Meet, July14-15, 2011, held at IGCAR, Kalpakkam.
2. Isotopic analysis of magnesium by thermal ionization mass spectrometry-A new sample loading approach for ion emission enhancement.
S. Bera, **R. Sajimol**, S. Nalini, R. Balasubramanian, T. S. Lakshmi Narasimhan, DAE-BRNS Theme Meeting on Recent Trends in Analytical Chemistry (TRAC-2012), August 30-31, 2012, held at VIT, Chennai.
3. PLD-IDMS studies towards direct measurement of Burn-up of nuclear fuel.
R. Sajimol, P. Manoravi, S. Nalini, R. Balasubramanian, Suranjan Bera, T.S. Lakshmi Narasimhan, M. Joseph, 12th ISMAS- Triennial International Conference on Mass Spectrometry, March 3-8, 2013, held at Goa.
4. Thermal Ionization Mass Spectrometric studies on sodalite- a candidate material for nuclear waste containment.
S. Bera, **R. Sajimol**, S. Nalini, R. Balasubramanian, T. S. Lakshmi Narasimhan, Theme meeting on recent trends in material chemistry, July 25-27, 2013, held at VIT, Chennai.
5. PLD-IDMS studies towards direct measurement of burn-up of nuclear fuel.
R. Sajimol, P. Manoravi, S. Nalini, R. Balasubramanian, S. Bera, M. Joseph, 28th ISMAS symposium cum workshop on mass spectrometry, march 9-13, 2014, held at Parwanoo, Himachal Pradesh.
6. IDMS studies on sodalite- a candidate material for nuclear waste containment.
S. Bera, **R. Sajimol**, S. Nalini, R. Balasubramanian, T. S. Lakshmi Narasimhan, march 9-13, 2014, held at Parwanoo, Himachal Pradesh.
7. Laser-Mass spectrometric studies on measurement of isotopic ratios of Sm and Nd- a comparative study using ns and ps pulsed laser.
R. Sajimol, P. Manoravi, M. Joseph, N. Sivakumar, National Symposium on Recent Trends in Spectroscopy, June 20-21, 2014, held at IIT, Chennai.
8. Observation of clusters of U_xO_y in laser mass spectrometric studies.
R. Sajimol, P. Manoravi, M. Joseph, N. Sivakumar, 29th International Seminar on Mass Spectrometry(ISMAS) , Feb 2 - 6, 2015, Jodhpur.

9. Observation of clusters of Te in laser desorption /ionization mass spectrometric studies.

R. Sajimol, P. Manoravi, U. K. Maity, M. Joseph, National Laser Symposium-25, Dec 20-23, 2016, held at KIT, Bhubaneswar.

Sajimol. R

*Dedicated to
my Brother, Biju*

ACKNOWLEDGEMENTS

First and foremost I express my deepest sense of gratitude to my Guide Dr. M. Joseph, whose deep and wide knowledge, intellectual approaches, proper guidance and hard work has helped me to overcome many crisis situations and to complete this thesis on time. I thank him for giving me the freedom to explore myself and for providing constant support and guidance whenever my steps faltered.

I express my obligations to Dr. P. Manoravi and Dr. N. Sivakumar whose instrumentation skill and technical support has helped me to improve the quality of my work.

I have been fortunate to work with a friend like Mr. Suranjan Bera, without his kind help and co-operation throughout the research, it would have been impossible to complete the work on time.

I thank Mrs. S. Nalini for sharing her knowledge and for constant encouragement throughout the course.

I express my indebtedness to Shri. R. Balasubramanian and Shri. R. Viswanathan for sharing their deep knowledge in mass spectrometry and associated topics.

I am grateful to Dr. N. Sivaraman for all the fruitful discussions and for critically correcting my manuscripts.

I express my sincere thanks to the doctoral committee, Dr. S. Anthonysamy (Chairman), Dr. N. Sivaraman (Member), Dr. B. S. Panigrahi (Member) and Dr. K. I. Gnanasekaran (Member) for their valuable suggestions.

I acknowledge Dr. S. Vijayalakshmi for making critical corrections in the thesis that could bring lot of improvements.

I specially thank Dr. T. S. Lakshmi Narasimhan for creating a determination in me to complete this thesis on time.

I am thankful to Dr. K. Sankaran for getting me the permission from PD, FRFCF to register for Ph. D, and for the continuous support thereafter.

I remember with gratitude for all the help I received in one or the other manner from Mr. Ujjwal Kumar Maity, Mr. P. Manikandan and Mr. V. V. Trinadh.

I thank all my dear friends Siva Kumar, Prasanth Kumar Nayak, Firdous, Tejaswi, Rajini P. Antony, Shima, Annapoorani, Satendra Kumar, Binoy Kumar Maji, Clinsha, Soja, Aiswarya, Meera, Priya, Sinosh, Suchithra and Benzy for their love, support and company.

I specially acknowledge Mr. George Thomas for his well wish and prayers.

I take pleasure to remember with gratitude my teachers Prof. Geetha Karunakaran, Dr. S. Suma, Prof. Reetha, Dr. Siva Prasad, Prof. Santha Kumari, Dr. Maria Starwin, Shri. K. Madhavan Nair, Shri. Muralidharan, Mrs. Lalitha and Shri. G. Beenish.

I thank my beloved parents for providing unlimited support and encouragement to complete this thesis, bearing lot of sacrifices .

I am blessed to have a brother who gave me wings to chase my dreams.

I thank my husband Reni Vasanth for his boundless support and for standing with me sharing my joys and crisis throughout the work.

I run short of words in expressing my gratitude to my little son Aarjav *alias* Kunjuni for bearing my long hours of absence, in his most needed time.

CONTENTS

	Page No.
I Synopsis	i
II List of figures	xi
III List of tables	xv
IV List of abbreviations	xvii
Chapter 1 Introduction	1
1.1 Mass Spectrometry	2
1.2 Applications of mass spectrometry in nuclear industry	4
1.3 Chronological development of mass spectrometry	5
1.4 Components of mass spectrometer	8
1.5 Characteristics of a mass spectrum	10
1.6 Different types of mass spectrometers	10
1.6.1 Secondary Ion Mass Spectrometer (SIMS)	10
1.6.2 Spark Source Mass Spectrometry (SSMS)	11
1.6.3 Glow Discharge Mass spectrometry (GDMS)	12
1.6.4 Inductively Coupled Plasma Mass Spectrometer (ICP-MS)	13
1.6.5 Matrix Assisted Laser Desorption/ Ionization Mass Spectrometry (MALDI)	14
1.6.6 Thermal Ionization Mass Spectrometry	16
1.6.6.1 Isotope Dilution Thermal Ionization Mass Spectrometry (ID-TIMD)	21
1.6.6.2 Applications of TIMS in nuclear industry	24
1.7 Scope of the present study	30
References	32
Chapter 2 Part A- Effect of laser parameters on measurement of U/Nd ratio using Pulsed Laser Deposition - Isotope Dilution Mass Spectrometry (PLD- IDMS)	40
2A.1 Introduction	40
2A.1.1 Pulsed Laser Deposition- Mass Spectrometry (PLD- MS)	40
2A.1.2 Interaction of laser with opaque surface	41

2A.1.3	Pulsed Laser Deposition (PLD)	42
2A.1.4	Motivation for the present study	43
2A.1.5	Previous studies in literature	43
2A.1.6	Scope of the present study	44
2A.2	Experimental	46
2A.2.1	The laser systems	46
2A.2.2	Sample preparation	48
2A.2.3	Instrumentation	49
2A.2.4	Procedure	50
2A.3	Results and discussion	55
2A.3.1	Optimization of laser parameters for best stoichiometric ablation	55
2A.3.2	Study on morphological changes on irradiation	62
2. A.4	Conclusions	64
Chapter 2	Part B- Laser-mass spectrometric studies on measurement of isotopic ratios of Li and rare earths – A comparative study using ps and ns pulsed lasers	65
2B.1	Introduction	65
2B.2	Experimental	65
2B.3	Results and discussion	69
2B.3.1	Measurements on Li	69
2B.3.2	Measurement on light rare earths	75
2B.4	Conclusions	80
	References	81
Chapter 3	Studies on Evaporation Behavior of Sm and Nd from their mixture, by Thermal Ionization Mass Spectrometry (TIMS)	87
3.1	Introduction	87
3.1.1	Thermal ionization	87
3.1.2	Principle of thermal ionization	88
3.1.3	Measurement of isotopic ratios	89
3.1.4	Evaporation rates of Sm and Nd	90

3.2	Experimental	91
3.2.1	Instrumentation-Thermal ionization mass spectrometer	91
3.2.2	Procedure	95
3.2.2.1	Measurement of filament temperature by optical pyrometer	95
3.2.2.2	Extent of Sm interference on isotopic ratios of Nd in 1:1 mixture	98
3.2.2.3	Study on variation of ion intensities of Sm and Nd with time, at constant temperature.	99
3.2.2.4	Effect of filament temperature on fractionation and rate of removal of Sm	102
3.3	Results and Discussion	102
3.3.1	Optimization of filament current (filament temperature)	102
3.3.2	Variation in ion intensities of ^{142}Nd and ^{147}Sm , with time at constant sample filament current	103
3.3.3	Evaporation behavior of various isotopes of Sm and Nd from their mixture	106
3.3.4	Isotopic composition of Nd measured at 0 and 130 minutes-effect of time on interference	108
3.3.5	Effect of filament temperature on fractionation and rate of removal of Sm	111
3.3.6	Effect of fractionation on isotopic ratios of Nd	112
3.4	Conclusion	113
	References	114
Chapter 4	Burn-up Determination of PHWR Spent Fuel by Direct Loading Method using Preferential Evaporation Behavior of Sm.	116
4.1	Introduction	116
4.1.1	Burn-up	116
4.1.2	Methods for burn-up determination	117
4.1.3	The present study	125
4.1.4	Previous studies in this area	126
4.2	Experimental	127

4.2.1	Instrumentation	127
4.2.2	Sample	127
4.2.3	Direct measurement of IC of heavy elements and fission product monitor	127
4.2.4	Isotope measurements by TIMS	128
4.2.5	Validation of the direct loading method with conventional method	128
4.2.5.1	HPLC separation of heavy elements and fission products for burn-up evaluation	129
4.3	Results and Discussion	131
4.3.1	Isotope composition of U and Nd present in the directly loaded dissolver solution	131
4.3.2	Burn-up measured by direct loading method	136
4.3.3	Separation of heavy elements and lanthanides by HPLC	139
4.3.4	Mass spectrometric measurements of U and Nd fractions separated by HPLC	140
4.3.5	Burn-up determination from U and Nd concentrations	141
4.4	Merits of the proposed direct loading method	142
4.5	Demerits	143
4.6	Conclusion	144
	References	144
Chapter 5	Part A- Direct burn-up determination of fast reactor mixed oxide (MOX) fuel by preferential evaporation of interfering elements	148
5A.1	Introduction	148
5A.2	Experimental	149
5A.2.1	Instrumentation	149
5A.2.2	Sample	149
5A.2.3	Sample preparation for IDMS	149
5A.2.4	Isotopic composition measurements by TIMS	150
5A.3	Results and Discussion	151
5A.3.1	Measurement of isotopic ratios of Pu in presence of U and Am	151

5A.3.2	Isotopic composition of constituent elements U, Pu and Nd	161
5A.3.3	Burn-up determination from U, Pu and Nd concentrations	162
5A.3.4	Features of the proposed direct loading method	165
5A.4	Conclusion	167
	Annexure 1	168
Chapter 5	Part B- Estimation of U/Pu of mixed carbide fuel irradiated in FBTR by direct loading method using TIMS	171
5B.1	Introduction	171
5B.2	Experimental	171
	5B.2.1 Pattern of analysis of isotopic composition	172
5B.3	Results and discussion	173
5B. 4	Conclusion	178
	References	178
Chapter 6	Laser Ionization Mass Spectrometric Studies of UC, U-O and Te systems	182
6.1	Introduction	182
6.2	UC system	182
	6.2.1. Experimental	184
	6.2.2 Results and discussion	184
6.3	U-O system	189
	6.3.1 Experimental	189
	6.3.2 Results and discussion	189
6.4	Te system	193
	6.4.1 Experimental	193
	6.4.2 Results and discussion	194
6.5	Conclusion	199
	References	199
Chapter 7	Summary and Conclusions	202
Chapter 8	Scope for future studies	206

SYNOPSIS

1. Introduction

Nuclear power is a robust facilitator of energy security in countries with inadequate domestic fossil and renewable energy resources, and also a way to deliver carbon free energy. Fission of single uranium nucleus produces energy higher by several orders of magnitude than burning of coal, oil or natural gas. Thus, a 1000 MWe power plant require ~160 tones of natural uranium per year; whereas for a thermal power plant of same capacity requires ~2.6 million tons of coal per year [1]. In the world, there are about 430 commercial nuclear power reactors based on nuclear fission operating with 370,000 MWe total capacity [2]. It is expected that the nuclear energy generation capacity will increase approximately to 1500 GWe in another 40 years. In India, 20 reactors are under operation and 7 reactors are under construction [3]. India has planned for a rapid increase in nuclear power capacity from the present capacity of 4120 MWe to 20,000 MWe by 2020, and 63,000 MWe by 2032. The amount of uranium available in India could set a limitation to the growth of nuclear energy as in the case of fossil fuels. However, the production of ^{239}Pu and ^{233}U fissile atoms in breeder reactors overcomes this limitation. Keeping this in view, India follows a three stage nuclear power program linking the fuel cycles of Pressurized Heavy Water Reactors (PHWR), Fast Breeder Reactors (FBR) and thorium based FBRs and Advanced Heavy Water Reactors (AHWR) [4]. Based on the neutron energy regime of nuclear fuel fission, reactors are broadly classified into two types- thermal and fast reactors. In thermal reactors, the fission is caused by neutrons with an average energy of ~ 0.025 eV, and in fast reactors, the fission is caused by fast neutrons with an average energy of 0.2 to 0.5MeV [5]. The PHWRs (thermal reactors) fuelled by natural uranium produce electricity while generating ^{239}Pu as a by-product. Natural uranium contains only 0.7 % of the fissile isotope ^{235}U , which undergoes fission to release energy. In the second stage, the FBRs are fuelled by mixed oxide of ^{238}U

and ^{239}Pu , recovered by reprocessing of the spent fuel from the first stage reactors. In FBRs, ^{239}Pu undergoes fission, generating energy and producing ^{239}Pu by transmutation of ^{238}U . FBRs produce more fuel than they consume, and hence are technically capable of growing the nuclear capacity to a very high level. ^{232}Th , which constitutes world's third largest reserves in India, is not fissile; therefore, it needs to be converted to a fissile material namely ^{233}U , by transmutation in FBRs [6]. This is to be achieved through the second stage of the program, by commercial operation of FBRs. The advanced nuclear reactor systems fuelled by ^{233}U and ^{232}Th , constitute the third stage of nuclear power program.

The fuel discharged from nuclear reactors is referred to as 'spent fuel' which contains fission fragments and transuranic actinides produced by the absorption of neutrons, in addition to the un-burnt fuel [7]. Detailed Post Irradiation Examination (PIE) of the nuclear fuel is carried out as a part of surveillance programme to monitor degradation properties and effective utilization of fuel [8]. PIE involves measurement of trace amounts of isotopes of U, Pu, Th, and fission products. Burn-up is the most important characteristic of spent nuclear fuel that indicates the degree of utilization of U or Pu. Mass Spectrometry holds a key role in the determination of fission products, which is a major concern for the characterization and complete inventory of nuclear fuels and burn-up determination [9]. Inductively coupled plasma mass spectrometry (ICP-MS) is a suitable method for actinide analysis at ultra trace concentration levels [10, 11], but the formation of uranium hydride ions and isobaric interferences due to molecular ions of lead/rare earth elements poses limitation to the method. After reprocessing, the fissile isotopes of plutonium (^{239}Pu and ^{241}Pu) can be used in combination with depleted or natural uranium as MOX in a nuclear reactor; where the other isotopes are capable of absorbing neutrons and becoming fissile. Therefore, the accurate determination of isotopic composition of Pu in the irradiated fuels is required, as it is used for the calculation of burn-up in UO_2 and MOX fuels. Though complete isotope composition of

plutonium can be determined by different mass spectrometric techniques [12], thermal ionization mass spectrometry (TIMS) is the standard technique for the isotopic analysis of U and Pu in different matrices [9, 13]. The present thesis deals with some of the applications of mass spectrometric techniques to characterize the nuclear fuel at different stages of fuel cycle.

2. Scope of the present study

The burn-up data determined by ASTM procedure of Isotope Dilution method using TIMS (ID-TIMS) is globally recognized as the most accurate technique, and the values are used for the validation of reactor physics codes [9]. The lengthy wet chemical sample preparation procedure involving dissolution of solid pellet into solution, two stage ion exchange separations of U, Pu and fission products followed by isotopic analysis and alpha spectrometric measurements, fade the merits of the technique in view of radiation exposure to the analyst and radioactive liquid waste generation. Replacement of conventional ion exchange procedure by High Performance Liquid Chromatography (HPLC) had significantly simplified the sample preparation procedure, but the destruction of fuel sample, high sample requirement and waste generation remains unsolved.

The present thesis addresses following aspects of nuclear fuel analysis, by mass spectrometry.

- i. Direct solid sampling by Pulsed Laser Deposition (PLD) and analysis by ID-TIMS; which minimizes the sample destruction to few micron depth and provides information on spatial profile of burn-up. Lasers of different wavelengths and pulse widths were employed for sampling and optimized the parameters for the near stoichiometric ablation of the sample. The study was extended to isotope composition measurements of Li and light rare earths (La, Ce, Nd and Sm) also, using an indigenously made time of flight mass spectrometer, as the data finds importance in nuclear technology.

ii. Analysis of spent fuel solution by TIMS, after directly loading the dissolver solution on to the filament without subjecting to elemental separation; by making use of differences in vapor pressures of analyte elements and interfering elements. Evaporation behavior of the fission product (Nd) and interfering element (Sm) was studied from their mixture, using TIMS. Based on the observations from this study, spent fuel dissolver solutions were analyzed by direct loading method and definite experimental patterns of analysis were reported for the first time, for complete isotopic measurements of heavy elements (U & Pu) and fission product (Nd). Studies on spent fuel from thermal, fast and research reactors were carried out towards this.

iii. Utility of carbide fuel in commercial fast breeder reactors is limited mainly because of bulk properties of the fuel pellet and the complexity associated with its reprocessing, due to generation of complex organic acids. An attempt was made to identify those dissolution products using a reflectron time of flight mass spectrometer (RTOF-MS). An extended study towards identification of clusters of U and O in nitric acid medium without the use of matrix, and that of Te was also carried out.

3. Organization of the thesis

Chapter 1

The first chapter deals with a brief introduction on mass spectrometry and its applications in nuclear industry. Emerging stages of mass spectrometry and different mass spectrometric techniques are briefly narrated in this chapter. Since majority of the studies described in this thesis employed Thermal Ionization Mass Spectrometer (TIMS), the technique is explained in detail with respect to working principle, instrumentation, sample loading techniques and theory of Isotope Dilution Mass Spectrometry (IDMS). This chapter covers a detailed study on the applications of TIMS in nuclear industry, and concludes with description on scope of the work.

Chapter 2

This chapter describes the studies on direct sampling of solid pellets by PLD, followed by concentration determination of constituent elements, by IDTIMS. Brief descriptions on pulsed laser deposition and laser mass spectroscopy are given in this chapter. The chapter is subdivided into Part A and Part B based on the samples analyzed. In part A, pellets of U and rare earths (La, Ce, Nd & Sm) of natural origin, and compositions similar to spent fuel of particular burn-ups were sampled by PLD using three types of lasers, namely Nd-YAG lasers of 8 ns and 100 ps pulse widths (of wavelengths 1064, 532 and 266 nm) and excimer laser of 30 ns pulse width (of 248 nm wavelength). The ablated samples collected on glass plates were subjected to ID-TIMS for concentration determination of elements of interest (U & Nd), which is a measure of burn-up, in the case of spent fuel. Isotope measurements of Nd was carried out in presence of its isotopically interfering elements like Ce and Sm, by applying correction factors based on their natural isotopic abundances, using the supportive software in TIMS. The study has optimized the laser parameters (i.e. 266 nm, ps laser) for most stoichiometric ablation of solid samples and hence to get the most accurate concentration values.

Part B of this chapter describes laser-mass spectrometric studies on isotopic ratios of Li and light rare earths (La, Ce, Nd and Sm) by an in-house developed Laser Ionization Mass Spectrometer (LIMS), using ps and ns pulsed lasers for ablation. The ps laser provided better accuracy compared to ns laser, furthermore, the 266 nm laser beam provided better precision compared to longer wavelengths, in agreement with the observations found in Part A.

Chapter 3

This chapter focuses on evaporation studies of Nd and Sm from their mixture, by measuring their ion intensities by TIMS. Nd produced as fission product in nuclear reactors is

isobarically interfered by Sm, which necessitates ion exchange separation of the latter from the dissolver solution, for quantification of Nd. As the vapor pressure of Sm is approximately five orders of magnitude higher than that of Nd at their melting points [14], a method to remove Sm by evaporation, by maintaining the sample at high temperature for longer duration, was attempted. Nd-Sm mixture loaded on Re filament was heated inside TIMS and studied the time dependent and temperature dependent changes in ion intensities of both the elements. The studies concluded that near complete elimination of Sm is possible, by maintaining the sample filament current at around 2.2 A for about 120 minutes. The effect of fractionation on isotopic ratios, caused by heating for long duration was also subjected to detailed investigation and described in this chapter.

Chapter 4

This chapter deals with application of the observations found in studies described in Chapter 3, for direct burn-up evaluation of spent nuclear fuel. A brief account of burn-up and the existing methods to evaluate the same are also discussed in this chapter. Spent fuel from PHWR of burn-up < 1 atom % was analyzed by directly loading the dissolver solution on Re filaments followed by isotopic measurements, without subjecting to chemical separation. Both pure solution as well as spiked sample were analyzed by this way, and all the elements of interest (U and Nd, in this case) were analyzed from the same filament. A sequential pattern of analysis could bring the ion intensities of interfering isotopes of Sm to a steady lowest level. The method was validated with the burn-up values obtained from another aliquot of the same sample analyzed by the conventional ASTM procedure of HPLC separation followed by ID-TIMS, and the deviation observed is 2.4 %. The merits and demerits of the proposed direct loading method are also described in this chapter.

Chapter 5

This chapter describes applicability of the proposed direct loading method for fast reactor spent fuel, where measurement of U, Pu and Nd are required for burn-up evaluation, which make the scenario more complex due to ^{238}U - ^{238}Pu and ^{241}Pu - ^{241}Am interferences, in addition to Nd-Sm interference. A sequential pattern of analysis was reported for the first time, considering the interference and vapor pressure factors. The large difference in vapor pressures of Am, Pu and U [15-17], made the sequential analysis of all the three elements present in the same filament, possible. This chapter is subdivided into Part A and Part B, based on the analysis of commercial fast reactor fuel and advanced fuel irradiated in a research reactor.

Part A discusses the analysis of U-Pu mixed oxide (MOX) fuel of composition ($\text{U}_{0.79}\text{Pu}_{0.21}\text{O}_2$) with U having an enrichment of 53.5% ^{235}U , irradiated in FBTR for a peak burn-up of ~ 112 GWd/t. The method was validated by comparing the results with the reported values [18] determined by ASTM procedure; the accuracy was found to be about 3.7 %. Part A is annexed by evaluation of the sources of error and their relative contributions to the total error associated with the burn-up determined by direct loading method.

Part B of this chapter deals with estimation of U/Pu of mixed carbide fuel (30% UC-70% PuC) irradiated in FBTR, by following the method adopted for MOX fuel. The U/Pu ratio evaluated has shown a deviation of 4.4 % from the reported value evaluated by ASTM procedure [19].

Chapter 6

This chapter deals with some nuclear applications of time of flight mass spectrometry in combination with laser desorption/ionization. It describes the studies on identification of dissolution products of uranium carbide in nitric acid during the first step of aqueous reprocessing. The soluble organic species consist of compounds which are probably highly

substituted aromatic compounds with $-\text{COOH}$ and $-\text{OH}$, forming an emulsion in the solvent extraction steps of Purex process [20]. The signals corresponding to oxalic acid and benzoic acid only could be ascertained by the present study. As the spectra obtained during this studies, consisted of clusters of U and O, in addition to dissolution products, a further study was carried out with uranyl nitrate sample, for identification of clusters. The study resulted in reporting of clusters up to $\text{U}_{13}\text{O}_{37}$, without the addition of any matrix. The study was further extended to Te system, which is known to form of long molecular chains. The study has reported clusters of size up to Te_{28} , for the first time.

Chapter 7

This chapter summarizes the conclusions of studies described in this thesis, which opened up novel approaches on sample treatment for mass spectrometric analysis of nuclear fuels. Direct sampling from solid pellets by laser ablation followed by TIMS analysis has proven to be applicable for quick estimation of burn-up with about 5% accuracy. The direct loading procedure based on preferential evaporation of interfering elements, put forwarded for burn-up evaluation of liquid samples holds many advantages over the conventional method, on radiation as well as waste generation points of view, compromising the accuracy to 3-4%. The analytical procedure was suitably modified to make it applicable for analysis of both thermal as well as fast reactor spent fuels. The in-house developed time of flight mass spectrometer was found applicable for the studies on inorganic clusters of U-O and Te.

Chapter 8

This chapter describes the perspectives of scope for future studies that are stemmed out of the studies described in this thesis.

References

1. Baldev Raj, U. Kamachi Mudali, Materials Science and Technology: Research and Challenges in Nuclear Fission Power, Proc. Indian Nat. Sci. Acad., 2015, 81, 801-826.

2. Baldev Raj, U. K. Mudali, Surface Engineering of steels and stainless steels for fast breeder reactor programme, *Steel Tech.*, 2008, 3, 26-31.
3. <http://worldnuclear.org/NuclearDatabase/rdResults.aspx>
4. <http://www.barc.ernet.in/about/anu1.html>
5. P. Chellapandi, P. Puthiyavinayagam, T. Jeyakumar, S. Chetal, Baldev Raj, IAEA-Technical Meeting on 'Design, Manufacturing and Irradiation Behavior of Fast Reactor Fuels', June-2011, IPPE, Russia.
6. Samuel Glasstone, Alexander Sesonske, *Nuclear Reactor Engineering*, 1986, CBS Publishers, Delhi.
7. K. R. Rao, Radioactive waste: The problem and its Management, *Curr. Sci.*, 2001, 81, 1534-1539.
8. Post-irradiation examination and in-pile measurement techniques for water reactor fuels, IAEA-TECDOC-CD-1635 (2009).
9. R. Balasubramanian, D. D. Albert Raj, S. Nalini, M. Sai Baba, Mass spectrometric studies on irradiated (U, Pu) mixed carbide fuel of FBTR, *Int. J. Nucl. Energy Sci. Technol.*, 2005, 1, 197-202.
10. S. F. Boulyga, J. S. Becker, Isotopic analysis of uranium and plutonium using ICPMS and estimation of burn-up of spent uranium in contaminated environmental samples, *J. Anal. At. Spectrom.*, 2002, 17, 1143-1147.
11. I. Glagolenko, B. Hilto, J. Giglio, D. Cummings, Fission yield measurements by inductively coupled plasma mass-spectrometry, *J. Radioanal. Nucl. Chem.*, 2009, 282, 651-655.
12. S. Chandramouleeswaran, Jayshree Ramkumar, Mass Spectrometry: A Boon to Nuclear Industry, *J. Anal. Bioanal. Techniques- Special Issue*, 2014, 6, 1-9.

13. 'Standard Test Method for atom percent fission in Uranium Plutonium Fuel (Neodymium-148 method)', Annual of ASTM Standards, 1996, E321, 96.
14. O. Knacke, O. Kubaschewski, K. Hesselmann, Thermo chemical properties of inorganic substances -II, 2nd Edition, 1991, Springer- Verlag.
15. M. H. Bradbury, R. W. Ohse, High temperature vapor pressure of pure Plutonium, J. Chem. Phys., 1979, 70, 2310-2314.
16. N. D. Erway, O. C. Simpson, The vapor pressure of Americium, J. Chem. Phys., 1950, 18, 953-960.
17. E. G. Rauh, R. J. Thorn, Vapor pressure of Uranium, J. Chem. Phys., 1954, 22, 1414-1418.
18. S. Bera, R. Balasubramanian, Arpita Datta, R. Sajimol, S. Nalini, T. S. Lakshmi Narasimhan, M. P. Antony, N. Sivaraman, K. Nagarajan, P. R. Vasudeva Rao, Burn-up measurements on dissolver solution of mixed oxide fuel using HPLC- Mass spectrometric method, Int. J. Anal. Mass Spec. Chrom., 2013, 1, 55-60
19. R. Balasubramanian, S. Nalini, R. Viswanathan, Proc. ISMAS (2009), Hyderabad, Nov 24-28, 2009, 377-379.
20. A. Palamalai, S. K. Rajan, A. Chinnusamy, M. Sampath, P. K. Varghese, T. N. Ravi, V. R. Raman, G. R. Balasubramanian, Development of an electro-oxidative dissolution technique for fast reactor carbide fuels, Radiochimica Acta, 1991, 55, 29-35.

LIST OF FIGURES

Figure No.	Title of the Figure	Page No.
Fig. 1.1	The first mass spectrum recorded by J.J. Thomsons positive ray parabola apparatus.	6
Fig. 1.2	Diagrammatic representation of sample-spike mixing in IDMS	22
Fig. 2A.1	Schematic of PLD	51
Fig. 2A.2	Photograph of the PLD chamber	52
Fig. 2A.3	Photograph of the sample loader inside PLD chamber	52
Fig. 2A.4	U/Nd concentration ratios obtained from TIMS for pellets with varying elemental composition of U & Nd. The concentrations of elements present in the films deposited by PLD at 532 & 1064 nm (ns pulsed laser) are compared against the sample taken from target pellet.	56
Fig. 2A.5	U/Nd concentration ratios obtained from TIMS for pellets with varying elemental composition of U & Nd. The elemental concentrations in the samples from PLD films deposited at 266, 532 & 1064 nm (ps pulsed laser) and 248 nm excimer laser show, unlike ns laser, a positive deviation from the corresponding values of the target pellet.	61
Fig. 2A.6	SEM images of pellet surfaces before laser irradiation	63
Fig. 2A.7	SEM images of pellet surface after ablation with laser beam of 532 nm wavelength	63
Fig. 2B.1	Schematic of LIMS facility	67
Fig. 2B.2	Photograph of the in- house developed Laser ionization- Time of flight mass spectrometer facility	68
Fig. 2B.3	Photograph of the Al sample holder with a tail cutting groove for the sample plate	68
Fig. 2B.4	Typical mass spectra of isotopes of Li obtained using (a) 8 ns and (b) 100 ps Nd-YAG lasers of 266 nm wavelength.	70

Fig. 2B.5	Mass spectra of isotopes of Li obtained using ps-Nd-YAG at different wavelengths; (a) 1064 nm; (b) 532 nm; (c) 266 nm. All other experimental conditions remain the same.	72
Fig. 2B.6	Measured isotopic abundance of Li present in natural Li_2CO_3 , using ns and ps lasers at 266 nm and compared with TIMS data	74
Fig. 2B.7	The mass spectra of La, Ce, Nd and Sm obtained from their nitrate solution dried on SS substrate, using three different laser wavelengths, namely 266 nm (UV), 532 nm (visible); and 1064 nm (IR) (a) using 8 ns pulse width; (b) using 100 ps pulse width.	76
Fig. 2B.8	Variation of intensity ratio of $^{152}\text{SmO}^+ / ^{154}\text{SmO}^+$ as a function of wavelength for both ps and ns lasers.	78
Fig. 2B.9	Variation of intensity ratio of $^{152}\text{NdO}^+ / ^{154}\text{NdO}^+$ as a function of wavelength for both ps and ns lasers.	79
Fig. 3.1	Photograph of the TIMS instrument used for the study	92
Fig. 3.2	Schematic of TIMS	92
Fig. 3.3	Schematic of functioning of optical pyrometer	97
Fig. 3.4	Peak centre coincidence of masses from 142 to 150 with respect to axial collector	101
Fig. 3.5	Mass spectra of Nd-Sm mixture at sample filament current of 2.0 A	104
Fig. 3.6	Mass spectra of Nd-Sm mixture at sample filament current of 2.25A.	104
Fig. 3.7	Variation of ion intensities of ^{142}Nd and ^{147}Sm with time at 2.25A sample filament current	106
Fig. 3.8	Variation in isotopic ratios involving interfering and un interfering isotopes, with time, at 2.25 A filament current.	107
Fig. 3.9	Mass spectra showing reduction in ion intensities of Sm from Nd - Sm mixture (of natural abundance) over successive measurements at different intervals of time (The double line in the spectra are due to a twice measurement).	110
Fig. 3.10	Effect of filament current on isotopic ratios of Nd	111

Fig. 4.1	Schematic of steps involved in the mass spectrometric determination of burn-up.	125
Fig. 4.2	Schematic of the HPLC system used for the present study	130
Fig. 4.3	Photograph of the components of HPLC system kept outside the FH	130
Fig. 4.4	Mass spectrum of Nd present in the directly loaded dissolver solution.	133
Fig. 4.5	Mass spectrum of Nd fraction of dissolver solution separation by HPLC.	133
Fig. 4.6	Mass spectrum of U and Pu present in the directly loaded dissolver solution.	135
Fig. 4.7	The expanded view of fig. 4.7, showing the abundances of Pu and U.	135
Fig. 4.8	Mass spectrum (m/z of 141 to 152) of spiked (with ^{142}Nd) dissolver solution, after heating for two hours at 5.5/2.2 A.	138
Fig. 4.9	Chromatogram obtained for PHWR dissolver solution using HPLC. Column: Reversed phase Monolith; mobile phase: CSA and HIBA; PCD with Arsenazo (III) at 655nm.	139
Fig. 4.10	Mass spectrum of U fraction of dissolver solution separated by HPLC.	140
Fig. 5A.1	Mass spectrum of dissolver solution showing appearance of only Am at 1.85 A	154
Fig. 5A.2	Mass spectrum of dissolver solution showing Pu and Am isotopes alone without U signals, at 1.95 A.	155
Fig. 5A.3	Mass spectrum of dissolver solution showing the reduction in intensity of ^{241}Am with successive scan at 1.95 A.	156
Fig. 5A.4	Expanded view of steady reduction of ion intensity of ^{241}Am , in consecutive runs, at constant filament current 1.95 A.	157
Fig. 5A.5	Appearance of U isotopes (at masses 233 and 238) in the mass spectrum of dissolver solution, after keeping the sample filament for about 40 minutes, at 1.95 A.	158
Fig. 5A.6	Mass spectra of dissolver solution showing reduction in intensity of $^{241}(\text{Pu}+\text{Am})$ over successive measurements at different intervals of time.	159

Fig. 5A.7	Variation of ion intensities of ^{241}Am , ^{239}Pu and their ratio with time, at a filament current of 2.25A.	160
Fig 5B. 1	Mass spectrum of dissolver solution showing appearance of only ^{241}Am at sample filament current of 1.55 A.	173
Fig 5B. 2	Mass spectrum of dissolver solution at filament current of 1.78 A, showing Pu and Am.	174
Fig. 5B.3	Mass spectrum of dissolver solution at filament current 5.5/2.2 A, indicating the presence of U, Pu and Am.	175
Fig. 6.1	A typical TOF mass spectrum of UC dissolved in nitric acid and subjected to laser ionization at a laser of frequency 1Hz	186
Fig. 6.2	Blank spectrum	188
Fig. 6.3	Typical mass spectrum obtained from uranyl nitrate at lower laser fluence of 0.002 J/cm^2	190
Fig. 6.4	Mass spectra showing higher clusters of U_xO_y at higher laser fluence of 0.03 J/cm^2	191
Fig. 6.5	Expanded view of Fig. 6.4 (a)- upto mass 2000 amu; (b) mass range 2000-4000 amu	192
Fig. 6.6	Laser desorption/ionization mass spectrum obtained over elemental Te	195
Fig. 6.7	Calculated and observed intensity for Te_2	196
Fig. 6.8	Calculated and observed intensity for Te_3	196
Fig. 6.9	TOF mass spectra obtained over elemental Te using different laser wave lengths.	198
Fig. 7.1	Variation in accuracy of U/Nd values measured, with lasers of different parameters used for PLD.	203

LIST OF TABLES

Table No.	Title of the Table	Page No.
Table 2A.1	Chemical composition of pellets prepared	49
Table 2A.2	Parameters of lasers used in the present study	51
Table 2A.3	Assigning masses in the 9 faraday cup collectors	54
Table 2A.4	U/Nd ratios observed with 532 & 1064 nm Nd-YAG laser (8 ns pulse width) and 248 nm of excimer laser of 30 ns pulse width.	57
Table 2A.5	U/Nd ratios observed with 266, 532 & 1064 nm laser with 100 ps pulse width	60
Table 2B.1	Full width half maxima (FWHM) and % of isotopes of Li as measured with different laser parameters.	73
Table 3.1	Work functions and melting points of some metals used for sample loading in TIMS	89
Table 3.2	Comparison of some properties of Nd and Sm relevant to the study	90
Table 3.3	Temperature measured by optical pyrometer and the corresponding filament current applied.	97
Table 3.4	Natural isotopic composition of isotopes of Nd and Sm	98
Table 3.5	Isotopic composition of Nd measured with and without applying interference correction	99
Table 3.6	Variation of ion intensities of ^{147}Sm and ^{142}Nd (from Nd-Sm mixture of natural isotopic composition), at filament current of 2.25 A.	105
Table 3.7	Isotope ratios (IR) of Nd measured at zero time (see text) and after 130 minute (from Nd-Sm mixture), at sample filament current of 2.25A.	109
Table 3.8	Isotopic ratios (IR) of Nd measured with interference correction at zero time and after	113
Table 4.1	Isotope composition of U and Nd present in dissolver solution before and after separation of the corresponding pure fractions.	134
Table 4.2	Thermal fission yield (Y) data for ^{235}U , ^{239}Pu and for 50% ^{235}U +50%	136

^{239}Pu

Table 4.3	Comparison of burn-up values arrived by the proposed direct loading method and the conventional method.	142
Table 5A.1	Comparison of some properties of Pu, Am and U relevant to the present study	153
Table 5A.2	Isotopic compositions of U, Pu and Nd present in dissolver solution, measured by direct loading method and with conventional method	163
Table 5A.3	Comparison of burn-up values determined by the proposed direct method and reported values (measured by conventional method).	164
Table 5A.4	Comparison of features of direct loading method with conventional methods	166
Table 5B.1	Relative abundances of U and Pu isotopes measured by the present direct loading method and by conventional method	177
Table 6.1	Time of arrival, corresponding masses and possible dissolution products of UC in nitric acid (in presence of NaOH) ionized with laser of frequency 1Hz.	187
Table 6.2	Time of arrival and corresponding masses of blank spectrum.	188
Table 7.1	Comparison of burn-up evaluated by the proposed direct loading method and conventional procedure.	205

LIST OF ABBREVIATIONS

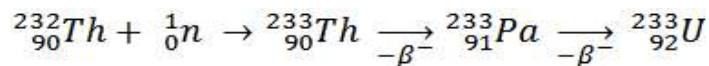
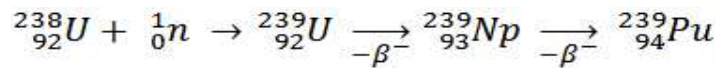
ASTM	- American Society for Testing Materials
CIRUS	- Canadian Indian Reactor Uranium System
DSO	- Digital storage Oscilloscope
EODT	- Electro Oxidative Dissolution Technique
FAB MS	- Fast Atom Bombardment Mass Spectrometry
FBR	- Fast Breeder Reactor
FBTR	- Fast Breeder Test Reactor
FT-TIMS	- Fission Track Thermal Ionization Mass Spectrometer
GC	- Gas Chromatography
GC-EIMS	- Gas Chromatography- Electron Impact Mass Spectrometer
GPIB	- General Purpose Interface Bus
HPLC	- High Performance Liquid Chromatography
IAEA	- International Atomic Energy Agency
IDTIMS	- Isotope Dilution Thermal Ionization Mass Spectrometer
LA-MC-ICPMS	- Laser Ablation Multi Channel Inductively Coupled Plasma Mass Spectrometer
LC	- Liquid Chromatography
LIMS	- Laser Ionization Mass Spectrometer
LRE	- Lighter Rare Earths
MALDI	- Matrix Assisted Laser Desorption and Ionization
MC-HR-ICPMS	- Multi Channel High Resolution Inductively Coupled Plasma Mass Spectrometer
MOX	- Mixed Oxide
NIST	- National Institute of Standards and Technology
N-TIMS	- Negative ion- Thermal Ionization Mass Spectrometer
NUMAC	- Nuclear Material Accounting
OD	- Outer Diameter
PFBR	- Prototype Fast Breeder Reactor

P-TIMS	- Positive ion- Thermal Ionization Mass Spectrometer
PWR	- Pressurized Water Reactor
PUREX	- Plutonium Uranium Redox Extraction
RIMS	- Resonance Ionization Mass Spectrometer
RF GDMS	- Radio Frequency Glow Discharge Mass Spectrometer
RSD	- Relative Standard Deviation
RTOF-MS	- Reflectron Time Of Flight Mass Spectrometer
SEM	- Secondary Electron Multiplier (p. 9, 19, 66) Scanning Electron Microscope (p. 62)
SIMS	- Secondary Ion Mass Spectrometry
SSMS	- Spark Source Mass Spectrometry
TOF- MS	- Time Of Flight Mass Spectrometry

Introduction

The fast growing energy demand, growing population and ever raising concerns about climate changes due to green house effect from fossil fuels make solar energy and nuclear energy to have key roles among other energy sources to satisfy future energy needs of India. The idea of making use of solar energy is very attractive, but considerable research and development will be required before generation of solar energy on a commercial scale for industrial applications. Of the available technology options, thermal reactors and fast breeder reactors (FBRs) with closed fuel cycle, i.e. with recovery of fuel materials from the irradiated fuel by recycle, are proven to be inevitable technology options to provide sustainable energy security for the nation.

Energy is produced in a reactor by nuclear fission. Fission is a nuclear reaction where a fissile atom is bombarded with a neutron and the fissile atom splits into mainly two atoms of nearly equal masses (fission products). Fission, apart from generating fission products, generates more than one neutron and also releases large amount of thermal energy. Such reactions are possible in heavy atoms such as ^{235}U , ^{239}Pu and ^{233}U , which are called fissile isotopes. Natural uranium contains about 0.7% ^{235}U and the rest is ^{238}U . Other two i.e. ^{239}Pu and ^{233}U are not naturally occurring isotopes. They are generated by a process called nuclear radioactive transmutation of ^{238}U and ^{232}Th as shown below [1]. These two are called fertile isotopes. Uranium and thorium are the naturally occurring nuclear fuel materials.



The energy generated by fission of one fissile nucleus is $\sim 3 \times 10^{-18}$ kWh. Since 1 kg of ^{235}U contains about 2.5×10^{24} nuclei, 1 kg of natural uranium containing about 7 g of ^{235}U can release energy equivalent to $\sim 52,500$ kWh [2]. The fractions of fissile isotopes of these elements are measured by mass spectrometry. With the limited nuclear resources available in the country and considering the recent substantial increase in uranium prices, FBR with closed fuel cycle, in view of its efficient utilization of uranium, is an inexorable option. Further, FBRs are essential for converting ^{232}Th to ^{233}U , required for third stage of Indian nuclear power programme [2]. Solid solutions of the oxides, carbides or nitrides of uranium and plutonium or U-Pu-Zr alloys are the candidates to be used as fast reactor fuels.

High density pellets of boron carbide containing boron enriched in ^{10}B isotope will be used in the control rods of fast breeder reactors [3]. Enrichment of boron is being carried out in India by both ion exchange process and BF_3 -diethylether distillation processes. By extensive research, it was established that elemental boron powder with a purity of 95-99 % could be produced using high temperature molten salt electro-winning process. The enrichment of boron is studied by isotopic analysis using mass spectrometry. The above discussions bring the fact into light that the isotopes and their relative abundances play a crucial role in the nuclear fuel performance as well as in reactor control, which is measured by mass spectrometric techniques.

1.1 Mass Spectrometry

Mass Spectrometry is a powerful analytical technique useful to identify the unknown compounds by determining their molecular weights, and their qualitative and quantitative determination in trace and ultra trace levels. The tool is applicable for both organic compounds and inorganic elements in different matrices. Mass spectrometry is used as a

reference technique in a wide variety of applications, especially when there are strict requirements for high accuracy, precision and need to know the isotopic composition. In view of its high sensitivity, selectivity and specificity, the technique provides valuable information in various branches of science like nuclear technology, biology, medicine, material science, environmental science, forensic science, archeology, astronomy etc. Some of the typical applications of mass spectrometry in diverse areas are listed below.

- i) Determination of isotopic composition of different elements
- ii) Precise and accurate determination of trace and ultra trace constituents in high pure matrices
- iii) Determination of molecular weights of organic compounds
- iv) Determination of organic compounds like cholesterol, glucose, urea etc. and trace elements in human body fluids
- v) Structure determination of newly synthesized compounds
- vi) Identifying irradiated and un-irradiated food materials
- vii) Discovering natural fission reactors
- viii) Determination of age of rocks and minerals and the half-lives of radioactive nuclides
- ix) Composition of molecular species found in space
- x) Location of oil deposits by measuring petroleum precursors in rock
- xi) Adulteration of food and beverages
- xii) Determination of drugs and their metabolites in human body fluids
- xiii) Monitoring of environmental pollutants like pesticides, herbicides etc.
- xiv) Detection of drugs of abuse in sports

1.2 Applications of mass spectrometry in nuclear industry

Detection and measurement of trace amounts of isotopes of U, Pu and Th finds extreme importance in nuclear industry as they are either fissile or fertile. The determination of fission products is a major concern for the characterization and complete inventory of nuclear fuels [4-9] and burn-up determination [10]. The characterization of fission products with respect to isotopic composition and elemental concentration can be carried out only with mass spectrometry. The low detection limits and availability of isotopic composition makes mass spectrometry a very useful and high potential characterization technique in nuclear industry [11-13]. The lanthanides are a major part of the stable and long-lived fission products of both ^{235}U and ^{239}Pu . The use of isotope dilution mass spectrometric procedure for the determination of Nd, U and Pu is used for the computation of burn-up of spent nuclear fuel. Burn-up is the most important characteristic of spent nuclear fuel that indicates the degree of utilization of fuel and also the amount of fission products and minor actinides produced during reactor operation. Accurate burn-up is evaluated by High Performance Liquid Chromatography- Isotopic Dilution Thermal Ionization Mass Spectrometry (HPLC-IDTIMS) method [14]. The determination of long-lived radionuclides is extremely important in nuclear waste management as the actinide isotopic composition is important for waste classification. Isotope speciation of elements like As, Cu, Cd etc. finds importance in environmental radiochemistry for understanding transfer/migration mechanisms [15, 16] and in age determination [17]. The complete record of fission products and actinides can be obtained using mass spectrometry with very good detection limits compared to radiometric methods [18-22]. Due to peculiar physical and geochemical reasons, the Pu concentration reaches 10^{-12} to 10^{-13} g/g in soils of the Northern hemisphere [23] but the concentration would

be higher in the regions contaminated with accidental fallout from nuclear reprocessing plants and nuclear power plants, e.g. in the Ural region (Russia) and Chernobyl (Ukraine) [24,25]. In spent nuclear fuel, the $^{236}\text{U}/^{238}\text{U}$ ratio is higher by several orders of magnitude than in non-contaminated natural uranium ores [26-28]. Thus, knowledge of the isotopic composition of artificial actinides is important for evaluating their origin in the environment. Out of two isotopes of Boron (having natural composition ^{10}B - 19.9% and ^{11}B - 80.1%), the neutron absorption properties depend on the content of ^{10}B isotope with an absorption cross section for thermal neutrons of more than 3.8 kilobarn (10^{-25} m^2). This isotope is an important neutron absorber used in shielding materials such as boron-alloyed steels for storage of spent nuclear fuel, reactor shielding and control, and in neutron detecting instruments. The rapid screening of ^{10}B enriched special steel samples for ^{10}B isotopic fraction is carried out using Laser Ablation- Multi Channel- Inductively Coupled Plasma Mass Spectrometer (LA-MC-ICPMS) [29].

The accurate determination of isotopic composition of enriched boron used as control rod is crucial for the safe operation of nuclear reactors, which is carried out by Thermal Ionization Mass Spectrometry (TIMS), with better than 0.1% accuracy.

1.3 Chronological development of mass spectrometry

The first systematic investigation of positive rays was undertaken by J. J. Thomson with his parabola mass spectrograph during the years 1910-1920. This instrument is considered as the first mass spectrograph [30,31]. From the mass spectrum recorded on a photographic plate, as shown in Fig. 1.1, it was concluded that neon is composed of atoms of two different atomic masses (Ne- 20 and Ne- 22). Around 1919, F. W. Aston created a mass spectrometer and could obtain two positive ray parabolas for neon at relative masses 20 and

22 with an intensity ratio of 10:1; the ions were dispersed by mass and focused by velocity. This design improved the mass spectrometer resolving power by an order of magnitude compared to that achieved by Thomson. These studies led to the receipt of Noble prize in Chemistry by Aston in 1922. A. J. Dempster developed a magnetic deflection instrument and also the first electron impact source around 1920. In Dempster's mass spectrometer, positive ions are obtained either by heating a salt on a platinum filament (thermal source) or by bombarding the sample with electrons from a heated filament.

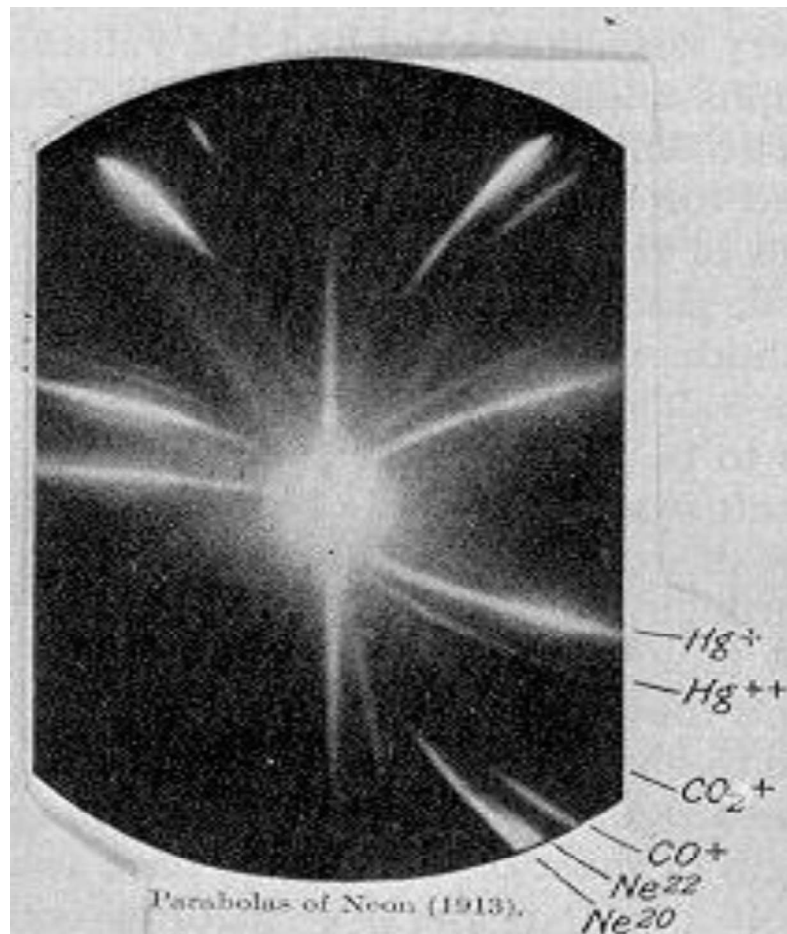


Fig. 1.1 The first mass spectrum recorded by J. J. Thomson's positive ray parabola apparatus [30].

The positive ions are accelerated with a potential of 500-2000 V and enter into a semicircular magnetic field of around 3000 G and detected by a quadrant electrometer detector. A true milestone in mass spectrometer instrumentation was achieved by Nier in 1940s with the introduction of a sector type of analyser. Nier's machine designed for gas and isotope analysis was 60° angular deflection instrument with a 15 cm radius of curvature and a resolution of 1 part in 100. In the same decade, Time-of-Flight Mass Spectrometer (1946) and Ion Cyclotron Resonance Mass Spectrometer (1949) were built. In the 1940s, the dominant commercial instrument, Model 21-101 analytical mass spectrometer was manufactured by Consolidated Engineering Corporation (Pasadena, Calif.), using Dempster's single-focusing design and was extensively used in the petroleum industry. The direct coupling of gas chromatograph (GC) and TOF-MS was accomplished in the mid-1950s by Gohlke and McLafferty. Quadruple mass filter was first reported in the mid of 1950s by Wolfgang Paul of the University of Bonn, who shared the 1989 Nobel Prize in Physics for his work on ion trapping, and was found to be perfect to couple with GC.

In the 1960s, Georges Slodzian developed the ion microscope (SIMS instrument that combined spatial and depth resolution along with isotopic analysis) to obtain high-resolution chemical images. In 1981, M. Barber developed fast atom bombardment MS (FAB MS), or 'liquid SIMS', in which beams of neutral atoms are used to ionize compounds gently from the surface of a liquid matrix enabling determination of large non-volatile organic molecules. Matrix Assisted Laser Desorption and Ionization Mass Spectrometer (MALDI MS) was developed by F. Hillenkamp and M. Karas in 1985 and the sample molecules are laser-desorbed from a solid or liquid containing a highly UV- absorbing matrix substance.

1.4 Components of a mass spectrometer

The three processes that occur in a mass spectrometer are i) ionization ii) sorting of ions iii) detection. Hence a mass spectrometer consists of sample introduction system, ion source, analyser, detector, data acquisition system and vacuum system. Samples in the solid, liquid or gas forms are introduced using a suitable inlet system. Usually, the singly charged positive ions are produced in the ion source. These ions are accelerated and sorted according to their mass to charge ratio (m/z) in the analyser. The sorted ions are detected either sequentially or simultaneously using a suitable detector. A vacuum system capable of producing pressure less than 10^{-6} torr in the ion source, analyser and detector forms an essential part of a mass spectrometer.

Inlet system

The solid samples can be introduced using a direct insertion probe. The effluents from liquid chromatography as well as gas chromatography columns can be introduced into the mass spectrometer using suitable interfaces. For gas analysis, static or dynamic mode can be used based on the amount of sample available.

Ion Source

The first step in using a mass spectrometer is to make the ions by either removing or sometimes adding a single electron to atom or molecule to produce a singly charged ion. Ions can also be produced by addition of proton to a molecule. Generally, ion production is accomplished in a variety of ways in different ion sources.

The ion sources commonly used in inorganic mass spectrometry are

- i. Thermal ionization or Surface ionization source
- ii. Electron ionization or Electron bombardment source

- iii. Spark source
- iv. Glow discharge source
- v. Inductively coupled plasma source
- vi. Secondary ion source

In the case of organic mass spectrometry, the ionization sources used are

- i. Electron impact ionization
- ii. Chemical ionization
- iii. Fast atom bombardment
- iv. Laser desorption & ionization
- v. Field emission
- vi. Electrospray ionization
- vii. Matrix Assisted Laser Desorption/ Ionization (MALDI)

Analyzer

Ions produced in the ion source are accelerated and mass separated into different ion beams according to their mass to charge ratios (m/z) using different physical principles. Most commonly used analyzers are magnetic, quadrupole, time of flight and ion cyclotron resonance.

Detector

After the separation of ions according to their m/z values, they are detected by a variety of detectors like Faraday cup, Secondary Electron Multiplier (SEM), ion-sensitive photographic plates, channeltron, ion counting system etc. When the amount of sample available is small, the ion current produced will be in the range of 10^{-14} to 10^{-16} A. Such low ion currents cannot be measured directly with a Faraday cup and further amplification is carried out using SEM.

1.5 Characteristics of a mass spectrum

A mass spectrum is a two dimensional representation of ion intensity (ordinate) versus m/z ratio (abscissa). This can be used

- i. To establish the molecular weight and structure of the compound analysed
- ii. To determine the isotopic composition of the element and for quantification of different elements/compounds present in the sample.

The mass spectrum of an organic compound is generally more complex compared to inorganic compounds. In the organic mass spectrometry, one can get peaks of the molecular ion (ionized parent molecule) and of the fragments resulting from breaking up of the molecule. The peak corresponding to the molecular weight of the compound is called molecular ion peak, generally denoted as M^+ ; the other peaks of lower m/z values are called the fragmentation peaks. The peak of highest intensity in the mass spectrum is called the 'base peak' and the intensities of other peaks are given relative to the base peak arbitrarily taken as 100% abundant. In the case of inorganic mass spectrum, the peaks of isotopes appear at their corresponding atomic masses with ion intensities corresponding to their relative abundances.

1.6 Different Types of Inorganic Mass Spectrometers

Based on the combinations of different types of inlet systems, ion sources, analyzers and detector systems, a variety of inorganic mass spectrometers are used for different applications. Some of the widely employed mass spectrometers are described below.

1.6.1 Secondary Ion Mass Spectrometer (SIMS)

SIMS is a very effective and powerful analytical technique for the chemical analysis of surfaces. The specimen under study is bombarded by a beam of energetic particles

(primary ions) in the energy range of 0.5 to 15 keV. The primary particle beam usually consist of ions (O^- , O_2^+ , Cs^+ , Ar^+ , Ga^+) or some neutral noble gas atoms. O_2^+ is typically used for the detection of electropositive species and Cs^+ for electronegative species. Some of the sputtered matter from the sample surface is emitted as positively or negatively charged atoms or molecules (secondary ions). These secondary ions carry information about the composition of specimen surface and are analysed with the help of a mass analyzer in SIMS. The neutral secondary species can also be post ionised either by electron impact or by laser ionization and can then be detected and this is known as Secondary Neutral Mass Spectrometry.

SIMS technique provides i) chemical characterization of uppermost surface layers of the specimen in the static SIMS mode ii) composition along with depth profiles in the dynamic SIMS mode and iii) lateral distribution of selected chemical species in the imaging SIMS mode. However, the SIMS technique is considered to be highly surface specific. Other special features of the technique include very high trace sensitivity (ppm to ppb range), excellent depth resolution (nm), wide dynamic range, isotopic analysis, hydrogen and other low Z element detection, ion imaging to provide three dimensional concentration maps and analysis of metals, semiconductors and insulators. SIMS has been used in all fields of material science, electronics industry, metallurgy, geology, biology and nuclear technology [32].

1.6.2 Spark Source Mass Spectrometry (SSMS)

In SSMS, the sample containing trace elements is taken in the form of cylindrical electrodes and a high radio frequency voltage is applied between the two electrodes, one of which contains the sample. The sample need to be made conducting by mixing with high

pure graphite, silver, aluminium or gold during electrode preparation. The ions generated due to RF-spark discharge are accelerated and passed through electrostatic and magnetic analysers. Both photoplate and electrical detection system are available. For quantification of results, the technique needs matrix matched trace constituent standards for calibration. SSMS finds application in analysis of standard reference materials, biological systems, environmental samples etc. Quantification of results is carried out by external calibration using standard reference materials [33]. Currently, this type of mass spectrometers are being replaced by LA-ICP-MS and GDMS.

1.6.3 Glow Discharge Mass Spectrometry (GDMS)

GDMS has been recognized as a powerful analytical technique for the determination of different trace constituents at ppb level present in a variety of matrices. The method is widely employed for surface analysis and depth profiling. The main advantage of the technique is that atomization and ionization processes are decoupled (unlike in SSMS) which leads to nearly uniform calibration factors for various elements in a given matrix.

The ion source is a dc glow discharge, where the sample acts as cathode and discharge is struck between the sample and the anode in an argon atmosphere. Plasma is sustained at a reduced pressure of 1 to 10 torr in an inert atmosphere. The quadrupole and magnetic sector analyzers have been used, respectively in low and high resolution GDMS. Faraday cup, Daly detector and SEM are used as detectors. Daly and SEM are used for trace and ultra trace level determination and Faraday cup for measuring high intensity ions. GDMS is employable for samples which are conductors, superconductors, semiconductors or insulators (RFGD-MS) [31].

1.6.4 Inductively Coupled Plasma source Mass Spectrometry (ICP-MS)

The ICP-MS technique has invigorated in the field of inorganic mass spectrometry since its commercial introduction in 1980s and is now used routinely in many laboratories for trace elemental analysis. ICP-MS consists of a conventional ICP torch mounted with a suitable sample introduction by pneumatic or ultrasonic nebulizer. Usually, solution samples are fed into the plasma through an aerosol generated by the nebulisers. The ions produced are extracted through a differentially pumped interface region into the high vacuum side of mass spectrometer consisting of ion lens system, a mass analyzer (usually a quadrupole) and a fast response detector (channeltron). To realise the full potential of ICP-MS in ultra trace analysis, a number of experimental parameters are optimised and improved. The major advantage of ICP-MS is the unique capacity for fast isotope ratio determination in solutions, with a precision 0.1-1% RSD.

ICP-MS in combination with separation techniques like Liquid Chromatography (LC) or Gas Chromatography (GC) are widely used for studies on elemental speciation. By coupling HPLC with ICP-MS, powerful and sensitive detection of elemental species in an online procedure is possible [31,34]. The nuclear applications of ICP-MS include trace and ultra trace level elemental analysis of nuclear fuel solutions, radioactive liquid waste, burn-up evaluation etc. The burn-up of simulated spent fuel solution containing U and rare earth elements La and Nd (fission products) of different compositions were analyzed by Maity et al by ICP-MS [35]. From the simultaneous measurement of intensity ratio of burn-up monitor to fissile atoms, the burn-up value was evaluated, with highest deviation of 1.5% from the reference value.

The Laser Ablation coupled ICP-MS (LA-ICP-MS) facility recently installed in the Fuel Chemistry Division of IGCAR enables direct solid sample analysis. Sample, in the form of pellet or thin film is subjected to ablation/ ionization by laser and the plume produced is flushed to the plasma source by Ar gas flow. The sensitivity of measurements was found comparable with that of liquid samples introduced by nebuliser. LA-ICP-MS finds special attention as it enables burn-up determination of spent nuclear fuel in pellet form, without dissolution. Moreover the facility enables remote handling of radioactive materials.

1.6.5 Matrix Assisted Laser Desorption /Ionization Mass Spectrometry (MALDI-MS)

Mass spectrometry of bio-molecules is complicated by two difficulties. One is the need of mass range of thousands of daltons with good resolution. Secondly, the analytes being a condensed phase with low vapor pressures, the molecules tend to break up under normal vaporization and ionization methods making it difficult to produce molecular ions. Both these problems are solved in MALDI-TOF-MS, in which the sample solution is mixed with a suitable matrix solution and allowed to dry; subsequently a laser causes desorption and ionization. The matrix plays two roles: absorption of laser and desorb the isolated analyte molecule along with matrix. Matrix also donates a proton (H^+) to the analyte molecule to form its molecular ion. When bio-molecules are dissolved in a matrix of an appropriate carboxylic acid which resonantly absorbs the laser radiation, the analyte molecules are desorbed as positive ions into the gas phase. Usually matrix to analyte ratio of greater than 100 is employed [36]. The matrices chosen are generally carboxylic acids such as nicotinic acid, 2,5-dihydroxy benzoic acid, sinapinic acid, succinic acid etc. which absorb strongly in the UV and IR region. The choice of laser is dictated by the need for resonant absorption of laser beam by the matrix. Nitrogen laser (337 nm), excimer laser (193, 248, 308, 266 nm),

Nd-YAG laser (266, 532, 1064 nm) etc. are good candidates of lasers. Though MALDI is well known for organic sample analysis, it found application for inorganic samples also, especially for cluster identification studies. Several studies on clusters of inorganic systems like Te, S, mixture of Te & S, U-O etc. are reported by researchers, using MALDI [37, 38].

Time of Flight Analyzer

MALDI-MS employs a time of flight analyzer in which the sorting out of masses from their mixture is achieved by taking advantage of the difference in velocities in a mono-energetic ion beam. When the singly charged ions are accelerated by a potential V , all the ions acquire kinetic energy ' eV ' (where e is the charge of ion), and $eV = \frac{1}{2}mv^2$. If this ion is allowed to drift a distance ' d ' in a field free region, the time taken for the travel ' t ' depends on the mass of ion and is given by,

$$t = \frac{d}{v} = \frac{dm^{1/2}}{(2eV)^{1/2}}$$
$$\frac{m}{e} = \frac{2Vt^2}{d^2}$$

Thus ions of different masses reach the detector at different points in time.

Reflectron TOF-MS

In RTOF-MS, the ion beam is reflected back at the end of its flight to the drift region and reaches the detector after travelling an equal distance in the reverse direction. This geometry provides energy compensation for ions of same m/z with different energy spread, and also an increase in the overall flight path; both these factors help to significantly increase the resolution. In TOF-MS, the gas samples are ionized with the help of lasers, due to their tunability in terms of wave length, resulting in RIMS (Resonance Ionization MS), a powerful tool for the detection of selected ions in very low concentration levels. Major advantages of

the reflectron type of TOF-MS are i) unlimited mass range ii) high resolution iii) high sensitivity due to very high transmission efficiency of ions (about 90%) compared to magnetic analyzer (<1%).

RTOF-MS is particularly suitable for the analysis of molecules of high mass for biological applications and in cluster studies. Worldwide many RTOF-MS are being used for various type of applications [39,40]. In India, the first RTOF-MS was fabricated at IGCAR, Kalpakkam which is being extensively used for organic sample analysis. This mass spectrometer is also used for identification of dissolution products of uranium carbide in nitric acid, identification of clusters of U and Te etc. [41,42].

1.6.6 Thermal Ionization Mass Spectrometry (TIMS)

Thermal ionization mass spectrometry involves vaporisation and ionization of the element, loaded and dried on the filament surface, by resistive heating (thermal ionization). The ions are accelerated and mass analysed by magnetic sector analyser and collected by Faraday cup or Daly scintillation detector or SEM. TIMS is a single element technique, and provides high precision and accuracy of better than 0.1%, hence TIMS is used as a definitive and reference method.

The filament materials generally used are high purity rhenium, tantalum, tungsten or platinum, as they have high melting point as well as high electronic work function since the formation of positive ions in TIMS is based on the Saha-Langmuir equation. Generally positive ions are employed for TIMS analysis. At times, the negative ions are also employed e.g. for boron, BO_2^- ion gives the highest sensitivity in negative TIMS (N-TIMS) [43,44] compared to Na_2BO_2^+ , Rb_2BO_2^+ or Cs_2BO_2^+ ions in positive TIMS (P-TIMS) [45]. The

generation of negative ions in surface ionisation requires high electron affinity of the element or molecule and low work function of the filament material.

The major components of TIMS are described below.

a. Thermal sources

Thermal sources consist of a filament assembly and a plate-slit system for the acceleration and shaping of the ion beam. There are three types of filament assemblies: single filament, multiple (double or triple) filament and specially prepared surfaces. Our laboratory uses all the three types of filaments, depending on the nature of the sample to be analyzed.

i) Single filament

In the simplest thermal source, few drops of sample solution or slurry is placed with a micro pipet on a filament ribbon which is about 0.01 mm thick, 15 mm long and 1 mm wide. The filament is then slowly heated by passing finite current through it to evaporate the solvent and fix the analyte over the filament. This is usually performed outside the mass spectrometer. The source assembly is then reinstalled inside the mass spectrometer, and after achieving vacuum of about 10^{-8} torr, the filament temperature is raised in a slow and steady manner; the vaporisation and ionization occurs on the same filament. Single filament is routinely used in our laboratory for the analysis of B which is loaded in the form of Na_2BO_2 .

ii) Triple filament

When elements of high ionization potential (I) are analysed, one has to operate at highest possible temperature for adequate ion intensity. When single filament is used, a compromise must be made between the efficiency of ionization and the duration for which the sample lasts. In triple filament system, the sample is evaporated from either of two symmetrically located filaments at a relatively low temperature (~ 1000 K), for long sample life, and the

neutral vapor produced is ionized by a central filament which is maintained at high temperature (~ 2800 K) for efficient ionization [30]. The main advantage of this arrangement is that sensitivity is increased without increase in sample consumption.

The triple filament system was used as ion source for all the studies described in chapter 3, 4 and 5 of this thesis.

iii) Specially prepared filaments

These filaments are specially prepared for specific nature of the sample. The following is an example of analysis of isotopic ratios of B in different kind of samples.

A thin layer of ultra high pure graphite slurry is coated over Ta/Re filament before loading elemental boron or boric acid samples (in the form of sodium borate, Na_2BO_2), for the removal of any oxide layer formed over the filament, and to expose the fresh metallic surface to the sample. After sample loading, a thin layer of mannitol is coated over the sample layer for controlled evaporation of sample [46]. However, for boron carbide (B_4C), graphite coating is not desirable as the sample itself act as source for carbon.

For elements of high ionization potential, we employ activators to improve the ion intensity. For e.g. ascorbic acid is loaded over Mo sample to form a complex species having lower ionization potential. Similarly, a mixture of boric acid and silica gel is employed for Zr analysis, in our laboratory.

b. Magnetic analyzer

The ions generated from thermal ionization source are collimated, accelerated and focussed into the mass analyser through an entrance slit. The low energy spread (< 0.2 eV) of the ions generated in thermal ionization source allows the use of only magnetic analyzer which

provides directional focusing. When a particle of charge e and velocity v moves across a magnetic field of flux density B at right angles to the field, a force, F is exerted upon it,

$$F_B = Bev$$

The ion, under the influence of a force whose magnitude is constant but direction is always at right angle to the velocity of the particle (Fleming's left hand rule), the orbit of particle becomes a circle, and the force become equal to the centripetal force, F_c

$$F_B = Bev = F_c = mv^2/r_m$$

Where v is the tangential speed and r_m is the radius of the circle described by the ion.

The above equation can be rearranged as

$$m/e = Br_m/v$$

The momentum filter becomes a mass filter when the condition of equal energy and equal charge are introduced. This property of magnetic field is the basis of majority of mass spectrometers. The constancy of ion energy is provided by accelerating the ion beam using a very high potential (V), depending on the initial energy spread of the ions formed after emerging from the ion source.

Thus, using the relations, $eV = 1/2mv^2$ and $Bev = mv^2/r_m$,

$$m/e = B^2 r_m^2 / 2V$$

c. Detector

Ions of different mass to charge ratios travel through the analyser in different trajectories. These ions which consist of different isotopes of a given element, pass through an exit slit and are collected and detected in a multi-Faraday cup detector system. All the latest commercial TIMS systems also incorporate a SEM for measuring minor isotopes of ion currents less than 10^{-15} A.

In Faraday cup detector, the positive ions arriving at the collector are neutralized by electrons arriving from the ground after passing through a high ohmic resistor. The potential drop across the resistor is the measure of the ion current. The bombarding of collector by energetic ions results in the formation of secondary electrons. In order not to change the actual current measured, secondary electrons must be returned to the collector. Similarly any negative ions generating from the bombardment of the slit must be prevented from reaching the collector to avoid peak height reduction and peak shape distortion. To eliminate these effects, a strong magnetic field around the collector or an additional slit which is negative (about -50 V) with respect to the collector plate is employed, called suppressor. The gains of different amplifiers used for various Faraday cups must be determined experimentally and the differences need to be accounted for isotopic measurements.

The most important advantage of Faraday cup detector is that the measured ion current is directly proportional to the number of ions and number of charges per ion, and is independent of the energy, mass and chemical nature of the ions. The detector is also characterised by constancy over long period of time, can be exposed to air without damage, reliability, inexpensiveness, long life and simple construction. A definite disadvantage is the relatively large time constant.

Electron multipliers used in mass spectrometry utilise the phenomenon of secondary electron emission. The ion current is converted into equivalent electron current by a conversion dynode and amplified by an array of amplification dynodes. The greatest advantage of electron multipliers is extremely high sensitivity and fast response. The important practical disadvantage with electron multipliers is large noise and desensitisation due to large ion currents and exposure to air.

The element to be analysed by TIMS should be in chemically pure form to eliminate the suppressive effect of ion formation by other impurity elements present in the sample. This requirement often demands the chemical separation and purification of the sample. This is usually done with ion exchange chromatography or by HPLC. This separation chemistry discourages the use of TIMS in earth science and biological fields, where ICP-MS have been widely accepted and used. However, for the analysis of radioactive elements like Pu, Am, Cm etc., TIMS still remain a work-horse and a gold standard in view of its high sensitivity, absence of any memory or carry over effect and elimination of the risk of generating any radioactive vapors as in ICP-MS.

Limitations of TIMS:

1. It is restricted to elements with ionization potential < 7 eV
2. No multi-element capability
3. Requires time-consuming sample preparation steps.

1.6.6.1 Isotope Dilution- Thermal Ionization Mass Spectrometry (ID-TIMS)

ID-TIMS is used to determine the concentration or total amount of an element present in a given sample solution [47]. It involves addition of a known amount of standard spike solution of the same element, to a known amount of sample solution, homogeneous mixing between the sample and the spike solutions and isotopic analysis of pure sample, pure spike and their mixture. Isotopic compositions of the sample, spike and their mixture are diagrammatically represented in Fig. 1.2.

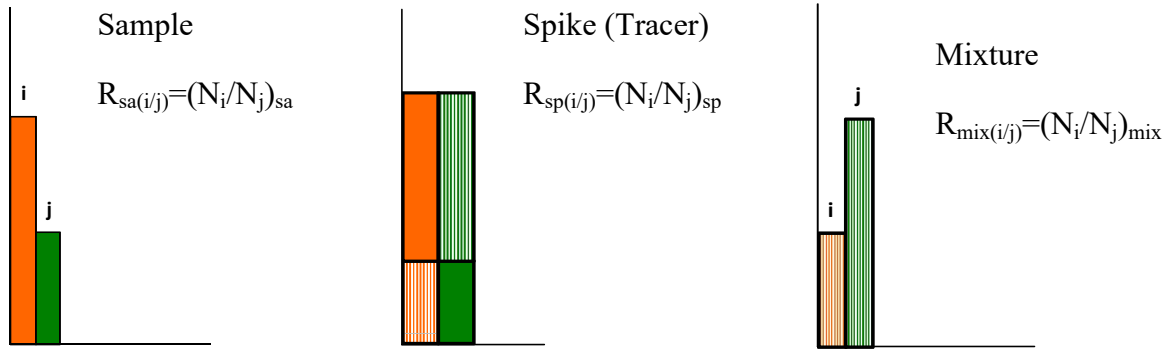


Fig. 1.2 Diagrammatic representation of sample-spike mixing in IDMS

$$R_{\text{mix}(i/j)} = (N_i/N_j)_{\text{mix}} = (N_{i,\text{sa}} + N_{i,\text{sp}}) / (N_{j,\text{sa}} + N_{j,\text{sp}})$$

From isotopic ratios, the IDMS equation [47] is deduced as

$$C^S = C^T * \frac{W^T}{W^S} * \left[\frac{R^T(i/j) - R^M(i/j)}{R^M(i/j) - R^S(i/j)} * \frac{1}{R^T(i/j)} * \frac{\langle A \rangle^S}{\langle A \rangle^T} * \frac{(A.F)_i^T}{(A.F)_j^S} \right]$$

where, C^S - concentration of sample; C^T - concentration of tracer (spike); W^T - weight of tracer; W^S - weight of sample; $\langle A \rangle^S$, $\langle A \rangle^T$ - average atomic weights of sample and tracer; $(A.F)_i^T$, $(A.F)_j^S$ - atom fractions of tracer and sample; $R^S_{(i/j)}$, $R^T_{(i/j)}$, $R^M_{(i/j)}$, - isotopic ratio of sample, tracer and mixture, respectively.

The concentration determination by IDMS depends only upon the change in isotopic ratio, and is not affected by incomplete recovery of the analyte during chemical separation and purification. In view of the inherent advantages of IDMS, ID-TIMS is termed as a definitive analytical methodology and is used as a reference technique to calibrate other analytical methodologies. The choice of spike isotope of an element is governed by many factors like:

1. The spike isotope should be absent or least abundant in the given sample.
2. The isotope should be stable or long lived.
3. It should not have any isobaric interference from the adjacent or other elements.

4. It should be easily available and should not be very expensive.
5. It should preferably be in the same chemical form as the element in the sample for easy homogenization or mixing.

For U and Pu, the most commonly used spikes are ^{233}U and ^{242}Pu , as they are the lowest abundant isotopes of the respective elements in most of the nuclear fuel samples [48]. Alternate spiking mechanisms for U and Pu had been tried by researchers and proven to work [49]. All the IDMS studies covered in this thesis have used ^{233}U spike for U, ^{239}Pu and ^{240}Pu spikes for Pu due to non-availability of the ideal spike (^{242}Pu). In our laboratory, Pu from Pressurized Heavy Water Reactor (with ~ 70 atom % ^{239}Pu) is estimated using Pu from research reactor (with ~ 93 atom % ^{239}Pu , from CIRUS reactor) as spike and vice versa. The spike solutions are calibrated by reverse IDMS using certified standards. The radioactive decay of Pu isotopes (mainly ^{241}Pu & ^{238}Pu) necessitates the certified values of concentration of Pu in spike to be corrected regularly. Moreover, there are chances for Pu spike to be unstable due to polymerisation which requires a suitable chemical treatment for isotopic homogenisation of Pu isotopes between the sample and the spike solutions. These problems are not very serious in the cases of Th and U.

The advantages of IDMS includes precise and accurate analysis, non-quantitative isolation of the substance to be analysed, ideal internal standardisation, feasibility of multielement and mono-element analysis, high sensitivity and low detection limit. However, the method has limitations such as destructive nature, necessity of chemical preparation of sample, time consumption and use of expensive spikes.

Sources of errors in IDMS

The sources of errors associated with an IDMS determination are as follows:

1. Chemical errors: can be caused by incomplete decomposition of the sample on the filament, incomplete mixing with tracer in the solution or by isotopic fractionation.
2. Purity, stoichiometry and quantity of the standard.
3. Isobaric interference.
4. Contamination from reagents, apparatus or the laboratory.

1.6.6.2 Applications of TIMS in nuclear industry

a) Isotopic composition and concentration determination

Isotopic composition of U is needed in ^{235}U enrichment facilities. Though the routine measurement using UF_6 gas (as UF_5^+ at m/z 330 and 333) is made by GC-Electron Impact Mass Spectrometer (GC-EIMS), TIMS is employed to check the memory effects in GC-EIMS and also for characterising the working standards to be used for GC-EIMS. When small changes in the $^{235}\text{U}/^{238}\text{U}$ ratio need to be measured during initial stages of enrichment studies using various enrichment methodologies, TIMS is the most dependable technique. The data on ^{235}U , ^{239}Pu and ^{241}Pu in U and Pu bearing nuclear fuels are obtained by TIMS to certify the fissile content as a part of chemical quality assurance of fuels. In the irradiated fuel, data on isotopic composition and concentrations of U and Pu are determined to calculate the burn-up from changes in the value of heavy element isotopic ratio and for nuclear material accounting at the reprocessing plants [50].

Boron carbide (B_4C) is widely used as control rod material both in thermal reactors such as Pressurized Water Reactors (PWR) and in Fast Breeder Reactors (FBR). The absorption cross-sections of ^{10}B and ^{11}B for thermal neutrons (~ 0.02 eV) are 3837 b and 5 mb, respectively; while the values for fast neutrons (~ 100 keV) are about 2.7 b for ^{10}B and a much smaller value (9.7×10^{-5} b) for ^{11}B [51]. The natural abundance of isotopes of boron

are: 19.89 % of ^{10}B and 80.11% of ^{11}B . Hence, B_4C pellets enriched in ^{10}B are used in the control rods for FBRs. The extent of enrichment varies from 60%, for a commercial fast reactor, to as high as 90% for small core test reactors, such as Fast Breeder Test Reactor (FBTR) [52]. The measurements of ^{10}B abundance need to be accurate within $\pm 1\%$. TIMS is the most reliable and widely employed method to measure the isotopic composition of B. Gd and Cd with adequate enrichment are other candidates for control rod materials; researchers are widely attempting the enrichment studies of these elements. TIMS is the most suitable technique to know the extent of enrichment with better than 0.1% accuracy.

b) Burn-up determination of irradiated nuclear fuels

TIMS is used to obtain the most reliable data on the burn-up of irradiated fuels and on the depletion and building up of U and Pu isotopes inside a nuclear reactor. The isotopic composition, along with concentrations of U, Pu and Nd (determined by triple spiked IDMS), provide accurate evaluation of burn-up. Burn-up can also be determined from changes in the heavy element isotopic composition. ID-TIMS provides the best possible data on burn-up with minimum uncertainty [53,54]. These experimental data are very useful to check and develop the computer codes for the build-up and depletion of different heavy element isotopes and for fuel management during reactor operation.

Burn-up studies were reported for irradiated fuels of natural U (PHWR) [48], enriched ($< 3\%$ ^{235}U) U, MOX fuels containing both U and Pu (FBR) [14,55] and for carbide fuel irradiated in test reactor [56]. Carbide fuel was analysed in our laboratory for U/Pu determination by ID-TIMS without pre-separation of individual elements, as explained in Chapter 5, part B.

c) Accountability of Pu and U in reprocessing plants

Determination of Pu and U in the input accountability tank of a reprocessing plant is carried out by ID-TIMS in an accurately measured aliquot of the solution. This involves uncertainties in the total volume or weight of solution in the tank and in the aliquot size. In order to minimize this error, a novel approach using a suitable tracer was developed [57], which involves the addition of a known amount of the tracer element to the storage tank, homogenization and mixing of the tracer with solution in the tank, and taking known aliquot from the solution. By determining tracer to Pu and tracer to U amount ratios by ID-TIMS, and knowing accurately the amount of tracer added, the total amount of Pu and U in the tank can be determined. The method eliminates the need to know the total volume of solution in the tank as well as the aliquot size.

d) Determination of half-lives

TIMS has played an important role in the determination of precise and accurate half-life values of different trans-uranium isotopes. A number of methods like daughter growth, specific activity and relative activity etc. were used to determine the half-life values experimentally. Half-life of ^{235}Np was determined by the parent decay method by measuring the changes in the $^{235}\text{Np}/^{236}\text{Np}$ ratio periodically for about 630 days, using TIMS [58]. The $^{235}\text{Np}/^{236}\text{Np}$ ratio decreased from 4.342 to 1.445 in 630 days and a half-life value of 396.1 ± 1.2 days was calculated. Aggarwal et al [59] determined the beta decay half-life of ^{241}Pu (14.4 years) using the same approach by preparing a synthetic mixture of Pu isotopes with almost equal amounts of ^{239}Pu , ^{240}Pu , ^{241}Pu and ^{242}Pu . The accurate half-lives of other radioactive isotopes like ^{238}Pu (87.7 years), ^{244}Cm (18 years), ^{232}U (70 years) etc., which are of interest in nuclear science and technology, were evaluated by employing the present

generation high sensitive TIMS [60]. The in-growth of daughter nuclides viz. ^{235}U from alpha decay of ^{239}Pu , and ^{241}Am from beta decay of ^{241}Pu was also determined by ID-TIMS.

The specific activity method [61] depends upon the availability of highly enriched isotope of the radio nuclide with high radiochemical purity. The number of atoms present in a given mass is determined by ID-TIMS. This method can be used for determining half- lives of several U, Pu and Am isotopes. In this method, the radioactive disintegrations per unit mass is obtained by alpha counting. Successful determination of half lives of ^{242}Pu , ^{232}U , ^{243}Am and ^{244}Pu by relative activity method, using another isotope of the same elements as a reference isotope, are also reported [62].

The different approaches mentioned above have also been used for the precise and accurate determination of half-lives of many other radioactive isotopes useful in geo-chronology and other fields.

e) Nuclear safeguards and nuclear forensics

TIMS is a unique analytical tool in nuclear forensics to find out the origin of the interdicted material and the age of the material (the time elapsed after the latest purification of U and/or Pu). Efforts are going on world-wide in different international laboratories to develop and confirm the suitability of different methodologies using TIMS to find out the accurate age of the materials. Different parent-daughter chronological couples e.g. ^{235}U - ^{231}Pa , ^{239}Pu - ^{235}U , ^{241}Pu - ^{241}Am have been used to validate the analytical methodology [63]. Efforts are also going on to produce certified reference materials of known age. IAEA, Vienna is the prime agency promoting this particular activity. The age of any radioactive sample can be determined by measuring the daughter/parent ratio as a function of decay time. Since the age of nuclear materials will not exceed a few decades compared to the long half-lives of

radioactive isotopes of U and Pu, the amounts of daughters grown are quite limited. This demands chemical separation followed by mass spectrometric or radiometric measurements.

Isotope ratio measurements on Sr, Nd and Pb present in uranium ore concentrate or any uranium sample can be used to trace the origin of uranium [64]. This is due to the fact that there would be small differences in the contents of ^{87}Sr (daughter of ^{87}Rb), ^{143}Nd (decay product of ^{147}Sm) and radiogenic lead isotopes (viz. ^{206}Pb , ^{207}Pb and ^{208}Pb) arising due to the geological history of the mine. The measurements require chemical separation of these elements to get them in the purest form using suitable ion exchange procedures and highly precise determination of isotopic composition by either TIMS or multi-collector high resolution inductively coupled plasma source mass spectrometry (MC-HR-ICPMS).

The $^{143}\text{Nd}/^{144}\text{Nd}$ isotope ratio is also a useful signature to assess the origin of U ore concentrates. This ratio provides a robust signature since it is less prone to weathering. This can be measured with high precision using TIMS or magnetic sector multi-collector ICP-MS. The $^{18}\text{O}/^{16}\text{O}$ isotope amount ratio in the actinide compounds is also proposed as a useful indicator for tracing their origin [65].

f) Fission Track analysis (FT-TIMS)

The method is used to discover the unrevealed nuclear activities. Swipe samples containing uranium bearing particles collected from surroundings of nuclear establishments are analyzed by TIMS. Finding out uranium bearing particles, transferring of single particle to TIMS and determination of isotopic composition are the three difficult steps involved in FT-TIMS. The particles present in swipe cotton are driven to isoamyl acetate solution using an ultrasonic bath and the mixture is dropped stepwise on to a collodion film and dried in air. The film is irradiated with thermal neutrons of fluence $\sim 9 \times 10^{15}$ neutrons/cm² in a reactor.

After irradiation, the films are etched with sodium hydroxide solution to amplify the fission tracks produced by each single uranium bearing particles. The etched film is viewed under a microscope to locate the stars made out of fission tracks where uranium particles are present. A small piece of film containing the track star is cut off with the help of a microscope and transferred onto a Re filament. A small drop of ethanol is dropped on the filament to dissolve the film and fix it on the filament. Isotopic composition of U is measured by TIMS , where each isotope is collected by Daly detector in peak jump mode. From the isotopic composition, age of the nuclear material, type of reactor (fast/thermal), enrichment level, geo-location etc. can be arrived at [66].

g) Discovery of natural reactors

The discovery of natural nuclear reactor (Oklo phenomenon) in 1972, which was solely due to the discrepancy noted in the fraction of ^{235}U isotope. Normally, the natural abundance of ^{235}U is 0.72%, while the samples received from uranium mines from Gabon Republic in West Africa by a French Company, had only 0.60%, a significant difference in isotopic composition. A series of measurements performed had shown that some regions of the mines with ^{235}U abundance as low as 0.44 atom%. Subsequent examination of other elements such as neodymium and ruthenium also had shown similar anomalies. A possible explanation was that the uranium ore had operated as a natural fission reactor. Other observations like presence of slightly enriched ^{235}U at some portions of the mine also led to the conclusion that self-sustaining nuclear chain reactions had occurred on earth about 2 billion years ago when the abundance of ^{235}U was about 3 atom%, where ground water acted as neutron moderator.

h) Tracing of nuclear materials in environment

TIMS has been used extensively for the determination of Pu and U isotopic ratios in a large number of environmental, biological and geological samples. However, the advent of MC-ICP-MS is quite attractive for obtaining these data in such samples containing less than microgram amounts of U and Pu. This is mainly because ICP-MS does not require the U and Pu to be in highly pure form, which eliminates the need for complex separation and purification and take less analysis time. Different mass spectrometric techniques provided data on the isotopic abundances and amounts of U, Pu and other actinides present in a variety of soil samples and effluents from accident reactor sites of Chernobyl and Fukushima [67,68].

1.7 Scope of the present study

Isotopic composition measurements of nuclear materials like U and Pu are the most important application of mass spectrometers in nuclear industry, along with other strategically important elements like B, Nd, Gd, Zr etc. The most accurate and precise measurements of U and Pu are important for burn-up evaluation and for nuclear material accounting (NUMAC). The performance of nuclear fuel inside a nuclear reactor is evaluated by the parameter burn-up, which is measured conventionally by a lengthy wet chemical procedure involving multi stage ion exchange separations followed by isotopic analysis. This leads to long time of exposure of radioactivity to the analyst and generation of large volume of radioactive liquid waste. Moreover, the data on spatial profile of burn-up is lost by dissolution of spent fuel. Therefore, a study on direct sampling of solid fuel pellets by ablation and deposition of microgram level of sample using pulsed laser, followed by isotopic analysis using TIMS was carried out. Simulated pellets of U doped with rare earths

were prepared and analyzed towards this to optimize the laser parameters in order to get the nearest stoichiometric ablation of solid samples, and hence to get the most accurate values for U/Nd concentration ratio. The method is characterized with amenability for remote handling of radioactive materials, reduced time consumption and minimum generation of radioactive liquid waste.

The present generation TIMS is equipped with advanced features for interference correction, which enable the measurement of isotopic composition of an element of natural origin, in presence of its isobarically interfering element, by measuring the corrected ion intensities of individual isotopes. Hence, in the above experiments with simulated pellets, isotopic composition of Nd could be measured using corrected ion intensities. Since the isotopic composition of elements present in irradiated nuclear fuel is different from that of natural origin, the above mentioned facility of TIMS cannot be employed for isobaric correction, which leads to necessity for chemical separation of individual elements of interest. This issue was addressed by making use of the high sensitive TIMS as well as the difference in physical properties like vapor pressure of the elements of interest. Interfering elements were removed from the matrix by evaporation inside TIMS. Direct loading of dissolver solution on to Re/Ta filaments followed by a sequential pattern of analysis of U, Pu and Nd was put forwarded by the present study and was found applicable for isotopic measurements and burn-up determination. Spent fuels from commercial reactors as well as research reactors were studied towards this. Hence, the present study is a probe into simplification of burn-up determination procedures making use of the advanced features of TIMS and the physical properties of elements of interest. Identification of dissolution products of UC in nitric acid

and cluster studies of U and Te using an indigenously made Reflectron Time of Flight Mass Spectrometer (RTOF-MS) are also form part of this thesis.

References

1. Samuel Glasstone, Alexander Sesonske, Nuclear Reactor Engineering, 1986, CBS Publishers, Delhi, pp. 13.
2. Baldev Raj, Materials science research for sodium cooled fast reactors, Bull. Mater. Sci., 2009, 32(3), 271–283.
3. V. Rajan Babu, S. Govindarajan, S. C. Chetal, Proc. of seminar on inherent engineered safety aspects of PFBR design, 1996.
4. C. H. Lee, M. Y. Suh, K. S. Choi, J. S. Kim, B. C. Song, Separation of fission products from spent pressurized water reactor fuels by anion exchange and extraction chromatography for inductively coupled plasma atomic emission spectrometric analysis, Anal. Chim. Acta, 2000, 428, 133-142.
5. S. F. Wolf, D. L. Bowers, J. C. Cunnane, Analysis of high burnup spent nuclear fuel by ICP-MS, J. Radioanal. Nucl. Chem., 2005, 263, 581-586.
6. S. F. Wolf, Y. Tsai, Application of ICP-MS and HR-ICP-MS for the characterization of solutions generated from corrosion testing of spent nuclear fuel, J. Radioanal. Nucl. Chem., 2005, 263, 575-579.
7. I. Glagolenko, B. Hilton, J. Giglio, D. Cummings, Fission yield measurements by Inductively coupled plasma mass-spectrometry, J. Radioanal. Nucl. Chem., 2009, 282, 651-655.

8. J. I. G. Alonso, F. Sena, P. Arbore, M. Betti, L. Koch, Determination of fission products and actinides in spent nuclear fuels by isotope dilution ion chromatography inductively coupled plasma mass spectrometry, *J. Anal. At. Spectrom.*, 1995, 10, 381-393.
9. M. Betti, Use of ion chromatography for the determination of fission products and actinides in nuclear applications, *J. Chromatogr. A*, 1997, 789, 369-379.
10. M. Joseph, D. Karunasagar, B. Saha, Laser mass spectrometric studies on rare earths doped UO₂, 1996, IGC report-184.
11. P. D. Blair, The application of inductively coupled plasma mass spectrometry in the nuclear industry, *Trends Anal. Chem.*, 1986, 5, 220-223.
12. S. Vijayalakshmi, R. Krishna Prabhu, T. R. Mahalingam, C. K. Mathews, A simple gas-liquid separator for continuous hydride introduction in ICP-MS, *At. Spec.*, 1992, 13, 26-28.
13. J. I. G. Alonso, D. T. Schultendorff, B. Giovanonne, L. Koch, H. J. Wiesmann, Performance characteristics of a glove box inductively coupled plasma mass spectrometer for the analysis of nuclear materials, *J. Anal. At. Spectrom.*, 1993, 8, 673-679.
14. S. Bera, R. Balasubramanian, A. Datta, R. Sajimol, S. Nalini, T. S. Lakshmi Narasimhan, M. P. Antony, N. Sivaraman, K. Nagarajan, P. R. Vasudeva Rao, Burn-up measurements on dissolver solution of mixed oxide fuel using HPLC- Mass spectrometric method, *Int. J. Anal. Mass Spec. Chrom.*, 2013, 1, 55-60.
15. J. Hoefs, *Stable Isotopes Geochemistry*, Springer, Berlin, 1987, 9, 387.
16. M. Shima, A summary of extremes of isotopic variations in extra-terrestrial materials, *Geochim. Cosmochim. Acta*, 1986, 50, 577-584.
17. G. Faure, *Principles of Isotope Geology*, 2nd edition, 1986, Wiley, New York.

18. J. S. Crain, Atomic spectroscopy perspectives: Applications of inductively coupled plasma-mass spectrometry in environmental radiochemistry, *Atomic Spectroscopy Perspectives*, 1996, 11, 30-39.
19. J. S. Becker, H. J. Dietze, Determination of long-lived radionuclides by double-focusing sector field ICP mass spectrometry, *Adv. Mass Spectrom.*, 1998, 14, 681-686.
20. C. K. Kim, R. Seki, S. Morita, S. Yamasaki, A. Tsumura, Application of a high resolution inductively coupled plasma mass spectrometer to the measurement of long-lived radionuclides, *J. Anal. At. Spectrom.*, 1991, 6, 205-209.
21. D. Solatie, P. Carbol, M. Betti, F. Bocci, T. Hiernaut, Ion chromatography inductively coupled plasma mass spectrometry (IC-ICP-MS) and radiometric techniques for the determination of actinides in aqueous leachate solutions from uranium oxide, *J. Anal. Chem.*, 2000, 368, 88-94.
22. R. A. Meyers, *Encyclopedia of Analytical Chemistry: Applications, Theory, and Instrumentation*, Volume 15, 2000, John Wiley & Sons.
23. S. Chandramouleeswaran, Jayshree Ramkumar, Mass Spectrometry: A Boon to Nuclear Industry, *J. Anal. Bioanal. Techniques- Special Issue*, 2014, 6, 1-9.
24. S. N. Begiche, A. A. Borovoj, E. V. Burlako, A. J. Gagarinsk, V. F. Demin, Radioactive releases due to the Chernobyl accident. In: Rogers JT, *Fission Product Transport Processes in Reactor Accidents*, Hemisphere, 1990, New York, USA, 717-734.
25. G. Kirchner, C. C. Noack, Core history and nuclide inventory of the Chernobyl core at the time of accident, *Nucl. Safety*, 1988, 29, 1-5.
26. D. L. Donohue, Strengthening IAEA safeguards through environmental sampling and analysis, *J. Alloys and Compounds*, 1998, 271, 11-18.

27. X. L. Zhao, M. J. Nadeau, L. R. Kilius, A. E. Litherland, The first detection of naturally-occurring ^{236}U with accelerator mass spectrometry, Nucl. Instrum. Methods Phys. Res. Sec. B, 1994, 92, 249-253.
28. D. Berkovits, H. Feldstein, S. Ghelberg, A. Hershkowitz, E. Navon, ^{236}U in uranium minerals and standards, Nucl. Instrum. Methods Phys. Res. Sec. B, 2000, 172, 372-376.
29. C. Kurta, L. Dorta, F. Mittermayr, K. Prattes, B. Hattendorf, Rapid screening of boron isotope ratios in nuclear shielding materials by LA-ICPMS – a comparison of two different instrumental setups, J. Anal. At. Spectrom., 2014, 29, 185-192.
30. John Roboz, Introduction to Mass Spectrometry- instrumentation and techniques. John Wiley & Sons, 1968, USA.
31. S. K. Aggarwal, H. C. Jain, Introduction to Mass Spectrometry, Indian Society for Mass Spectrometry, 1977, Mumbai.
32. R. B. Jeffrey, K. L. Linge, L. V. Vaeck, Atomic spectrometry update-Atomic mass spectrometry, J. Anal. At. Spec., 2005, 20, 763–802.
33. F. A. Mellon, Mass Spectrometric methods for studying nutrient, mineral and trace element absorption and metabolism in humans using stable isotopes, Analyst, 1994, 119, 2491-2518.
34. A. R. Date, A. I. Gray, Inductively Coupled Plasma Mass Spectrometry, 1989, Chapman and Hall, New York.
35. U. K. Maity, P. Manoravi, N. Sivaraman, M. Joseph, A precise and fast determination of burn-up using ICP-MS (private communication).
36. F. Hillenkamp, M. Karas, R. C. Beavis, B. T. Chait, Matrix Assisted Laser Desorption Ionization Mass Spectrometry of Biopolymers, Anal. Chem., 1991, 63A, 1193-1202.

37. M. Alberty, O. Sedo, J. Havel, Laser ablation synthesis and TOF mass spectrometric identification of tellurium, sulfur and mixed tellurium–sulfur clusters, *Polyhedron* , 2003, 22, 2601-2605.
38. V. S. Ban, B. E. Knox, Mass spectrometric studies of laser-produced vapor species, *J. Chem. Phys.*, 1969, 51, 524-526.
39. S. Wei, A. W. Castleman, Using reflection time-of-flight mass spectrometer techniques to investigate cluster dynamics and bonding, *Int. J. Mass Spec.*, 1994, 131, 233-241.
40. D. F. Barofsky, G. Brinkman , P. Hakansson, B. U. R. Sundqvist, Ion Processes, *Int. J. Mass Spec.*, 1994, 131, 283-289.
41. R. Sajimol, P. Manoravi, M. Joseph, N. Sivakumar, Mass spectrometric studies on dissolution products of UC in nitric acid, *Proc. Chemistry Research Scholars Meet- July14-15, 2011, held at IGCAR, Kalpakkam.*
42. R. Sajimol, P. Manoravi, U. K. Maity, M. Joseph, Observation of clusters of Te in Laser Ionization Mass Spectrometric studies, *Proc. National Laser Symposium, KIIT-Bhubaneswar, Dec. 20-23, 2016, 63-66.*
43. S. K. Aggarwal, B. S. Wang, C. F. You, C. H. Chung, Boron analysis by Negative Thermal Ionization Mass Spectrometry based on BO_2^- ions and using the $^{18}\text{O}/^{16}\text{O}$ ratio from ReO_4 for internal normalization, *Anal. Chem.*, 2009, 81, 7420–7427.
44. K. G. Heumann, M. Koppe, M. Wachsmann, New developments in Negative Thermal Ionization Mass Spectrometry and its applications, *Proc. 37th ASMS Conf. Mass Spectrometry and Allied Topics*, 1989, 414–416.
45. R. M. Rao, A. R. Parab, S. K. Aggarwal, The preparation and use of synthetic isotope mixtures for testing the accuracy of the PTIMS method for $^{10}\text{B}/^{11}\text{B}$ isotope ratio

- determination using Boron-Mannitol complex and NaCl for the formation of Na_2BO_2^+ , *Anal. Methods*, 2012, 4, 3593–3599.
46. R. M. Rao, A. R. Parab, K. Sasibhushan, S. K. Aggarwal, A robust methodology for high precision isotopic analysis of boron by thermal ionization mass spectrometry using Na_2BO_2^+ ion, *Int. J. Mass Spec.*, 2009, 285, 120–125.
47. K. G. Heumann, *Isotope Dilution Mass Spectrometry*, *Int. J. Mass Spec. Ion Processes*, 1992, 118, 575–592.
48. B. Saha, R. Bagyalakshmi, G. Periaswami, V. D. Kavimandan, S. A. Chitambar, H. C. Jain, C. K. Mathews, *Determination of nuclear fuel burn-up using mass spectrometric techniques*, 1977, BARC Report-891.
49. A. Hasozbek, K. J. Mathew, G. Orlowicz, N. Hui, B. Srinivasan, M. Soriano, U. Narayanan, Uranium isotope dilution mass spectrometry using NBL certified reference materials as spikes, *J. Radioanal. Nucl. Chem.*, 2013, 296, 447–457.
50. S. K. Aggarwal, *Thermal Ionisation Mass Spectrometry in nuclear science and technology*, *Anal. Methods*, 2016, 8, 942–957.
51. A. G. R. Ahmed, S. Sen, V. Goplalakrishnan, *Cross-sections of some control rod materials for PFBR*, 2003, IGC Report- RPD/NDS/103.
52. P. Manoravi, M. Joseph, N. Sivakumar, P. R. Vasudeva Rao, Quasi-non-destructive isotopic ratio measurement of boron in irradiated control rod B_4C pellets using a home-built reflectron time-of-flight mass spectrometer, *Int. J. Mass Spec.*, 2012, 309, 148-153.
53. R. Sajimol, S. Bera, S. Nalini, N. Sivaraman, M. Joseph, T. Kumar, Preferential removal of Sm by evaporation from Nd- Sm mixture and its application in direct burn-up determination of spent nuclear fuel, *J. Radioanal. Nucl. Chem.*, 2016, 3092, 563-573.

54. R. Sajimol, S. Bera, N. Sivaraman, M. Joseph, Direct burn-up determination of fast reactor mixed oxide (MOX) fuel by preferential evaporation of interfering elements, *J. Radioanal. Nucl. Chem.*, 2017, 311, 1593-1603.
55. S. K. Aggarwal, P. G. Jaison, A. R. Parab, Experimental determination of burn-up of mixed-oxide fuels irradiated in PWL, CIRUS using Thermal Ionisation Mass Spectrometry, BARC Report- E/012/2011.
56. R. Balasubramanian, D. D. Albert Raj, S. Nalini, M. Sai Baba, Mass spectrometric studies on irradiated (U, Pu) mixed carbide fuel of FBTR, *Int. J. Nucl. Energy Sci. Technol.*, 2005, 1, 197–203.
57. S. K. Aggarwal, V. D. Kavimandan, S. N. Acharya, H. C. Jain, C. K. Mathews, Lead tracer technique for the accountability of Plutonium (LEADTRAP), BARC Report- 904/1976.
58. J. H. Landrum, Mass spectrometric determination of the half-life of ^{235}Np , *J. Inorg. Nucl. Chem.*, 1970, 32, 2131–2132.
59. S. K. Aggarwal, A. R. Parab, S. A. Chitambar, H. C. Jain, Half-life of ^{241}Pu , *Phys. Rev. C*, 1985, 31, 1885–1890.
60. S. K. Aggarwal, H. C. Jain, Half-life of ^{241}Pu : Past and present, *J. Radioanal. Nucl. Chem.*, 1987, 109, 183–200.
61. D. Brown, K. Glover, M. King, G. Phillips, F. R. Rigters, Wiltshire, A re-determination of the half-life of ^{239}Pu by specific activity measurements, *J. Radioanal. Nucl. Chem.*, 1981, 64, 181–193.

62. S. K. Aggarwal, D. Alamelu, P. M. Shah, N. N. Mirashi, Precise and accurate determination of the half-life of the α -decay nuclide ^{243}Am using ^{241}Am as the reference isotope, *Nucl. Instrum. Methods Phys. Res., Sect. B*, 2007, 571, 663–668.
63. G. R. Eppich, R. W. Williams, A. M. Gaffney, K. C. Schorzman, ^{235}U - ^{231}Pa age dating of uranium materials for nuclear forensic investigations, *J. Anal. At. Spectrom.*, 2013, 28, 666–674.
64. J. Krajko, Z. Varga, E. Yalcintas, M. Wallenius, K. Mayer, Application of neodymium isotope ratio measurements for the origin assessment of uranium ore concentrates, *Talanta*, 2014, 129, 499–504.
65. L. Pajo, G. Tamborini, G. Rasmussen, K. Mayer, L. Koch, A novel isotope analysis of oxygen in uranium oxides: Comparison of Secondary Ion Mass Spectrometry, Glow Discharge Mass Spectrometry and Thermal Ionisation Mass Spectrometry, *Spectrochim. Acta, Part B*, 2001, 56, 541–549.
66. K. T. Esaka, F. Esaka, J. Inagawa, K. Iguchi, Chi-Gyu Lee, S. Sakurai, K. Watanabe, S. Usuda, Application of fission track technique for the analysis of individual particles containing Uranium in safeguard swipe samples, *Jap. J. Appl. Phys.*, 2004, 43/7A, 73-80.
67. S. K. Sahoo, Y. Nakamura, K. Shiraishi, A. Masuda, Accurate measurement of uranium isotope ratios in soil samples using Thermal Ionization Mass Spectrometry equipped with a WARP energy filter, *Int. J. Environ. Anal. Chem.*, 2004, 84, 919–926.
68. Y. Shibahara, T. Kubota, T. Fujii, S. Fukutani, K. Takamiya, M. Konno, S. Mizuno, H. Yamana, Determination of isotopic ratios of plutonium and uranium in soil samples by thermal ionization mass spectrometry, *J. Radioanal. Nucl. Chem.*, 2016, 307, 2281–2287.

Effect of laser parameters on measurement of U/Nd ratio using Pulsed Laser Deposition - Isotope Dilution Mass Spectrometry (PLD - IDMS)

2A.1 Introduction

2A.1.1 Pulsed Laser Deposition - Mass Spectrometry (PLD-MS)

The techniques available for elemental analysis may be divided into two broad categories- those suitable for analysis of sample in solution form and those developed for direct analysis of solid materials. Though the number of techniques routinely used for trace elemental analysis of solution is relatively small, thousands of instruments around the world perform this kind of work, as a result of high sensitivity of the established methods and the uniform physical nature of liquid samples. Direct introduction of solid sample into atomization and excitation sources of spectrometers is of interest as it broadens the capability of the technique since the laborious sample dissolution process can be avoided, especially for radioactive samples like nuclear fuel. Lasers play an important role in elemental analysis of solids because a suitable focused beam of a pulsed laser is capable of vaporizing or ablating all materials [1]. Laser is highly directional, high intensity beam and is highly monochromatic having power ranging from 10^{-9} to 10^{20} W [2]. The wavelength of laser ranges from microwave to soft X-ray spectral regions with corresponding frequencies from 10^{11} to 10^{17} Hz. The ability of laser to precisely target a small feature of interest is an important advantage compared to techniques with little or no spatial resolution such as spark source and GDMS. At moderate laser irradiances ($>10^7$ W/cm²), interaction between the laser and sample causes rapid heating and ejection of a plume of material from the sample surface [3].

Sample introduction by laser ablation gives compositional analysis at medium spatial resolution ($\sim 100 \mu\text{m}$) and is applicable to all materials without restriction of physical properties such as electrical conductivity. The plume contains vaporized atomic and molecular species as well as particulates [4]. Ground and excited state atomic species and ions formed in the micro plasma can be detected directly by Time of flight mass spectrometer, ICP-OES or the plume can be deposited on a glass substrate kept at a suitable distance from the target material, subsequently make the deposited film into a solution and analyze by Thermal Ionization Mass Spectrometer.

2A.1.2 Interaction of laser with opaque surface

When a high power laser beam is absorbed by an opaque surface, the effects involve heating with or without change of phase. The absorbed power of laser per unit area is denoted by the quantity laser flux density (W/cm^2).

In metals, light is absorbed by interaction with electrons. A quantum of optical energy is absorbed by an electron and is raised to a higher energy state in the conduction band. The excited electrons collide with lattice phonons and with other electrons and give up their energy, the same collision process governs the transfer of heat. The mean free path between collisions of electrons in a conductor is of the order of 10^{-13} m [5]. In time of the order of the duration of laser pulse, the electrons which absorb the photons will make many collisions, both among themselves and with lattice phonons. Thus the energy absorbed by an electron will be distributed and passed on to the lattice, i.e. the optical energy is instantaneously turned into heat at the point at which the light is absorbed. This assumption may break down for the case of picoseconds (ps) pulse. During the absorption of a ps duration pulse, there will not be time for the energy to be distributed among many particles by the collision processes.

2A.1.3 Pulsed Laser Deposition (PLD)

PLD is a physical vapor deposition process, carried out in a vacuum system, having characteristics common with molecular beam epitaxy and with sputter deposition. In PLD, a pulsed laser is focused on to a target of the material to be deposited. With sufficiently high laser energy density, each laser pulse vaporizes or ablates a small amount of the material creating a plasma plume. The ablated material is ejected from the sample in a highly forward directed plume, which provides material flux for film growth [6]. Several features make PLD particularly attractive for complex material film growth, such as stoichiometric transfer of material from the target, generation of energetic species, hyper thermal reaction between ablated ions and background gas in the plasma, and compatibility with background pressures ranging from ultra high vacuum to 1 Torr.

With PLD, the thickness distribution from a stationary plume is quite non-uniform due to the highly forward-directed nature of the plume. One of the most important and enabling characteristics in PLD is the ability to realize stoichiometric transfer of ablated material from multi cation targets. For low laser fluence and/or low absorption at the laser wavelength, the laser pulse would simply heat the target, with ejected flux due to thermal evaporation of target species. In this case, the evaporated flux from a multi component target would be determined by the vapor pressures of the constituents. As the laser fluence is increased, an ablation threshold is reached where laser energy absorption is higher than that needed for evaporation. The ablation threshold is dependent on the absorption co-efficient of material and wavelength of laser. At still higher fluence, absorption by the ablated species occurs resulting in the formation of plasma at the target surface. With appropriate choice of the

ablation wavelength, high energy densities are absorbed by a small volume of material, resulting in vaporization that is independent of the vapor pressures of constituent cations.

2A.1.4 Motivation for the present study

PLD is a powerful tool to fabricate thin films with stoichiometry reflecting that of target material, and mass spectrometry for elemental analysis. Combination of the two techniques can enable elemental analysis of solid samples for depth profiling, elemental mapping etc. This method catches special interest in nuclear industry as it can provide information on spatial distribution of elemental concentration of spent fuel pellet, with remote sample handling amenability. In conventional methods of analysis, the fuel is first dissolved in nitric acid and the solution is employed for elemental analysis, which provides an average burn-up value. The scope for remote handling and the fact that direct sampling from solid pellet using spatially coherent laser beam followed by isotopic analysis can provide data on spatial (radial and axial) distribution of burn-up, has motivated for the present study.

2A.1.5 Previous studies in literature

Several studies were carried out by many researchers for determination of U by PLD-ICP-MS and PLD-ICP-OES [7-10]. Wang Wei et al determined the isotopic composition of U from micro particles of U, by fixing the particles on adhesive tape followed by LA-ICP-MS; the measured relative uncertainties for $^{(235/238)}\text{U}$, $^{(234/238)}\text{U}$ and $^{(236/238)}\text{U}$ were reported less than 0.050%, 1.7% and 1.8% respectively [7]. Maria Betti et al characterized the micro particles stemming from different release scenarios of radioactivity (nuclear forensic studies) by ICP-MS and its hyphenation with other techniques for resolving isobaric interferences. The application of glow discharge and laser ablation in combination with secondary ion

mass spectrometry, accelerator mass spectrometry, resonance ionization mass spectrometry, and thermal ionization mass spectrometry were reported for the determination of the isotopic composition of U and Pu in micro particles [8]. Zamzov et al measured the concentration of uranium in soil for large number of sites in an area suspected to have uranium contamination, by in situ LA-ICP-AES, utilizing a field-deployable mobile analytical laboratory [9]. Samples containing UO₂ doped with lighter rare earths (La, Ce, Sm and Nd) were analyzed by Joseph et al using a laser mass spectrometry system comprising of an in-house developed Reflectron Time Of Flight Mass Spectrometer (RTOF-MS) [10]. Preliminary results indicated that this method has potential for direct determination of burn-up of irradiated nuclear fuel, but holds an uncertainty of about 10%.

2A.1.6 Scope of the present study

The performance of nuclear fuel in a reactor is monitored by burn-up analysis which is an estimate of the total number of heavy atoms undergone fission [11,12]. Out of various techniques available [13,14], the chemical methods [15,16] involving dissolution of the irradiated fuel sample, followed by laboratory analysis were demonstrated to provide the most accurate information on burn-up, and is prescribed by ASTM [12], which is explained in detail in Chapter 4. The ASTM procedure involves separation of fission products from the spent fuel followed by separation of burn-up monitor (usually Nd), both the steps are carried out by anion exchange method [16-18]. The separated burn-up monitor and the fuel elements are then quantified by Isotope Dilution Mass Spectrometry (IDMS) using TIMS [19,20]. The overall procedure yields best accuracy for determination of average burn-up, but unable to provide information on spatial profile of distribution of heavy elements (U and Pu) and fission products [21,22]. At high burn-up, the composition of nuclear fuel changes in a non-

homogeneous manner within its radius, due to various reasons like neutron capture by ^{238}U in the rim region, temperature gradient between the center and the rim of a fuel pellet, diffusion properties of constituent elements in the fuel matrix, difference in their vapor pressures etc. Hence the high burn-up fuel requires an experimental database to support the fuel-integrity, safety analysis, shielding design and multiplication factor of storage systems. Apart from the core design improvements, the radial and axial mapping of the burn-up is also essential for repositioning of sub-assemblies, especially if such a sub-assembly is positioned into the inner part of the core after a reloading [22].

A direct burn-up determination method of irradiated pellet can overrule the conventional method by virtue of shorter time of radiation exposure, feasibility of remote handling of sample and minimum release of radioactive waste [23,24]. Pulsed laser ablation is a well known technique to deposit thin films of complex oxides and other multi-component materials. The instruments involved in laser ablation are simple and amenable for sampling highly radioactive materials. Moreover, the amount of material in deposited films are in ng to μg level and hence the radiation exposure during post deposition analytical procedures is minimized. Laser Ablation (LA) inside Hot-Cell using an engineered laser beam with suitable beam conditioner can be used to take out a small amount of representative sample in vapor form from a very small area of the order of few tens of $(\text{microns})^2$ at the fuel pellet surface. Such vapor sample is introduced to an ICP-MS and subjected to mass analysis would be the best suited technique for burn-up profile measurement on irradiated fuel pellets [25]. However, if such a LA-ICP-MS facility is not available, a procedure involving pulsed laser deposition of spent fuel matrix followed by Isotope Dilution Mass Spectrometry (IDMS) using TIMS, can be adopted for burn-up profile measurements. Therefore, in the present

study, we use PLD-IDTIMS technique for the analysis of simulated inactive samples having heavy element (U) and fission products (Nd, La etc.). The effect of laser parameters like wavelength and pulse width on stoichiometry of ablation of the sample, thereby, on accuracy of measurements is also discussed.

2A.2 Experimental

2A.2.1 The laser systems

In the present study, two types of lasers are used, namely

1. Nd:YAG lasers of ns and ps pulse widths
2. Excimer ns laser

A brief account of these lasers are given below.

Neodymium:YAG lasers

The Nd ion when doped into a solid-state host crystal produces the strongest emission at a wavelength beyond $1\mu\text{m}$ [3]. The two host materials most commonly used for this are yttrium aluminum garnate (YAG) and glass. When doped in YAG ($\text{Y}_3\text{Al}_5\text{O}_{12}$), the Nd:YAG crystal produces laser output primarily at $1.064\mu\text{m}$. Nd also lases at $0.94\mu\text{m}$ and at $1.32\mu\text{m}$ from the same upper laser level, although these transitions have lower gain. The Nd:YAG laser incorporates a four level system and consequently has a much lower pumping threshold than that of ruby laser. The emission and gain line widths are 0.45 nm for YAG and the laser transition is homogeneously broadened by thermally activated lattice vibrations. The Nd:YAG crystal has good optical quality and high thermal conductivity, making it possible to provide pulsed laser output at repetition rates of up to 100 Hz . Doping concentrations for Nd:YAG crystals are typically of the order of 0.725% by weight, which corresponds to approximately 1.4×10^{26} atoms per cubic meter [4].

Nd-YAG ns laser

The laser provided by Continuum-NY (61-10) series, U. S. A was used for the studies of pulsed laser deposition with ns laser. The maximum pulse energy associated with the three wavelengths available are 225 mJ, 100 mJ and 35 mJ for 1064 nm, 532 nm and for 266 nm wavelengths, respectively. The laser heads are located on the laser bench and are utilized as either oscillator or amplifiers. Each laser head is a module incorporating a rod, flash lamp and coupling medium. All have linear flash lamps which are in a close coupled configuration surrounded by a magnesium oxide diffuser. The heads are designed to pump Nd³⁺ doped YAG, the doping levels vary from 0.9 to 1.4 %. The rod lengths for all the laser head is 115 mm measured along the optical axis. The diameter of the rods ranges from 6 mm to 7 mm. The laser heads are pumped by linear flash lamps. The discharge system of the flash lamps use a negative pulse (-1.8 kV max) with a duration of 200 μ s full width half maximum. The flash lamps are cooled by deionized water, and the gas filled is Xenon with a pressure of 1-3 atmospheres. The capacitor banks store the energy needed to run the flash lamps, also to convert the 24 volt trigger pulse from a power unit to a high voltage spike to initiate ionization in the flash lamps.

Nd-YAG ps laser

The laser model G-SUB-100, custom built by Geola Digital Uab, Lithuania was employed for pulsed laser deposition with ps laser. The maximum pulse energy associated with the three wavelengths available are 250 mJ, 125 mJ and 25 mJ for 1064 nm, 532 nm and 266 nm wavelengths, respectively. The pulse energy stability per 250 pulses is ≤ 3 %. The laser pulse duration is 100 ± 20 ps. The laser system comprises a laser head and power supply rack and a computer with laser control software.

Excimer laser

Excimer lasers are a group of pulsed lasers that incorporate electronic transitions within excited molecules. Such lasers are most often composed of combination of rare gas atom and a halogen atom. The excimer laser used in the present study is KrF laser of 248 nm wavelength, 450 mJ (maximum) pulse energy with a repetition rate of 200 Hz and with duration of 30 ns FWHM; supplied by Lambda Physik, U. S. A (model Compex 205). The laser operates with a total gas pressure of 2 atmospheres and with partial pressures of 10 torr F_2 , 30 torr Ar and an approximately 1400 torr He.

2A.2.2 Sample preparation

Pellets of UO_2 doped with rare earth (RE) fission products (La, Ce, Sm and Nd) were prepared by combustion synthesis method. Nuclear grade U_3O_8 was converted to UO_2 by heating at $600^\circ C$ for 4 hrs in a furnace of reducing atmosphere of Ar/ H_2 . All the rare earth oxides (CeO_2 , La_2O_3 , Sm_2O_3 and Nd_2O_3) were of spectroscopic grade (99.9% pure), from M/s Indian Rare Earths. Accurately weighed amounts of UO_2 and the rare earth oxides were dissolved independently in Quartz Distilled (Q D) HNO_3 (Ce_2O_3 was dissolved in presence of HF with heating under IR lamp for 5 hrs in PTFE beaker). The rare earths and uranium were weighed corresponding to their fission yields and the residual heavy element atoms in a spent fuel [26] after undergoing different levels of burn-ups, as per Table 2A.1. All the solutions were mixed together and stirred well to attain uniformity, and the mixture was dried on a hot plate, and re-dissolved in water. To this aqueous solution, 0.1M citric acid solution was added. The solution was then dried under IR lamp and the resulted powder was ground well and made pellets of about 5 mm diameter and 2-3 mm thickness, by applying a pressure of 5 tons. The pellets sintered at $1400^\circ C$ for 4 hrs were used as target for pulsed laser deposition.

Table 2A.1 Chemical composition of pellets prepared

Burn-up (atom %)	Weight of U and fission products (g/g of matrix)				
	U	La	Nd	Sm	Ce
5 (P1)	0.830	1.77×10^{-3}	4.46×10^{-3}	9.94×10^{-4}	4.42×10^{-3}
9 (P2)	0.788	3.18×10^{-3}	8.50×10^{-3}	1.99×10^{-3}	7.06×10^{-3}
17 (P3)	0.703	5.94×10^{-3}	17.2×10^{-3}	4.42×10^{-3}	12.1×10^{-3}
25 (P4)	0.619	8.62×10^{-5}	25.8×10^{-3}	7.21×10^{-3}	16.6×10^{-3}

2A.2.3 Instrumentation

PLD experiments were performed using (i) a flash lamp pumped Q-switched Nd-YAG laser of pulse width 8ns (ii) diode pumped Nd-YAG laser of pulse width 100ps and (iii) KrF Excimer Laser of pulse width 30ns. The Nd-YAG ps laser has a Q-switched diode pumped master oscillator with a pulse width of 3 ns. The laser beam is then pulse compressed by Stimulated Brillouin Scattering (SBS) technique in CCl_4 medium and further amplified by three successive flash lamp pumped single pass Nd-YAG amplifiers. While the ns laser has a transverse beam profile of TEM_{00} mode, both excimer and Nd-YAG ps lasers have a quasi-Gaussian, near top-hat spatial beam profile. All three lasers were operated at a repetition rate of 10 Hz. The second harmonic (532 nm) and fourth harmonic (266 nm) beams were generated from the fundamental (1064 nm) by frequency doubling and quadrupling using non-linear crystals like β -Barium Borate (in ps laser) and Potassium Dihydrogen Phosphate (in ns laser) [27]. Films of UO_2 doped with rare earth oxides were deposited using three wavelengths- 1064, 532 and 266 nm from both ns and ps Nd-YAG

lasers and 248 nm from KrF excimer laser. The laser parameters used in the present study are tabulated in Table 2A.2.

2A.2.4 Procedure

Oxide pellets containing U and RE corresponding to burn-up of 5, 9, 17 and 25 atom % were used as targets for PLD. Thin films were deposited using laser pulse energy for wavelengths 1064 nm (IR), 532 nm (visible) and 266 nm (UV) were about 60, 30 and 15 mJ, respectively [28], focused on an area of diameter ~2 mm, with a pulse width of 8 ns (thermal ablation). A quartz lens with a focal length of 50 cm was used for focusing the laser beam and the target was positioned after the focus, the substrate-target distance was maintained at ~1.5 cm. The focal area was kept such that power density is $< 1 \times 10^8 \text{ W/cm}^2$ [28] to minimize the particulate ejection and change in isotopic composition of the plume [29].

Since the purpose of PLD is to collect sub-microgram amount of sample for further analysis, deposition on a glass substrate was carried out at rough vacuum ($\sim 5 \times 10^{-3}$ torr). Ablation of each pellet with different laser wavelengths were made under identical experimental conditions in terms of background pressure, target-substrate distance etc. (the experimental set up is schematically given in Fig. 2A.1). The deposited material was dissolved in about 100 μl of Q D nitric acid. The solution was then evaporated to dryness under IR lamp and the residue was then re-dissolved in $\sim 200 \mu\text{l}$ of 0.75 M nitric acid. This solution was divided into two portions- one for isotopic composition (IC) measurement of U and Nd, and the other for isotope dilution measurements for concentration determination of the elements. The photograph of PLD chamber and the sample loader are shown in Fig. 2A.2 and 2A.3, respectively.

Table 2A.2 Parameters of lasers used in the present study

Nd-YAG laser				
Wavelength (nm)	Pulse width (ns)	Pulse energy (mJ)	Pulse width (ps)	Pulse energy (mJ)
1064	8	60	100	450
532	8	18	100	180
266	8	8	100	80
KrF excimer laser				
248	30	300		

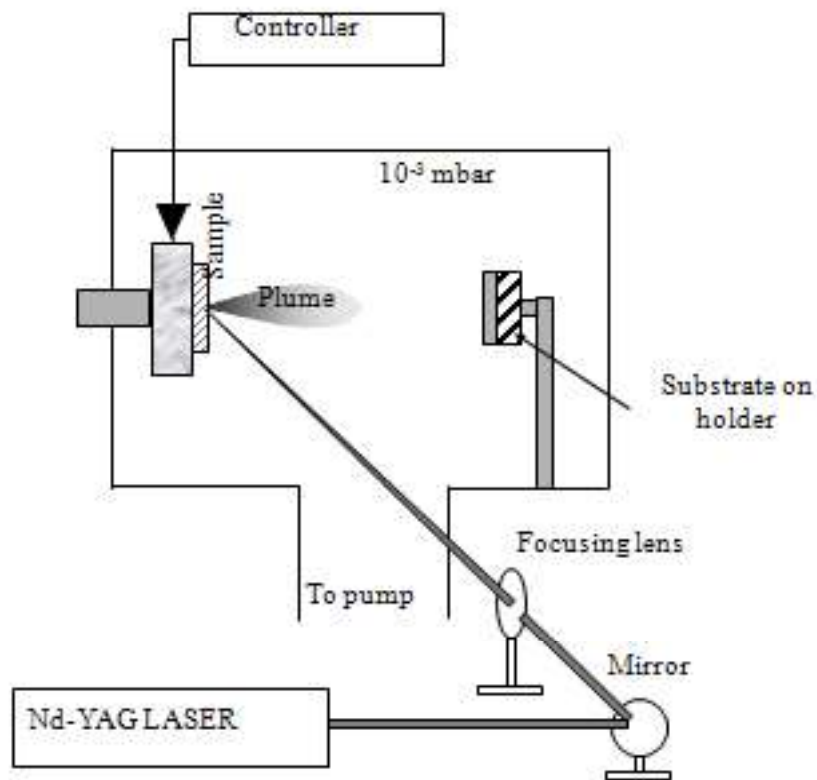


Fig. 2A.1 Schematic of PLD facility

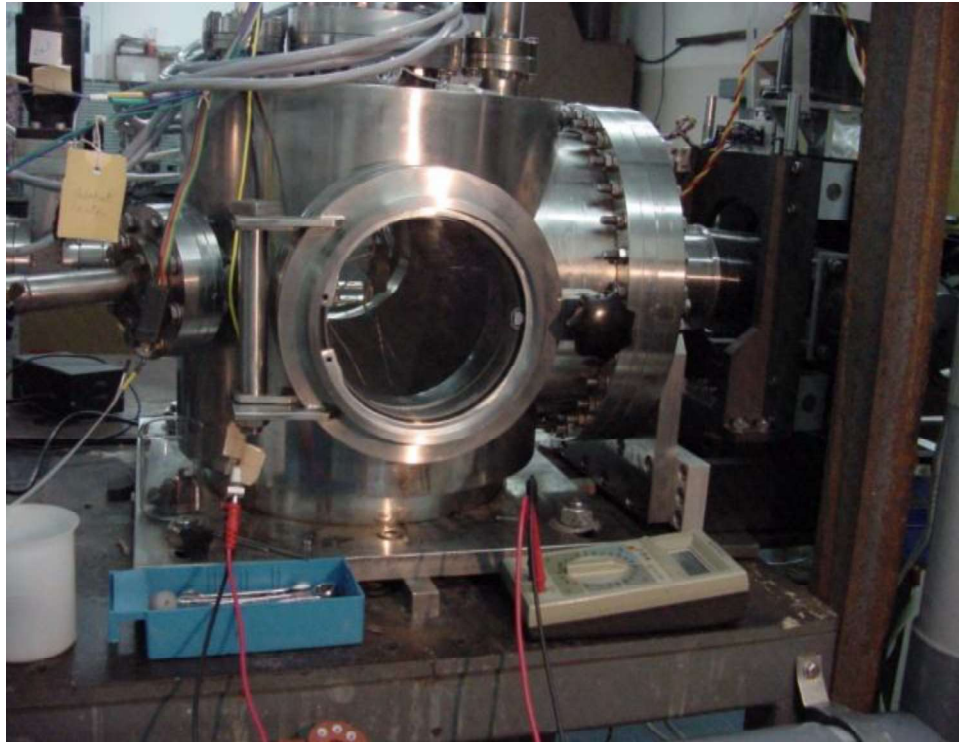


Fig. 2A.2 Photograph of the PLD chamber

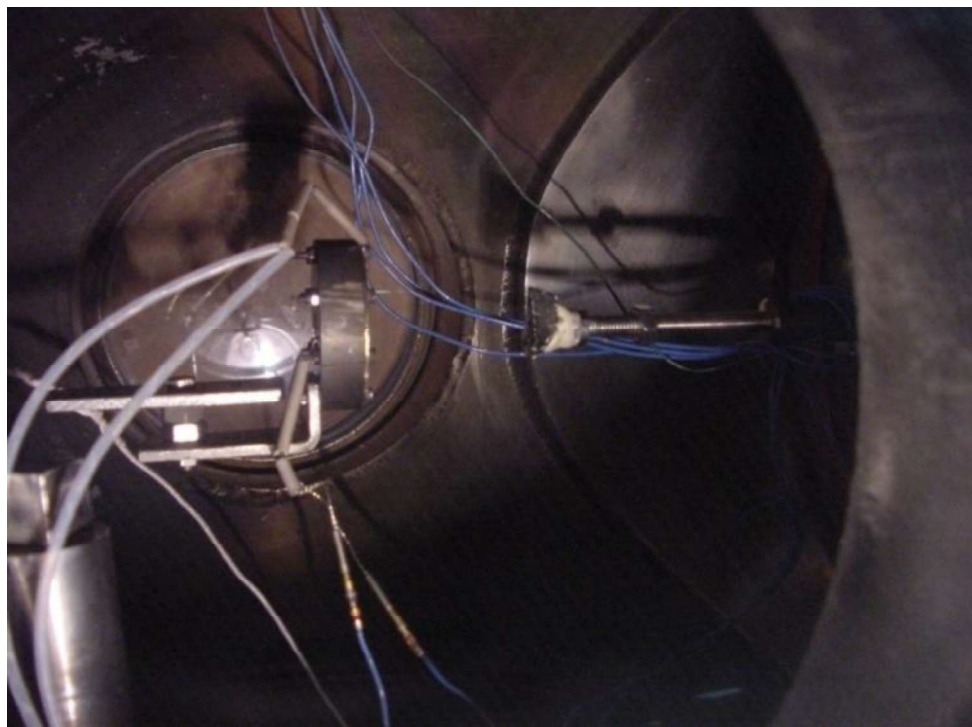


Fig. 2A.3 Photograph of the sample loader inside PLD chamber

Isotope Dilution- Thermal Ionization Mass Spectrometry (ID-TIMS)

The mass analysis was carried out by a multi-collector thermal ionization mass spectrometer-model Isoprobe-T supplied by IsotopX (U. K). This magnetic sector analyzer is equipped with 9 faraday cup detectors for simultaneous measurement of isotopes and operates at an acceleration voltage of 6 kV at vacuum of 10^{-8} - 10^{-9} torr. Accurately weighed amount of the sample solution was mixed with known quantities of suitable spikes (enriched with ^{150}Nd for Nd, and ^{233}U for U) of standard concentrations and isotopic compositions. The double spiked mixture was evaporated to dryness and residue was made into a homogeneous solution in minimum volume ($\sim 10 \mu\text{l}$) of 0.75 M HNO_3 and loaded on to a tantalum filament. The filament was then heated outside the mass spectrometer (by ohmic heating) to evaporate the solvent and to fix the residue on the filament. The filament is then taken into ion source of TIMS for isotopic analysis. The ratios of appropriate isotopic pairs of RE element and U under investigation ($^{150}\text{Nd}/^{142}\text{Nd}$ and $^{233}\text{U}/^{238}\text{U}$) were measured by thermal ionization mass spectrometric procedure to deduce the concentrations of U and Nd in the sample. During mass spectrometric analysis, the isotopic ratios of U were measured first, followed by Nd, though the ionization energy of Nd is slightly lesser than that of U, because of two reasons:

- i) ion intensities of Nd were found to exist for a longer time owing to its lower vapor pressure
- ii) ion intensities of Ce and Sm isotopes (interfering with Nd) were found to get reduced to negligible levels by their exposure to high temperature during uranium measurements.

Nevertheless, isobaric interference was corrected by measuring the corrected ion intensities of each isotope by applying correction factor based on the natural abundance of isotopes of

Ce and Sm [30,31]. Assigning of isotopes in the available 9 faraday cup collectors was made as shown in Table 2A.3. Intensity of ^{142}Nd was corrected based on the intensity of ^{140}Ce and intensities of ^{144}Nd , ^{148}Nd and ^{150}Nd were corrected based on the intensity of ^{147}Sm . However, this correction factor is not applicable for spent fuel analysis as the isotopic composition of reactor produced Sm and Nd (fission products) are different from their natural abundances. In this scenario, an attempt was made to minimize the interference by extending the time of exposure of sample to high temperature, so that Sm and Ce will get evaporated to the maximum extent, which is explained in detail in chapter 3.

Table 2A.3 Assigning of masses in the 9 faraday cup collectors

Collector	L3	L2	AX	H1	H2	H3	H4	H5	H6
Isotope	140	142	143	144	145	146	147	148	150
Elements	Ce	Ce, Nd	Nd	Nd,Sm	Nd	Nd	Sm	Nd,Sm	Nd,Sm

From the IDMS data, concentrations of U and Nd in the sample were arrived by the following equation [19]

$$C^S = C^T * \frac{W^T}{W^S} * \left[\frac{R^T(i/j) - R^M(i/j)}{R^M(i/j) - R^S(i/j)} * \frac{1}{R^T(i/j)} * \frac{\langle A \rangle^S}{\langle A \rangle^T} * \frac{(A.F)_i^T}{(A.F)_j^S} \right]$$

where, C^S - conc. of sample; W^T -weight of tracer (g); C^T - conc. of tracer (spike); W^S – weight of sample (g); $i = 233$ and $j = 238$ for U; $i = 150$ and $j = 142$ for Nd; $\langle A \rangle^S$, $\langle A \rangle^T$ - average atomic weights of sample and tracer; $(A.F)_i^S$, $(A.F)_j^T$ - atom fractions of sample and tracer; $R^S_{(i/j)}$, $R^T_{(i/j)}$, $R^M_{(i/j)}$ - isotopic ratios of sample, tracer and mixture, respectively.

Reproducibility of the U/Nd concentration ratio obtained has been checked by repeating IDMS analysis on the scrapped samples from PLD target.

In PLD experiments using ns laser with fluences much above the ablation threshold, though the vaporization may be highly incongruent at any given instant, the cumulative component fluxes approach congruency over the entire pulse width [32,33]. However, the ablated plume and hence the deposited material on the substrate contains a large amount of particulates due to various processes [34,35]. Use of pico second pulse width tends to produce particulates of relatively smaller size [36]. Apart from the size, the faster surface recession in shorter laser pulse was expected to produce reduced fractionation effect in ablation and hence nearer stoichiometric deposition. Ultra short laser pulse is known to produce particulates, of sub-micron size range compared to the much larger size range when pulses of several nano second are employed for ablation [37]. So, a fresh set of pellets maintaining the composition similar to the previous batch was prepared and the above experiments were repeated with laser of 100 ps pulse width, maintaining other parameters the same. PLD was carried out with all the three available wavelengths of Nd-YAG laser (1064, 532 and 266 nm) and 248 nm of excimer laser, on pellets of four different compositions, followed by IDMS with the plume deposited. To expose the fresh surface to laser, pellet surface was polished after each set of irradiation [38].

2A.3 Results and discussion

2A.3.1 Optimization of laser parameters for nearest stoichiometric ablation

The compositions of U and Nd present in four pellets irradiated with 532 nm, 1064 nm and 248 nm of 8 ns pulse width laser beam are given in Table 2A.4. The amount of sample deposited as films were reasonably sufficient for IDMS measurements. However, the quantity of material deposited using 266 nm laser beam was found to be not sufficient for IDMS procedure, even after deposition for 45 minutes, due to very small laser pulse energy

from the laser available with us. The U/Nd ratio shows large deviation on the negative side from the actual value (up to 33%) using 1064 nm laser, whereas this deviation gets reduced (up to 13%) by using 532 nm, as depicted in Fig. 2A.4. The improved results for shorter wavelength is because of better stoichiometric ablation in PLD films [39,40] with reduced exfoliated particulates [34] and lesser elemental fractionation in analytical applications as reported for shorter wavelength lasers [36,41].

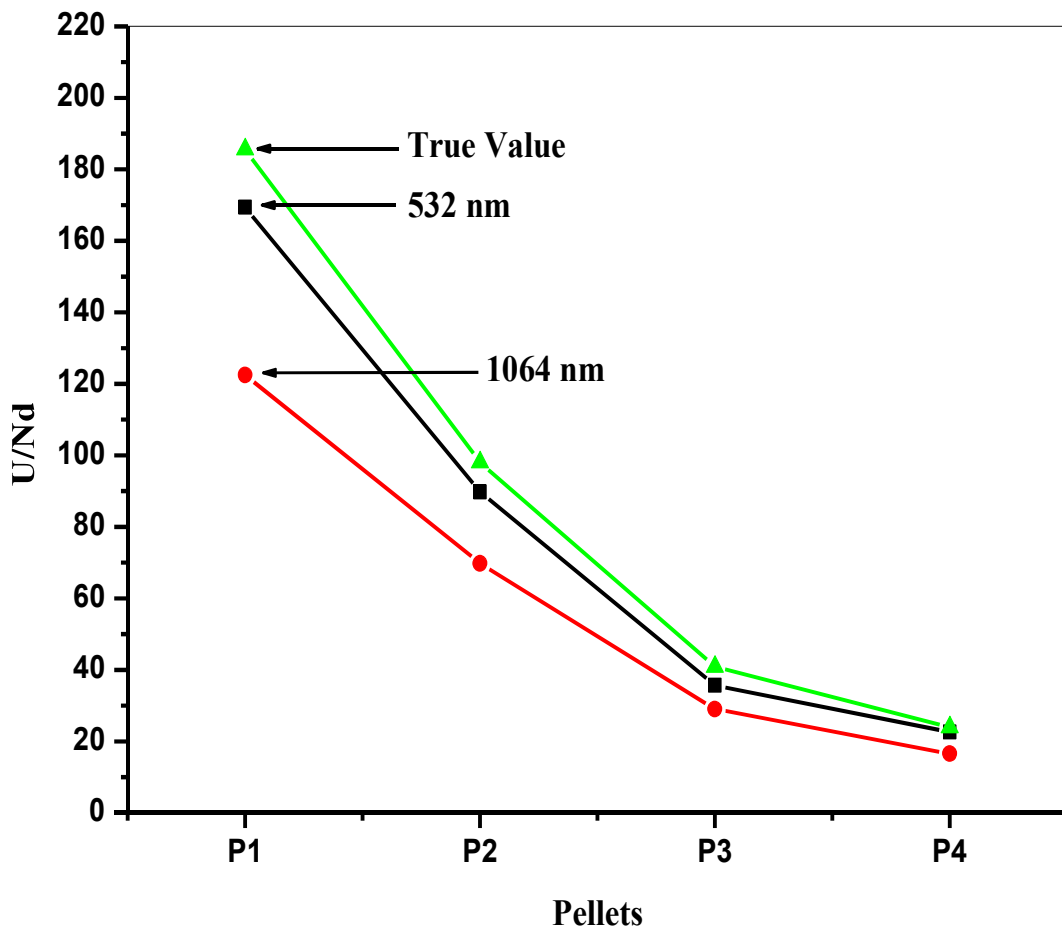


Fig. 2A.4 U/Nd concentration ratios obtained from TIMS for pellets with varying elemental composition of U & Nd. The concentrations of elements present in the films deposited by PLD at 532 & 1064 nm (ns pulsed laser) are compared against the sample taken from target.

Table 2A.4 U/Nd ratios observed with 532 & 1064 nm Nd-YAG laser (8 ns pulse width) and 248 nm of excimer laser of 30 ns pulse width.

Pellet no.	532 nm wavelength				Liquid target (pellet 4)	1064 nm wavelength				Excimer (248 nm)			
	1	2	3	4		1	2	3	4	1	2	3	4
(U/Nd) _{true}	185.55	98.02	40.97	24.02	24.02	185.55	98.02	40.97	24.02	184.12	93.24	41.46	22.43
(U/Nd) _{obs.}	169.4 ± 0.35	89.68 ± 0.23	35.65 ± 0.29	22.56 ± 0.43	23.92 ± 0.15	122.5 ± 0.51	69.8 ± 0.64	29.3 ± 0.77	16.6 ± 0.48	202.7 ± 0.47	102.4 ± 0.62	49.17 ± 0.50	26.14 ± 0.76
Error (%)	10.15	8.5	13.0	6.1	0.42	33.0	28.7	28.3	30.8	10.1	9.8	18.6	16

The relation between the amount of material ablated and the wavelength of laser used for ablation/ ionization is given by the following equation [42]

$$M=110[F_a^{1/3}](10^{14})\lambda^{-4/3}$$

where, M is the loss of sample mass due to laser ablation (kg/cm^2), F_a is the absorbed laser intensity on the surface (W/cm^2) and λ is the laser wavelength (nm). According to above equation, 266 nm laser is more efficient in terms of quantity of material ablated than 532 nm and 1064 nm laser. However, in our laser system, 266 nm was found to produce least amount of plume due to the loss of pulse energy during harmonic generations.

As can be seen from Table 2A.4, better stoichiometry could be observed for samples of pellet 4 in liquid form, as laser target. Since the sample gets dried during evacuation of the PLD chamber, the shape of sample container and substrate- target alignment were adjusted over several trials to avoid the sample splash during laser ablation. Laser ablation for few minutes without splashing could be achieved by holding a semisolid form of sample in a deep narrow container with optimal alignment with the substrate. However, the use of such solution-dried samples as laser ablation target defeats the present objective as it fails to provide the spatial burn-up profile of irradiated nuclear fuel pellets.

The measured concentration ratios of U and Nd after ablation with lasers of shorter pulse width (100 ps) for all three wavelengths 266, 532 and 1064 nm are summarized in Table 2A.5. PLD with all the three wavelengths provided sufficient quantity of sample required for IDMS analysis. Measurements with 266 nm stands on top in terms of reproducing the stoichiometry, followed by 532 and 1064 nm respectively, as observed in nanosecond laser ablation experiments. The highest deviations in concentration of U/Nd values from original composition are 6.5%, 15.9% and 26.7% with 266, 532 and 1064 nm, respectively.

Figures 2A.4 and 2A.5 together show the deviation of U/Nd composition with different wavelengths for all the three type of lasers used for ablation. Fig. 2A.4 shows an increased value of Nd in the ns PLD films compared to the un-ablated target. Such deviation is more pronounced for the films ablated using 1064 nm wavelength. Laser ablation using ns laser pulses, especially with longer wavelengths, is known to produce such elemental fractionation effects due to deeper penetration of laser inside material surface [43,32] and is governed by the vaporization behavior of the constituent elements . The oxide of Nd has higher vapor pressure compared to the oxide of U, hence higher Nd content is expected in the deposited film [44]. Such an effect is also observed for the films ablated using 532 nm wavelength, though at a lesser scale because of shallow penetration depth causing a better ablation [43].

Fig. 2A.5 shows a positive deviation in the U/Nd ratio (enhanced Nd fractionation in the PLD film) compared to the un-ablated target. It can also be seen that the samples ablated by both excimer (248 nm, 30 ns) and ps Nd-YAG lasers display a positive deviation in U/Nd ratio for all the pellets. Sub-nanosecond laser pulses are known to produce efficient ablation with less elemental fractionation due to reduced thermal and increased non-thermal ablation process [45,46]. The lesser deviation in composition with ps- PLD film compared to that of ns-PLD film is shown in Table 2A.5 and Fig. 2A.5. Apart from laser induced material removal, plasma shielding effect of the laser-plume with the tailing part of the laser pulse also play a major role in the film deposition process. The non-linear interaction of the plume front formed in the picosecond time regime with the trailing part of the laser pulse will be significantly lower in ps laser pulses compared to the ns pulses.

Table 2A.5 U/Nd ratios observed with 266, 532 & 1064 nm laser with 100 ps pulse width

Pellet no.	266 nm wavelength				532 nm wavelength				1064 nm wavelength			
	1	2	3	4	1	2	3	4	1	2	3	4
(U/Nd>true	184.12	93.24	41.46	22.43	184.12	93.24	41.46	22.43	184.12	93.24	41.46	22.43
(U/Nd)obs.	187.3 ±0.13	96.1 ±0.20	44.2 ±0.19	23.8 ±0.32	201.3 ±0.39	106.9 ±0.28	48.1 ±0.48	25.3 ±0.69	213.1 ±0.63	108.8 ±0.39	52.5 ±0.27	28.4 ±0.48
Rel. Error (%)	1.7	3.1	6.5	5.8	9.3	14.7	15.9	12.8	15.7	16.8	26.7	24.8

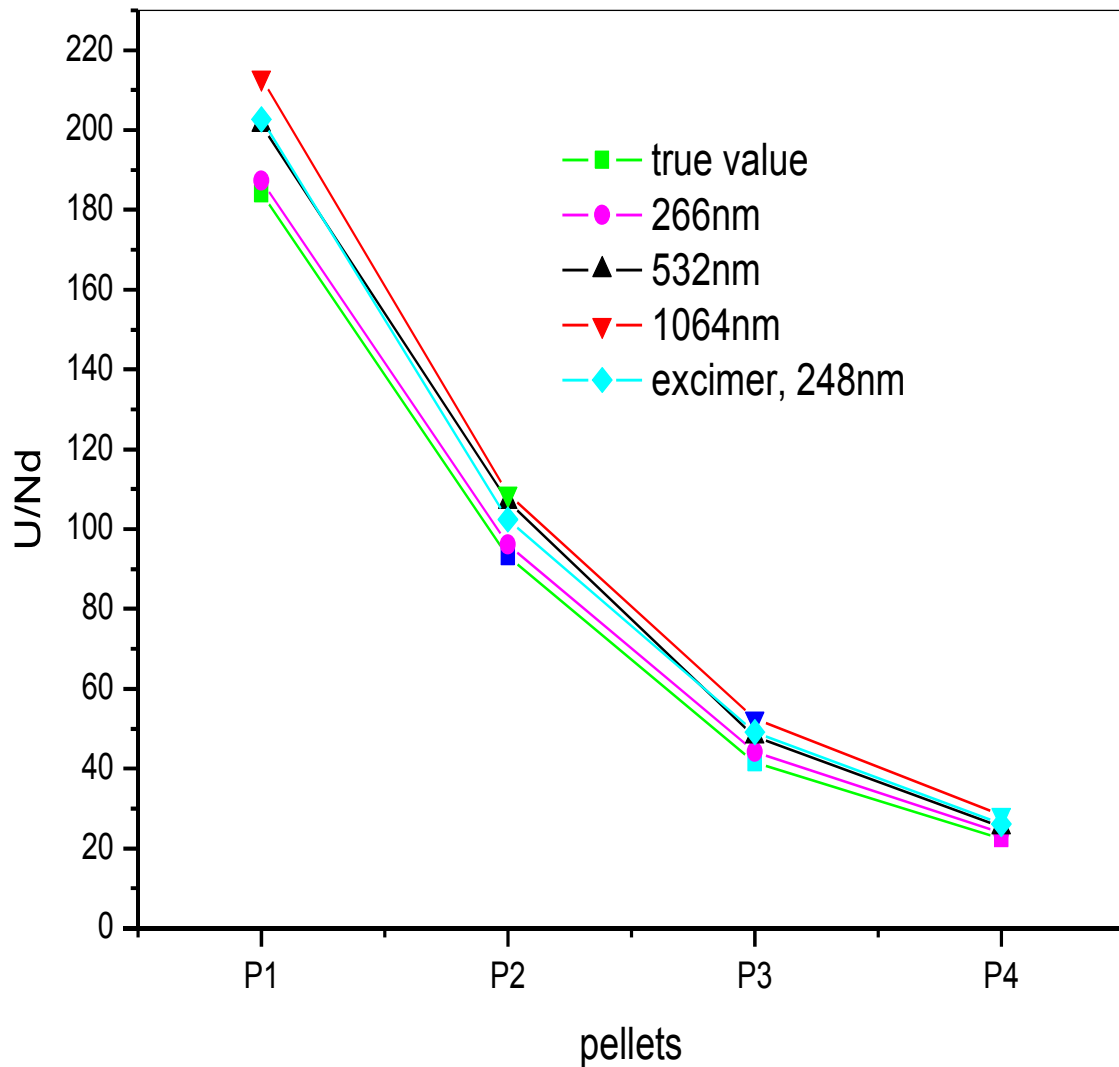


Fig. 2A.5 U/Nd concentration ratios obtained from TIMS for pellets with varying elemental composition of U & Nd. The elemental concentrations in the samples from PLD films deposited at 266, 532 & 1064 nm (ps pulsed laser) and 248 nm excimer laser show, unlike ns laser, a positive deviation from the corresponding values of the target pellet.

Among the composition within the laser plume, the Nd species will have larger interaction due to the Nd-luminescence of the Nd-YAG laser and hence Nd bearing species will get more energized kinetically and sputter the Nd atoms out of the PLD film causing a net Nd deficiency in the film. Hence, a positive deviation in the U/Nd values are expected in the ps laser ablated plume. The plasma shield effect is more for longer laser wavelength and hence the U/Nd offset from actual values is observed more with 1064 nm compared to 266 nm pulses [35].

Even though the KrF excimer laser used here has much longer laser pulse duration (30 ns) compared to the ns Nd-YAG laser (8 ns), the highly efficient ablation at UV wavelength is responsible for the lesser elemental fractionation effects compared to ns laser with 1064 nm. Table 2A.5 reveals that PLD films using ps laser, though produces a deviation in U/Nd values, it is less compared to that with ns laser pulses. Moreover, the 266 nm ps pulses produce films that have least deviation in elemental compositions compared to that of the actual values. The above results implies that the UV lasers with ps pulse width is better suitable for analytical applications such as PLD compared to longer wavelengths and ns pulse width.

2A.3.2 Study on morphological changes on irradiation

The morphological changes of the sample on laser irradiation were studied by Scanning Electron Microscope (SEM). The SEM images of surface before and after irradiation with 532 nm laser are given below. Fig. 2A.6 show the fresh, un-irradiated surface of the pellet. Irradiation has modified the surface morphology of the pellet by forming craters due to penetration of the beam into the sample, as shown in Fig. 2A.7, which leads to surface boiling and exfoliation. This necessitates removal of the outer layers of the pellet by polishing, before the surface get exposed to irradiation with laser of another wavelength.

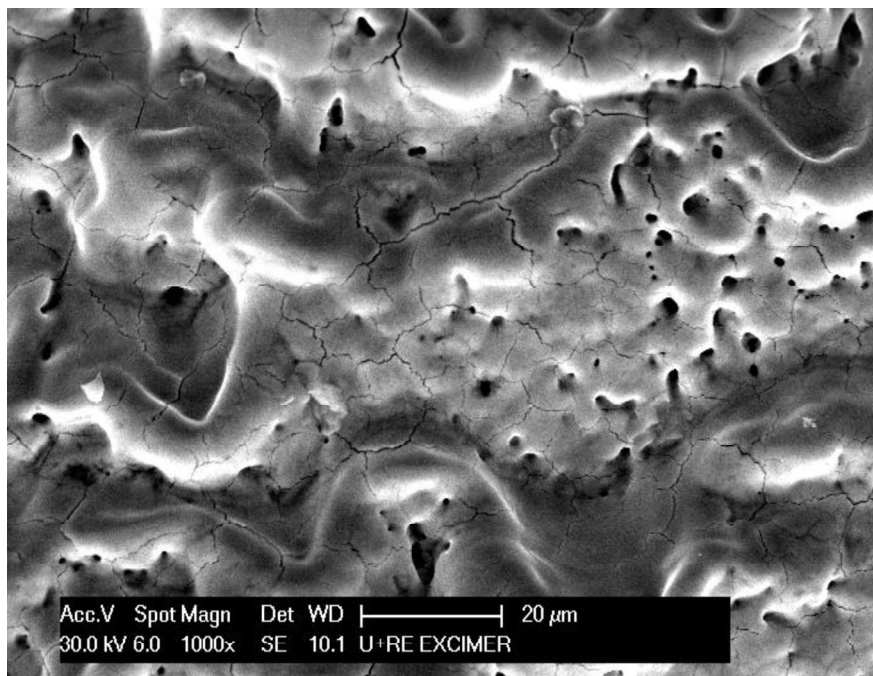


Fig. 2A.6 SEM images of pellet surfaces before laser irradiation

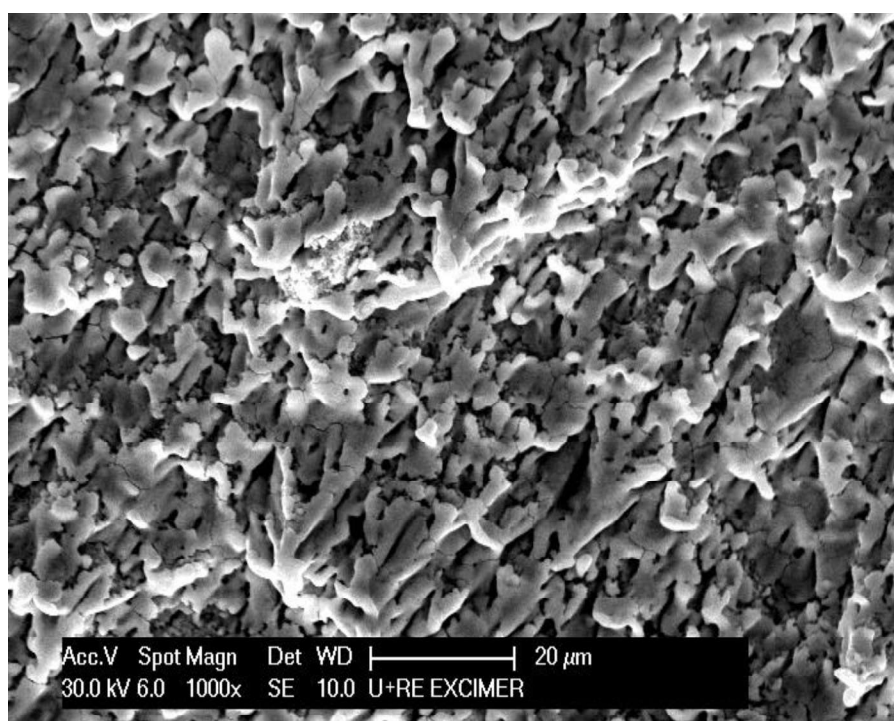


Fig. 2A.7 SEM images of pellet surface after ablation with laser beam of 532 nm wavelength

2.A.4 Conclusions

Laser ablation- IDMS method was employed to measure the U/Nd ratios in simulated samples of U and Nd (a potential burn-up monitor in the spent nuclear fuel). Studies on optimization of laser parameters to evaluate U/Nd ratio, with lasers of different wavelengths and pulse widths revealed that measurement with 266 nm, ps laser offers best agreement (minimum error 1.7 % and maximum error 6.8 %) with the actual value. The method is attractive as the laser ablation sampling can be done at rough vacuum condition; hence amenable for easy and remote sample handling. The procedure is characterized with very little production of radioactive liquid waste and generation of spatial profile of nuclear fuel pin.

The greatest difficulty faced in the method was isobaric interference of Ce and Sm isotopes in the determination of Nd by TIMS, which was overruled by interference correction method as the elements were of natural origin. Since the elements of reactor origin have got an entirely different isotopic composition compared to that of natural origin, the online correction method becomes invalid for the analysis of spent nuclear fuel samples. The effort to solve this difficulty had led to evaporation of interfering elements preferentially from the analyte matrix, making use of their higher vapor pressures, as explained in Chapter-3.

The spatial profiling of U and Nd could not be carried out in the present study since the simulated pellets are homogeneous in nature. In order to measure the spatial profile of U/Nd ratio, either out of pile simulated fuel pellets or the fuel pellets irradiated in a nuclear reactor need to be examined, which demands setting up of new experimental facilities.

Laser-mass spectrometric studies on measurement of isotope ratios of Li and rare earths – A comparative study using ps and ns pulsed lasers

2B.1 Introduction

Enrichment studies of ^6Li isotopes (80-90%) finds application in nuclear science, as it is used as breeder blanket in fusion technology. The accuracy required for such enrichment studies can be limited to within few percentage levels. Time Of Flight - Mass Spectrometers (TOF-MS), which is home built and less expensive, coupled to a pulsed laser as a desorption/ionization source is a convenient method for quick measurements in such elemental analysis, especially for radioactive and chemically hazardous samples. Apart from isotopic ratio measurement of the same element, there is also a requirement for isotope ratio analysis of selected isotopes between two different elements like Nd, Sm etc. (fission products), which are involved in the estimation of burn-up [10]. The present study describes the measurement of isotopic ratio of Li, Sm and Nd samples of natural abundance by the use of a home-made Reflectron TOF-MS coupled to laser ionization, generally referred to as Laser Ionization Mass Spectrometry (LIMS) [47]. Laser desorption/ ionization is a non-linear process and the ion yield varies for different elements for the same laser parameters and optimization of laser parameters becomes necessary. The present study reports measurements of isotopic ratio of Li, and of Lighter Rare Earths (LRE) such as Sm and Nd by laser ablation using Nd-YAG lasers having picosecond (ps) and nanosecond (ns) pulse widths at different wavelengths of 1064 nm (IR), 532 nm (visible) and 266 nm (UV), followed by mass spectrometric analysis.

2B. 2 Experimental

The LIMS experimental facility contains an indigenously made Reflectron RTOF-MS having a resolution of about 1000 for gas samples, comparable to any commercial

instrument. Schematic of the experimental facility and its photograph are shown in Fig. 2B.1 and Fig. 2B.2, respectively. In the photograph, the LIMS facility is indicated with part number 3 and 4, namely the sample chamber and the time of flight drift tube, respectively. This LIMS is part of the whole laser mass spectrometer facility. Part no. 1 and 2 forms the laser induced vaporization mass spectrometer [47], where part no. 1 is the PLD chamber which is discussed in detail in section 2A.2.4.

Two types of lasers were used in this study- one with a pulse width of 8 ns and the other is a pico second (100 ps) laser, details of them are already explained in Part A of this chapter. A thin film made by evaporating few micro liters of sample solution on a stainless steel plate was positioned by an aluminum sample holder. The vacuum chamber containing the sample and the mass spectrometer was maintained at a base pressure below 1×10^{-6} torr by a turbo molecular pump (1000 L/s).

Detector

A secondary electron multiplier (SEM) having a sensitive area of $\sim 10 \times 25$ mm, rise time of ~ 2.0 ns, and recovery time of < 5 ns is used as the detector. The typical gain of the detector is $\sim 1 \times 10^6$ at 2.8 kV, the optimized operating voltage in these measurements. The bare SEM detector was mounted on a 6" OD CF flange with the required electrical connectors for high voltage and signal leads. Signal from the SEM is pre-amplified and then recorded using a fast digital storage oscilloscope (DSO), interfaced to a PC through a GPIB (general purpose interface bus) for data collection. The DSO is triggered externally by a fast photodiode illuminated by a diffusive reflection of the laser beam. Hence, each laser pulse yields one sweep. Each spectrum is obtained for 1000 sweeps, and summation average mode (available in the DSO) is used to improve the signal to noise ratio [11,48].

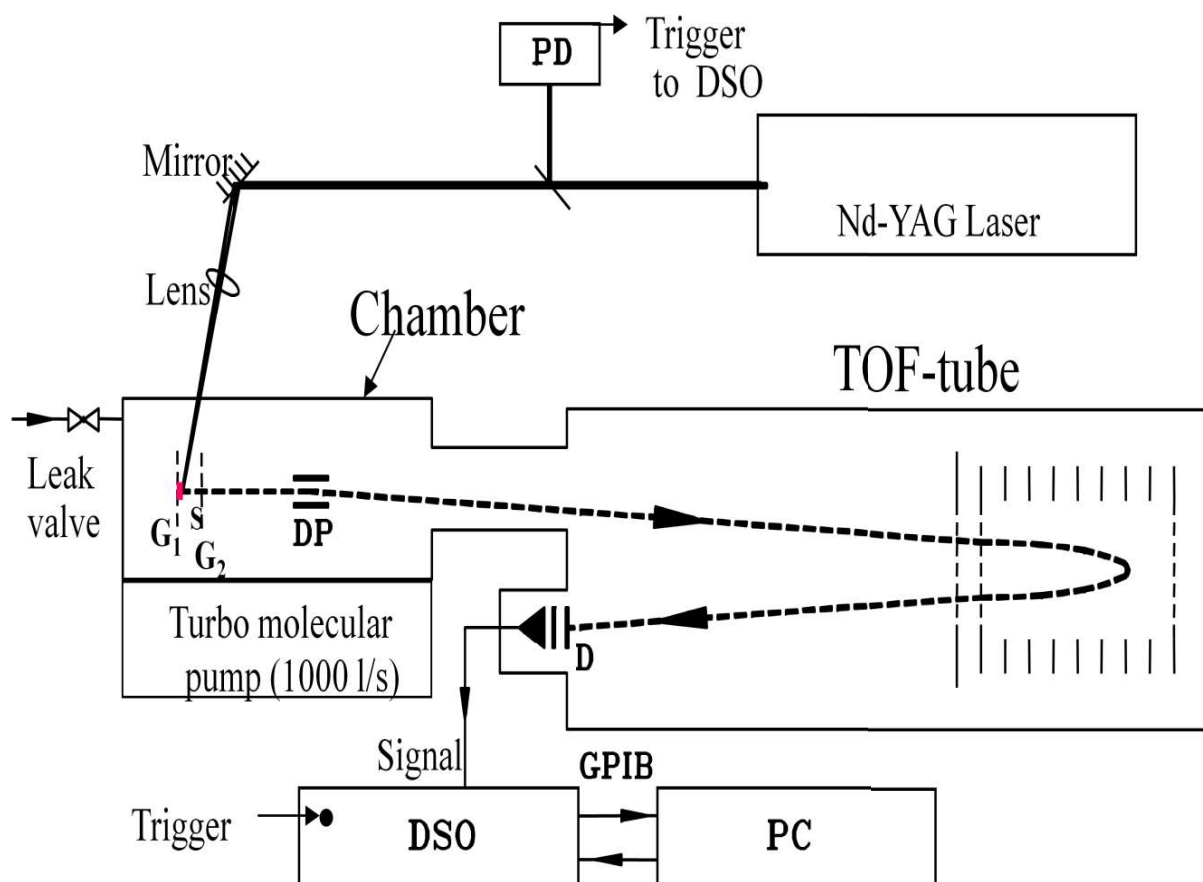


Fig. 2B.1 Schematic of LIMS facility



Fig. 2B.2 Photograph of the in- house developed Laser ionization- Time of flight mass spectrometer facility (1- PLD chamber, 2- QMS chamber, 3- sample chamber, 4- TOF drift tube)



Fig. 2B.3 Photograph of the Al sample holder with a dow tail cutting groove for the sample plate

Sample

A solution of Li_2CO_3 in water was used for isotope measurements of Li. For the lighter rare earths (La, Ce, Sm and Nd), a mixture of their nitrate solutions was used. Few μl of the sample solution was loaded on a stainless steel (SS) sample plate, dried and introduced into the mass spectrometer, using a sample holder. The sample holder consists of a groove, to fix the metal plate for laser irradiation (as shown in Fig. 2B.3). All samples used in this study were of natural isotopic abundance.

2B.3 Results and discussion

2B.3.1 Measurements on Li

Typical mass spectra obtained for Li isotopes using ps and ns lasers are compared in Fig. 2B.4, which shows the result obtained using 266 nm beam for desorption and ionization. Value of the isotope ratio (${}^7\text{Li}/{}^6\text{Li}$) obtained for the two spectra corresponding to ps and ns lasers are: 11.81 ± 0.48 and 10.67 ± 0.95 , respectively, as against the natural abundance of 12.18 [49].

As the figure indicates, the peaks obtained are very broad for the ns pulsed laser beam, with the full width half maxima (FWHM, Δt) of about $0.07 \mu\text{s}$ for the ${}^7\text{Li}$ peak, whereas, for the ps pulsed laser, the FWHM is about $0.03 \mu\text{s}$. The corresponding resolutions ($t/2\Delta t$) are 77 and 180 for the use of the ns and ps pulsed lasers, respectively. Since the absorption of trailing part of the laser beam by the vapor, for the ps pulse is less (i.e. energy carried by ps laser pulse is spent more on the desorption and ionization process than interacting with the species that are coming out of the sample), the ps laser pulse produces a colder beam giving sharp mass peaks compared to ns laser pulses [50,51].

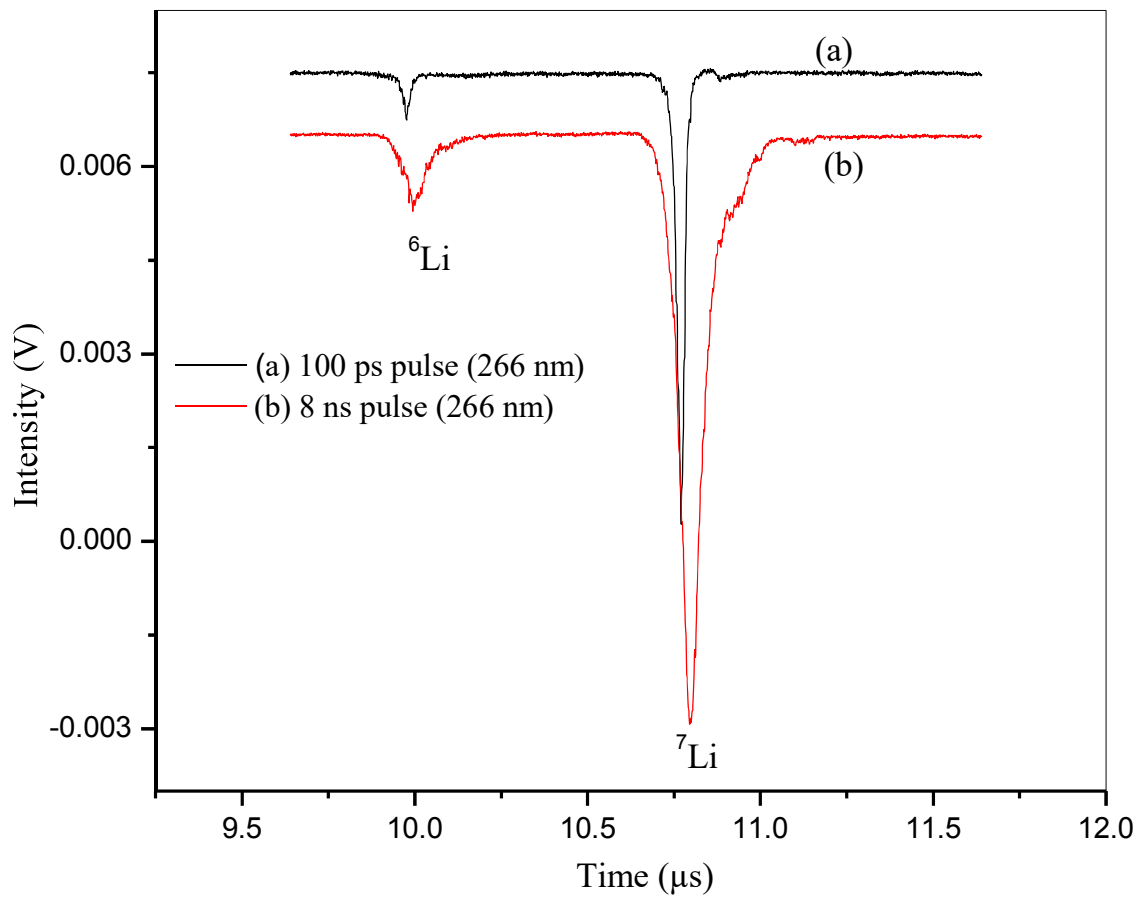


Fig. 2B.4 Typical mass spectra of isotopes of Li obtained using (a) 8 ns and (b) 100 ps Nd:YAG lasers of 266 nm wavelength.

The wavelength dependent mass spectrum obtained for the ps laser is shown in Fig. 2B.5. As can be seen, the FWHM obtained for the three wavelengths, namely 1064, 532 and 266 nm are: 0.01, 0.01 and 0.03 μ s, respectively. This trend is expected, as the pulse energy stability is poorer at 266 nm compared to the other two wavelengths. Also, at 1064 nm, the peak profile shows a hump, indicating that there are different mechanisms [50] by which ions are formed (may be thermally and photolytically), as the SS sample plate has larger optical absorbance at 1064 nm and hence this wavelength is better absorbed compared to the other two wavelengths. A summary of FWHM of ${}^7\text{Li}^+$ signal and the % abundance obtained for both the isotopes of Li as a function of laser parameters are shown in Table 2B. 1.

For ns beam, the FWHM is higher than that of the ps laser. The spectrum obtained using the ns beam is expected to be broader as the ions come off the surface for a longer duration and further, the ions formed from the leading part of the ns laser pulse can interact with the trailing part of the ns laser beam, leading to a larger kinetic energy spread, resulting in wider detector signal.

As can be seen from Table 2B.1, the average isotopic abundance obtained for ${}^6\text{Li}$ and ${}^7\text{Li}$ using ps laser at 266 nm are 7.82 ± 0.28 % and 92.18 % and this value has lower scatter and closer to the true value as measured using TIMS, which is in good agreement with the natural abundance, namely, 7.59 % of ${}^6\text{Li}$ and 92.41 % of ${}^7\text{Li}$ [49]. This table also indicates that the error spread (1σ) is less (0.3 %) with 266 nm compared to longer wavelengths (0.7 %). Even though the energy stability is expected to be poorer at 266 nm compared to longer wavelengths, the difference in ion production mechanisms could be the reason for the larger standard deviation with longer wavelengths.

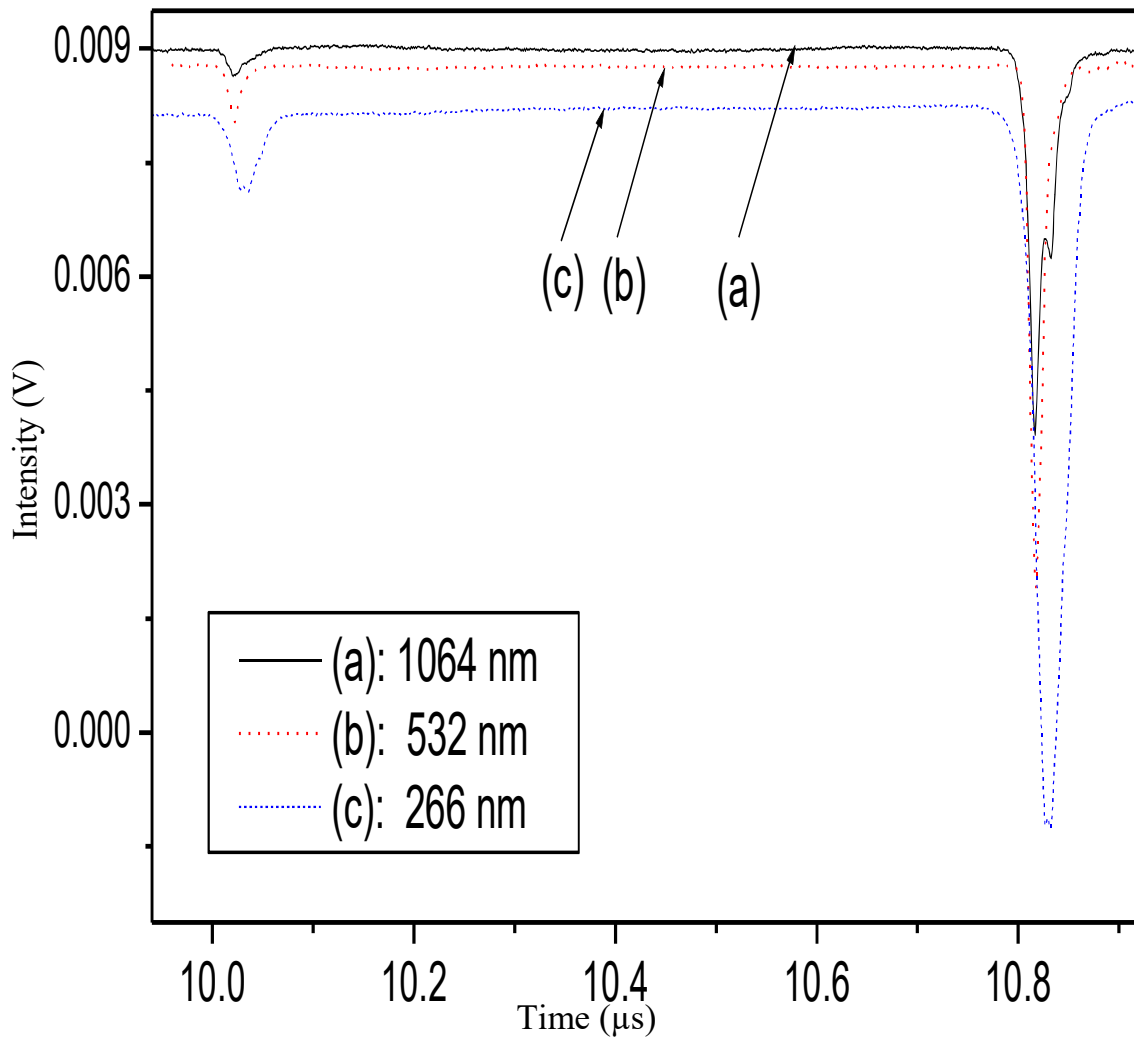


Fig. 2B.5 Mass spectra of isotopes of Li obtained using ps Nd-YAG at different wavelengths; (a) 1064 nm; (b) 532 nm; (c) 266 nm. All other experimental conditions remain the same.

Table 2B.1 Full width half maxima (FWHM) and % of isotopes of Li as measured with different laser parameters.

Parameter	ps laser beam			ns laser beam		
	1064	532	266	1064	532	266
FWHM for ${}^7\text{Li}^+$ peak (μs)	0.01	0.01	0.03	0.04	0.04	0.07
% of ${}^7\text{Li}$	92.03 ± 0.68	91.82 ± 0.59	92.18 ± 0.26	92.20 ± 0.66	92.10 ± 0.69	91.5 ± 0.64
% of ${}^6\text{Li}$	7.97 ± 0.67	8.18 ± 0.60	7.82 ± 0.28	7.80 ± 0.67	7.9 ± 0.70	8.5 ± 0.65

A typical result of % isotopic abundance for both the isotopes of Li, using the ns and ps pulsed lasers operated at 266 nm are shown in Fig. 2B.6.

When the signal intensity is considered in terms of peak height, the result obtained was found to have more scatter and more error. For instance, using ps laser (266 nm), the % abundance obtained for ${}^7\text{Li}^+$, based on peak intensity is $90.31 \pm 1.14\%$, whereas the same data obtained based on peak area is $92.18 \pm 0.26\%$.

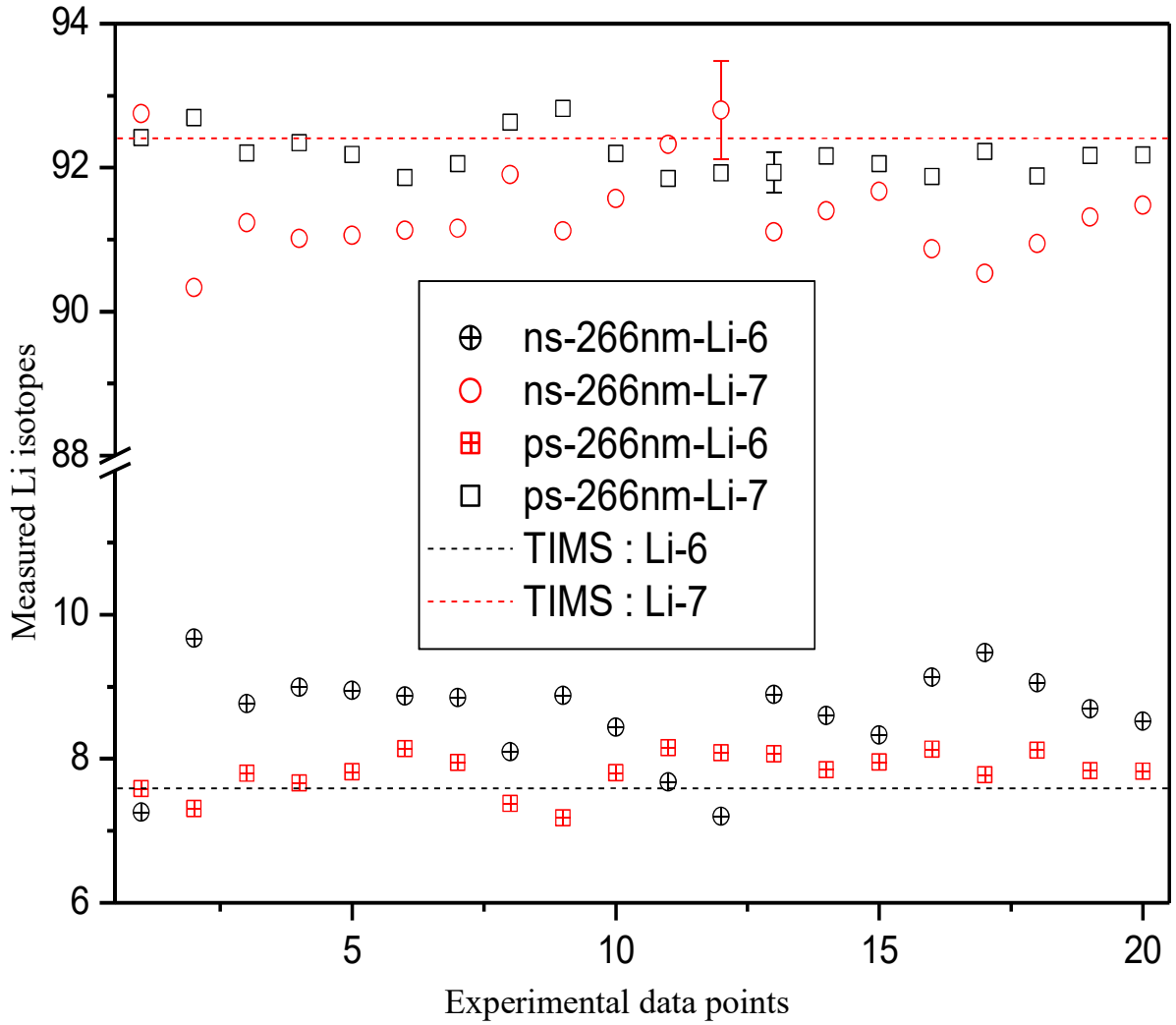


Fig. 2B.6 Measured isotopic abundance of Li present in natural Li_2CO_3 , using ns and ps lasers at 266 nm and compared with TIMS data.

2B.3.2 Measurement on light rare earths

Unlike the isotopic abundance measurements on Li, pure samples of light rare earths (LRE) are not considered, rather a mixture of LRE is studied. This is done because study of a mixture has a bearing on the determination of burn-up of a nuclear fuel [10]. In order to get good resolution, it is necessary to use very low laser energy density for laser desorption/ ionization, as reported by our laboratory [10,52]. Under such conditions, for LRE, the predominant species are their respective monoxide ions (REO^+) rather than atomic ions (RE^+), as the ionization potential of the former is lesser than that of the latter [53]. Typical mass spectra obtained for the LRE using three different wavelengths, namely 1064, 532 and 266 nm using the ns and ps pulse laser is shown in Fig. 2B.7 (a) and (b).

As can be seen from these figures, a nearly base line separation is obtained for all the three wavelengths. For the most intense peak of the above mass spectrum, namely LaO^+ , the FWHM values obtained are: 0.05, 0.04 and 0.05 μs , respectively, for three wavelengths of 1064, 532 and 266 nm using ns laser. The values obtained using the ps laser is about 0.03 μs for all the three wavelengths. This shows that at higher mass, the FWHM is less sensitive to the wavelength used. The spectrum obtained at 532 nm has poorer signal-to-noise ratio compare to the spectra obtained at 1064 and 266 nm, even though all these spectra are sum averaged for the same 1000 sweeps. This low signal-to-noise at 532 nm could be due to the high reflection of the 532 nm beam from the SS sample plate surface and hence reducing the laser energy coupled for desorption/ ionization causing less ion yield. Accordingly, the signal strength for 532 nm is less and hence displays poor signal to noise ratio compared to the other two wavelengths. While 1064 nm is readily absorbed by SS sample plate and causing more thermal vaporization of the sample, the 266 nm beam is readily absorbed by the sample layer itself.

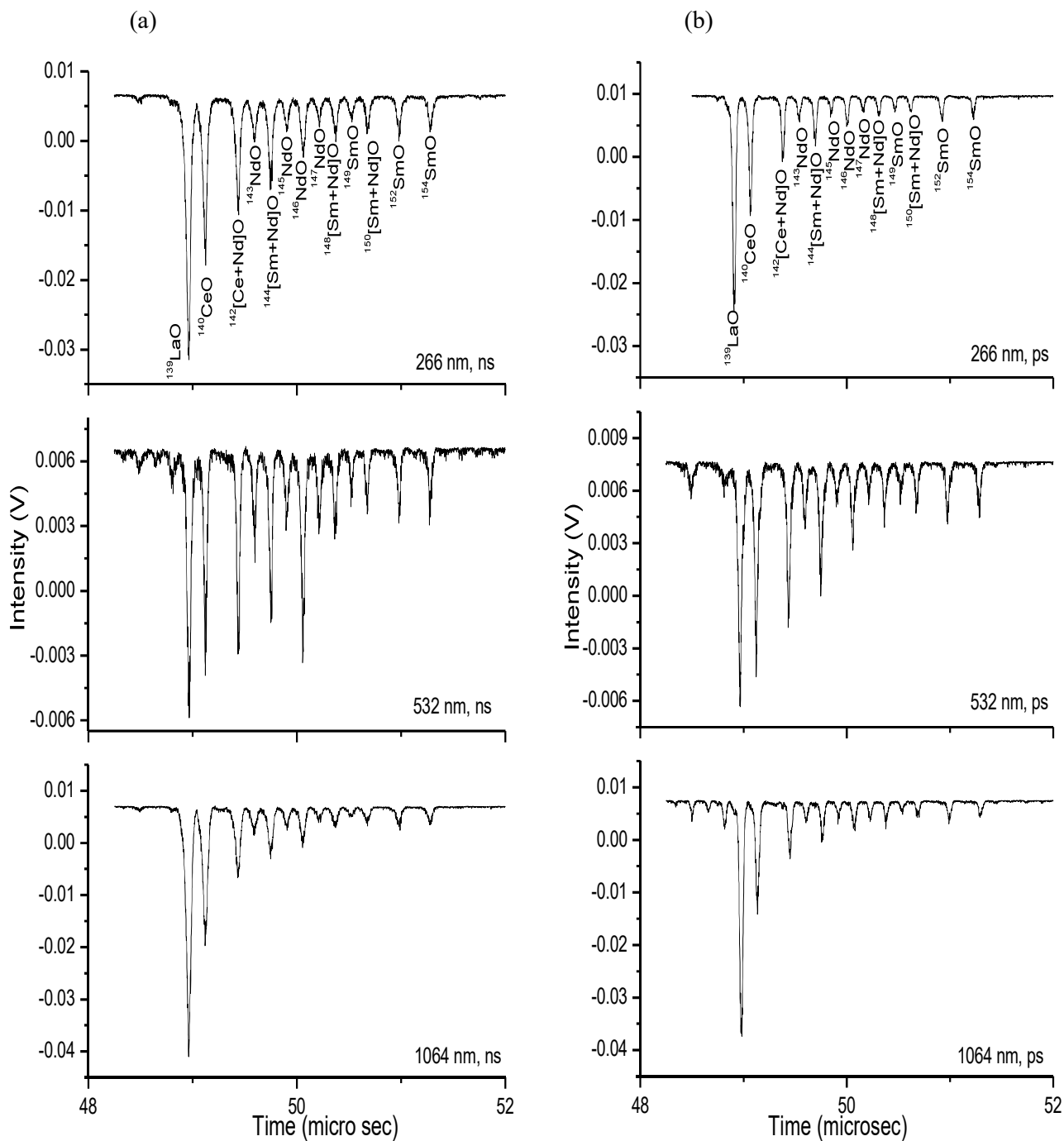


Fig. 2B.7 The mass spectra of La, Ce, Nd and Sm obtained from their nitrate solution dried on SS substrate, using three different laser wavelengths, namely 266 nm (UV), 532 nm (visible); and 1064 nm (IR) (a) using 8 ns pulse width; (b) using 100 ps pulse width.

Mass spectra obtained for the rare earth oxides (REO^+) using the ps pulsed laser is shown in Fig. 2B.7 (b) which shows a similar pattern as that with ns laser. The intensities for CeO^+ and SmO^+ observed for 532 nm are larger than those observed for 1064 and 266 nm, as obvious from Fig. 2B.7 (a) and (b). Even though the exact reason is not known, there could be near resonance ionization at 532 nm. However, no such data is reported in the literature. The spectrum obtained using 266 nm is better in terms of mass resolution, and the signal values are comparable to those obtained using 1064 nm laser. The isotopic ratios obtained for $^{152}\text{SmO}^+ / ^{154}\text{SmO}^+$ and $^{143}\text{NdO}^+ / ^{146}\text{NdO}^+$ at different wavelengths and pulse widths are compared in Figs 2B.8 and 2B.9, respectively.

As can be seen from figure 2B.8, the standard deviation is least corresponding to 266 nm, ps pulse, and the intensity ratios obtained corresponding to isotope ratios are very close to that given by natural abundance [49]. For instance, the $^{152}\text{SmO}^+ / ^{154}\text{SmO}^+$ ratio obtained is: 1.183 ± 0.06 for 266 nm, ps laser beam; whereas the natural abundance is 1.176, resulting in abundance measurements uncertainty within $\pm 1\%$. (i.e., the % abundance obtained for ^{152}Sm is $26.8 \pm 0.6\%$, against the natural abundance of 26.7%).

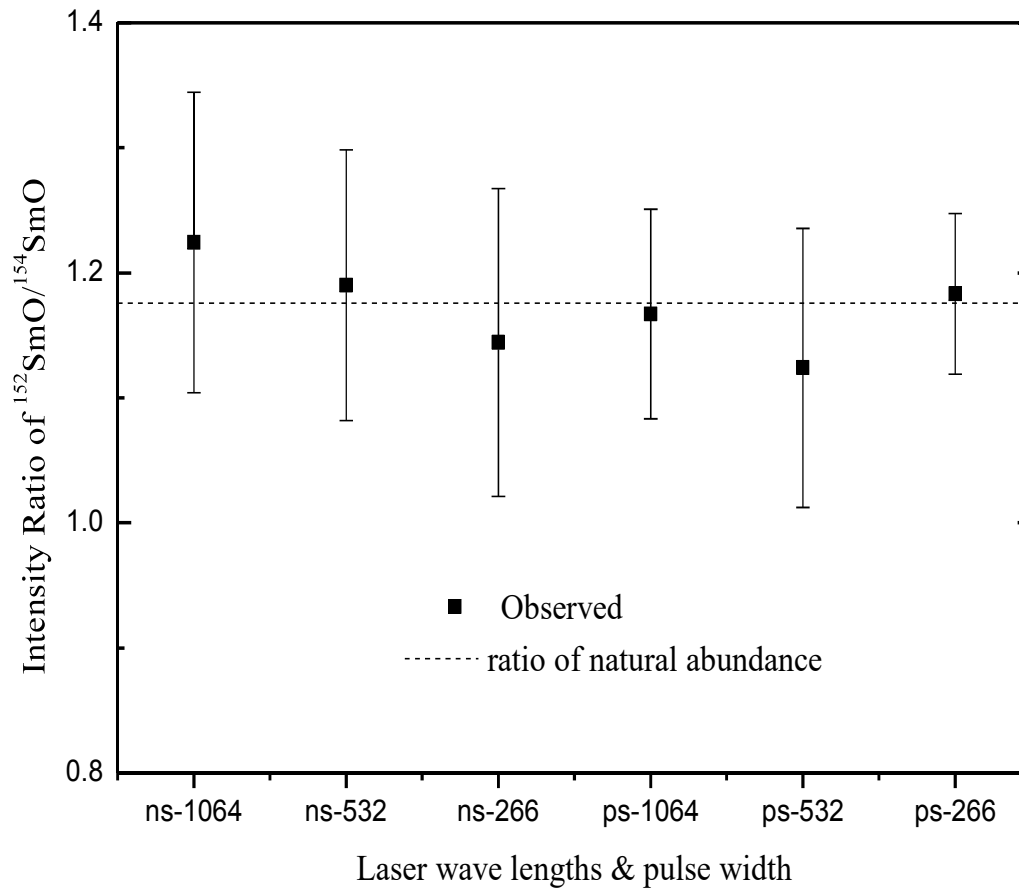


Fig. 2B.8 Variation of intensity ratio of $^{152}\text{SmO}^+ / ^{154}\text{SmO}^+$ as a function of wavelength for both ps and ns lasers.

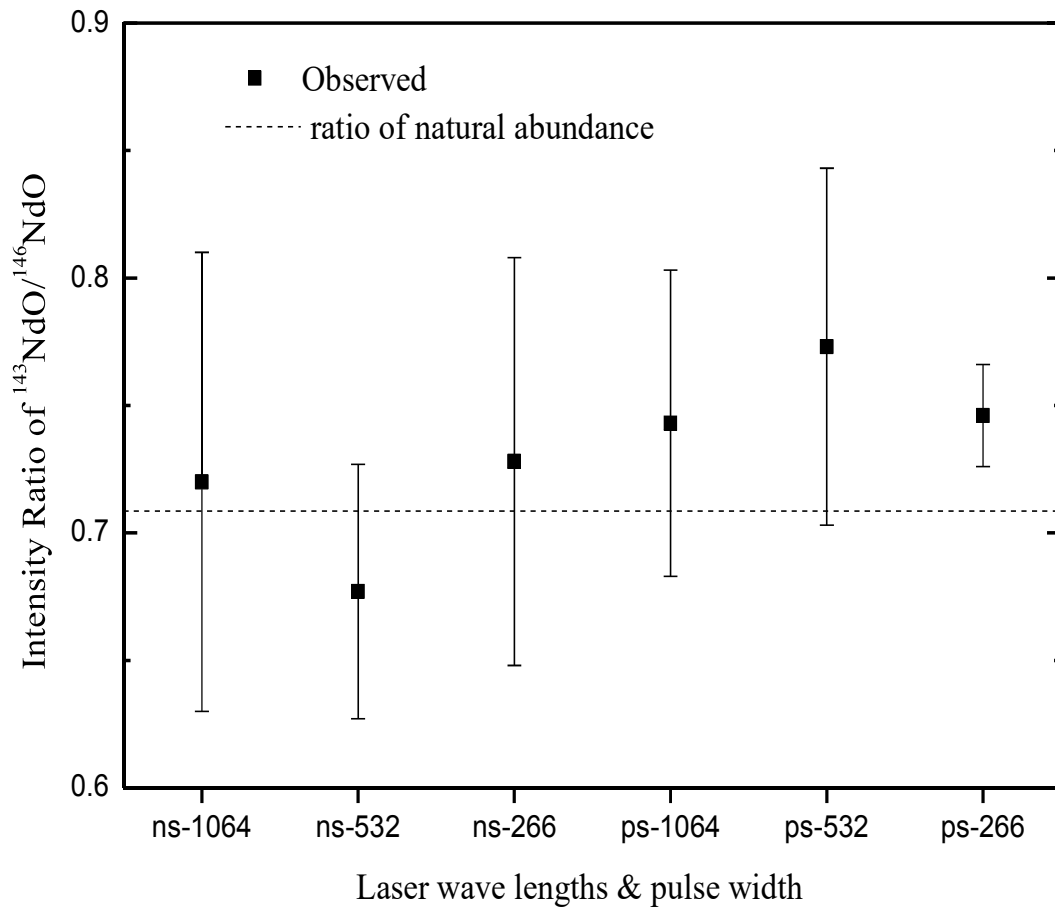


Fig. 2B.9 Variation of intensity ratio of $^{152}\text{NdO}^+ / ^{154}\text{NdO}^+$ as a function of wavelength for both ps and ns lasers.

But in the case of $^{143}\text{NdO}^+ / ^{146}\text{NdO}^+$, as shown in Fig 2B.9, though the scatter is low for ps-266 nm compared to results obtained for all other laser parameters, the accuracy is poor (0.746 ± 0.02 against the natural abundance of 0.708, leading to about 3% error in the % abundance). The inaccuracy with Nd ratio could be due to the possible contribution to $^{143}\text{NdO}^+$ from relatively more intense adjacent mass peaks. In the case of Sm, the two isotopes considered are well separated (due to the 2 amu difference). These results indicate that the 266 nm ps pulse seems to provide less standard deviation and better resolved mass spectrum. This can be expected in terms of laser pulse width, i.e., with ns pulse the ions have more time to interact with the laser beam, leading to a larger spread in their kinetic energy, compared to a ps pulse. Similarly, in terms of wavelength, for 266 nm the absorption coefficient of the sample is large, leading to very small absorption depth, and therefore most of the ions originate from the top surface layer. From the practical point of view, with regard to precise laser beam alignment under restricted human access environment (for radioactive samples with lead shielding), 532 nm (green) beam is more convenient than the 1064 nm and 266 nm beams. Even though laser beam alignment using 266 nm is not an issue in this work because the samples are non-radioactive, tracing the beam during handling of radioactive samples (for example, in the nuclear burn-up measurements) will be difficult. Hence we recommend not to filter away the 532 nm residual green beam completely from the 266 nm UV beam generated by the harmonic generator of the laser, so that a trace intensity of 532 nm can guide the laser alignment without difficulty when radioactive samples are studied.

2B.4 Conclusions

Li isotope ratio measurements were carried out using an in-house developed LIMS, with ps and ns pulsed laser beams. The ps laser produced sharper spectrum and better precision compared to that of ns laser. Furthermore, the FWHM of 266 nm beam

was found more than the other two wavelengths of both the pulse widths. However, the average isotope abundance of ${}^6\text{Li}$ and ${}^7\text{Li}$ measured with 266 nm, ps laser was found closer to the true value.

Similarly, for LREs analysis, the peaks were found to be sharper (FWHM 0.03 μs) with ps laser of all the three wavelengths, compared to that with ns pulses (FWHM \sim 0.05 μs). The spectrum obtained with 532 nm was found to have a poor signal to noise ratio compared to the other two wavelengths, irrespective of their pulse widths. Among the available combinations, the 266 nm, ps laser produced the spectrum with best mass resolution and lowest standard deviation.

This study revealed the applicability of LIMS to measure the isotopic ratios to within \pm 1% accuracy.

References

1. Marvin J Weber, Hand book of Lasers, 2001, CRC press, USA.
2. <https://www.rp-photonics.com/lasers.html>
3. Principles of Lasers, Orazio Svelto, 1976, Plenum press, USA.
4. M. Sargent, M. O. Scully, W. E. Lamb, Laser Physics, 1974, Addison-Wesley Publishing Company, USA.
5. William T Silfvast, Laser Fundamentals, 1998, Cambridge University Press, Florida, USA.
6. Robert Eason, Pulsed Laser Deposition of Thin Films, 2007, John Wiley & Sons, Inc., New Jersey, USA.
7. W. Wei, L. Z. Ming, X. Jiang, Z. L. Hua, Determination of uranium isotope ratios in uranium particles by Laser Ablation- Multiple Collector Inductively Coupled Plasma Mass Spectrometry, Chinese J. Anal. Chem., 2015, 43, 703-708.

8. M. Betti, L. Aldave, G. Tamborini, Mass spectrometric determination of transuranium elements, *Applied Spectroscopy Reviews* 2006, 41, 491-514.
9. D. S. Zamzow, D. P. Baidwin, S. J. Weeks, S. J. Bajlc, A. P. D'Silva, In situ determination of uranium in soil by laser ablation-inductively coupled plasma atomic emission spectrometry, *Environ. Sci. Technol.*, 1994, 28, 352-358.
10. M. Joseph, P. Manoravi, N. Sivakumar, R. Balasubramanian, Laser mass spectrometric studies on rare earth doped UO₂, *Int. J. Mass Spect.*, 2006, 253, 98–103.
11. M. Joseph, N. Sivakumar, Development of a laser induced vaporization mass spectrometric facility, *Instrumentation Sci. and Tech.*, 1998, 26, 81-94.
12. Standard test method for atom percent fission in uranium plutonium fuel (neodymium-148 method), Designation 321-96, *Annual of ASTM Standards*, 1996, 12.02.
13. W.N. Bishop, High-Resolution Inductively Coupled Plasma Atomic Emission Spectrometry for the determination of burn-up in spent nuclear fuel, Nuclear Regulatory Commission, Washington DC., 1997, Vol.1, Report NUREG/CP004, p 469-475.
14. B. B. Bevard, J. C. Wagner, C. V. Parks, M. Aissa, Review of information for spent nuclear fuel burn-up confirmation”, Nuclear Regulatory Commission, Washington DC., 2009, Report NUREG/CR-6998.
15. P. Deregge, R. Boden, Determination of neodymium isotopes as burn-up indicator of highly irradiated (U,Pu)O₂ LMFBR fuel, *J. Radioanal. Chem.*, 1977, 35, 173-184.
16. N. Sivaraman, S. Subramaniam, T. G. Srinivasan, P. R. Vasudeva Rao, Burn-up measurements on nuclear reactor fuels using high performance liquid chromatography, *J. Radioanal. Chem.*, 2002, 253, 35-40.

17. K. Joe, Y. S. Jeon, J. S. Kim, S. H. Han, J. G. Kim, W. H. Kim, Separation of burn-up monitors in spent nuclear fuel samples by Liquid Chromatography, *Bull. Korean Chem. Soc.*, 2005, 26, 569-574.
18. J. S. Kim, Y. S. Jeon, S. D. Park, B. C. Song, S. H. Han, J. G. Kim, Dissolution and burn-up determination of irradiated U-Zr alloy nuclear fuel by chemical methods, *Nuclear Eng. and Tech.*, 2006, 38, 301-310.
19. K. G. Heumann, *Isotope Dilution Mass Spectrometry in Inorganic Mass Spectrometry*, Edited by F. Adams, R. Gijbels and R. Van Grieken, 1988, John Wiley & Sons, New York. p.301-376.
20. I. L. Koumenis, M. L. Vestal, A. L. Yergey, S. Abrams, S. N. Deming, T. W. Hutchens, Quantitation of metal isotope ratios by laser desorption time-of-flight mass spectrometry, *Anal. Chem.*, 1995, 67, 4557.
21. R. Prokopowicz, K. Pytel, Z. Marcinkowska, M. Tarchalski, Measuring the axial profile of spent nuclear fuel burn-up by spontaneous fission neutrons. <https://www.euronuclear.org/meetings/rrfm2017/pdf/RRFM2017-A0055.pdf>
22. Y. K. Ha, J. Kim, Y. S. Jeon, S. H. Han, H. S. Seo, K. Song, Local burn-up characteristics of PWR spent nuclear fuels discharged from Yeonggwang-2 Nuclear power plant, *Nuclear Engg. and Tech.*, 2009, 42, 79-88.
23. Management of small quantities of radioactive waste, IAEA-Tecdoc-1041 (1998).
24. Handling and processing of radioactive waste from nuclear applications, IAEA-Tecdoc-402 (2001).
25. Y. K. Ha, S. H. Han, H. G. Kim, W. H. Kim, K. Y. Jee, Radial Distribution of U, Pu in a 55,000 MWd/Mt U spent nuclear fuel, *Nucl. Eng. and Technol.*, 2008, 40, 311-318.

26. K. Kanno, T. Hirose, Melting temperature of simulated high burn-up mixed oxide fuels for fast reactors, *J. Nucl. Sci. Technol.*, 1999, 36, 596.
27. P. Manoravi, R. Sajimol, M. Joseph, N. Sivakumar, Laser-mass spectrometric studies on measurement of isotopic ratios – A comparative study using ps and ns pulsed lasers, *Int. J. Mass Spectr.*, 2014, 367, 16-20.
28. P. Manoravi, R. Sajimol, M. Joseph, N. Sivakumar, Laser-Mass spectrometric studies on measurement of isotopic ratios of Li -A comparative study using ps and ns pulsed lasers, *Int. J. Mass Spectr.*, 2014, 367, 16-20.
29. M. Joseph, P. Manoravi, Boron isotope enrichment in nanosecond pulsed laser-ablation plume, *Appl. Phys. A*, 2003, 76, 153-156.
30. K. J. R. Rosman, P. D. P. Taylor, Isotopic compositions of the elements, *Pure Appl. Chem.*, 1998, 70, 217-235.
31. G. Audi, A. H. Wapstra, The atomic mass evaluation: Atomic mass table, *Nucl. Phys. A*, 1993, 565, 1-65.
32. D. R. Olander, *Materials Chemistry at High Temperatures*, 1990, Vol. 2, Edited by J. W. Hastie, Humana Press, New Jersey, USA, p 411.
33. D. R. Olander, S. K. Yagnik, C. H. Tsai, Laser-pulse vaporization of uranium dioxide and other refractory materials, *J. Appl. Phys.*, 1988, 64, 2680-2689.
34. D. B. Chrisey, G. K. Hubler, *Pulsed Laser Deposition of Thin Films*, John Wiley & Sons Ltd., USA, 1994.
35. R. E. Russo, X. L. Mao, S. S. Mao, The Physics of laser ablation in microchemical, *Anal. Chem.*, 2002, 70A, 74-79.
36. M. E. Shaheen, J. E. Gagnon, B. J. Fryer, Femtosecond (fs) lasers coupled with modern ICP-MS instruments provide new and improved potential for in situ elemental and isotopic analyses in the geosciences, *Chemical Geology*, 2012, 260, 330-337.

37. S. Barcikowski, J. Walter, A. Hahn, J. Koch, H. Haloui, T. Herrmann, A. Gatti, Picosecond and femtosecond laser machining may cause health risks related to nanoparticle emission, *J. Laser Micro/Nanoeng.*, 2009, 4, 159-164.
38. Robert Eason, *Pulsed Laser Deposition of Thin Films*, John Wiley & Sons Ltd., USA, 2006.
39. A. E. Hussein, P. K. Diwakar, S. S. Harilal, A. Hassanein, The role of laser wavelength on plasma generation and expansion of ablation plumes in air, *J. Appl. Phys.*, 2013, 113, 1063-1069.
40. Q. Lu, S. S. Mao, X. Mao, R. E. Russo, Theory analysis of wavelength dependence of laser-induced phase explosion of silicon, *J. Appl. Phys.*, 2008, 104, 301-307.
41. M. Guillong, *Laser Ablation Inductively Coupled Plasma Mass Spectrometry: Laser ablation system developments and investigations on elemental fractionation*, PhD Thesis, ETH, 2004, URL: <http://e-collection.library.ethz.ch/eserv/eth:27150/eth-27150-02.pdf>
42. K. Song, H. Cha, D. Kim, K. Min, Determination of the isotope ratio for metal samples using a laser ablation/ionization Time-of-flight Mass Spectrometry, *Bull. Korean Chem. Soc.*, 2004, 25, 101-105.
43. R. E. Russo, X. L. Mao, O. V. Borisov, Haichen Liu, Influence of wavelength on fractionation in laser ablation ICP-MS, *J. Anal. At. Spectrom.*, 2000, 15, 1115-1120.
44. Wei-E Wang, D. R. Olander, T. B. Lindemer, Vaporization thermodynamics of urania-neodymia mixed oxides, *J. Nucl. Materials.*, 1994, 211, 85-91.
45. A. C. Ciocan, X. L. Mao, O. V. Borisov, R. E. Russo, Optical emission spectroscopy studies of the influence of laser ablated mass on dry inductively coupled plasma conditions, *Spectrochim. Acta, B*, 1998, 53, 463-468.

46. R. E. Russo, X. L. Mao, H. Liu, J. Gonzalez, S. S. Mao, Laser ablation in analytical chemistry- a review, *Talanta*, 2002, 57, 425-432.
47. M. Joseph, N. Sivakumar, P. Manoravi, *Materials Under Extreme Conditions: Recent Trends and Future Prospects*, Edited by Tyagi and Banerjee, Elsevier, 2017, p.533-573.
48. D. Leena, Laser pulse energy based high speed trigger controller for mass spectrometry (M. Tech. Thesis), 2013, Anna University, Chennai, India.
49. Hand Book of Chemistry and Physics, 73rd ed., CRC Press, 1992–1993, p. 11.
50. E. E. B. Campbell, I. V. Hertel, C. Kusch, R. Mitzner, B. Winter, Nanosecond and picosecond laser desorption of C₆₀, *Synthetic Metals*, 1996, 77, 173-180.
51. H. Sobral, R. Sanginés, Comparison of plasma parameters and line emissions of laser-induced plasmas of an aluminum target using single and orthogonal double nanosecond/picosecond pulses, *Spectrochim. Acta B*, 2014, 1, 94-99.
52. M. Joseph, N. Sivakumar, P. Manoravi, R. Balasubramanian, Determination of boron isotope ratio in boron carbide using a laser mass spectrometric method, *Rapid Commun. Mass Spectrom.*, 2004, 18, 231-235.
53. R. J. Ackermann, E. G. Rauth, R. J. Thorn, The thermodynamics of ionization of gaseous oxides; the first ionization potentials of the lanthanide metals and monoxides, *J. Chem. Phys.*, 2008, 65, 1027-1034.

Studies on Evaporation Behavior of Sm and Nd from their mixture, by Thermal Ionization Mass Spectrometry (TIMS)

3.1 Introduction

The advanced Thermal Ionization Mass Spectrometer with multi collectors enables determination of isotopic composition of elements of natural origin, in presence of their interfering isotopes, with the help of an inbuilt software. By this way, the rates of evaporation of Nd isotopes and their interfering counterparts of Sm were studied, by measuring their ion intensities. A study on preferential evaporation behavior of Sm over Nd finds special importance in nuclear industry as the latter is universally accepted as the ideal candidate for burn-up monitor [1] for performance evaluation of spent nuclear fuel. The isobaric interference caused by Sm necessitates chemical separation of Nd from the fuel matrix, for burn-up determination. As the vapor pressures of Sm isotopes dominate than that of Nd isotopes, it could be possible to remove Sm from Nd-Sm mixture, by evaporation. Hence, a study on the evaporation behavior of these elements from their mixture was attempted using TIMS. This chapter describes the studies on effect of time and temperature on evaporation rates of Sm and Nd isotopes, and the influence of fractionation on isotopic composition due to long time exposure of the elements to high temperatures.

3.1.1 Thermal ionization

Heating a metal wire to high temperature in vacuum causes emission of electrons from the metal surface. Thermal ionization or surface ionization is a process which involves heating a sample to high temperature on a metal filament to produce characteristic positive ions [2]. The sample treatment for thermal ionization is as follows:

- i. The sample solution is loaded on to the surface of a metal filament and then evaporate the solvent by passing a current of ~0.7 A (i.e. ohmic heating) at ambient conditions.
- ii. The filament is placed into the source housing of TIMS and the chamber is evacuated to high vacuum (better than 10^{-7} torr). Vacuum is required for the measurement of emitted ions, and also to facilitate the evaporation of sample.
- iii. An electric current is passed through the filament. This heats up the sample, causing positive ions and neutral species to desorb from the surface.
- iv. The ions are analyzed for m/z values and the corresponding abundances to give accurate and precise isotopic ratios.

As a result of high temperature involvement, only certain refractory elements can be used as filament material. The elements generally used are Pt, Re, W and Ta, as they are metallic and can be heated to temperatures of 1200-2300 K. A further important criterion for the filaments is that they should not readily react chemically with either the sample or with surrounding gas.

3.1.2 Principle of thermal ionization

The process of thermal ionization is based on the fact that when neutral atoms or molecules having first ionization potential I are heated on or impinged upon a hot metallic surface of work function W , at temperature T , there is a probability that ions will also evaporate in addition to neutral particles. The ratio of number of positive ions formed to the total number evaporated (i.e. ionization efficiency) is given by the Langmuir-Saha equation [2],

$$\frac{n^+}{n^0} = \exp \left[e \frac{(W-I)}{kT} \right] \quad (1)$$

where k is Boltzmann's constant and e is the electronic charge.

For higher ionization efficiency (n^+/n^0), the work function of the surface must be larger than the ionization potential of the sample and the temperature as low as possible consistent with efficient evaporation. When sample is loaded on a metal surface having high work function, the electron cloud of the sample atoms will experience more attraction from the metal surface than from its own nucleus, leading to formation of large number of positive ions. The average work function and melting points of the commonly used filaments are given in Table 3.1.

Table 3.1 Work functions and melting points of some metals used for sample loading in TIMS

Element	Thermionic Work Function (eV) [3]	Melting point (K) [3]
Tantalum	4.19	3269
Rhenium	5.12	3453
Tungsten	4.52	3653
Platinum	5.32	2042

3.1.3 Measurement of isotopic ratios

To measure the abundance of a particular ion in a sample, the sample must be evaporated over a period of time. Generally, in TIMS, ratios of isotopic abundances need to be obtained and not individual total ion yields. To measure the ratio of two isotopes M1 and M2, the abundances of the isotopes must be measured simultaneously. The abundances are measured as ion currents recorded by the ion collectors.

For two isotopes, the ion yields are given by the following equations

$$\frac{n_1^+}{n_1^0} = C_1 e^{(W-I_1)/kT} \quad (2)$$

$$\frac{n_2^+}{n_2^0} = C_1 e^{(W-I_2)/kT} \quad (3)$$

Dividing equation (2) by (3) gives

$$\frac{\left(\frac{n_1^+}{n_1^0}\right)}{\left(\frac{n_2^+}{n_2^0}\right)} = C e^{\left(\frac{\Delta I}{kT}\right)} \quad (4)$$

i.e. relative ionization efficiency depends upon the difference in ionization potential (ΔI) of the isotopes and the filament temperature.

3.1.4 Evaporation rates of Sm and Nd

When multi elements are loaded on the same filament and heated inside TIMS, the rate of evaporation of the elements depends upon their vapor pressures and temperature of the filament. Dependence of vapor pressure on temperature is given by the Clausius-Clapeyron equation [4,5]

$$d \ln p = \left(\frac{\Delta H_v}{RT^2} \right) dT \quad (5)$$

where p- vapor pressure, ΔH_v - enthalpy of vaporization, R- gas constant and T- temperature.

On comparing the vapor pressures of Nd and Sm, it can be seen that heat of vaporization of Sm is ~1.6 times lesser than that of Nd, as shown in Table 3.2.

Table 3.2 Comparison of some properties of Nd and Sm relevant to the present study

Element	Fission yields with thermal neutrons (for ^{235}U ; ^{239}Pu)	Heat of vaporization, ΔH_{298}° (kJ/mol) [6-9]	Vapor pressure at melting point (torr.) [10,11]	Ionization energy (eV) [2]
Nd	20.515; 16.641	327.88 ± 0.21	3.4×10^{-5} ($T_m=1297\text{K}$)	5.5
Sm	4.376; 5.252	203.04 ± 0.22	5.8 ($T_m=1345\text{K}$)	5.6

3.2. Experimental

3.2.1 Instrumentation-Thermal ionization mass spectrometer

Model ISOPROBE-T from M/s ISOTOPX, U.K, shown in Fig. 3.1 was used in the present study. The layout of Isoprobe-T is shown schematically in Fig. 3.2. This instrument is equipped with a turret magazine of 20 samples loaded on single or triple filament system, and operates at an acceleration voltage of 6kV at a vacuum of 10^{-8} - 10^{-9} mbar. A 90° magnetic sector analyzer with 26.5° oblique incidence provides better mass dispersion and the resolved ions are detected by 9 Faraday cups and an axial secondary electron multiplier (for isotopes of very low abundance- having ion current less than 10^{-16} A). The ions generated in the ion source by the process of thermal ionization over a hot filament are focused into a beam which is directed towards the entrance slit of the mass spectrometer. The ion beam is separated in the magnetic analyzer according to their mass -to-charge ratio. Ions of a chosen mass-to-charge ratio are focused in the collector system by selecting the appropriate magnetic field or radius of curvature. The ions are then measured either by Faraday cups or by Secondary Electron Multiplier (SEM) and the digitized ion currents are displayed.

Detailed description of TIMS used in the present study is given below.

The ion source

The source housing made out of electro polished stainless steel holds the turret which can accommodate up to 20 bead blocks of separately loaded samples. The filaments are heated via resistive heating by the filament wiper assembly. The view port provided in the source flange allows the filament under analysis to be observed, to ensure that the filament is heating up. In addition, a pyrometer option is available to monitor and control temperature of



Fig. 3.1 Photograph of the TIMS instrument used for the present study

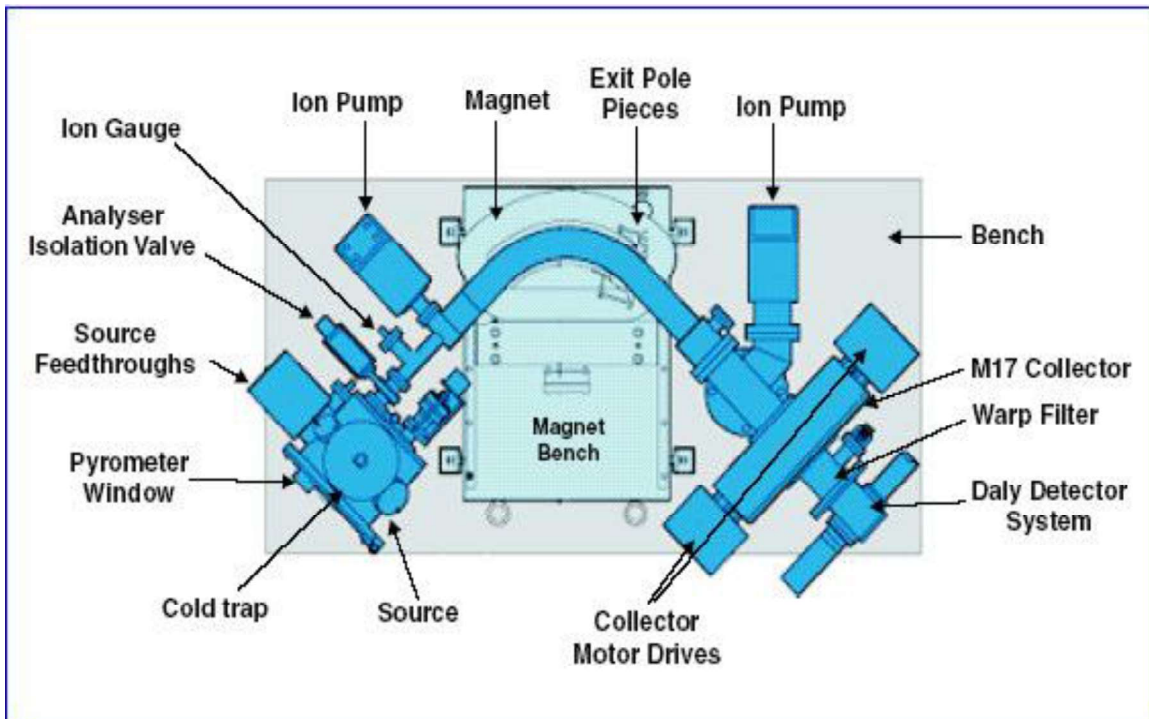


Fig. 3.2 Schematic of TIMS

the ionizing filament. The pre-heat option allows sample to be pre-conditioned prior to measurement, whilst one sample is being run, which increases the sample throughput.

Magnetic sector analyzer

Ions pass through the single focusing magnetic sector analyzer are separated according to their mass-to-charge ratios. The magnet is fitted with adjustable exit pole faces to give stigmatic focusing. The extended geometry eliminates ion reflection effects caused by ion hitting the collector walls, which will otherwise cause perturbation in the baseline. The 8 cm wide flight tube allows the measurement of ~17% relative mass separation, which enables determination of Li isotopes. The nominal radius of the ion optical system is 270 mm for normal ion beam entry into the magnet. The entrance and exit angles double the dispersion length, i.e. the distance between effective boundary of the magnet and the image, to 540 mm with unit magnification. The increased dispersion improves abundance sensitivity to <10 ppm and allows the use of wider slits for same resolving power, and hence to improve the transmission efficiency.

The magnet pole pieces tilt the magnetic field boundaries to approximately 26.5°, causing additional Z- focusing of the ion beams thus improving ion beam transmission even further.

The magnetic field is controlled by a Hall probe, situated between the inner radius of the flight tube and the magnet. Hall probe senses the strength of the magnetic field and relays this signal to the magnet control unit. This forms a feedback loop that defines operation of the magnet as requested by the user.

The strength of the magnetic field required to turn the ions through a radius r can be calculated from the equation,

$$\frac{m}{e} = B^2 r^2 / 2V$$

where, B is the magnetic field (gauss), m is isotopic mass (amu), V is acceleration voltage (volts) and r is the radius of curvature (cm).

The nominal mass range of the instrument is 280 amu at a magnet current of 5A and an operating voltage of 6 kV.

The Ion Collector assembly

The mass separated and focused ion beams are detected by an array of nine Faraday cup collectors and an optional Secondary Electron Multiplier (SEM). The ion beam passing through the flight tube may collide with residual gas molecules and undergo an energy loss and fall at a point on the focal plane where ions of lesser mass is assigned for, which will lead to overlapping of ion peak of lesser mass (M) by tailing part of adjacent mass (M+1), leading to abundance sensitivity issues. Hence, the ion beams are passed through a wide aperture retarding potential (WARP) filter, before reaching the counting devices. Both Faraday and electron multipliers are positioned at 2.2 mm apart, which gives unit mass spacing for Pu. The positioning of all the adjustable collectors is controlled by an optical read back system.

Faraday collectors

Faraday detectors are the principal ion detectors. In front of each faraday cup, there is an entrance slit with a fixed width of 1 mm. The ion beam arriving at the collector has a width of 0.3 mm which is defined by the source slit. The combination of narrow ion beam and a wide collector allows the measurement of flat topped peaks. The ion beam measured at any point on the peak flat has the same intensity. As a result, ion intensities can be measured very accurately despite small fluctuations in magnetic field or ion focusing. Routine and rapid measurement of isotopic ratios is achieved using a static magnetic field and several Faraday

cups. The Faraday cups are coated with carbon in order to reduce the emission of secondary ions. As a result, the conversion of ion charge to the measured ion current is highly reproducible (constant cup efficiency). Each Faraday cup is connected to a separate amplifier board which is mounted in an evacuated housing called decabin. The decabin is cooled internally to 16°C by a Peltier cooling device. Faraday collectors can be used to measure ion signals in the range 10^{-15} to 10^{-10} A. The noise on Faraday collector is $\sim 2 \times 10^{-16}$ A (10 seconds integration). The measuring resistor for the collector is 10^{11} ohms, so that a current of 10^{-10} A corresponding to an output of 10 V is produced from the amplifier.

Collector Calibration Gain (CC gain)

A programmed collector gain calibration has to be carried out to cross calibrate the gain of Faraday amplifiers. The calibration involves switching a low reference current, simulating the base line and a high reference current, simulating the signal, successively into each amplifier. The gain of each collector is baseline corrected and then calculated as a ratio relative to the axial Faraday. The results of CC gain calibration are automatically uploaded into the collector properties for each Faraday cup.

3.2.2 Procedure

3.2.2.1 Measurement of filament temperature by optical pyrometer

The study on Nd-Sm system involves investigation of rate of evaporation of Sm with filament temperature and the corresponding changes in isotopic ratios of Nd. Temperature of the filament is varied by changing the filament current. Thus, the current passed through filament is a measure of temperature experienced by the sample. Hence, a correlation data was made by measuring the filament temperatures corresponding to different filament currents in the operational range, using an optical pyrometer.

Procedure for temperature measurement

The thermal radiation emitted by the source is captured by the optical objective lens of the pyrometer. The lens helps in focusing the thermal radiation onto the reference bulb. The process was observed through the eye piece and corrected it in such a manner that the reference lamp filament has a sharp focus and the filament was super-imposed on the source image, and changed the current in the reference lamp [12]. The change in current can result in the following situations.

1. The filament is dark. That is, cooler than the source.
2. Filament is bright. That is, hotter than the source
3. Filament disappeared, there is equal brightness between the filament and the source.

At this time, the current that flows in the reference lamp was measured; its value is a measure of temperature of the filament. Schematic of the temperature measurement is given in Fig. 3.3, and the results are tabulated in Table 3.3

Optical Pyrometer - Temperature Measurement

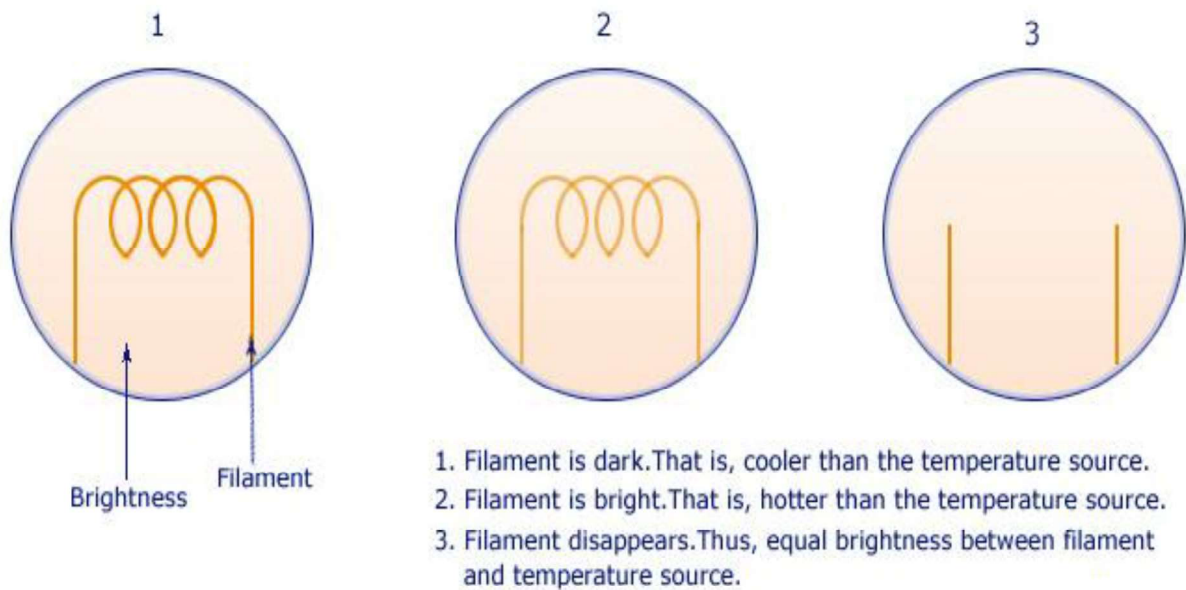


Fig. 3.3 Schematic of functioning of optical pyrometer

Table 3.3 Temperature measured by optical pyrometer and the corresponding filament current applied.

Filament Current (A)	2.0	2.4	3.0	3.2	3.4	3.6	3.8	4.0	4.35	4.6	4.75	4.9	5.2
Temp. (K)	1264	1390	1535	1625	1721	1812	1880	1955	2065	2140	2187	2234	2293

3.2.2.2 Extent of Sm interference on isotopic ratios of Nd in 1:1 mixture

In order to evaluate the severity of Sm interference in the measurement of isotopic ratios of Nd when both the elements are equally present, a study was carried out with a mixture of spectroscopic grade Nd and Sm solutions (in nitrate form), having natural isotopic composition. The natural abundances of isotopes of Nd and Sm are given in Table 3.4.

Table 3.4 Natural isotopic composition of isotopes of Nd and Sm

Isotope mass	142	143	144	145	146	147	148	149	150	151	152	153	154
Nd (%)	27.1	12.2	23.8	8.3	17.2	-	5.76	-	5.64	-	-	-	-
Sm (%)	-	-	3.10	-	-	15.0	11.3	13.8	7.40	-	26.7	-	22.7

Nitrate solutions containing about 500 ng of each element were mixed together and loaded on to Re filament and evaporated the solvent by ohmic heating. The sample was then loaded in TIMS in a triple filament assembly (Re-Re-Re) and heated both sample filament (evaporation filament) and ionization filament slowly at a heating rate of 0.001 A/s and 0.002 A/s, respectively by an inbuilt heating program. At 2.25/5.5 A, when Sm and Nd intensities were sufficiently high, isotopic composition of Nd was measured. In order to study the extent of contribution of interfering isotopes of Sm on the measured isotopic ratio, another set of measurements were made after applying interference correction for Sm. The corrected ion intensities of interfering isotopes of Nd were measured based on the natural isotopic abundance of Nd and Sm, using the supportive software of TIMS. That is, the intensity of an interfered isotope is corrected based on the intensity of an un interfered isotope. In the present study, contribution of Sm isotopes on Nd isotopes is corrected based on the intensity

of an un-interfered isotope, ^{147}Sm (see Table 3.4). Isotopic composition of Nd measured with and without applying correction are given in Table 3.5.

Table 3.5 Isotopic composition of Nd measured with and without applying interference correction

Isotope ratio	IR (without applying interference correction)	IR (after applying interference correction)	Error due to isobaric interference (%)
$^{143}\text{Nd}/^{142}\text{Nd}$	0.4469±0.0002	0.4468±0.0001	0.02
$^{144}\text{Nd}/^{142}\text{Nd}$	1.3247±0.0012	0.8781±0.0002	50.9
$^{145}\text{Nd}/^{142}\text{Nd}$	0.3036±0.0002	0.3034±0.0002	0.1
$^{146}\text{Nd}/^{142}\text{Nd}$	0.6286±0.0002	0.6276±0.0001	0.2
$^{148}\text{Nd}/^{142}\text{Nd}$	1.8447±0.0037	0.2027±0.0002	810.1
$^{150}\text{Nd}/^{142}\text{Nd}$	1.2732±0.0025	0.1918±0.0002	563.8

The results depict immense contribution of Sm isotopes leading to huge error in isotopic composition of Nd. Maximum error was observed for the ratio $^{148}\text{Nd}/^{142}\text{Nd}$ (810%) followed by $^{150}\text{Nd}/^{142}\text{Nd}$ (564%) and $^{144}\text{Nd}/^{142}\text{Nd}$ (51%), in accordance with the relative abundances of Sm isotopes (Table 3.4).

3.2.2.3 Study on variation of ion intensities of Sm and Nd with time, at constant temperature.

Sample preparation:

Spectroscopic grade oxides of Sm and Nd of natural isotopic composition (BDH chemicals Ltd, U. K) were mixed in 1:4 ratio (20 mg:80 mg), since the Sm/Nd ratio in the

dissolver solution of PHWR fuel varies from 1:3 to 1:5 depending on the fractional fission contributions [13] from ^{235}U and ^{239}Pu . The Nd-Sm mixture was dissolved in 250 μl of Q D nitric acid and evaporated to dryness under IR lamp. The residue was then made into a solution using 50 μl of 0.75 M nitric acid, a small droplet of the solution was loaded on to Re filament using a micro pipette and evaporated the solvent by ohmic heating for Thermal Ionization Mass Spectrometric studies.

Procedure:

The filament containing mixture of Sm and Nd was heated slowly to 1.5 A, and ionization filament to 5.5A, by applying a heating rate of 0.001 A/s and 0.002 A/s, respectively. The focusing conditions were optimized using Re^+ signal. On stepwise increase of sample filament current, Sm ions started to appear at 1.70 A and Nd signals started to appear at 2.0A. All the peak centers from mass 142 to 150 were made coinciding with respect to the axial collector, as shown in Fig. 3. 4.

After attaining sufficiently high ion intensities at 2.25 A, one set of isotopic ratios of Nd was measured with corrected ion intensities for interfered isotopes, based on the natural isotopic abundance of Nd and Sm, using the supportive software of TIMS. The start of isotopic ratio measurements, after the filament current reached a value of 2.25 A, is arbitrarily fixed as 'zero' time and the corresponding isotopic ratios are considered as 'base-values'. The effect of isobaric interference and fractionation were studied with respect to this base values. Keeping the filament current at 2.25A, the ion intensities of Nd and Sm, and isotopic ratios of Nd were measured, without applying any correction for interference, at various time intervals and monitored for the variation in isobaric interference with time due to relatively higher evaporation rate of Sm. The ion intensity of ^{147}Sm , an un-interfered isotope was

monitored with time, and found to be feeble and steady after 130 minutes (i.e. similar to the dissolver solution of long cooled PHWR fuel, where most of the ^{147}Pm would have been converted to ^{147}Sm). After this time interval, isotopic composition measurements with corrected ion intensities were repeated to study the effect of fractionation due to preferential evaporation of lighter isotopes on prolonged exposure to high temperature.

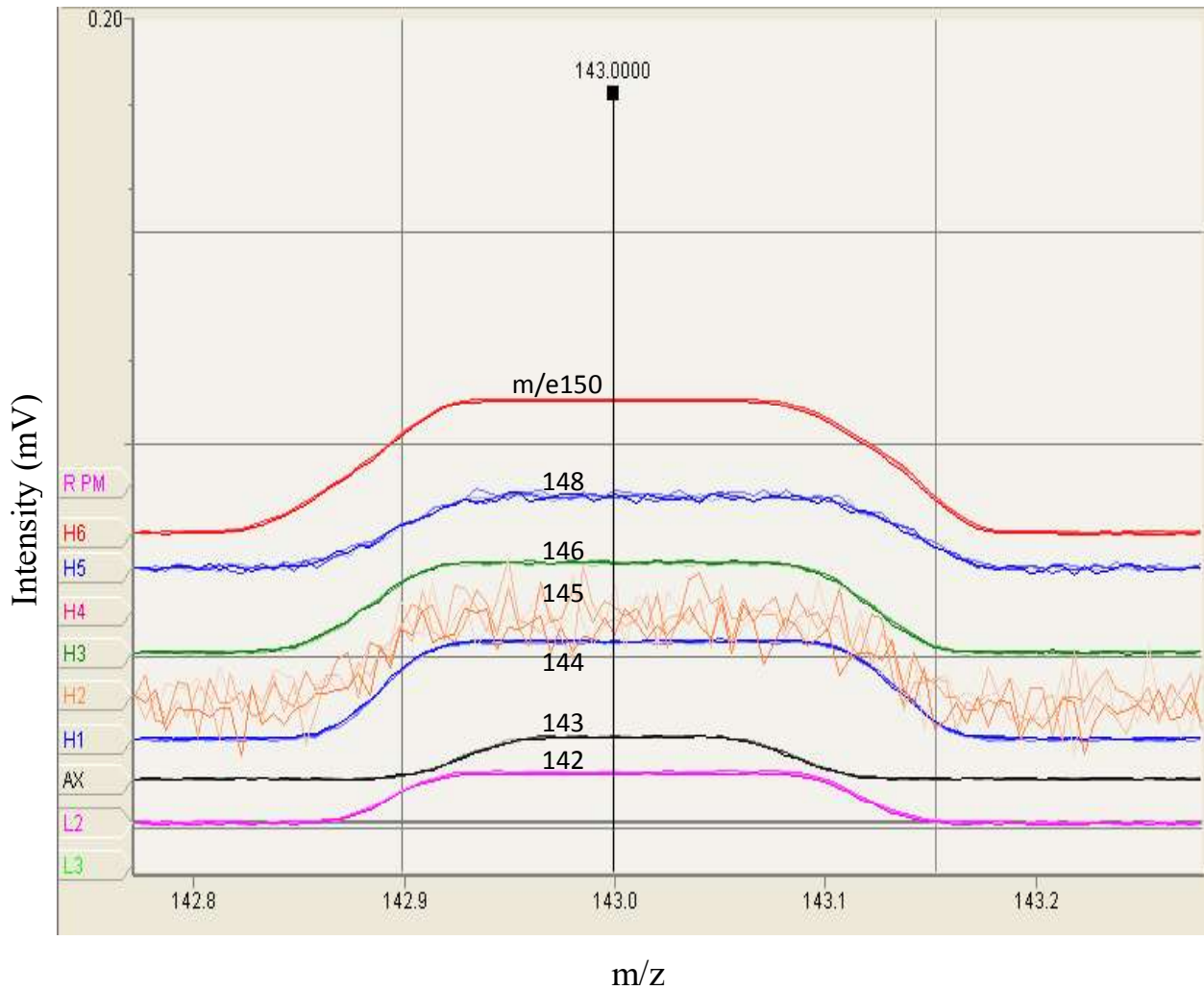


Fig. 3.4 Peak centre coincidence of masses from 142 to 150 with respect to axial collector

3.2.2.4 Effect of filament temperature on fractionation and rate of removal of Sm

An enhancement in filament temperature will accelerate the rate of removal of Sm and the isobaric interference is expected to diminish faster than that at lower temperature [14]. However, elevated temperature catalyses fractionation as well, and the effect will become more prominent for ratios involving isotopes with larger difference in their mass numbers [15]. Isotopic compositions at different filament currents, namely 2.25, 2.3, 2.35 and 2.4 A (and the corresponding temperature ranges of ~ 1260 to 1390 K) were measured after equal duration of exposure (130 minutes) and compared for the extent of fractionation. Separate sample filaments were employed for fractionation studies at individual filament currents, as there will be cumulative effect when the same sample was taken to higher temperature after finishing measurements at immediate lower temperature.

3.3 Results and Discussion

3.3.1 Optimization of filament current (filament temperature)

On stepwise increase of sample filament current, Sm ions started to appear at 1.70 A and their intensities were found to increase with filament current. Though Sm and Nd (1:4 ratio) were loaded in their nitrate form, measurements were made based on the intensities of elemental ions since their nitrates decompose to their respective oxides at higher temperature [16] and ultimately to elemental ions, as do the nitrates of U and Pu [17]. i.e., a steady increase in intensities of the elemental ions with temperature was observed, where as that of oxide ions decrease. At 1.95 A, ion intensity of ^{147}Sm reached a maximum of 261 mV and remained almost steady for few minutes and then started to fall. As the filament current reaches 2.0 A, Nd ions started to appear, but the ion intensities were still dominated by the Sm isotopes, as seen in Fig. 3.5. With further increase of filament current, ion intensities of

Sm, which initially shown an increasing trend, started to fall as soon as the current was made steady. At higher filament currents, Sm intensities followed an accelerated rate of fall, and Nd intensities kept rising up. As the filament current reached 2.25 A, Nd isotopes had attained sufficient ion intensities for isotopic composition measurements with fairly good accuracy for un-interfered isotopes, and with reduced isobaric interference from Sm for interfering isotopes, as obvious from Fig. 3.6.

3.3.2 Variation in ion intensities of ^{142}Nd and ^{147}Sm , with time at constant sample filament current

In this study, the ion intensities of ^{142}Nd and ^{147}Sm isotopes with time at constant filament current (2.25 A) were measured, and the results are given in Table 3.6. Intensity of ^{146}Nd , being an un-interfered isotope (see Table 3.4) was also monitored as a function of time, to compare with the change in intensity of ^{147}Sm . It was observed that intensity of ^{142}Nd increased with time and that of ^{147}Sm kept decreasing. The large difference in vapor pressures [10] of the elements (given in Table 3.2) resulted in early removal of Sm from the filament compared to Nd; moreover, the comparatively lower amount of Sm also assisted for intensity reduction. This is evident from the $^{147}\text{Sm}/^{142}\text{Nd}$ values shown in Table 3.6, which started with 0.573 at zero time and reached 0.003 after 130 minutes, where as $^{146}\text{Nd}/^{142}\text{Nd}$ ratio maintained a constant average value of 0.6308 for a long time and approached 0.6312 after prolonged heating, due to fractionation. Steady decrease in ion intensity of ^{147}Sm in the course of successive measurements is obvious from Fig. 3.7; and was found to be very small (~ 2 mV) and almost steady after 130 minutes. Also, it is to be noted that in the case of dissolver solution of long cooled PHWR fuel, most of the ^{147}Pm would have been converted to ^{147}Sm .

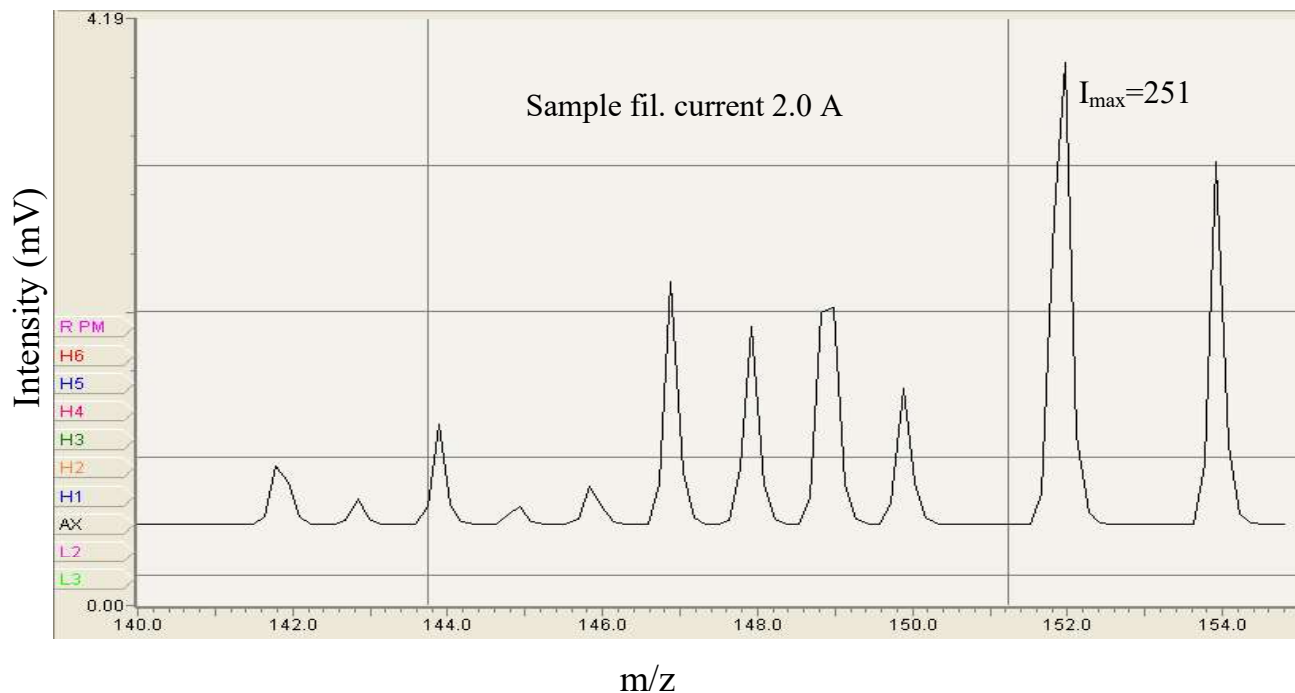


Fig. 3.5 Mass spectrum of Nd-Sm mixture at sample filament current of 2.0 A

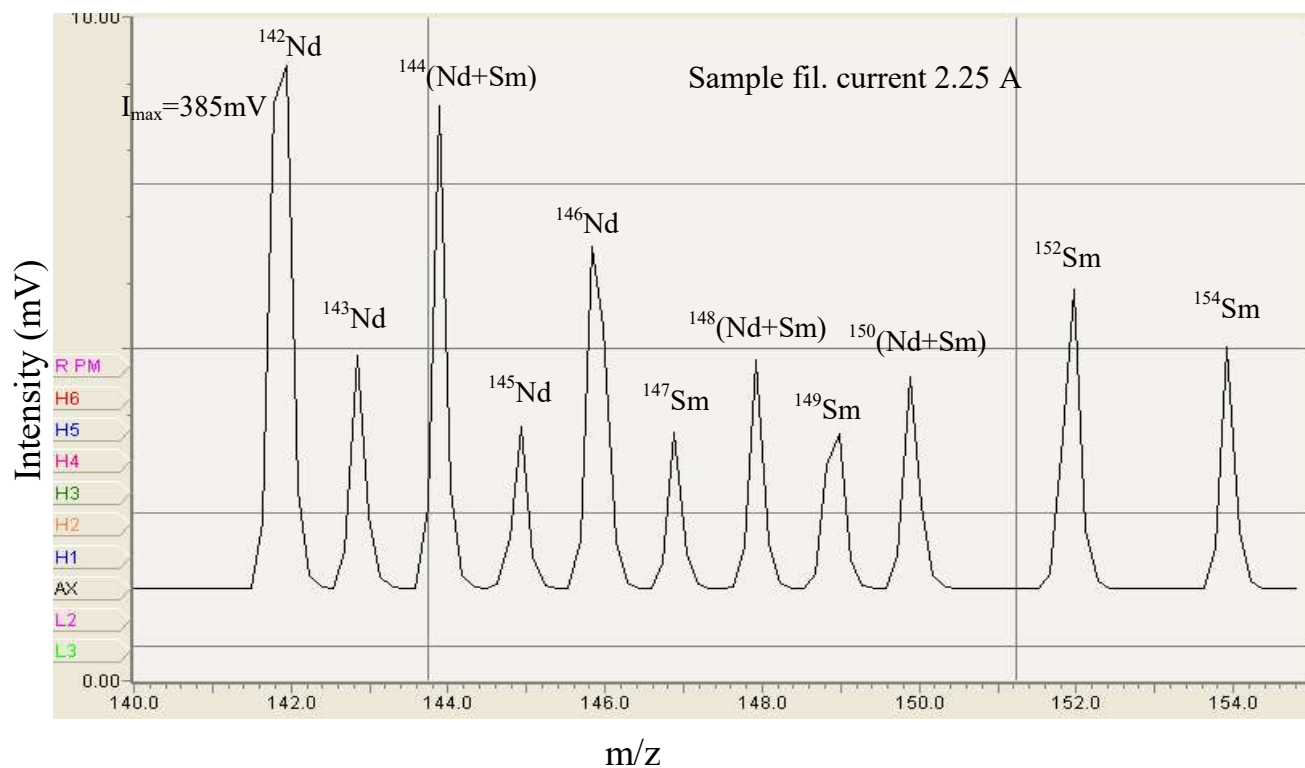


Fig. 3.6 Mass spectrum of Nd-Sm mixture at sample filament current of 2.25A.

Table 3.6 Variation of ion intensities of ^{147}Sm and ^{142}Nd (from Nd-Sm mixture of natural isotopic composition), at filament current of 2.25 A.

Time (min.)	Intensity of ^{142}Nd (mV)	Intensity of ^{147}Sm (mV)	$^{147}\text{Sm}/^{142}\text{Nd}$	$^{146}\text{Nd}/^{142}\text{Nd}$
0.00	44	26	0.5733	0.6308
10.00	57	23	0.4110	0.6305
20.00	87	22	0.2479	0.6308
30.00	83	13	0.1646	0.6306
35.00	126	13	0.1059	0.6307
41.00	129	9.4	0.0754	0.6309
50.00	112	6.1	0.0547	0.6306
55.00	132	5.3	0.0399	0.6307
65.00	150	4.3	0.0289	0.6306
70.00	208	4.1	0.020	0.6308
85.00	326	3.8	0.012	0.6309
100.00	537	3.5	0.007	0.6311
115.00	606	2.9	0.005	0.6310
130.00	744	2.2	0.003	0.6312

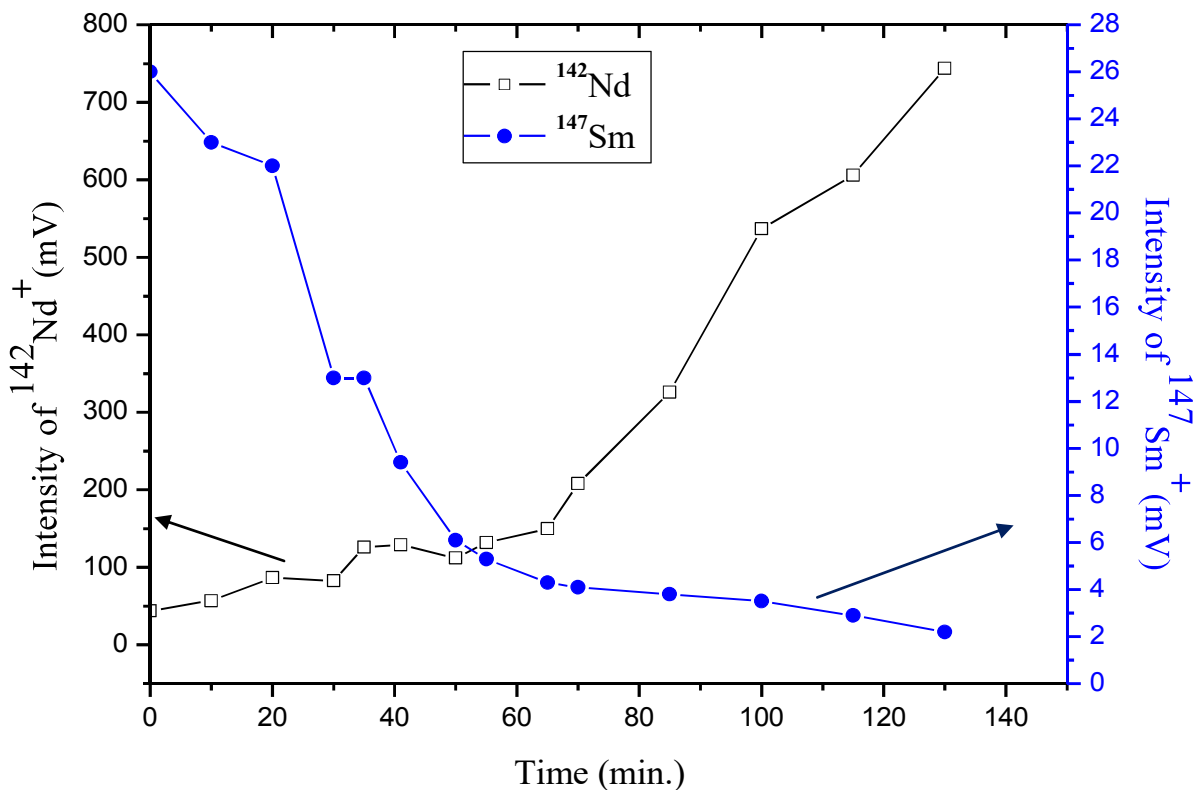


Fig. 3.7 Graphical representation of variation in ion intensities of ^{142}Nd and ^{147}Sm with time at 2.25A sample filament current

3.3.3 Evaporation behavior of various isotopes of Sm and Nd from their mixture

Variation of isotopic ratios as a function of time is shown in Fig. 3.8, which shows that isotopic ratios which do not involve interfering isotopes, like $^{143}\text{Nd}/^{142}\text{Nd}$, $^{145}\text{Nd}/^{142}\text{Nd}$ and $^{146}\text{Nd}/^{142}\text{Nd}$ remains steady with time, whereas the ratios influenced by interfering isotopes of Sm, like $^{144}\text{Nd}/^{142}\text{Nd}$, $^{148}\text{Nd}/^{142}\text{Nd}$ and $^{150}\text{Nd}/^{142}\text{Nd}$ exhibited a steady drop in their values and approached close to their natural values after getting exposed to high temperature for long duration. The ratio $^{147}\text{Sm}/^{142}\text{Nd}$ exhibited highest rate of fall from 0.5732 to 0.0121 within 130 minutes, which practically establishes the preferential evaporation of Sm over Nd. As mentioned earlier, isotopic interference can be reduced at a

faster rate by maintaining the sample filament at an elevated temperature, but it may lead to an enhancement in fractionation.

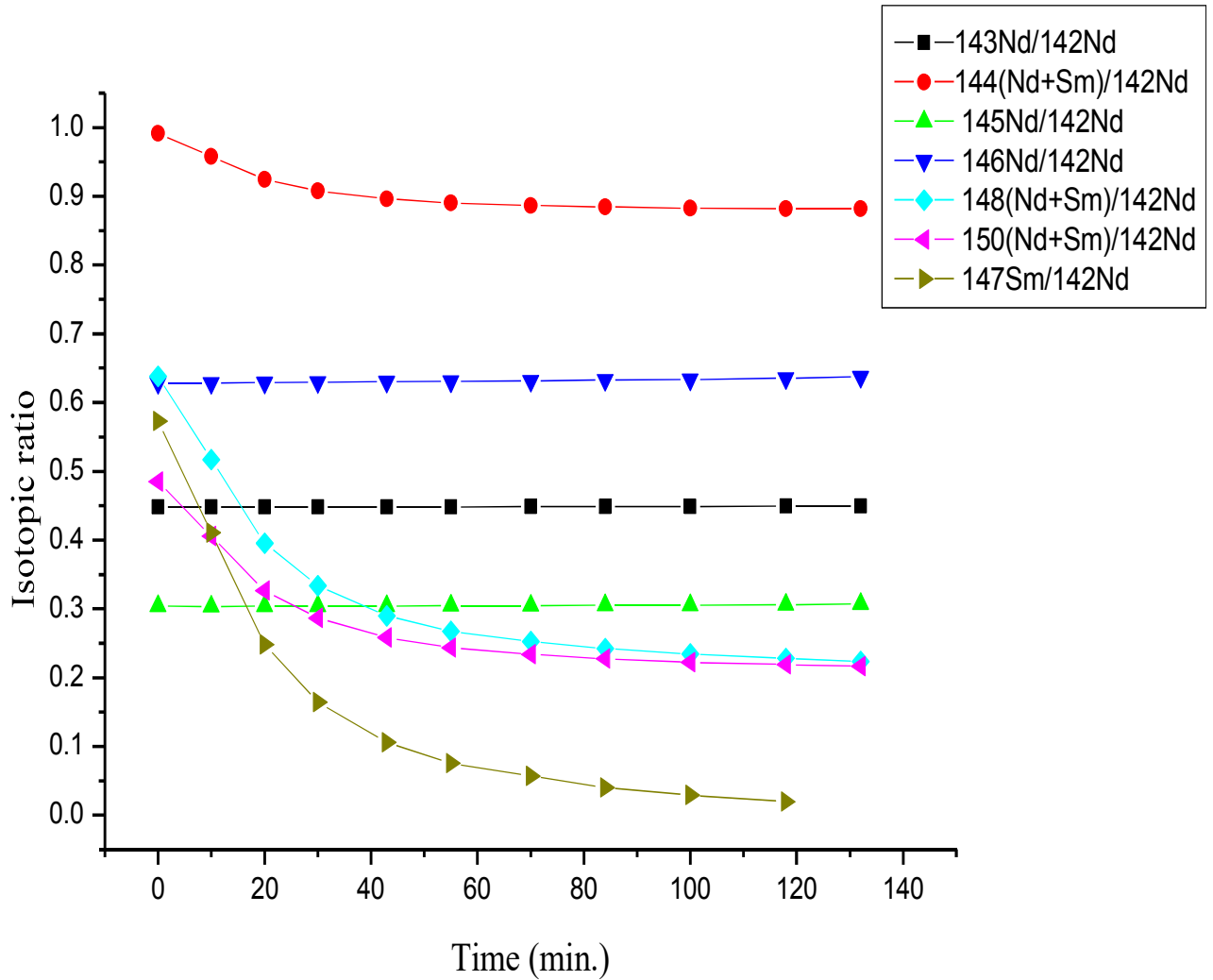


Fig. 3.8 Variation in isotopic ratios involving interfering and un-interfering isotopes, with time, at 2.25 A filament current.

3.3.4 Isotopic composition of Nd measured at 0 and 130 minutes- effect of time on interference

The isotope ratios measured with and without interference correction at zero time and after 130 minutes are given in Table 3.7, which shows that maximum deviation from true value occurred for $^{148}\text{Nd}/^{142}\text{Nd}$ and $^{150}\text{Nd}/^{142}\text{Nd}$, namely 202 % and 135 %, respectively, due to isobaric interference. This deviation gets reduced to 5.7% and 4.7%, respectively after heating for 130 minutes. The isotopic ratios (IR) without correction at zero time were measured immediately after finishing IR measurements with correction at zero minute (for base values). Practically it took about 5 minutes to complete the base value measurements, but it is considered that the second measurement is also made at 0 min; same concept is valid for measurements at 130 minutes also.

The array of spectra showing steady reduction in intensities of isotopes which are affected by interference, is given in Fig. 3.9. The figure clearly portrays the intensities of ^{147}Sm , ^{149}Sm , ^{152}Sm and ^{154}Sm which had prominent peaks in the beginning, got reduced in peak heights (intensities) with time and almost vanished after 130 minutes of heating, whereas the isotopes of Nd maintained increasing trend in their ion intensities.

Table 3.7 Isotope ratios (IR) of Nd measured at zero time and after 130 minute (from Nd-Sm mixture), at sample filament current of 2.25A.

Isotopic ratio	IR with correction (0 minute) (base value)	IR without correction (0 minute)	% Error due to isobaric interference (0 minute)	IR without correction (130 minute)	% Error due to isobaric interference (130 minute)
143/142	0.4483 ±0.0002	0.4480 ±0.0004	*NA	0.4492 ±0.0003	NA
144/142	0.8752 ±0.0003	0.9915 ±0.004	13.29	0.8819 ±0.0003	0.76
145/142	0.3044 ±0.0009	0.3039 ±0.0006	NA	0.3070 ±0.0001	NA
146/142	0.6313 ±0.0002	0.6308 ±0.0006	NA	0.6312 ±0.0003	NA
148/142	0.2112 ±0.0001	0.6382 ±0.001	202	0.2233 ±0.0004	5.7
150/142	0.2066 ±0.0001	0.4847 ±0.009	135	0.2164 ±0.0001	4.7

*NA-not applicable, as there is no isobaric interference from Sm

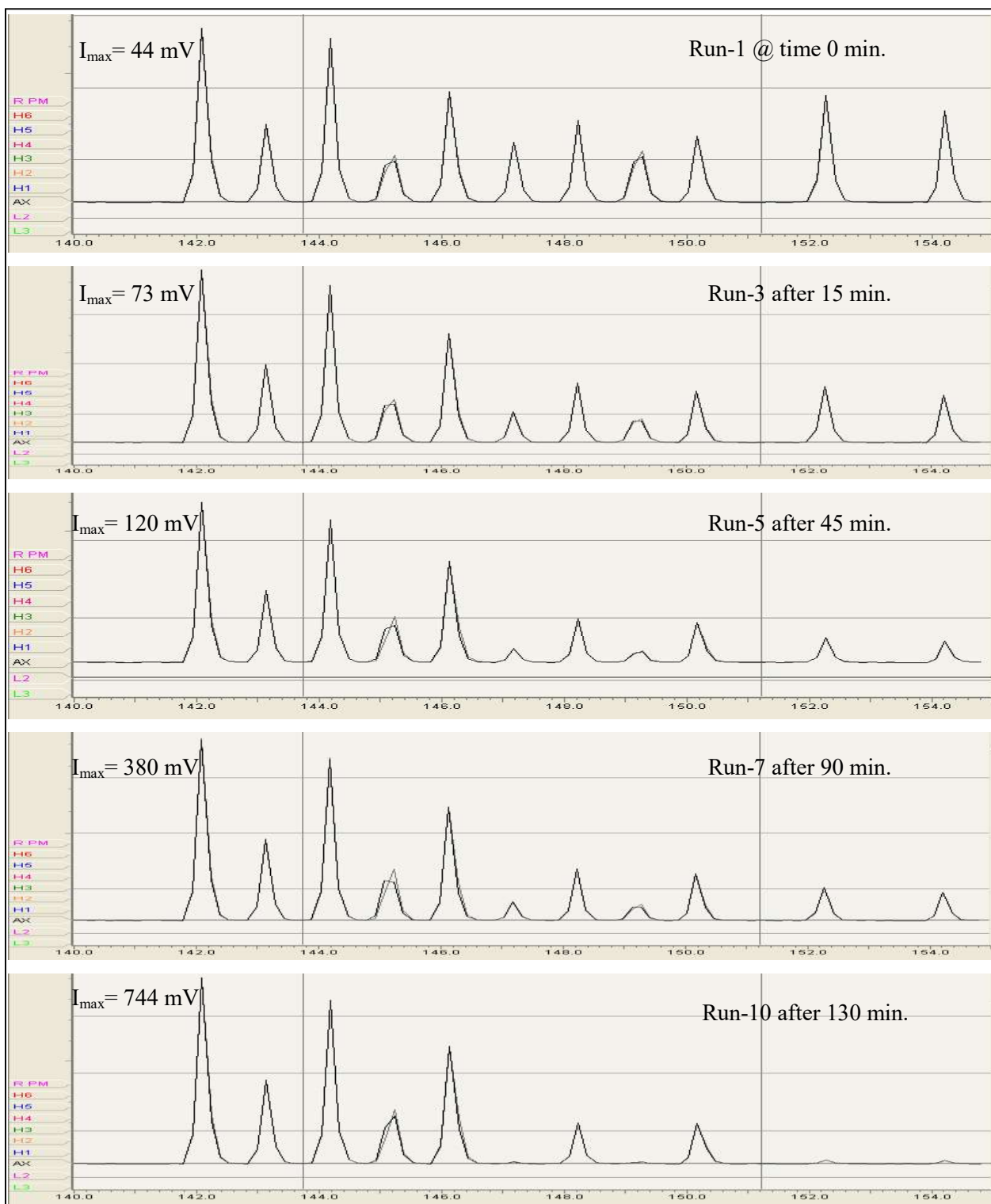


Fig. 3.9 Mass spectra showing reduction in ion intensities of Sm from Nd - Sm mixture (of natural abundance) over successive measurements at different intervals of time (the double line in the spectra are due to a twice measurement).

3.3.5 Effect of filament temperature on fractionation and rate of removal of Sm

Isotope fractionation during thermal ionization mass spectrometry is a mass and temperature dependent process [18]. An enhanced filament temperature can accelerate the rate of evaporation of Sm and the isobaric interference will be diminished faster. However, elevated temperature is expected to increase the fractionation as well, and the effect will become more prominent for ratios involving isotopes with larger difference in their mass numbers, as shown in Fig. 3.10.

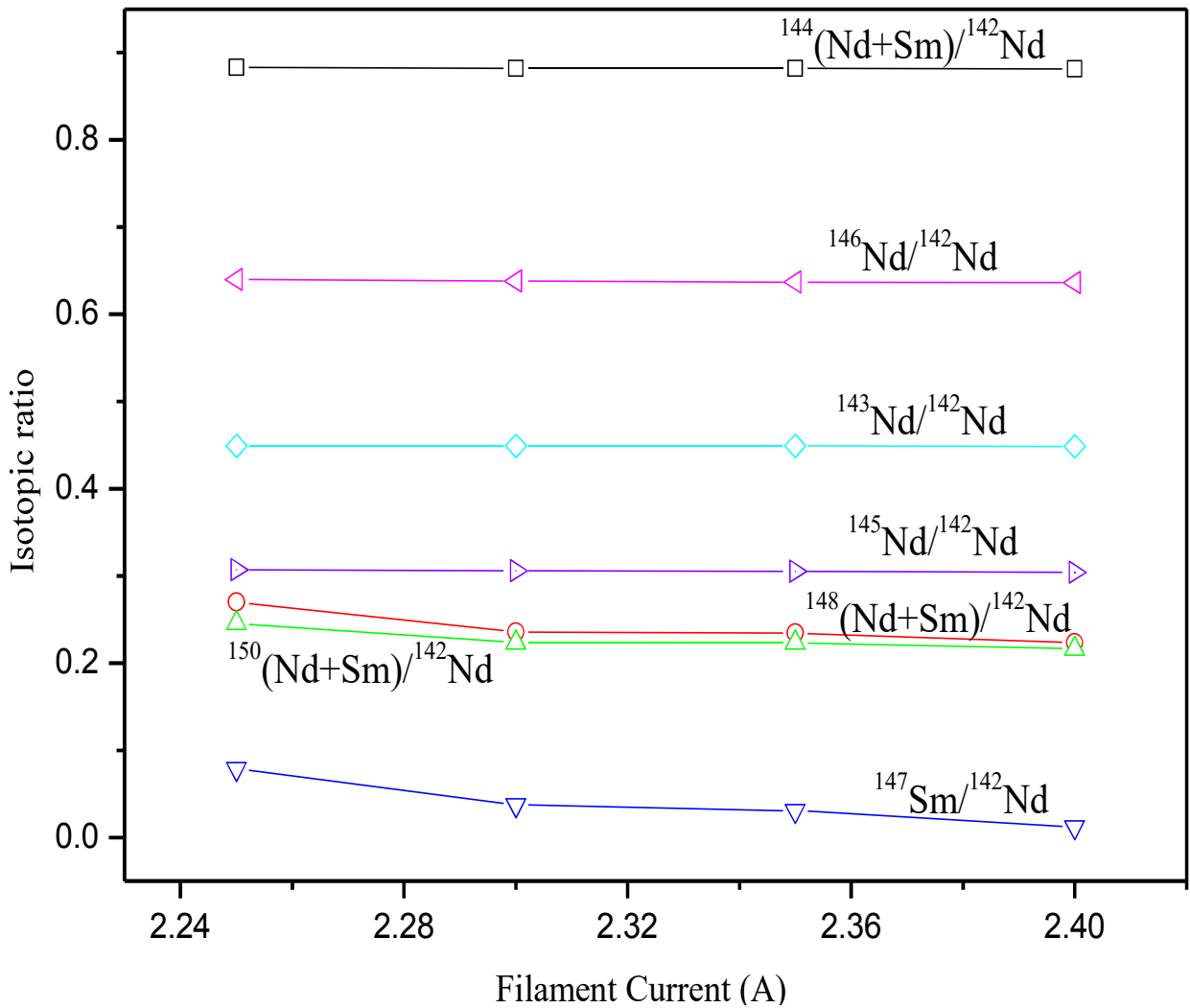


Fig. 3.10 Effect of filament current on isotopic ratios of Nd

From the Tables 3.7 and 3.8, it is evident that error due to fractionation is not as prominent as that due to isobaric interference. Effect of temperature on fractionation was studied by heating the individual sample filaments at different filament currents for equal duration followed by isotopic composition measurements, after applying correction. Fig. 3.10 implies that there is only very mild deviation in the ratios involving non-interfering isotopes of adjacent mass numbers, whereas $^{148/142}\text{Nd}$ and $^{150/142}\text{Nd}$ exhibited noticeable deviation from their true values. It is also obvious from the figure that the rate of decrease of $^{147}\text{Sm}/^{142}\text{Nd}$ ratio is higher with increase in filament current, than any other isotopic ratios.

3.3.6 Effect of fractionation on isotopic ratios of Nd

Prolonged exposure of sample to high temperature leads to enhanced evaporation of lighter isotope, making isotopic composition inaccurate, which was studied by comparing the IR (with correction) measured after 130 minutes with that measured at 0 min. as shown in Table 3.8. Fractionation is more for isotopes of larger mass difference; accordingly, the ratio $^{143/142}\text{Nd}$ was least affected (0.2%) and $^{150/142}\text{Nd}$ was most affected (1.45%) by fractionation. Effect of mass difference on the isotopic ratio measured is evident from the following equation [19].

$$r = \left(\frac{C_1}{C_2}\right) * \left(\frac{M_2}{M_1}\right)^{1/2} = R * \gamma$$

where r is the ratio of molar concentration of the isotopic species in the vapor, C_1 and C_2 are concentrations of masses M_1 and M_2 respectively, remaining on the filament, $R = C_1/C_2$ and $\gamma = (M_2/M_1)^{1/2}$, the fractionation factor.

Table 3.8 Isotopic ratios (IR) of Nd measured with interference correction at zero time and after 130 minute (from Nd-Sm mixture) at a sample filament current of 2.25A.

Isotopic ratio	IR with correction (0 minute) (base value)	IR with correction (130 minute)	Error due to fractionation (%)
143/142	0.4483 ± 0.0002	0.4494 ± 0.0001	0.20
144/142	0.8752 ± 0.0003	0.8786 ± 0.0002	0.39
145/142	0.3044 ± 0.0009	0.3065 ± 0.0001	0.69
146/142	0.6313 ± 0.0002	0.6362 ± 0.0001	0.78
148/142	0.2112 ± 0.0001	0.2135 ± 0.0002	1.10
150/142	0.2066 ± 0.0001	0.2096 ± 0.0001	1.45

3.4 Conclusion

The evaporation behavior of Sm and Nd was studied by measuring the ion intensities using TIMS, from their mixture. It was observed that the evaporation rate of Sm is highly dominated than that of Nd, making the isotopes of Nd nearly free from interference, by adopting an extended heating program. The error originated out of fractionation due to heating for long duration was found negligible compared to the error caused by isobaric interference. The observations were employed for direct burn-up evaluation of spent nuclear fuels, without chemical separation of Nd from the fuel matrix, which is explained in Chapter 4.

References

1. Standard Test Method for Atom Percent Fission in uranium Plutonium Fuel (neodymium-148 method), Annual of ASTM Standards, 1996, E321, 96.
2. John Roboz, Introduction to Mass Spectrometry- instrumentation and techniques, 1968, John Wiley & Sons, USA.
3. W. A. Gordon, G. B. Chapman, Determination of work functions near melting points of refractory metals by using a Direct Current Arc, 1972, NASA TECHNICAL NOTE, NASA TN D-6888.
4. Ahindra Ghosh, Text Book of Materials and Metallurgical Thermodynamics, 2003, Prentice Hall of India, Pvt. Ltd., p120.
5. Max Planck, Treatise on Thermodynamics, 1910, DOVER Publications, Inc., Germany, p147.
6. Habermann, Vapor Pressures of the Rare Earth Metals, Ph. D thesis, 1963, Iowa State Univ. Sci. Tech., Iowa, USA.
7. D. White, P. K. Walsh, H. W. Goldstein, D. F. Dever, Rare earths. II. A mass spectrometric determination of the heats of sublimation (or vaporization) of Neodymium, Praseodymium, Gadolinium, Terbium, Dysprosium, Holmium, Erbium and Lutetium, J. Phys. Chem., 1961, 65, 1404-1416.
8. R. G. Johnson, D. E. Hudson, Mass Spectrometric Study of Phase Changes in Aluminum, Praseodymium, and Neodymium, J. Chem. Phys., 1956, 25, 917-1002.
9. W. R. Savage, D. E. Hudson, F. H. Spedding, Mass Spectrometric Study of Heats of Sublimation of Dysprosium, Samarium, Thulium, and Ytterbium, J. Chem. Phys., 1959, 30, 221-227.

10. A Lanthanide Lanthology, Part-II, M-Z, Collection of Notes Concerning Lanthanides and Related Elements, 1994, Molycorp., Mountain Pass, USA.
11. O. Knacke, O. Kubaschewski, K. Hesselmann, Thermo chemical properties of inorganic substances -II, 2nd Edition, 1991, Springer- Verlag.
12. R. E. Bentley, Hand book of Temperature and Humidity Measurement, 1998, Springer.
13. E. A. C. Crouch, Atomic Data and Nuclear Data Tables: Fission Product Yields from Neutron Induced Fission, 1977, Academic Press, New York.
14. B. Wunder, A. Meixner, R. L. Romer, W. Heinrich, Temperature-dependent isotopic fractionation of lithium between clinopyroxene and high-pressure hydrous fluids, Contributions to mineralogy and petrology, 2006,151,112-117.
15. Mukul Sharma, Cynthia, Chen, Neodymium isotope fractionation in the mass spectrometer and the issue of ¹⁴²Nd anomalies in early Archean rocks, Precambrian Research, 2004, 135, 315-319.
16. S. M. C. L. Gioia, M. M. Pimentel, The Sm-Nd Isotopic Method in the Geochronology Laboratory of the University of Brasília, An. Acad. Bras. Ciênc. 2000, 72 , 376-382.
17. D. D. Albert Raj, S. Nalini, R. Viswanathan, R. Balasubramanian, Thermal ionization mass spectrometric study of U-Pu-O system, 1999, Proc. of 8th International Seminar on Mass Spectrometry held at Mumbai, India, p 857.
18. D. Upadhyay, E. E. Scherer, K. Mezger, Fractionation and mixing of Nd isotopes during thermal ionization mass spectrometry: implications for high precision ¹⁴²Nd/¹⁴⁴Nd analyses, J. Anal. At. Spectrom., 2008, 23, 561-565.
19. H. Kanno, Isotopic Fractionation in a Thermal Ion Source, Bulletin of the Chemical Society of Japan, 1971, 44, 1808-1816.

**Burn-up Determination of PHWR Spent Fuel by Direct Loading Method
Using Preferential Evaporation Behavior of Sm.**

4.1 Introduction

The rate of evaporation of Sm and Nd from their nitrate mixture was studied based on their elemental ion intensities by using Thermal Ionization Mass Spectrometry (TIMS), as described in previous chapter. Making use of the large difference in vapor pressures of the two elements, isotopic composition (IC) of Nd, which is close to free from Sm interference could be measured. This study has opened up the possibility of IC measurements of Nd (the fission product monitor) present in a spent nuclear fuel matrix without subjecting it to chemical separation, and hence the evaluation of atom % fission. Present study deals with determination of burn-up of spent nuclear fuel from a Pressurized Heavy Water Reactor (PHWR) by the proposed direct loading method - a simple and time effective method, compared to the conventional burn- up evaluation procedure.

4.1.1 Burn-up

The amount of thermal energy produced by unit mass of a nuclear fuel during its life in a reactor is evaluated by the parameter 'burn-up'. Burn-up data is important in fuel management, fuel development and in evaluation of fuel performance [1]. Burn-up finds importance in nuclear material accounting (NUMAC) also, to evaluate the inventory difference of heavy elements [2-4]. Burn-up measurements play an important role in evaluating fuel performance characteristics like power levels, fuel and clad temperatures and fuel-clad gap conductance [5,6]. For fuels used in experimental reactors, the determination of total fissions provides basic operating parameters for the evaluation of irradiation behavior to eventually assess the power generating costs. For the purpose of fuel management, burn-up

data for each fuel subassembly is required and this is predicted by suitable reactor physics codes [7]. However, the validity of these codes must be often verified by experimental measurements; TIMS is the most accurate and widely accepted technique for the same.

Generally, burn-up is expressed in terms of megawatt days/tonne (MWd/t). It can also be expressed in terms of ‘atom percent fission’ as the energy liberated in a nuclear fuel is proportional to the number of fissions. ‘Atom percent fission’ is defined as the number of fissions per hundred heavy element atoms (of mass greater than 225) initially present in the fuel. The mass limit of 225 is used to ensure all fissile and fertile atoms likely to be present in the fuel are included.

Atom % fission is expressed as follows:

$$\text{Atom \% fission} = \frac{\text{Total fissions} \times 100}{\text{Total atoms of } (U + Pu)} \quad (1)$$

Atom percent fission is a convenient measure of burn-up as most irradiation measurements and burn-up codes arrive at number of fissions first, and not the energy released. Atom percent fission is related to MWd/tonne by a constant factor which depends on nature of the fuel, fissioning nuclide and the kind of reactor system.

4.1.2 Methods for burn-up determination

The conventional methods for burn-up evaluation of spent nuclear fuel can be broadly classified into non-destructive methods and destructive methods.

a) Non-destructive methods [8] involve

- i. Calorimetry
- ii. Neutron flux dosimetry
- iii. Gamma scanning
- iv. Ion probe method

v. Electron probe method

These methods are fast measurement techniques involving 10-15% error in reported value.

b) Destructive methods

Destructive methods involve dissolution of the fuel specimen and analyzing a portion of the aliquot employing a suitable chemical method. Owing to the high radioactivity associated with the fission products in addition to the fissile materials in the spent fuel, a shielded facility like 'hot cell' is employed for carrying out the dissolution. After dissolution, analysis is carried out by spectrophotometry, X-ray fluorescence spectrometry or mass spectrometry.

i. Spectrophotometry

The method involves separation of U and Pu from rare earths (RE) and other fission products by adsorbing them as chloride complexes on an anionic resin. Subsequently, the U and Pu fractions are eluted using different concentrations of HCl, and the fission product effluent is further subjected to an anion exchange separation involving methanol-nitric acid medium to separate the RE fraction (the burn-up monitor). Finally the U, Pu and RE fractions are analyzed by spectrophotometry using Arsenazo-III as chromogenic reagent [9]. The most important requirement for the technique is that the burn-up monitor should have a high fission yield to allow high sensitivity without excessive radioactivity levels. So the total rare earths are considered as the burn-up monitor, in view of the higher fission yield (the summed up fission yield value for 14 rare earths nuclide is 50% for thermal reactor fuel and 45 % for fast reactor fuel) [10]. The method offers an accuracy of about 5% compared to mass spectrometric values.

ii. X-ray fluorescence spectrometry (XRF)

In XRF spectrometry, the sample is excited by irradiating with X-rays from an X-ray source, and the emitted X-rays or fluorescent X-rays are analyzed. The wavelength or energy of the

X-rays reveals the identity of the elements present in the sample; from the intensity of the characteristic X-rays, the concentration of the emitter element in the sample is derived [11].

A sample - spike solution containing known amounts of added fission product element (of natural origin) and uranium, is analyzed by XRF, for individual amounts of the elements. Accuracy of the method is about 3%.

iii) Mass spectrometry

Mass spectrometry remains the method with wide applicability for burn-up measurements. In mass spectrometry, the sample for burn-up measurement is taken in microgram quantity, ionized by suitable ionization method, mass separated and the ion signals pertaining to each isotope is detected by a suitable detector. The comparison of ion intensities provides isotopic ratio essential for deducing the burn-up.

Among all the mass spectrometric techniques, thermal ionization mass spectrometry in conjunction with isotopic dilution technique (ID-TIMS) is an accredited one. American Society for Testing Materials (ASTM) has documented the procedures of heavy elements method and fission product method for burn-up evaluation, employing mass spectrometry [12].

1) Heavy elements methods

- a) Heavy elements isotopic ratio method: The method involves measurement of isotopic ratios of heavy elements (generally U and Pu) present in dissolved fuel specimens before and after irradiation, and application of nuclear cross section data to evaluate burn-up.
- b) Heavy elements difference method: The method involves measurement of the contents of heavy elements in dissolved specimens of both irradiated and un-irradiated fuel.

The major disadvantage of both the above methods is the practical difficulty in availability of un- irradiated fuel sample of the particular spent fuel campaign.

2) Fission Product method

This method is based on measurement of a chosen fission product monitor and the residual heavy atom contents of an irradiated fuel specimen and using the fission yield value of the fission product monitor chosen [13]. The expression for burn-up from this method is given as

$$\text{Burn - up (at \%)} = \left(\frac{\left(\frac{A}{Y} \right)}{\left(H + \frac{A}{Y} \right)} \right) \times 100 \quad (2)$$

where A represents the number of atoms of fission product monitor nuclide or element/g of the dissolver solution; Y is its fission yield for either thermal or fast neutrons; H represents the number of residual heavy elements (generally U and Pu)/ g of the dissolver solution.

Fission product method is most widely used for burn-up evaluation of both thermal and fast reactor fuels.

Among large number of fission products, Nd has the following properties to recommend it as an ideal burn-up indicator [14]:

1. It is not volatile, does not migrate in solid fuels below their re-crystallization temperature, and has no volatile precursors that migrate; therefore local burn-up determinations are possible.
2. It is non-radioactive and requires no decay corrections.
3. It has a low destruction cross section and low formation cross section from adjacent mass chains.
4. Its fission yield is nearly the same for ^{235}U and ^{239}Pu and is essentially independent of neutron energy.

5. It has a shielded isotope, ^{142}Nd which can be used for correcting natural Nd contamination
6. It is not a normal constituent of un-irradiated fuel.
7. Nd has good ion emission characteristics for thermal ionization mass spectrometric measurements.

The analysis of Nd in irradiated fuel does not depend on the availability of pre-irradiation sample data or irradiation history. Atom percent fission is directly proportional to the Nd -to-residual heavy elements ratio in the irradiated fuel sample.

Procedure recommended by ASTM - the conventional method for burn-up determination by fission product method [13,14]:

Step 1: Preparation of a working sample of dissolver solution- Prepare a diluted fuel dissolver solution with 1:1 HNO_3 to obtain a concentration in the range of 100 to 1000 mg of (U + Pu) /liter.

Step 2: Separation of Nd, U and Pu fractions by ion exchange method- In a 100 ml beaker, place 1000 μl of dissolver solution and add about 0.1 ml of 0.1 M ferrous sulfate solution (or few drops of fresh H_2O_2 solution) to convert all the oxidation states of Pu to Pu(IV) and U to U(VI). Prepare a 5 cm long (4 mm dia.) anion exchange column of Dowex resin and wash the column with 10 Column Volumes (CV) of 1:1 nitric acid. Transfer the sample solution on to the column, ensuring complete adsorption of sample onto the resin by washing down walls of the column, above the resin level.

Elute Nd fraction along with other fission products using 2 CV of 1:1 nitric acid (~ 7.5 M) into a 5 ml beaker.

Elute U fraction with 5 CV of 1:5 (~ 3 M) nitric acid into another 5 ml beaker.

Wash the column with 2 CV of 1:5 nitric acid for removal of tailing U fraction.

Finally elute Pu fraction with 1:15 (~ 0.1 M) nitric acid and collect in a 5 ml beaker.

Purification of Nd fraction:

Evaporate the Nd fraction to near dryness and re-dissolve the residue in 500 μ l of 1:1 nitric acid. Prepare a 5 cm long (4 mm dia.) anion exchange column and quantitatively transfer the solution into the column. Elute the column with 14 CV of methanolic nitric acid eluent (prepared by pipetting 10 ml of 1:500 nitric acid into a 100 ml volumetric flask and dilute to the mark with absolute methanol). Discard first 4 CV of eluent and collect remaining 10 CV of eluent containing Nd, along with other lanthanide fission products. Evaporate the solution into dryness. Re-dissolve the residue in 500 μ l of 1:1 nitric acid. Add 1 ml of 70 % HClO₄ and again evaporate to dryness. Re-dissolve the residue in 500 μ l of loading solution (freshly prepared by pipetting 1 ml of 1:1 nitric acid into a 100 ml flask and dilute to the mark with absolute methanol).

Prepare a 6 cm long anion exchange column and transfer the above sample solution containing Nd fraction into the column. Pass 30 CV of wash solution (prepared by pipetting 10 ml of 1:100 nitric acid into a 100 ml flask and dilute to the mark with absolute methanol) through the column. This amount of wash solution is sufficient to elute the other rare earth elements (Pm and heavier) and the actinide elements (Am and heavier). Then strip Nd fraction from the column with 6 CV of eluent (prepared as mentioned above), collect the Nd solution in a 5 ml centrifuge tube. Evaporate this solution to dryness in a hot water bath and dissolve in few drop of 0.75 M nitric acid, load and evaporate on a Re filament for mass spectrometric analysis.

Similarly, evaporate the U and Pu fractions, re-dissolve in few drops of 0.75 M nitric acid and load on Re filaments and affix by evaporation, for mass spectrometric determination of isotopic ratios, atom fractions and average atomic weights.

Step 3: Isotope Dilution Mass Spectrometry (IDMS)

Another aliquot of the dissolver solution (of known weight) is mixed with exactly weighed tracers of U, Pu and Nd (the respective elements enriched with ^{233}U , ^{242}Pu and ^{150}Nd are the recommended tracers) and mixed well to attain homogeneity. The U, Pu and Nd fractions are separated from the homogenous solution by following the chromatographic procedure described above. Individual fractions are collected, evaporated to dryness, re-dissolved in 0.75 M nitric acid and loaded on a Re filament for mass spectrometric determination of $^{233}\text{U}/^{238}\text{U}$, $^{242}\text{Pu}/^{239}\text{Pu}$ and $^{150}\text{Nd}/^{143}\text{Nd}$ ratios from the spiked mixture. From isotopic ratios, concentration of the elements are evaluated using the following IDMS equation.

$$C^S = C^T * \frac{W^T}{W^S} * \left[\frac{R^T(i/j) - R^M(i/j)}{R^M(i/j) - R^S(i/j)} * \frac{1}{R^T(i/j)} * \frac{\langle A \rangle^S}{\langle A \rangle^T} * \frac{(A.F)_i^T}{(A.F)_j^S} \right] \quad (3)$$

where, W^T - weight of tracer; W^S - weight of sample;

$i=233$ and $j=238$ for U, $i=242$ and $j=239$ for Pu & $i=150$ and $j=142$ for Nd;

C^S - concentration of sample; C^T - concentration of tracer (spike);

$\langle A \rangle^S$, $\langle A \rangle^T$ - average atomic weights of sample and tracer;

$(A.F)_i^T$, $(A.F)_j^S$ - atom fractions of tracer and sample;

$R^S_{(i/j)}$, $R^T_{(i/j)}$, $R^M_{(i/j)}$ - isotopic ratio of sample, tracer and mixture, respectively.

Thus, the conventional burn-up determination of spent fuel by wet chemical method is a laborious, lengthy procedure involving multi stage ion exchange separations. Isobaric interference caused by Sm necessitates this tedious separation procedure. As ^{142}Nd is not produced in fission (unlike its natural composition), ^{142}Ce will not make any interference in the measurement of Nd. Also, for long cooled spent fuel, most of the ^{144}Ce would have been converted to ^{144}Nd , as ^{144}Ce has a relatively short half life of 284 days. Hence, the interference for Nd is confined to isotopes of Sm alone, and is free from Ce, in the dissolver

solution. Isotopic ratio measurements by TIMS, by applying correction factor for interfering isotopes is not applicable for fission product monitor, as the isotopic composition (I C) of elements formed as fission products differ from their natural composition. The High Performance Liquid Chromatography (HPLC) offers reasonably accurate results of burn-up for vital theoretical calculations for effective fuel management, but necessitates minimum 5 to 10 μg of Nd per mL of aliquot (corresponding to ~ 10 mg/mL of heavy elements for 1 atom % burn-up) in the dissolver fuel solution for separation [16], leaving considerable volume of radioactive liquid waste and radiation exposure to the personnel. The schematic representation of conventional burn-up determination procedure is shown in Fig. 4.1.

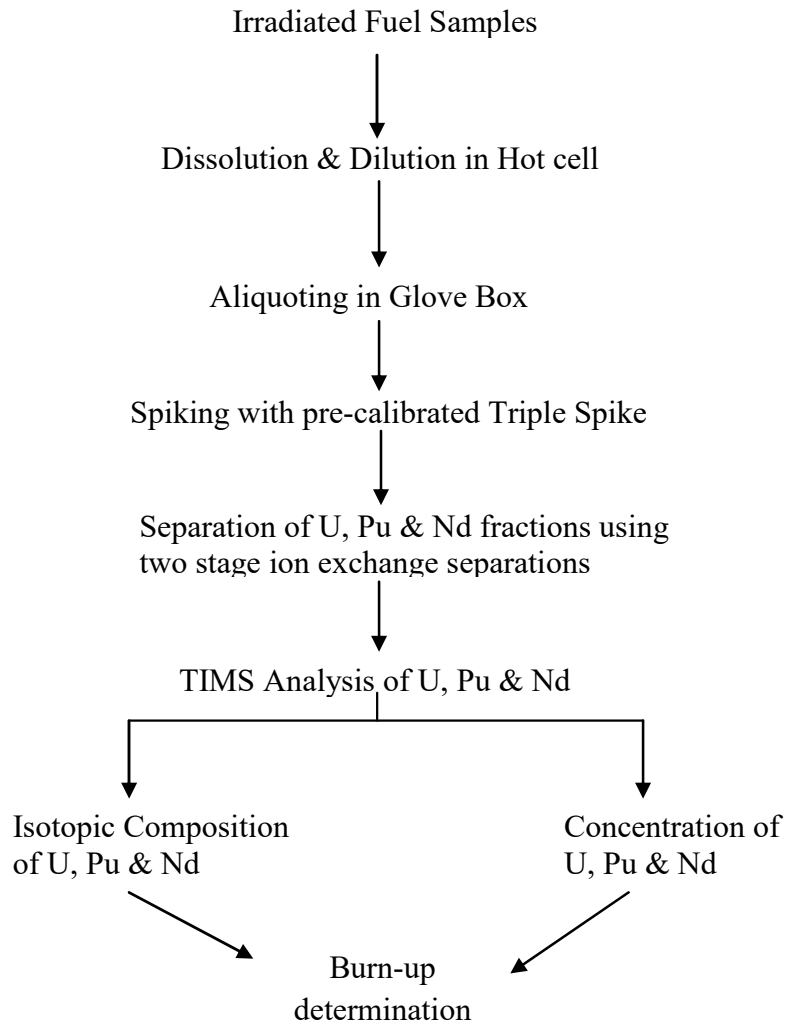


Fig. 4.1 Schematic of steps involved in the mass spectrometric determination of burn-up.

4.1.3 The present study

Present study probes into the feasibility of burn-up determination using sub-microgram quantity of Nd in presence of Sm, by preferentially evaporating the latter making use of its comparatively lower heat of vaporization. The study deals with burn-up evaluation of spent nuclear fuel by direct IDMS method, without subjecting to ion exchange separation of heavy elements and fission product monitor. Spent fuel from Pressurized Heavy Water Reactor (PHWR) was analyzed for burn-up by the proposed method and the results are compared with that determined by conventional method involving HPLC separation of fission product and heavy elements, followed by IDMS.

4.1.4 Previous studies on burn-up measurements

Several burn-up examinations have been reported for irradiated fuels of natural U, MOX fuels containing both U and Pu, advanced fuel like U, Pu mixed carbide, as well as thorium fuel bundles irradiated in research reactors; all were based on either the conventional fission product method or by non-destructive methods. Bera et al reported the burn-up measurement of irradiated mixed oxide (MOX) test fuel pellet, by HPLC-TIMS technique [17]. In another study, Aggarwal et al evaluated the burn-up of spent UO_2 fuel from Kakrapar Atomic Power Station (KAPS) by chemical separation of U and Nd from the fuel matrix followed by IDMS [18]. Irradiated (U, Pu) mixed carbide fuel of Fast Breeder Test Reactor (FBTR), was analyzed by Balasubramanian et al for IC and concentrations of U, Pu and Nd by HPLC separation followed by ID-TIMS technique to deduce the burn-up [19]. Burn-up studies on ThO_2 bundles irradiated in KAPS by separation and determination of Th, U and Nd by conventional procedure was also been reported [20]. Several post irradiation studies of nuclear fuels by non-destructive methods have also been globally reported [21-23].

Several HPLC based studies have been carried out to simplify and reduce the separation time, by many researchers. Joseph et al employed HPLC for the separation and estimation of lighter rare earths by making use of an anion exchanger or a dynamically modified reverse phase column as a cation exchanger; relative performance of both the methods was assessed for the determination of burn-up of nuclear fuels [24]. In another study, Datta et al determined the concentrations of Nd, U and Pu present in spent MOX fuel sample, using HPLC with post-column derivatisation technique using arsenazo (III) as the post-column reagent [25]. Jaison et al reported the development of an HPLC method for the determination of lanthanides, in presence of Th and U, without involving any pre-separation procedure for the matrix elements (Th, U), based on dual gradient elution. This method facilitates the use of

a minor fission product as an internal standard for the accurate and precise quantification of lanthanides [26]. The above studies contributed heavily to fasten the separation process of fission product monitor and heavy elements from the fuel matrix, though helped little towards reduction in waste generation, and sample requirement. However, any approach towards burn-up evaluation based on preferential removal of interfering elements from the fuel matrix by evaporation, could be hardly found in literature.

4.2 Experimental

4.2.1 Instrumentation

Thermal ionization mass spectrometer- model ISOPROBE-T of M/s ISOTOPX, U.K. was used in the present study. The instrumental details are explained in Chapter 3, section 3.2.1. The HPLC system used is of M/s JASCO, Japan.

4.2.2 Sample

Dissolver solution of natural uranium irradiated in Pressurized Heavy Water reactor (PHWR) of burn-up less than 1 atom % was used for the present study.

4.2.3 Direct measurement of IC of heavy elements and fission product monitor

For the present study, accurately weighed dissolver solution of 0.0916 g (~90 μL) was taken in a teflon boat and evaporated to dryness under IR, the residue was dissolved in ~10 μL of 0.75 M nitric acid and loaded on Re filaments (in duplicate) for IC measurements. Two sample aliquots weighing 0.0315 g (~30 μL) and 0.0470 g (~45 μL) were used for spiking in duplicate. Each fraction was double spiked with accurate quantities of standard tracers of U (enriched with ^{233}U) and Nd (enriched with ^{150}Nd) and mixed well. The homogeneous solutions were then evaporated to dryness under IR lamp and re-dissolved in about 10 μL of 0.75 M nitric acid and loaded on Re filaments (in duplicate). The solvent was evaporated by heating the filament by passing current of about 1A, using the sample loading

unit kept in ambient conditions. All the above procedures were carried out in a radioactive fume hood. The filament left with sample residue was loaded in the turret of TIMS for IC measurements.

4.2.4 Isotope measurements by TIMS

The ionization filament and sample filament were heated by passing filament currents of 5.5 A and 1.5 A, simultaneously (with a rate of increment of 0.002 A/s and 0.001 A/s respectively), and optimized the focus parameters with Re^+ ions emitted from the filament. As seen in our earlier studies, the IC measurements of U and Nd present in the same filament is easily possible, in a sequential manner [27]. For un-spiked (pure) dissolver sample, mass spectrometric analysis of U was carried out first at 5.5/2.2 A filament currents. After completing U measurements, the filaments were maintained at the same currents for about two hours, for the removal of Sm present in the sample, by evaporation. Ion intensity of ^{147}Sm was monitored periodically to assess the amount of Sm left in the sample. Ion intensity of ^{147}Sm has shown a steady decrease with time. Once it attained a minimum, nearly steady value (about 2mV), isotopic measurements of Nd were carried out. The spiked sample was also analyzed following the same pattern. From IC, concentrations of U and Nd were evaluated by the IDMS equation. Using the concentrations of U and Nd, burn-up of the dissolver solution was computed.

4.2.5. Validation of the direct loading method with conventional method

In order to evaluate the accuracy of burn-up values determined by direct loading method, an experiment based on routine procedure of HPLC separation of fission monitor (Nd) and actinides (U & Pu) followed by mass spectrometric analysis was carried out with another aliquot of the same dissolver solution.

4.2.5.1 HPLC separation of heavy elements and fission products for burn-up evaluation

The HPLC system kept inside fume hood was employed for separation of the individual lanthanide fission products and actinides (U and Pu) in the dissolver solution. The components such as Rheodyne sample injector, chromatographic column and UV-Vis detector were kept inside the fume hood, whereas the high pressure pumps for the delivery of mobile phase and post column reagent were placed outside, as shown in the schematic in Fig. 4.2, and the photograph of the HPLC components kept outside the fume hood is given in Fig. 4.3.

A reversed phase monolithic column (Merck) with dimension 100 mm x 4.6 mm, surface area $300 \text{ m}^2\text{g}^{-1}$, macro porous structure of $2 \text{ }\mu\text{m}$ and meso porous structure of 13 nm was used for separation. The data acquisition from the UV-Vis detector was connected to a computer through Borwin software interface. Post Column Derivatization (PCD) technique was employed for the detection of lanthanides and actinides. In the PCD method, effluent from the column was mixed with coloring reagent arsenazo (III) using a “T” connector and the metal complex was passed on to a UV-Vis detector. Lanthanides and actinides were separated and eluted using α - Hydroxy Iso Butyric Acid (α -HIBA) as complexing reagent. The mobile phase (0.02M Camphor Sulfonic Acid + 0.1M α -HIBA with pH adjusted to 3.1 with dil. ammonia) was passed through the reverse phase column to establish a dynamic ion exchange surface prior to separation of lanthanide fission products. Fuel solution containing about $10 \text{ }\mu\text{g}$ per ml of Nd was required for HPLC separation (with $100 \text{ }\mu\text{l}$ sample loop); therefore 6.2785 g of dissolver solution was used for the separation, so that the amount of Nd in the solution now meet the requirement for chromatographic separation. Similarly, for IDMS, 3.5819 g of sample was used for spiking, remaining amount of Nd required for HPLC separation was contributed by calculated quantity of Nd tracer added to the solution.

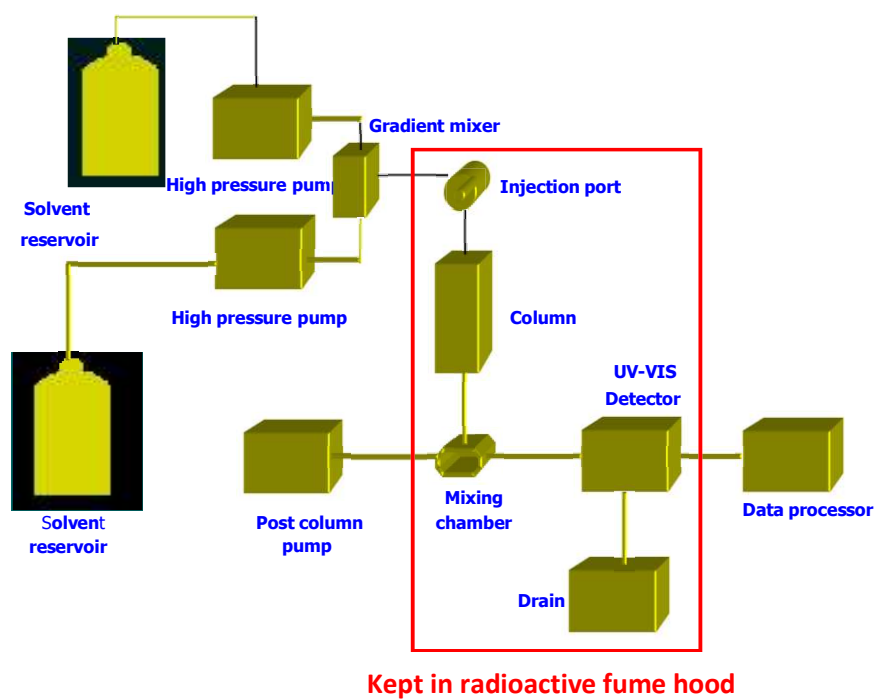


Fig. 4.2 Schematic of the HPLC system used for the present study



Fig. 4.3 Photograph of the components of HPLC system kept outside the fume hood.

The neat dissolver solution (for IC measurements) and the spiked dissolver sample (for concentration measurement) were subjected to HPLC separation of actinides and lanthanides. The eluted fractions of U and Nd collected from HPLC were evaporated to dryness under IR after adding conc. nitric acid; the process was repeated about 10 times for complete removal of the organics present in the fractions. The clear residues were then dissolved in 10 μl of 0.75 M nitric acid and loaded on Re filaments using micro pipette of 10 μl capacity, and evaporated the solvent by ohmic heating. The residues affixed on the filaments were subjected to IC measurements by TIMS. From the mass spectrometric values, atom fractions and mass fractions of individual isotopes were evaluated, which led to the average atomic weights of both the elements. The concentrations of U and Nd in the dissolver solution were determined by the IDMS equation, and thereby computed the atom % fission. The values were then compared with that obtained by the proposed direct loading method.

4.3 Results and Discussion

4.3.1 Isotopic composition of U and Nd present in the directly loaded dissolver solution

The mass spectrum corresponding to m/z 141 to 151, comprising all the isotopes of Nd present in the dissolver solution is shown in Fig. 4.4, and the isotopic abundances are indicated in Table 4.1. It was observed that the abundances of isotopes like ^{145}Nd , ^{146}Nd , ^{148}Nd and ^{150}Nd are in agreement with the expected thermal fission yields (FY), whereas the abundances of ^{143}Nd (18.9%) and ^{144}Nd (29.35%) were found to be different from their reported fission yield values. The value of $^{(144/143)}\text{Nd}$ was found to be 1.55, instead of expected value of 0.91 for ^{235}U or 0.86 for ^{239}Pu based on thermal fissions [10,28]. The $^{(144/143)}\text{Nd}$ ratio remained steady for more than three hours for duplicate filaments. Also, the ratio remained the same for both spiked and un-spiked samples with different amounts of fuel solutions. Any role of ^{144}Sm towards this observation was ruled out by analyzing the Nd

fraction of dissolver solution separated by HPLC in which isotopic abundance of ^{143}Nd and ^{144}Nd were found to be 19.09 and 29.62 respectively with $^{(144/143)}\text{Nd}$ ratio of 1.55 (as obvious from Table 4.1 & Fig. 4.5). This observation is in agreement with an earlier study carried out in our laboratory with PHWR fuel of 0.9 atom% burn-up, in which the $^{(144/143)}\text{Nd}$ ratio was found to be 1.77 [29]. The possible explanation for this observation is the neutron capture process leading to conversion of ^{143}Nd to ^{144}Nd over the long cooling period of 13 years (from July 2001 to June 2014) seen by the present fuel. This is in agreement with the high neutron absorption cross section [30] of ^{143}Nd (325 b) compared to that of other isotopes, of values ^{144}Nd (3.6 b), ^{145}Nd (42 b), ^{146}Nd (1.3 b), ^{148}Nd (2.48 b) & ^{150}Nd (1.2 b). Also, for long cooled spent fuel, most of the ^{144}Ce would have been converted to ^{144}Nd , as ^{144}Ce has a relatively short half life of 284 days.

Isotopic ratios, atom fractions and average atomic weights of U and Nd determined by direct method (without separating Nd and U) and by conventional method (after HPLC separation) are given in Table 4.1. There is no significant change in the values with U isotopes in both the methods. In the case of Nd, the values are matching for un-interfered isotopes (^{143}Nd , ^{145}Nd and ^{146}Nd); whereas, among the interfering isotopes (^{144}Nd , ^{148}Nd and ^{150}Nd), nominal deviation is observed with ^{144}Nd , followed by ^{148}Nd and the highest deviation is with ^{150}Nd . This is because of the fractionation due to prolonged heating at high temperature. Also, the effect of fractionation is more with $^{150}\text{Nd}/^{143}\text{Nd}$ as the difference in masses is highest for it, as explained in chapter 3. The mass spectrum of U and Pu present in the directly loaded dissolver solution is shown in Fig. 4.6, at 5.5/2.2A (ionization filament current/ sample filament current). The relative abundance of ^{238}U is so high that other isotopes of U and Pu are almost invisible in the spectrum. The expanded view of the spectrum (Fig. 4.7) shows that the relative abundance of Pu is too less compared to that of U.

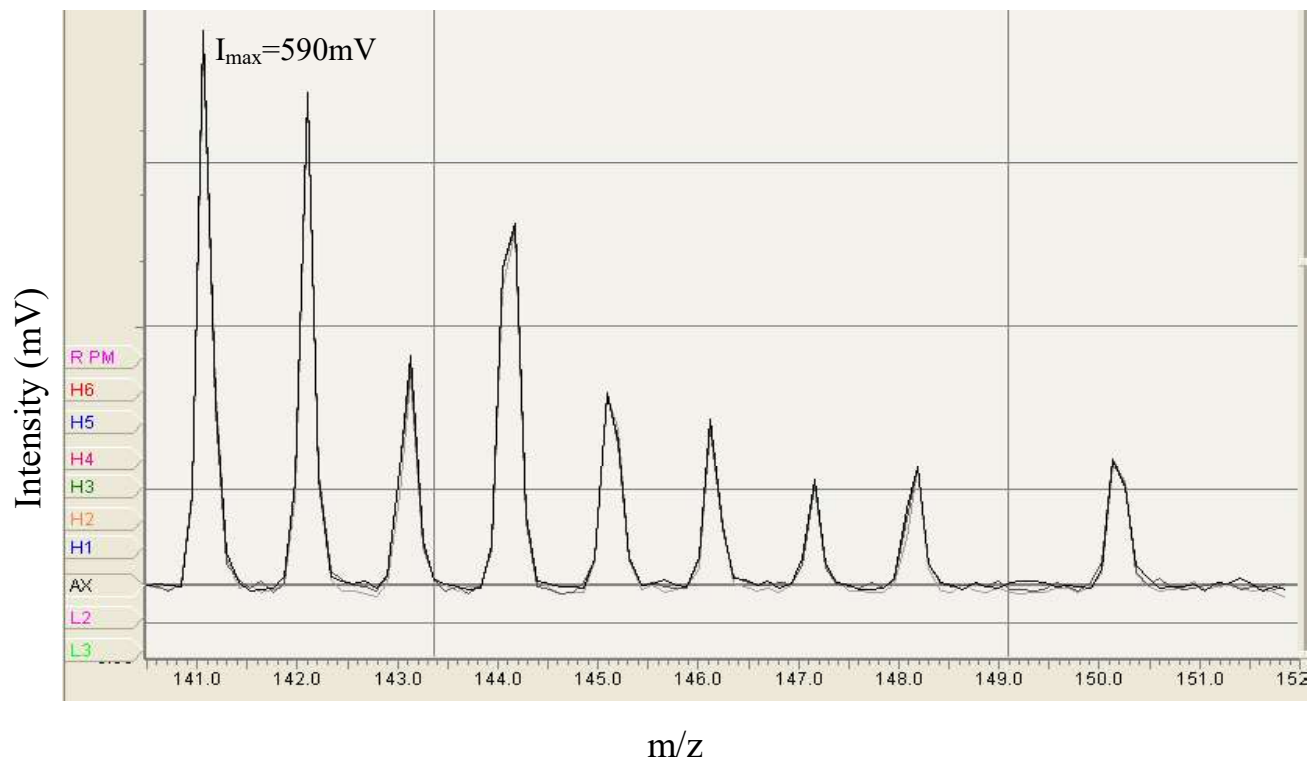


Fig. 4.4 Mass spectrum of Nd present in the directly loaded dissolver solution.

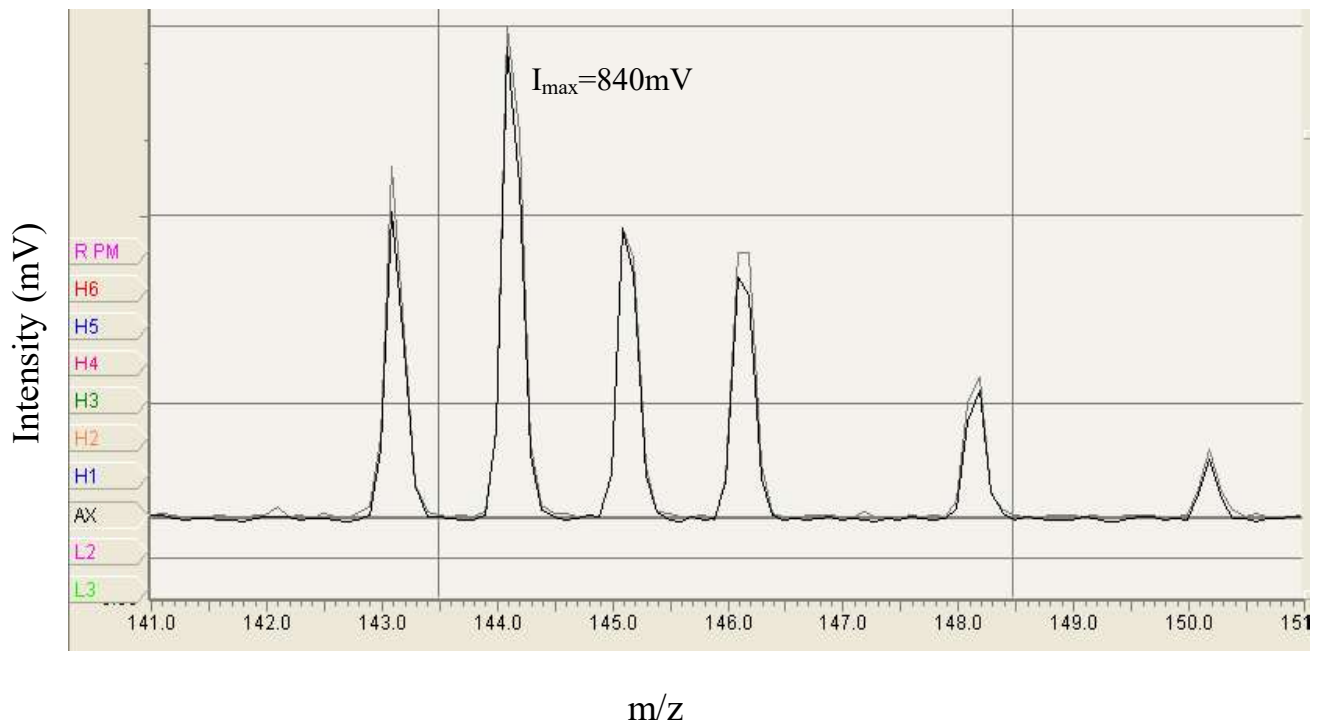


Fig. 4.5 Mass spectrum of Nd fraction of dissolver solution separation by HPLC.

Table 4.1 Isotope composition of U and Nd present in dissolver solution before and after separation of the corresponding pure fractions.

Without separation (direct loading method)			After HPLC separation	
Mass No.	IR w.r.t 238	Atom fraction	IR w.r.t 238	Atom fraction
234	4.4E-05	4.4E-05	2.8E-05	2.8E-05
235	0.0023	0.0023	0.0023	0.0023
236	0.0007	0.0007	0.0007	0.0007
238	1	0.9969	1	0.9968
	Average AW	238.0421	Average AW	238.0421
	IR w.r.t 143		IR w.r.t 143	
143	1	0.1890	1	0.1909
144	1.5527	0.2935	1.5516	0.2962
145	0.8519	0.1610	0.8538	0.1630
146	0.7669	0.1449	0.7657	0.1462
148	0.5293	0.1001	0.5204	0.0994
150	0.5890	0.1113	0.5461	0.1043
	Average AW	145.2430	Average AW	145.2001

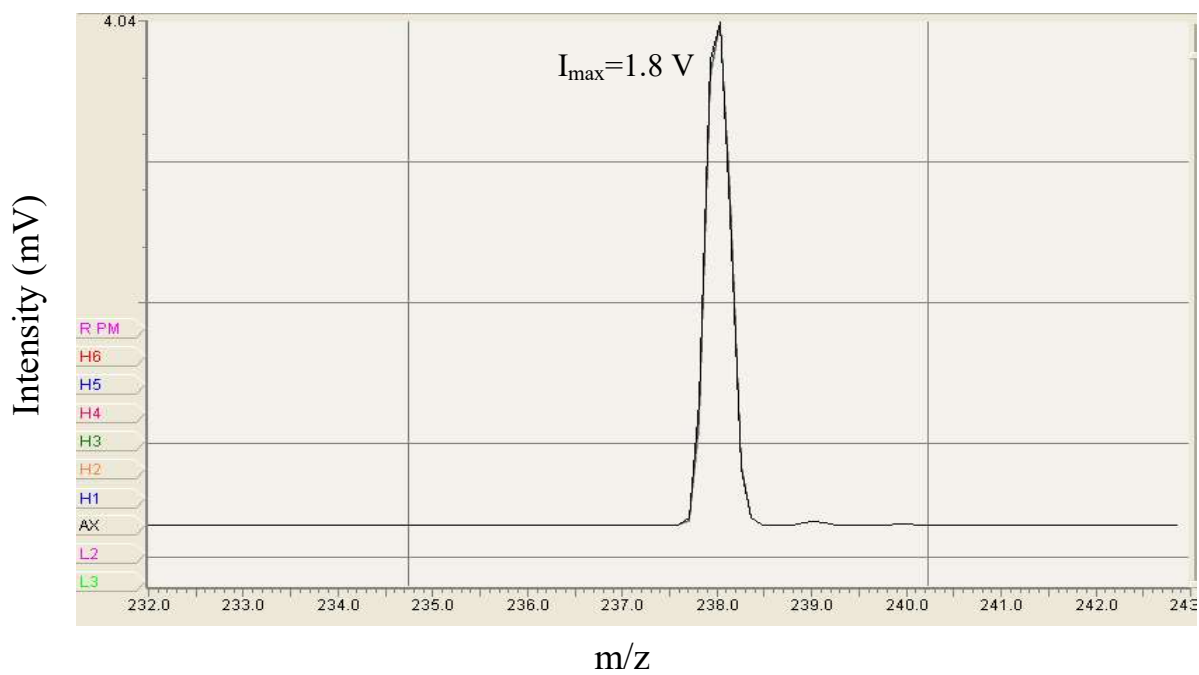


Fig. 4.6 Mass spectrum of U and Pu present in the directly loaded dissolver solution.

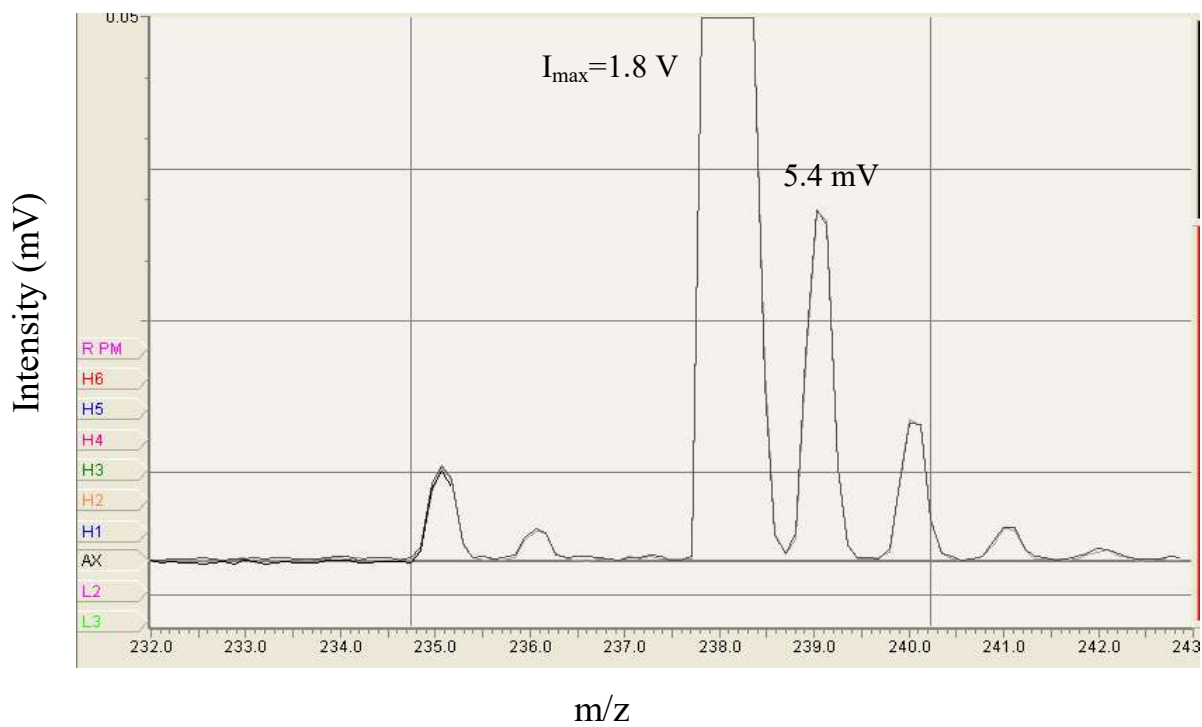


Fig. 4.7 The expanded view of fig. 4.7, showing the abundances of Pu and U.

4.3.2 Burn-up measured by direct loading method

Burn-up was computed using following equation,

$$\text{Burn-up (at \%)} = \left(\frac{\left(\frac{A}{Y}\right)}{\left(H + \frac{A}{Y}\right)} \right) \times 100$$

The fractional fission yield (Y) was computed by comparing the observed value of $^{(143+144)}\text{Nd}$ / ^{148}Nd with different fractional combinations of U and Pu, and found to be ~ 50% from ^{235}U and 50% from ^{239}Pu . The fission yield data used for calculation of burn-up is given in Table 4.2

Table 4.2 Thermal fission yield (Y) data for ^{235}U , ^{239}Pu and for 50% ^{235}U +50% ^{239}Pu

Fission product monitor	Y value for ^{235}U [10]	Y value for ^{239}Pu [10]	Y value for 50% ^{235}U +50% ^{239}Pu
Nd-143	5.94	4.47	5.205
Nd-144	5.38	3.82	4.60
Nd-145	3.92	3.12	3.52
Nd-146	2.96	2.53	2.745
Nd-148	1.67	1.71	1.69
Nd-150	0.645	0.991	0.818
Nd-total	20.515	16.641	18.578

Initially, IDMS was carried out with ^{150}Nd tracer, which yielded U/Nd ratio deviating much in positive direction compared to the reference value (determined by HPLC-IDTIMS method), and correspondingly reflected in burn-up values also. This is because of the

interference of residual ^{150}Sm in $(^{150/143}\text{Nd})_{\text{sam}}$ and in $(^{150/143}\text{Nd})_{\text{mix}}$ values, while $(^{150/143}\text{Nd})_{\text{tracer}}$ remains unaffected.

In order to overcome this scenario, IDMS was repeated for dissolver solution, with ^{142}Nd tracer (enriched with 98.3% ^{142}Nd) advantage being the isotope is present only in tracer, not in the dissolver sample. Any signal corresponding to mass 142 in sample is only of ^{142}Ce isotope, which made it possible to correct for $[(^{142}\text{Nd}+^{142}\text{Ce})/^{143}\text{Nd}]_{\text{mix}}$, where as this correction is not possible with the use of ^{150}Nd tracer, as the corresponding isotope of Sm is present both in sample as well as in mixture. The correction is applied as indicated below.

$$\text{IR}_{\text{sam}} = ^{142}\text{Ce}_{\text{sam}}/^{143}\text{Nd}_{\text{sam}}$$

$$\text{IR}_{\text{mix}} = (^{142}\text{Ce}_{\text{sam}} + ^{142}\text{Nd}_{\text{spk}})/(^{143}\text{Nd}_{\text{sam}} + ^{143}\text{Nd}_{\text{spk}})$$

As atom fraction of $^{143}\text{Nd}_{\text{spk}} \ll ^{143}\text{Nd}_{\text{sam}}$,

$$\text{IR}_{\text{mix}} = (^{142}\text{Ce}_{\text{sam}} + ^{142}\text{Nd}_{\text{spk}})/^{143}\text{Nd}_{\text{sam}}$$

Corrected value of IR_{mix} , denoted as $\text{IR}_{\text{mix}}^{\text{corr}} = \text{IR}_{\text{mix}} - \text{IR}_{\text{sam}}$

For making this correction, IR_{mix} was measured after exactly following the same heating pattern and equal hold up time (about two hours) as that for IR_{sam} measurements, to minimize the time dependent error.

In this way, contribution of Sm in burn-up determination gets confined to its effect on average atomic weight of Nd alone, as the interfering isotopic ratios are not involved in any step of its calculation. The mass spectrum of Nd present in sample-spike mixture, after heating for about 2 hours is shown in Fig. 4.8. The U/Nd ratios determined by direct loading method using ^{150}Nd and ^{142}Nd as tracers, and that obtained by conventional method are given in Table 4.3 .

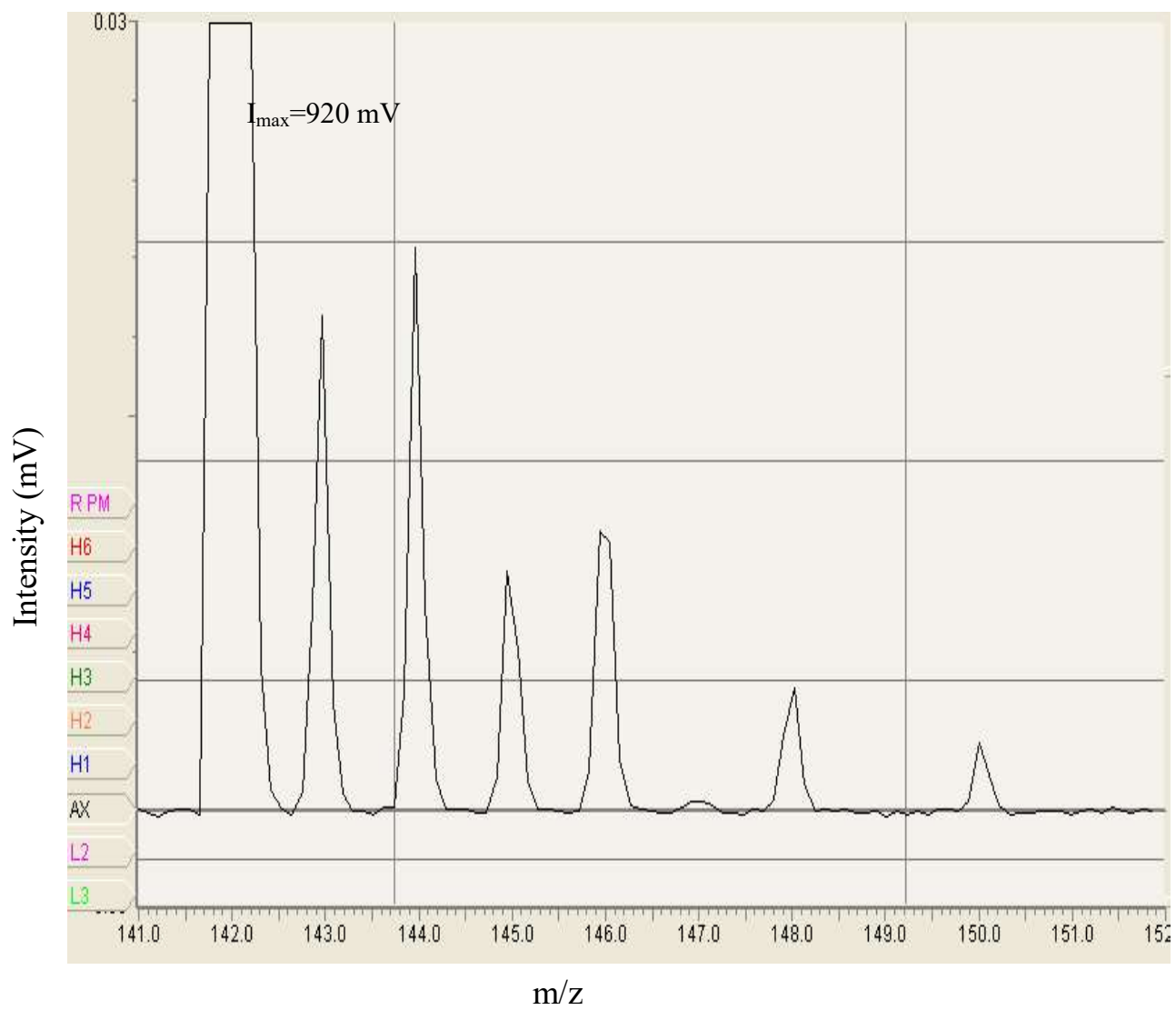


Fig. 4.8 Mass spectrum (m/z of 141 to 152) of spiked (with ^{142}Nd) dissolver solution, after heating for two hours at 5.5/2.2 A.

4.3.3 Separation of heavy elements and lanthanides by HPLC

Direct injection of pure dissolver solution and its double spiked mixture subjected to HPLC separation yielded heavy elements and fission product fractions, as shown by the chromatogram in Fig. 4.9. The relative amount of Pu was so small that its signal was masked by U peak which appeared at a retention time of 2.9 min., whose abundance was much higher than that of rest of the elements. The fission product, Sm was found to appear at 6.4 min. and Nd had a retention time of 13 minutes.

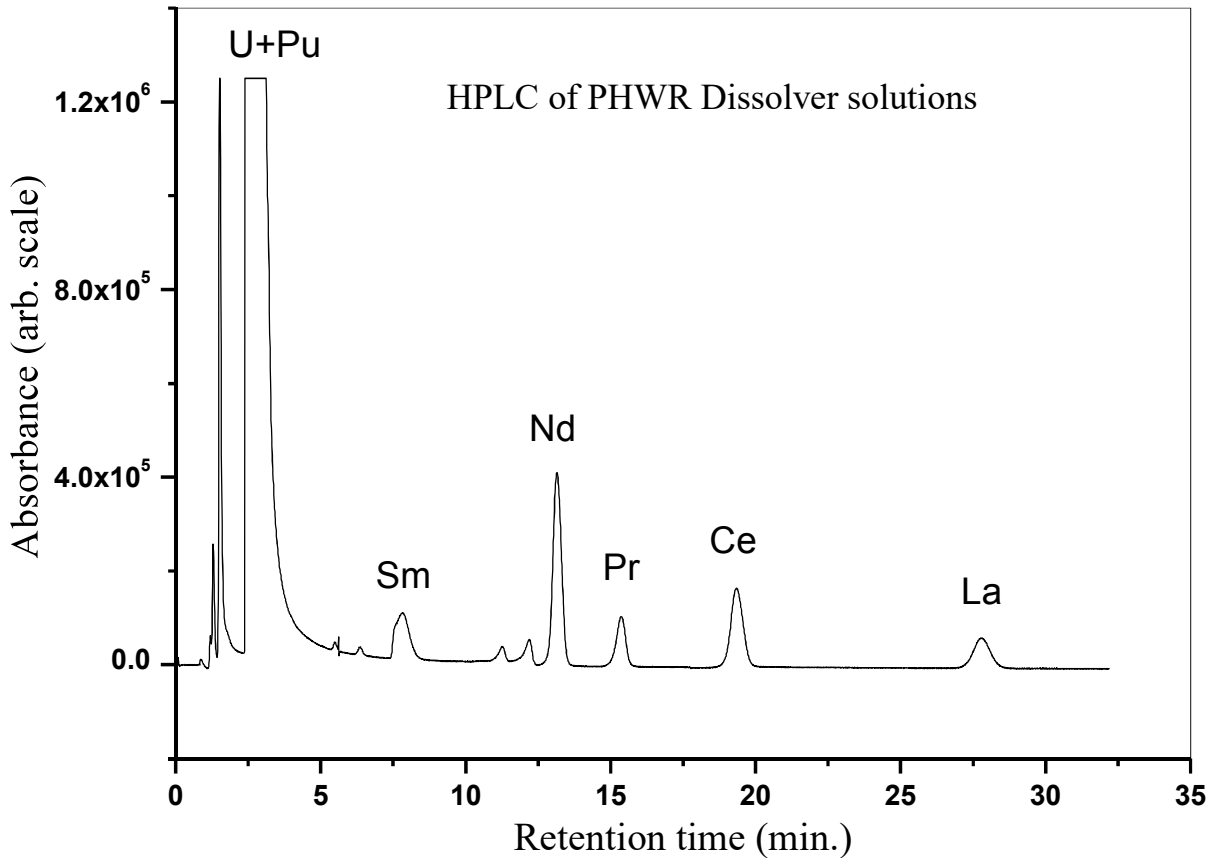


Fig. 4.9 Chromatogram of PHWR dissolver solution using HPLC.

Column: Reversed phase Monolith; mobile phase: CSA and HIBA; PCD with Arsenazo (III) at 655nm.

4.3.4 Mass spectrometric measurements of U and Nd fractions separated by HPLC

The U and Nd fractions loaded on individual filaments were analyzed independently, by TIMS. The filament current was raised to 5.5/1.0A, and optimized the focusing parameters with Re^+ . The filament (with U fraction) current was further raised to 5.5/2.2 A and measured the isotopic composition of U. The spectrum was free of Pu peaks, as shown in Fig. 4.10. Measurement of Nd was also carried out in the same way at 5.5/2.25 A, and the spectrum is shown earlier, in Fig. 4.5.

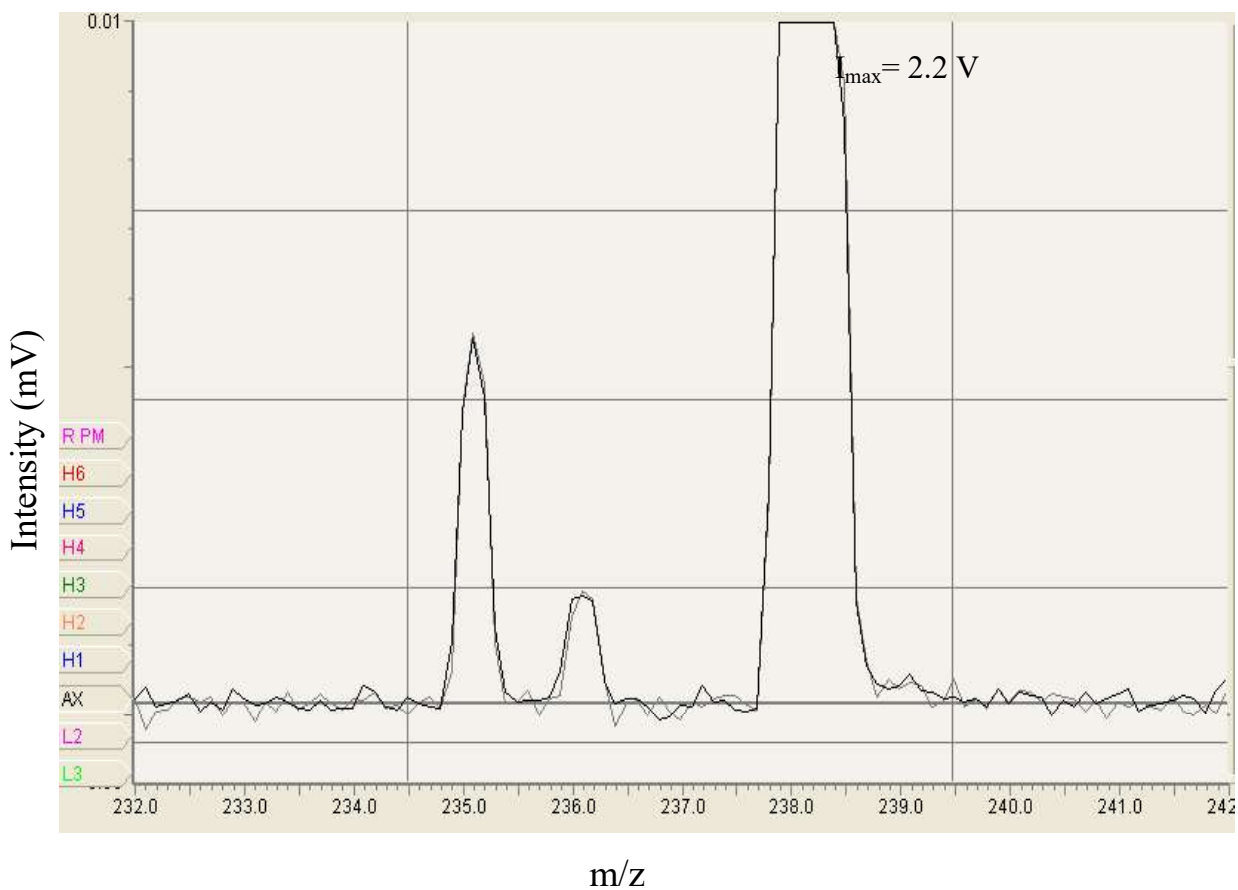


Fig. 4.10 Mass spectrum of U fraction of dissolver solution separated by HPLC.

4.3.5 Burn-up determination from U and Nd concentrations

The Pu content of the dissolver solution was determined by HPLC technique and found to be only 0.3% of that of U. Hence in this study, for the computation of total heavy element content, Pu was not taken into account.

Table 4.3 shows the burn-up values determined by direct method based on total Nd (0.84 at %), compares well in terms of accuracy considering the true value as 0.82 at % (determined by HPLC-TIMS method). Atom % burn-up values obtained based on ^{143}Nd was too low (0.60) as its abundance is lower than that expected, because of its possible conversion to ^{144}Nd by neutron capture. Similarly, with ^{148}Nd , atom % burn-up was found to be higher (0.93) than the reference value (0.81) as ^{148}Nd was interfered by residual ^{148}Sm . The atom fraction of ^{148}Nd after HPLC separation is 0.0994, and that without separation is 0.1001 (see Table 4.1). The above explanation given for ^{148}Nd is valid for ^{150}Nd also. Better accuracy (2.4%) was observed with burn-up estimated based on total Nd, rather than that with individual isotopes of Nd, and by using ^{142}Nd tracer. This is because of the following facts. (i) in IDMS equation [(equation (3))] for concentration measurement, IR_{sam} and IR_{mix} of $^{(142/143)}\text{Nd}$ are unaffected by Sm isotopes; (ii) the effect due to deviation in average atomic weight was found to be very small; (iii) deviation in individual atom fractions were not affected in burn-up evaluation. Thus the atom % burn-up determined by the direct method shows a deviation of < 3% compared to the conventional method.

Table 4.3 Comparison of burn-up values determined by the proposed direct loading method and the conventional method.

Burn-up monitor used	Burn-up measured by Direct loading method		Burn-up measured by Conventional method (HPLC- TIMS method)
	(with ^{150}Nd tracer)	(with ^{142}Nd tracer)	(with ^{150}Nd tracer)
	U/Nd ratio- 1400.7 Burn up (at %)	U/Nd ratio- 1036.9 Burn up (at %)	U/Nd ratio- 1074.2 (with ^{150}Nd tracer)
Total Nd	0.65	0.84	0.82
Nd-143	0.52	0.57	0.60
Nd-(143+144)	0.60	0.77	0.83
Nd-(145+146)	0.60	0.77	0.82
Nd-148	0.57	0.93	0.81

4.4 Merits of the proposed direct loading method

In direct loading method, the quantity of dissolver sample solution used for isotopic composition measurement was only 90 μl (containing ~ 106 ng of Nd). For two duplicate spike mixtures (A & B) with ^{150}Nd tracer, the samples taken were 30 μl (36 ng of Nd) and 45 μl (54 ng of Nd), respectively. For experiments with ^{142}Nd spike, the quantities of dissolver solution were still reduced to 40 μl (for IC), 20 μl and 30 μl for spike mixtures, A and B, respectively (because of the possible evaporation of solvent during the time gap of about two months between the two sets of experiments). Even with few tens of nanograms of Nd, ion intensity of about 200 mV was observed for ^{144}Nd , the most abundant isotope in this dissolver solution and it remained steady for more than 2 hours. For HPLC separation,

minimum of about 10 μg of Nd must be present in the solution to be separated; and the corresponding amount of dissolver solution required is ~ 6.3 g for isotopic composition and 3.6 g for spike mixing. The above comparison, on the amount of sample needed for the burn-up evaluation indicates that only extremely small amount of sample is required for the direct loading method. This is advantageous in view of radiation exposure, sample economy and minimum generation of radioactive waste. Moreover, in direct method, the sample was directly loaded on to the filament. Hence both heavy elements and burn-up monitor present in the same filament can be analyzed in a sequential manner, without changing the filament, which reduces the filament requirement to one third of that required in conventional procedure, which correspondingly reduces the radioactive solid waste generation. The method also offers convenience of double spiking (or even triple spiking, if Pu also to be quantified) with same sample aliquot and it doesn't demand any reagents, chemicals (except nitric acid) or equipments for sample preparation.

4.5 Demerits

The accuracy of burn-up values determined by direct loading method (2.4%) is not close to that offered by conventional method ($\sim 1\%$). Though prolonged exposure of sample to higher temperature for more than a couple of hours minimizes the error due to isobaric interference, it introduces an additional error in isotopic composition due to fractionation. The rate of preferential evaporation of Sm is quite faster at the initial hour of exposure to high temperature and slows down towards the end, leaving a minimum, but non negligible contribution in the atom fractions of ^{148}Nd and ^{150}Nd , which contribute towards an enhancement in average atomic weight of Nd. Time dependent error in measurement of $^{142}\text{Ce}/^{143}\text{Nd}$ ratio in sample to correct the value of IR_{mix} can be minimized by following

similar heating and measurement patterns for both sample and mixture analysis, after reaching desired temperature in equal heating rate.

4. 6 Conclusion

A method based on preferential evaporation of Sm was studied for an easy, cost and time effective determination of burn-up of spent nuclear fuel, by ID-TIMS, without any prior separation of heavy elements and burn-up monitor. Burn-up values based on the total amount of Nd and its isotopes are compared with the corresponding values obtained by conventional method. As the technique doesn't involve any ion exchange separation procedure, it is free of liquid waste generation and demands use of only micro liter level of sample, which makes it less prone to operational radiation exposure. The method is less accurate compared to the conventional one, but competitive with the accuracy of ICP-MS (2-3 %) which generates radioactive vapor as well as liquid waste. Hence the proposed direct loading method can be treated as a fast, simple and most fuel economic procedure for applications which can bear an error of ~ 3%, particularly useful to evaluate reactor physics codes, as large number of burn-up measurements are to be carried out for fuel pins from different locations in the core.

References:

1. J. E. Rein, B. F. Rider, Burn-up determination of nuclear fuels, Progress Report, AEC Re- search and Development Report, 1962, TID-17385.
2. C. K. Mathews, H. C. Jain, V. D. Kavimandan, S. K. Aggarwal, Tracer techniques in the input accountability of plutonium in reprocessing plants, Nucl. Technol., 1979, 42, 297–303.
3. P. R. Trincerini, H. Ullah, S. Facchetti, Input measurements in reprocessing plants, Nucl. Sci. Technol., 1980, 2, 295–303.
4. F. Franssen, W. Franzel, Input tank calibration at the Eurochemic plant, 1969, ETR 236

5. M. Rahgoshay, Y. Rahmani, A study of the effects of changing burn-up and gap gaseous compound on the gap convection coefficient (in a hot fuel pin) in VVER-1000 reactor, NUKLEONIKA, 2007, 52, 93-98.
6. Water reactor fuel element modeling at high burn-up and its experimental support, Proceedings of a Technical Committee meeting, 1994, IAEA-TECDOC-957.
7. B. F. Rider, C. P. Ruiz, J. P. Peterson, R. S. Seymour, J. L. Jaech, F. R. Smith, Burn-up- A code for calculation of nuclear fuel burn-up from U, Pu and Nd mass spectrometric measurements, U. S. Atomic Energy Commission Report, 1965, GEAP-4811.
8. S. T. Hsue, T. W. Crane, W. L. Talbert, J. C. Lee, Nondestructive assay methods for irradiated nuclear fuels, 1978, LA-6923.
9. K. Dhamodharan, A. Pius, Determination of plutonium present in highly radioactive irradiated fuel solution by spectrophotometric method, Nuclear Engg. Tech., 2016, 48, 727-732.
10. E. A. C. Crouch, Atomic Data and Nuclear Data Tables: Fission Product Yields from Neutron Induced Fission, 1977, Academic Press, New York.
11. E. L. T. Reis, M. Scapin, M. E. B. Cotrim, V. L. Salvador, M. A. F. Pires, Impurities determination on nuclear fuel element components for the IEA-R1 research reactor by analytical methods based on ED-XRF and ICP-OES, International Nuclear Atlantic Conference - INAC, 2009, Rio de Janeiro, RJ, Brazil.
12. 'Atom percent fission in uranium and plutonium fuel (mass spectrometric method)', American Society for Testing & Materials Standard Method, 1974, ANSI/ASTM E-244-69.
13. 'Standard Test Method for atom percent fission in Uranium Plutonium Fuel (Neodymium-148 method)', Annual of ASTM Standards, 1996, E321,96.

14. Standard Test Method for atom percent fission in Uranium and Plutonium fuels (Neodymium-148 method), American Society for Testing Materials, 1974, E321, 69.
15. K. G. Heumann, Isotope Dilution Mass Spectrometry in Inorganic Mass Spectrometry, 1988, John Wiley & Sons, New York, p301-376.
16. N. Sivaraman, S. Subramaniam, T. G. Srinivasan, P. R. Vasudeva Rao, Burn-up measurements on nuclear reactor fuels using high performance liquid chromatography, J. Radioanal. Nucl. Chem., 2002, 253, 35-40.
17. S. Bera, R. Balasubramanian, A. Datta, R. Sajimol, S. Nalini, T. S. LakshmiNarasimhan, M. P. Antony, N. Sivaraman, K. Nagarajan, P. R. V. Rao, Burn-up measurements on dissolver solution of mixed oxide fuel using HPLC-Mass spectrometric method, Int. J. Anal. Mass Spectrom. Chromatogr., 2013, 1, 55-59.
18. S. K. Aggarwal, P. G. Jaison, V. M. Telmore, P. S. Khodade, R. V. Shah, R. Govindan, V. L. Sant, P. M. Shah, Determination of burn-up of irradiated PHWR fuel samples from KAPS-1 by mass spectrometry, BARC Report, 2007, BARC/E/020.
19. R. Balasubramanian, D. D. Albert Raj, S. Nalini, M. Sai Baba, Mass spectrometric studies on irradiated (U, Pu) mixed carbide fuel of FBTR, Int. J. Nucl. Energy Sci. Technol., 2005, 1, 197-202.
20. S. K. Aggarwal, P. G. Jaison, V. Telmore, R. V. Shah, V. L. Sant, K. Sasibhushan, A. R. Parab, D. Alamelu, Burn-up determination of Thoria samples by Isotope Dilution-Thermal Ionisation Mass Spectrometry, BARC Report, 2010, BARC/E/003.
21. R. I. Dobrin, T. Craciunescu, M. Pavelescu, Candu, Triga fuel burn-up determination using axial and tomographic gamma scanning, Romanian Reports in Physics, 2011, 6, 1009-1014.

22. S. N. Jha, A. Kadam, S. K. Kapoor, N. C. Das, Determination of impurities in thorium based fuel using wavelength dispersive X-ray fluorescence technique, BARC report, 2002, BARC/ E/ 024.
23. K. Joe, Y. S. Jeon, J. S. Kim, S. H. Han, J. G. Kim, W. H. Kim, Separation of burn-up monitors in spent nuclear fuel samples by Liquid Chromatography, Bull. Korean Chem. Soc., 2005, 26, 569-574.
24. M. Joseph, D. Karunasagar, B. Saha, Development of high performance liquid chromatography for rapid determination of burn-up, 1996, IGC report-184.
25. A. Datta, N. Sivaraman, T. G. Srinivasan, P. R. Vasudeva Rao, Rapid separation of lanthanides and actinides on small particle based reverse phase supports, Radiochimica Acta, 2010, 98, 277-285.
26. P. G. Jaison, N. M. Raut, S. K. Aggarwal, Direct determination of lanthanides in simulated irradiated thorium fuels using reversed-phase high-performance liquid chromatography, J. Chromatography A, 2006, 1122, 47-53.
27. R. Sajimol, P. Manoravi, S. Bera, M. Joseph, Effect of laser parameters on the measurement of U/Nd ratio using Pulsed Laser Deposition followed by Isotopic Dilution Mass Spectrometry, Int. J. Mass. Spec., 2015, 387, 51-55.
28. E. A. Melaika, M. J. Parker, J. A. Petruska, R. H. Tomlinson, The relative abundances of neodymium and samarium isotopes in the thermal neutron fission of ^{235}U and ^{233}U , Canadian Journal of Chemistry, 1955, 33, 830-836.
29. R. Balasubramanian, S. Nalini, N. Sivaraman, Burn-up determination of Pressurized Heavy Water Reactor fuel by Thermal Ionization Mass Spectrometry, 2001, private communication.
30. Karlsruhe's chart of the nuclides (1974).

Direct burn-up determination of fast reactor mixed oxide (MOX) fuel by preferential evaporation of interfering elements

5A.1 Introduction

For sodium cooled fast reactors, U, Pu Mixed Oxide (MOX) fuel is chosen as the driver fuel due to its high burn-up potential, high melting point and ease of fuel fabrication and reprocessing [1]. The Prototype Fast Breeder Reactor (PFBR) located at Kalpakkam (India) is expected to attain criticality soon, using MOX fuel. For PFBR, the target burn-up is expected to be about 100 GWd/t. In order to assess the performance of the fuel for the proposed target burn-up, a test fuel assembly consisting of 37 MOX fuel pins was irradiated in Fast Breeder Test Reactor (FBTR) [2]. After attaining a peak burn-up of ~112 GWd/t, post irradiation examination was carried out to evaluate the fuel performance. Burn-up of this fuel was determined in our laboratory by Bera et al by conventional ASTM procedure using HPLC separation of U, Pu and Nd fractions followed by isotopic composition measurement by TIMS [3].

The results of study carried out for burn-up evaluation of PHWR fuel by direct loading method was found to be comparable with the results obtained by conventional method. Therefore, the proposed direct loading method was attempted with irradiated fast reactor MOX fuel, by following a sequential pattern of analysis. The present study deals with evaluation of burn-up of fast reactor spent fuel by direct loading method without separation of any constituent elements, and comparison of the observed values with the reported data [3] evaluated by conventional method [4,5]. In the case of fast reactor fuel, isobaric interference of ^{238}U with ^{238}Pu and that of ^{241}Am with ^{241}Pu necessitates ion exchange separation of the constituent elements, in addition to Sm-Nd isobaric interference. The fact that heat of

vaporization of Am is 1.49 times lower than that of Pu was utilized for its removal by an extended heating program. Interference from ^{238}U makes it necessary to correct the ratio $^{238}\text{Pu}/^{239}\text{Pu}$ by alpha spectroscopy [6] in conventional method. Whereas, in direct loading method, by making one set of isotopic ratio ($^{238}\text{Pu}/^{239}\text{Pu}$) measurements before building up of uranium signals (as can be seen from the appearance of other isotopes of U, such as ^{235}U or ^{233}U), the $^{238}\text{Pu}/^{239}\text{Pu}$ ratio can be determined almost free from uranium interference. Very low contribution of ^{238}Pu isotope towards the total amount of Pu makes any trace interference of ^{238}Pu on ^{238}U less serious. Concentrations of individual elements were determined by IDMS by the addition of known quantities of proper spikes for each element of interest. This chapter deals with all the above points in detail, as described below.

5A.2 Experimental

5A.2.1 Instrumentation

Thermal ionization mass spectrometer (ISOPROBE-T, of M/s ISOTOPX, U. K) was employed in the present work, details of the instrumentat is given in Chapter 3, section 3.2.1.

5A.2.2 Sample

Uranium- Plutonium mixed oxide (MOX) fuel of composition $(\text{U}_{0.79} \text{Pu}_{0.21})\text{O}_2$ with U having an enrichment of 53.5% ^{233}U irradiated in FBTR was used as the sample [7]. The plutonium isotopic abundance is: ^{238}Pu (0.23%); ^{239}Pu (72.89%); ^{240}Pu (24.20%); ^{241}Pu (1.55%); ^{242}Pu (1.13%) [3].

5A.2.3 Sample preparation for IDMS

In the proposed direct loading method (i.e., without any ion exchange separation of individual elements like U, Pu & Nd), dissolver solution of MOX irradiated in FBTR was used. About 40 μl of dissolver solution was evaporated to dryness under IR lamp in a teflon boat. The residue was subsequently re-dissolved in about 8 μl of 0.75 M nitric acid and

loaded on to Re filament (in duplicate) for isotopic composition measurements. Accurately weighed sample aliquot of 0.0412 g (~40 μ l) was used for spiking. The sample was triple spiked with accurate quantities of standard tracers of natural U (as the sample was enriched with ^{233}U), Pu (which was mainly ^{239}Pu) and Nd (enriched with ^{142}Nd) and mixed well. The homogeneous solution was subsequently evaporated to dryness under IR lamp and re-dissolved in about 8 μ l of 0.75 M nitric acid and loaded on to two Re filaments for IDMS measurements.

5A.2.4 Isotopic composition measurements by TIMS

Prior to making isotopic composition measurement of sample, a collector gain calibration was carried out, as the measurements were done in static multi-collection mode. The filament loaded with neat dissolver solution (for isotopic composition measurement) was heated by raising the current slowly to 1.5 A, and the ionization filament to 5.5 A, regulating the heating rates as 0.001 A/s and 0.002 A/s, respectively with the help of an in-built heating program. Using the Re^+ signal that originated from the filament material, beam focus conditions were optimized. From our earlier studies [8,9] it was well established that for U-Nd system, isotopic composition measurement of U and Nd present in the same filament has been easily possible in a sequential manner. As the present sample contained Pu in significant quantities, the sequence of analysis was started with Pu, then U and finally Nd, followed by a re-analysis of Pu (only for unspiked sample), considering the interference and vapor pressure factors which is explained in detail in 'Results and Discussion' section.

When the sample filament current reached 1.95A, ion intensities corresponding to Pu isotopes started to appear. After attaining sufficient ion intensities at 1.96A, one set of isotopic ratios were measured for $^{238}\text{Pu}/^{239}\text{Pu}$, before the appearance of ^{238}U signal, (the absence of U can be ascertained by looking for the signal at mass ^{233}U and ^{235}U).

Subsequently the filament current was slowly raised to 2.25A to accelerate the preferential evaporation of Am, and isotopic ratios $^{240}\text{Pu}/^{239}\text{Pu}$ and $^{242}\text{Pu}/^{239}\text{Pu}$ were measured, which are not affected with isobaric interference. The measurements of $^{241}\text{Pu}/^{239}\text{Pu}$ could not be done at this stage as there existed considerable intensity of ^{241}Am . Subsequently, the isotopic composition measurement of U was carried out at same filament current, 2.25 A. Then the filament temperature was maintained constant for about 2 hours, in order to evaporate and remove Sm and Am from the sample simultaneously, before moving on to isotopic composition measurement of Nd. After ensuring near complete elimination of Sm, the collector positions were adjusted for ion intensity measurements of Nd isotopes, and isotopic composition measurement of Nd was carried out. Subsequently, the collector positions were readjusted for measurements of Pu isotopes, mainly for $^{241}\text{Pu}/^{239}\text{Pu}$ ratio, which was almost free of interference from ^{241}Am at this juncture.

The triple spiked dissolver sample was analyzed for $^{240}\text{Pu}/^{239}\text{Pu}$, $^{233}\text{U}/^{238}\text{U}$ followed by $^{142}\text{Nd}/^{143}\text{Nd}$. The Pu and U ratios were measured at 2.25 A, as soon as the ion intensities gained sufficient intensities. However for measuring Nd ratio, the same filament current and equal hold up time were maintained as that of the sample filament during IC measurements, in order to account for cerium correction [8]. From isotopic composition and sample-spike mixture analysis, concentration of U, Pu and Nd were evaluated by the IDMS equation [10] and atom % burn-up was computed and the results were compared with the reported data, determined by conventional method.

5A.3 Results and Discussion

5A.3.1 Measurement of isotopic ratios of Pu in presence of U and Am

The isotopic analysis of dissolver solution without separating constituent elements resulted the following: out of the five isotopic intensities (^{238}Pu , ^{239}Pu , ^{240}Pu , ^{241}Pu and ^{242}Pu)

required for Pu determination, ^{238}Pu is interfered by ^{238}U signal; similarly, ^{241}Pu is interfered by intensity of ^{241}Am . During slow and steady rise of filament temperature, ^{241}Am appeared first at 1.85A itself (Fig. 5A.1), the intensity of which was found building up with time and temperature. Consecutively, Pu isotopes started to appear at 1.95A, but the ion intensity was still dominated by Am. There were no signals at mass 233 or 235 in the spectrum (Fig. 5A.2), which indicated the absence of U isotopes at this stage (a peak at mass 238 is of ^{238}Pu).

The observation is supported by the fact that the heat of vaporization of U is much higher than that of both Pu and Am (Table 5A.1). Measurement of $^{238}\text{Pu}/^{239}\text{Pu}$ at this stage provided the most un-interfered value.

Subsequently, the ion intensities of Am isotopes were found decreasing with time, which was clearly observed in successive mass scans (each scan took about 10 seconds duration) as shown in Fig. 5A.3. However, even by maintaining the filament current constant (1.95 A), U signals started to appear after about 40 minutes (appearance of peak at mass 233, as seen in Fig. 5A.5) and isotopic intensities were found to build up with time. Hence measurement of $^{238}\text{Pu}/^{239}\text{Pu}$ ratio before this stage was preferred. The correction of ratio, $^{238}\text{Pu}/^{239}\text{Pu}$ using alpha spectrometry was not possible in the present study, as the sample contains Am in addition to U and Pu, leading to complexity in alpha spectrometry [17,18]. The complexity arises due to the fact that alpha energies of ^{238}Pu (5.495, 5.452 MeV) and ^{241}Am (5.486, 5.443 MeV) being close to each other and interfere during measurement (the parameter which is measured by alpha spectrometry is the ratio $^{238}\text{Pu}/[^{239}\text{Pu}+^{240}\text{Pu}]$).

Table 5A.1 Comparison of some properties of Pu, Am and U relevant to the present study

Element	Heat of vaporization, ΔH°_{298} (kJ/mol) [11-13]	Vapour pressure at temperature 1800 K (Torr.) [13-15]	Liquid range (K)	Ionization energy (eV) [16]
Am	234	5.52	1431 ($T_m=1449$ K) ($T_b=2880$ K)	5.99
Pu	349	1.34e-2	2593 ($T_m=912$ K) ($T_b=3505$ K)	6.06
U	487	4.2e-5	2999 ($T_m=1405$ K) ($T_b=4404$ K)	6.1

During the measurement of $^{238}\text{Pu}/^{239}\text{Pu}$, intensity of ^{241}Am was too high that the intensity of $^{241}(\text{Pu}+\text{Am})$ was found to be almost equal to that of ^{240}Pu as seen in Fig. 5A.6(a), but the actual proportion of $^{240}\text{Pu}:^{241}\text{Pu}$ is $\sim 17:1$ as reported by Bera et al [3]. In order to accelerate the rate of removal of Am and Sm, filament current was raised to 2.25 A, which also helped to increase the ion intensities of U isotopes for its composition measurements with good precision. The typical mass spectra obtained for mass number 238 to 242 as function of time is shown in Fig. 5A.6(a)-(d).

Ion intensities of ^{239}Pu , $^{241}(\text{Pu}+\text{Am})$ and their ratio measured at regular intervals of time is given in Fig. 5A.7; as the ion intensity of ^{241}Am was falling continuously, the ratio of $^{241}(\text{Pu}+\text{Am})/^{239}\text{Pu}$ was found to decrease with time.

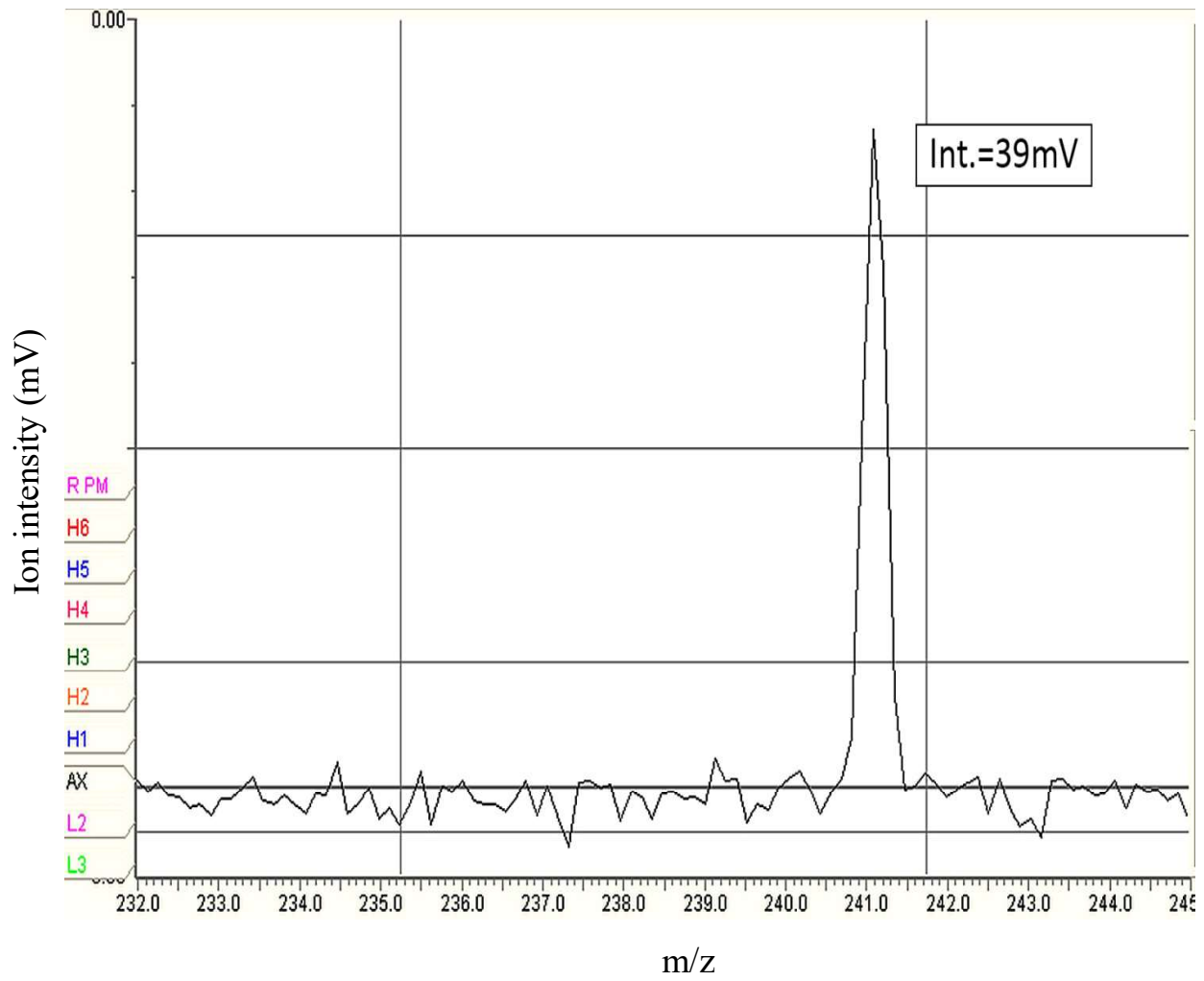


Fig. 5A.1 Mass spectrum of dissolver solution showing ion peak of only ^{241}Am at 1.85 A sample filament current.

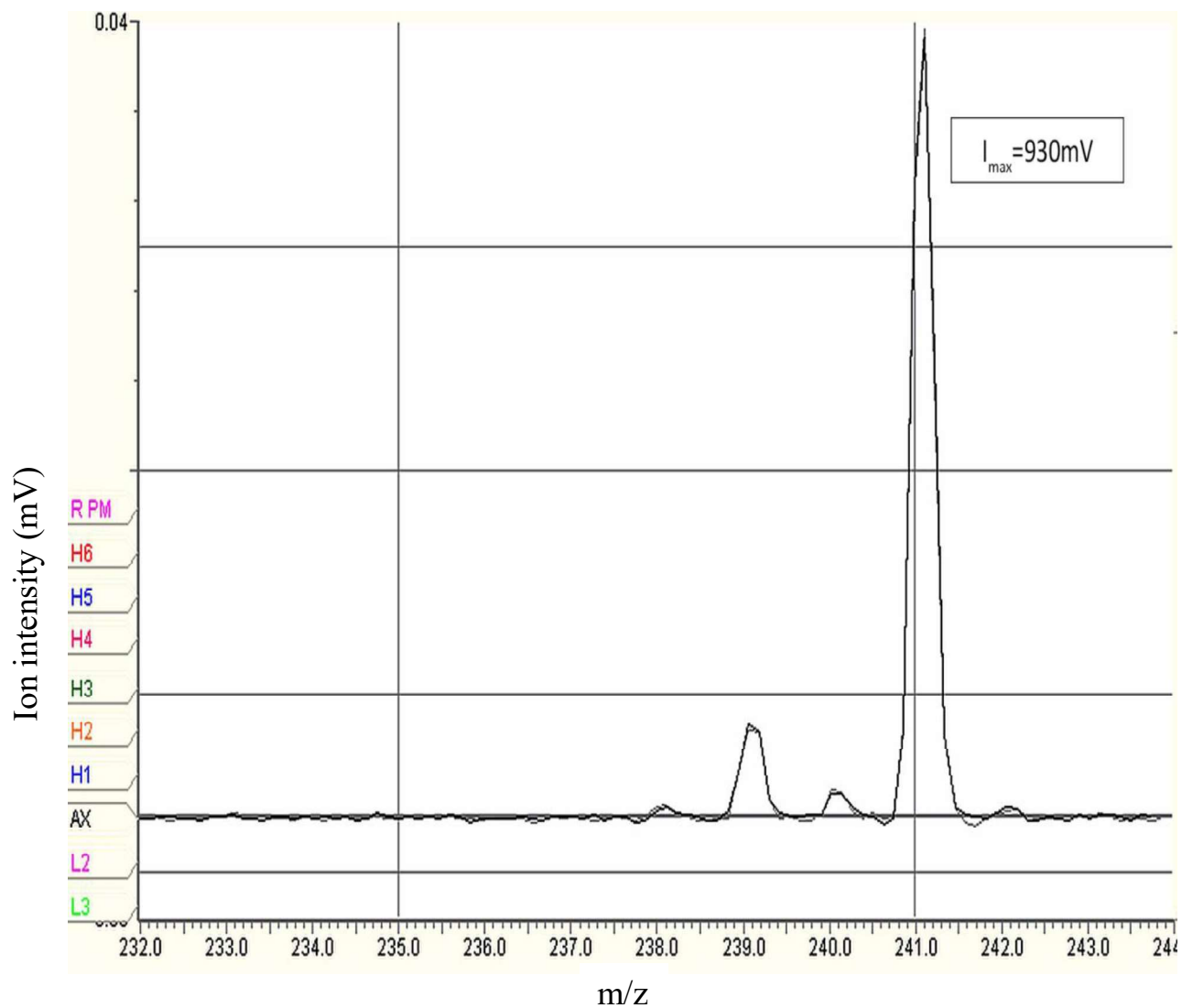


Fig. 5A.2 Mass spectrum of dissolver solution showing Pu and Am isotopes alone without U signals, at 1.95 A sample filament current.

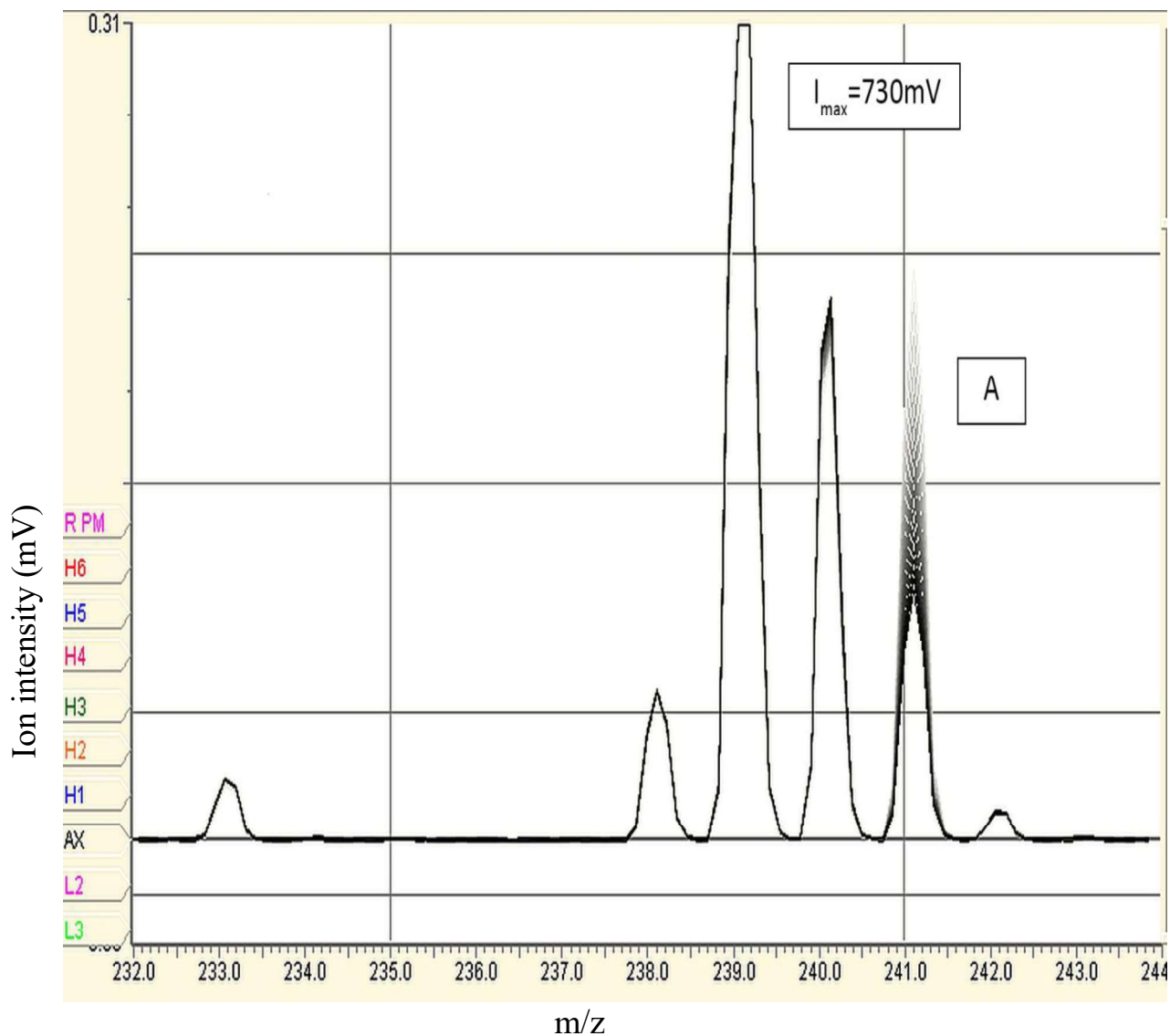


Fig. 5A.3 Mass spectrum of dissolver solution showing the reduction in intensity of ^{241}Am with successive scan at 1.95 A sample filament current.

The expanded view of steady reduction of intensity of ^{241}Am (indicated as A in the above figure) is depicted in Fig. 5A. 4.

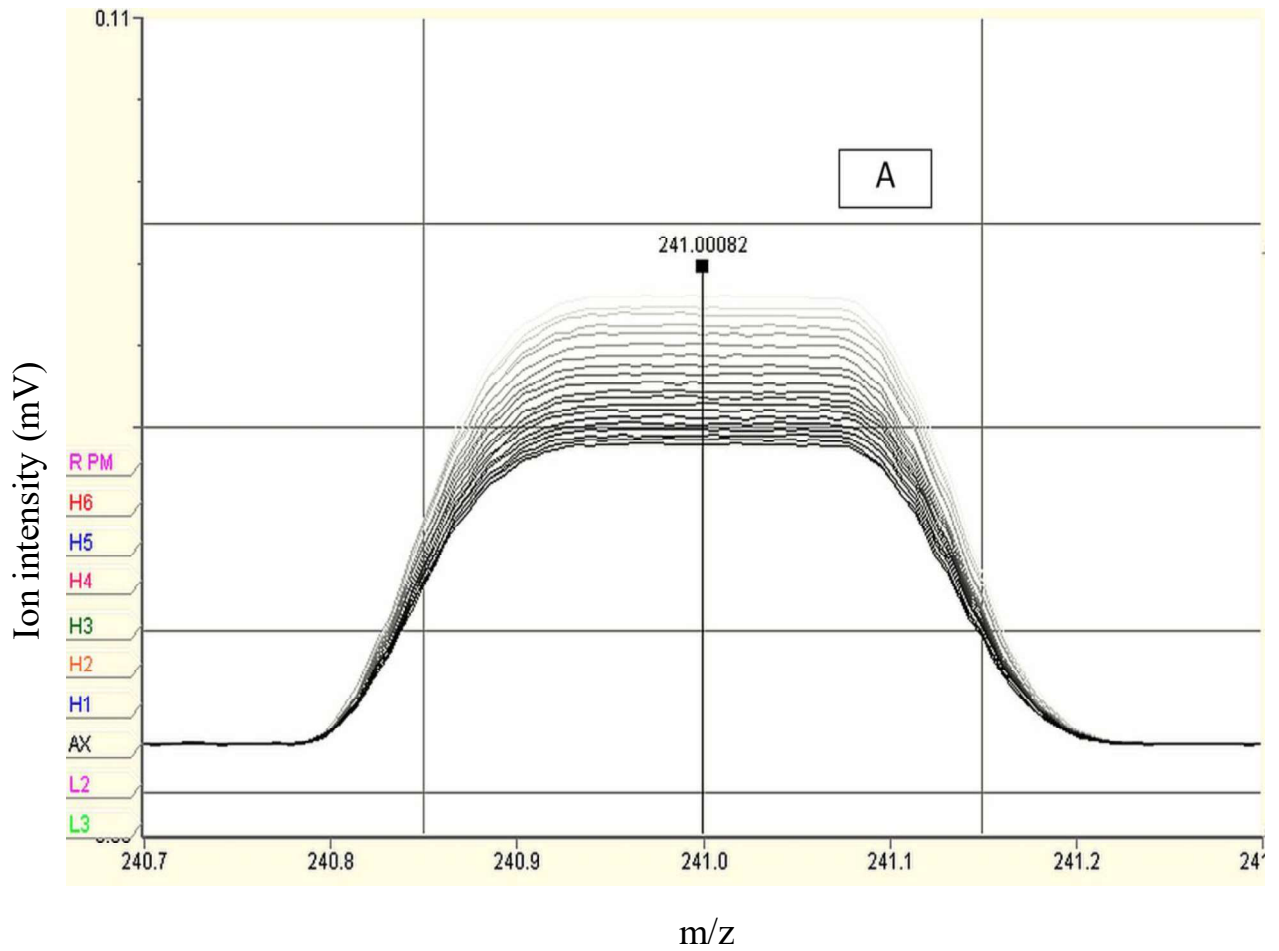


Fig. 5A.4 Expanded view of steady reduction of ion intensity of ^{241}Am , in consecutive runs, at constant sample filament current 1.95 A.

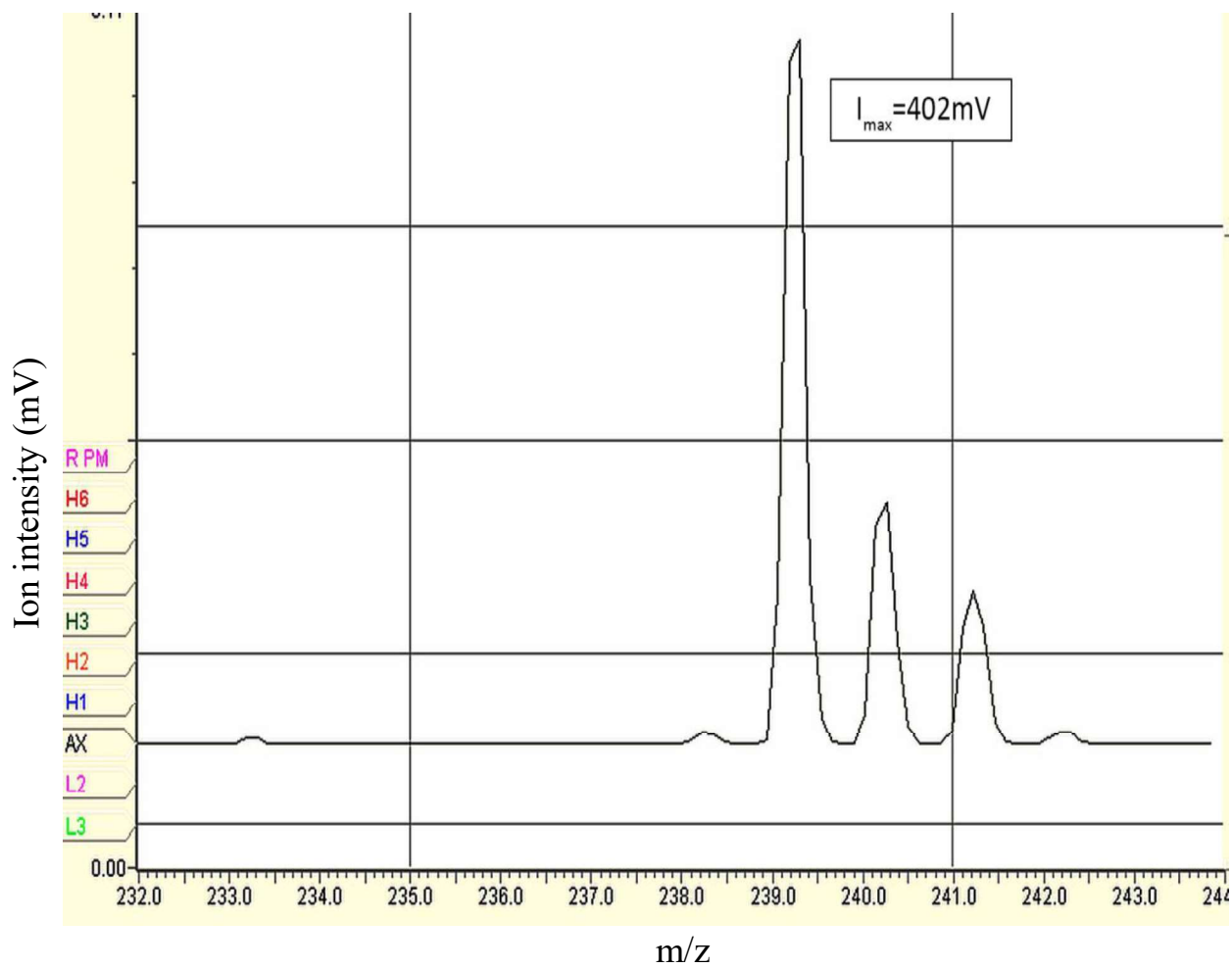


Fig. 5A.5 Appearance of U isotopes (at masses 233 and 238) in the mass spectrum of dissolver solution, after keeping the sample filament for about 40 minutes, at 1.95 A.

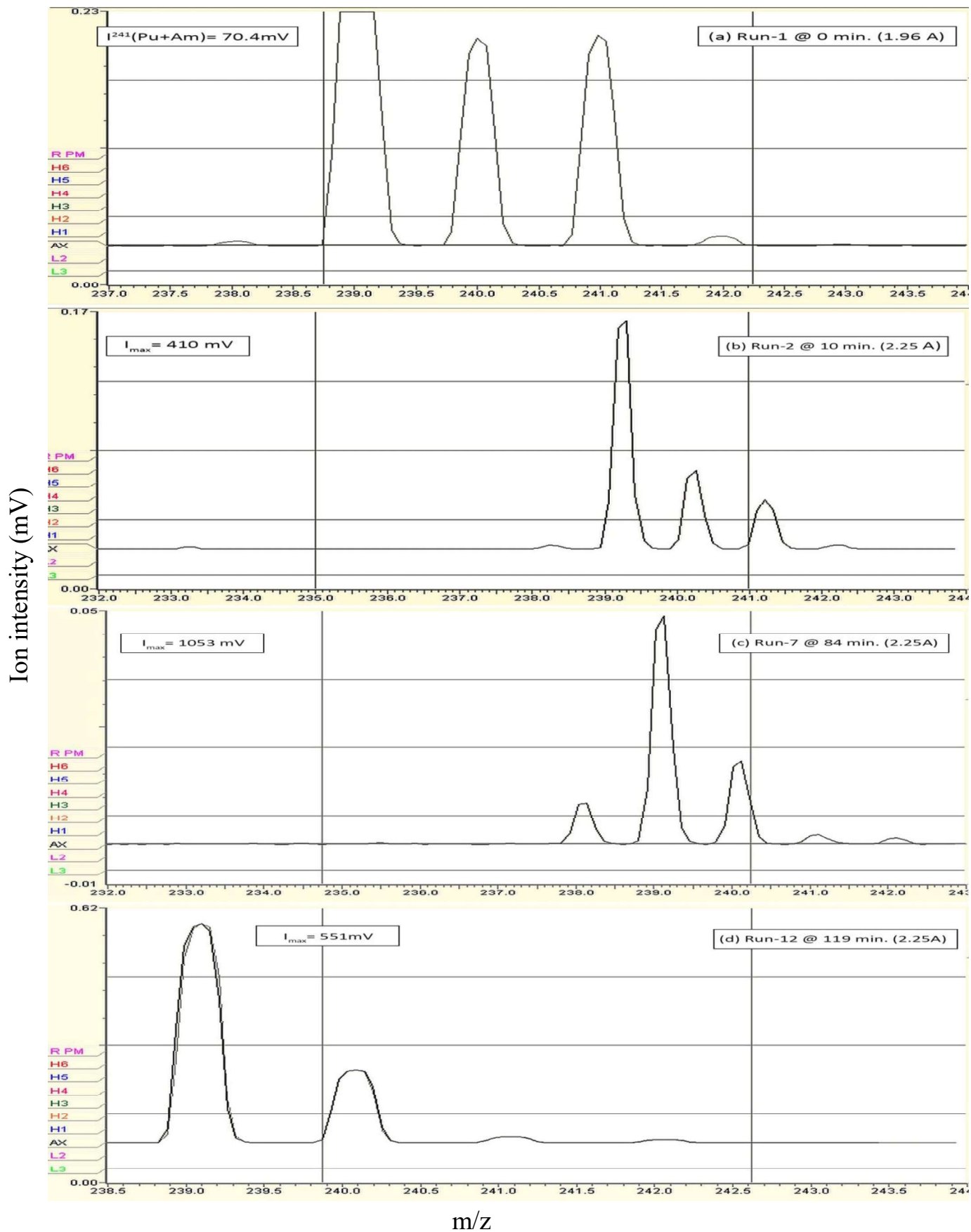


Fig. 5A.6 Mass spectra of dissolver solution showing reduction in intensity of $^{241}\text{Pu+Am}$ over successive measurements at different intervals of time.

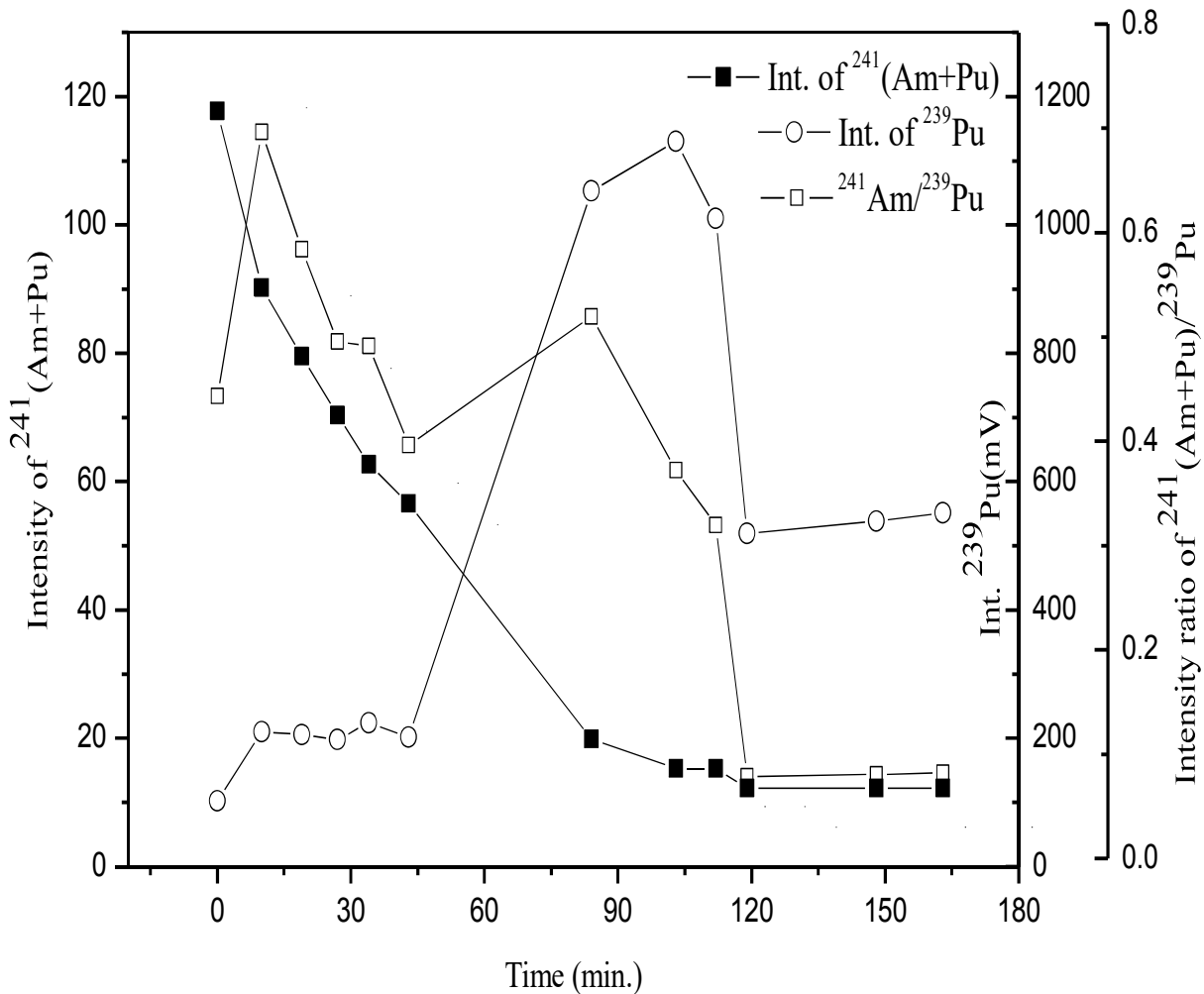


Fig. 5A.7 Variation of ion intensities of ^{241}Am , ^{239}Pu and their ratio with time, at sample filament current of 2.25A.

Hence, the lower heat of vaporization and shorter liquid range of Am was utilised for its elimination from the sample by evaporation, by maintaining high filament temperature. After increasing the sample filament current to 2.25A, measurements were made for rest of the ratios, namely, $^{240}\text{Pu}/^{239}\text{Pu}$ and $^{242}\text{Pu}/^{239}\text{Pu}$. Subsequently, the sample was analyzed for U isotopic composition. The errors associated with ^{238}U signal due to ^{238}Pu contribution is negligible as its atom fraction towards the total Pu is only $\sim 0.2\%$ compared to that of ^{238}U ($\sim 55\%$).

As described in our earlier study [8], samarium contribution was eliminated by maintaining the filament at same elevated temperature (2.25A) for about two hours, followed by isotopic composition measurements of Nd. At this stage, ^{241}Am intensity was also nearly eliminated and $^{241}\text{Pu}/^{239}\text{Pu}$ was found to be steady and close to the reported value [3]. Hence the isotopic composition measurements of Pu can be accomplished with minimum interference from U and Am by making use of the difference in their vapour pressures. Prolonged exposure of sample to higher temperature results in uncertainties in the isotopic ratios due to the preferential evaporation of lighter isotopes (fractionation). But, it was already observed that the errors originate out of fractionation were far less compared to that caused by isobaric interference [8]. Moreover, fractionation is more severe for ratios involving isotopes of larger mass differences [19]; accordingly the ratio $^{241}\text{Pu}/^{239}\text{Pu}$ (which was measured after prolonged evaporation) is less affected, as the mass difference between isotopes is only 2.

5A.3.2 Isotopic composition of constituent elements- U, Pu and Nd

The isotopic ratios, atom fractions and the average atomic weights of individual elements determined by both direct loading method and conventional method are compared in Table 5A.2. It is obvious that U isotopic composition is very much comparable and is in good agreement with that of reported data, except minor variations in the atom fraction of

^{238}U , which is due to a minimum interference from ^{238}Pu . The isotopic ratio of $^{238}\text{Pu}/^{239}\text{Pu}$ varies by one order of magnitude (see Table 5A.2, observed: 0.0199 and reported by standard method: 0.0031). However, the contribution of ^{238}Pu towards the total atom fraction is far too less to make any significant change in the average atomic weight (239.35 & 239.36, respectively). The residual intensity of ^{241}Am , even after prolonged evaporation has resulted the isotopic ratio $^{241}\text{Pu}/^{239}\text{Pu}$, marginally higher than the reported value (0.0269 & 0.0212, respectively). Isotopic ratios, atom fractions and average atomic weight of Nd were found to be very close to the reported data.

5A.3.3 Burn-up determination from U, Pu and Nd concentrations

The atom percent burn-up determined by direct loading method as well as by the conventional method is shown in Table 5A.3. The atom % burn-up determined based on total Nd (11.2 at %) is in agreement with the reported value (10.8 atom %) with 3.7 % relative deviation. Based on the atom fraction of ^{148}Nd , burn-up is found to be 11.1 atom % compared to the reported value of 10.9 atom % (with a relative deviation of 1.8 %). Similarly, based on the summation of atom fractions of ($^{145}\text{Nd} + ^{146}\text{Nd}$), the burn-up determined is 11.3 atom % whereas the reported value was 10.9 at %, with a deviation of 3.7% .

The sources of error and their relative contributions are determined and given in **Annexure**.

1).

Table 5A.2 Isotopic compositions of U, Pu and Nd present in dissolver solution, measured by direct loading method and by conventional method.

Element	Isotopic composition (IC) measured by Direct loading method			IC measured by Conventional method (Reported data [3])	
	Mass No.	IR w.r.t 238	Atom fraction	IR w.r.t 238	Atom fraction
U	233	0.7882 ± 0.014	0.4334	0.8014	0.4374
	234	0.0226 ± 0.0004	0.0124	0.0230	0.0126
	235	0.0070 ± 0.0002	0.0039	0.0073	0.0040
	236	0.0007 ± 0.0002	0.0004	0.0007	0.0004
	238	1	0.5499	1	0.5457
		Average AW	235.82	Average AW	235.80
			IR w.r.t 239		IR w.r.t 239
Pu	238	0.0199 ± 0.008	0.0143	0.0031	0.0023
	239	1	0.7201	1	0.7289
	240	0.3318 ± 0.0002	0.2389	0.3320	0.2420
	241	0.0269 ± 0.0003	0.0153	0.0212	0.0155
	242	0.0157 ± 0.0001	0.0113	0.0154	0.0113
		Average AW	239.35	Average AW	239.36
		IR w.r.t 143		IR w.r.t 143	
Nd	143	1	0.2944	1	0.2959
	144	0.8301 ± 0.0004	0.2444	0.8090	0.2394
	145	0.6313 ± 0.0003	0.1859	0.6324	0.1872
	146	0.5014 ± 0.0004	0.1476	0.5045	0.1493
	148	0.2878 ± 0.0004	0.0847	0.2873	0.0850
	150	0.1458 ± 0.0004	0.0429	0.1456	0.0431
		Average AW	144.69	Average AW	144.70

IR – Isotopic Ratio; w.r.t – with respect to; AW – Atomic Weight

Table 5A.3 Comparison of burn- up values determined by direct loading method with the reported values (measured by conventional method).

Burn-up monitor used	Observed values of Burn up in atom % (Direct method)	Reported values of Burn up in atom % (Conventional method) [3]	Relative error (%)
Total Nd	11.2	10.8	3.7
¹⁴³ Nd	11.2	NA	NA
¹⁴⁴ Nd	11.4	NA	NA
(¹⁴⁵ + ¹⁴⁶)Nd	11.3	10.9	3.7
¹⁴⁸ Nd	11.1	10.9	1.8

NA- not available

Burn-up was computed using the following expression:

Atom% burn-up = $(A/Y) \times 100 / [(H+ (A/Y))]$; where 'A' is the total atom contents of fission product monitor nuclide, 'Y' fractional fission yield of nuclide [20] and 'H' is total number of fissile atom contents (U+Pu) in the given aliquot.

The error associated with burn-up values obtained for the present MOX fuel (about 3.7%) is found to be more than that obtained with similar direct burn-up determination of thermal reactor spent fuel (2.4%, based on total Nd) [8]. This could be because of the additional error contributed by Pu analysis, due to unavoidable minimum interferences from isotopes of Am and U.

5A.3.4 Features of the proposed direct loading method

Comparison of features of the proposed direct loading method with conventional methods is given in Table 5A.4. In the direct loading method, quantity of dissolver sample solution employed for isotopic composition measurements of three constituent elements is only 40 μ l (containing \sim 185 ng of Nd). The radiation dose associated with the sample was only 11.5 mR/h. The conventional method involving ion exchange separation of constituent elements requires 8-10 μ g of Nd in the sample. As per the concentration of Nd in the present sample, the minimum sample requirement is about 1.7 g for separation by HPLC. This will have a radiation dose of about 490 mR /h (\sim 43 times more than that with directly loaded sample). The quantity of sample used for triple spiking with tracers of three different elements was only 0.0412 g (containing \sim 189 ng of Nd), and the associated dose is 11.8 mR/h. In conventional method, \sim 4-5 μ g of Nd is required in the sample for spiking (remaining quantity of Nd will be contributed by the added spike) and the corresponding sample requirement is \sim 0.85 g, the associated dose will be \sim 243 mR /h (\sim 21 times more than the dose with directly loaded sample). The extremely small sample requirement makes the direct method based on preferential evaporation of interfering elements attractive and advantageous in view of sample economy and radiation safety. The method is also characterized by zero radioactive liquid waste generation as it doesn't demand any sample preparation. Since all the three elements of interest are measured sequentially from the same sample filament, there is three times reduction in the number of filaments used, leading to minimisation of radioactive solid waste also. Duration of sample exposure to higher temperature depends on the difference in vapor pressures of interfering elements; for e.g. in the case of dissolver solution from thermal reactor fuel, it took only two hours of heating [8] to bring the interference of Sm to a minimum steady level (ΔH_{vap} . of Sm: Nd is 1:1.61)

whereas, in the case of fast reactor fuel, removal of Am in addition to Sm, necessitates extension of sample heating for slightly longer durations (ΔH_{vap} of Am: Pu is 1:1.49) to achieve steadiness in $^{241}\text{Pu}/^{239}\text{Pu}$ ratio. Thus the proposed direct burn-up determination method for fast reactor fuel has definite advantage features over the conventional method though it is difficult to get the accuracy close to that provided by the well established traditional procedure.

Table 5A.4 Comparison of features of direct loading method with conventional methods.

Ideally looking for	ASTM	HPLC	Direct loading method
Precision & accuracy	~1%	~4%	~4%
Personel exposure to radiation	x	x	0.02x
Fast & less tedious	Slow, tedious	Fast (separation), tedious	Faster, less tedious
Small sample size	~ 2 μg of Nd	8-10 μg of Nd	<100 ng of Nd
Waste generation	moderate	moderate	Nil/ minimum
Spatial profile	No	No	Yes (with LA- TIMS)

5A.4 Conclusion

Based on the vapour pressure differences of isobarically interfering elements, a direct method for burn-up determination of spent fast reactor fuel (MOX) was examined. The dissolver sample solution was heated inside the mass spectrometer to remove the interfering elements by evaporation, making use of their elevated vapour pressures. A sequential pattern of analysis of three constituent elements (Pu, U and Nd) has enabled the measurements of almost un-interfered isotopic compositions. Accordingly, Pu was first analyzed at lowest filament temperature (at 1.96 A with Re filament) for $^{238}\text{Pu}/^{239}\text{Pu}$; subsequently, the filament temperature was raised to 2.25A for isotopic measurements of $^{240}\text{Pu}/^{239}\text{Pu}$, $^{242}\text{Pu}/^{239}\text{Pu}$ and all the isotopic ratios of U; the filament was maintained at this temperature for about 2 hours for simultaneous removal of Sm and Am, and carried out the analysis of Nd, followed by measurement on $^{241}\text{Pu}/^{239}\text{Pu}$. The method provided atom % burn-up with an uncertainty of 3.7% from the reported value. The proposed method is less time consuming and adaptable for applications which can accommodate uncertainties in these levels. The proposed method has additional advantages with respect to zero radioactive solution waste generation, reduction in solid waste and drastic reduction in radiation exposure to the analyst.

Annexure 1

This annexure indicates the identification of sources of error and their relative contributions to the total error associated with the evaluated burn-up. It is based on the analysis of propagation of systematic error by derivative method, as explained below. The concentration of the elements are determined by the IDMS equation,

$$C^S = C^T W^T / W^S [(R_{(i)}^T - R_{(j)}^M) / (R_{(i)}^M - R_{(j)}^S) (\frac{1}{R_{(i)}^T}) (<A>^S / <A>^T) (A.F)_i^T / (A.F)_j^S] \quad (i)$$

where, W^T : weight of tracer; W^S : weight of sample; $i=233$ and $j=238$ for U; $i=142$ and $j=143$ for Nd; C^S : concentration of sample; C^T : concentration of tracer (spike); $<A>^S$, $<A>^T$: average atomic weights of sample and tracer; $(A.F)_i^T$, $(A.F)_j^S$: atom fraction of tracer and sample; $R_{(i/j)}^S$, $R_{(i/j)}^T$, $R_{(i/j)}^M$: isotopic ratio (IR) of sample, tracer and mixture respectively.

The simplified form of error associated with concentration (ΔC) can be expressed as,

$$\Delta C = \left[\frac{P}{(x_2 - x_1)^2} \right] [(x_2(x_2 - Q)\Delta x_1) - (x_1(x_1 - Q)\Delta x_2)] \quad (ii)$$

Where $P = P_1 * P_2$

$$P_1 = C^T \times (W^T / W^S)$$

$$P_2 = \left[\frac{(A.F)_i^T}{(A.F)_j^S} \times \left(\frac{<A>^S}{<A>^T} \right) \right]$$

$$x_1 = IR^M, x_2 = IR^S \text{ and } Q = IR^T$$

For U, natural U was taken as spike; $^{233}\text{U}/^{238}\text{U} = 0$, ie $Q = 0$, hence

$$\Delta C = \left[\frac{P}{(x_2 - x_1)^2} \right] [(x_2)^2 \Delta x_1 - (x_1)^2 \Delta x_2] \quad (iii)$$

On substituting the values of P , x_1 and x_2 , in equation (iii),

$$\Delta C^U = 0.4046$$

Hence, concentration of U, $C^U = 227.2454 \pm 0.4046$

Similarly,

$$C^{Pu} = 127.1886 \pm 0.0528 \text{ and}$$

$$C^{Nd} = 4.6330 \pm 0.0158$$

No. of atoms of an element present in the sample, $z = (N_A \times C \times W^S)/M$

Where N_A : Avagadro number and M : average atomic weight

Uncertainty associated with the number of atoms, $\Delta z = (N_A \times W^S \times \Delta C)/M$

Uncertainty associated with the number of atoms of U, $\Delta z^U = 5.6872e14$

Total no. of atoms of U, $z^U = 2.3913e16 \pm 5.6872e14$

Similarly,

$$z^{Pu} = 1.3187e16 \pm 1.6380e13$$

$$z^{Nd} = 7.9463e14 \pm 9.1e12$$

From concentrations of U, Pu and Nd, the burn-up is evaluated by the following expression,

$$Burn - up = \left(\frac{\left(\frac{A}{Y} \right)}{\left[H + \frac{A}{Y} \right]} \right) \times 100 \quad (iv)$$

where A is the no. of atoms of burn-up monitor, Y is its fission yield, H is the total no. of atoms of U and Pu.

Uncertainty associated with burn-up,

$$\Delta(Burn - up) = \left[\frac{100}{(H + A')^2} \right] [(H \times \Delta A') - (A' \times \Delta H)] \quad (v)$$

Where $A' = (A/Y)$

Based on the total no. of atoms of Nd (z^{Nd}),

$$\Delta(\text{Burn up}) = 0.35$$

Therefore, Burn-up = 11.24 ± 0.35

No. of ^{148}Nd isotopes = Atom Fraction (A.F) of ^{148}Nd * Total Nd atoms (z^{Nd})

$$\Delta(^{148}\text{Nd}) = \Delta(\text{A.F}) * \Delta z$$

$$\Delta(\text{A.F})$$

$$= \frac{[(1 + R_2 + R_3 + R_4 + R_5)dR_1 - R_1(dR_2 + dR_3 + dR_4 + dR_5)]}{(1 + R_1 + R_2 + R_3 + R_4 + R_5)^2} \quad (vi)$$

where,

$$R_1 = ^{148}\text{Nd}/^{143}\text{Nd}$$

$$R_2 = ^{144}\text{Nd}/^{143}\text{Nd}$$

$$R_3 = ^{145}\text{Nd}/^{143}\text{Nd}$$

$$R_4 = ^{146}\text{Nd}/^{143}\text{Nd}$$

$$R_5 = ^{150}\text{Nd}/^{142}\text{Nd}$$

Based on the no. of atoms of ^{148}Nd ,

$$\Delta(\text{Burn-up}) = 11.12 \pm 0.24$$

Based on the no. of atoms of ($^{145}\text{Nd} + ^{146}\text{Nd}$),

$$\Delta(\text{Burn-up}) = 11.28 \pm 0.35$$

Based on the no. of atoms of ^{143}Nd ,

$$\Delta(\text{Burn-up}) = 11.16 \pm 0.34$$

Uncertainty associated with burn-up evaluated based on total no. of Nd atoms is 11.24 ± 0.35 ; i.e. 3.13%.

The reported error is 3.7%. The remaining uncertainty is contributed by the random errors associated with the measurements.

Estimation of U/Pu of mixed carbide fuel irradiated in FBTR by direct loading method using TIMS

5B.1 Introduction

The Fast Breeder Test Reactor (FBTR) at Kalpakkam, India is the only operating reactor in the world with high plutonium content, hyperstoichiometric mixed carbide as driver fuel. FBTR is a 40 MWt (13.2MWe), sodium cooled fast reactor for research purpose [21]. Plutonium rich mixed uranium-plutonium carbide fuel of two compositions namely (30% UC-70% PuC) as Mark I and (45% UC-55% PuC) as Mark II are being used as driver fuel in FBTR [22]. The carbide fuel is characterised by high thermal conductivity and metal density suitable for compact core and high breeding ratio. Performance of this fuel has been excellent and achieved record burn-up of 1,65,000 MWd/t [23]. Post irradiation examinations of the spent carbide fuel were carried out to evaluate the irradiation behavior of the fuel [24]. Burn-up measurements of the fuel was carried out by Balasubramanian et al [25] by following the conventional ASTM procedure. The present chapter deals with analysis of irradiated Mark I (U, Pu) mixed carbide fuel of FBTR for U and Pu concentrations by direct loading method, employing the large differences in vapor pressures of U, Pu and the interfering element Am, as explained in Part A of this chapter. The method found its applicability for PHWR spent fuel (10000 MWd/t) [26] as well as for (U, Pu) mixed oxide [27] fuel of 100 GWd/t, with less than 4 % uncertainty in burn-up. Applicability of the technique with advanced fuel like carbide fuel is discussed in this chapter.

5B.2 Experimental

Thermal ionization mass spectrometer- model ISOPROBE-T of M/s ISOTOPX, U.K. was used in the present work.

Sample:

Dissolver solution of irradiated mixed carbide of 30% UC-70% PuC.

Procedure:

About 40 μl of dissolver solution of mixed carbide fuel, without subjecting to any chemical separation was evaporated to dryness under IR lamp in a teflon boat for isotopic composition measurements. Another aliquote of 0.0409g ($\sim 40 \mu\text{l}$) sample was mixed with 0.5833g of Pu spike (Pu of thermal reactor origin with comparatively more ^{240}Pu content) and 0.9978 g of U spike (enriched with ^{233}U), mixed well to attain homogeneity and evaporated to dryness under IR lamp, for IDMS measurements. Residues in both the boats were then dissolved in $\sim 10 \mu\text{l}$ of 0.75 M nitric acid and loaded on to Re filaments (in duplicate) for mass spectrometric analysis.

5B.2.1 Pattern of analysis of isotopic composition

The triple filament assembly containing virgin dissolver solution was heated slowly to 5.5/1.5A with constant heating rates. At 1.55 A, ^{241}Am signal started to appear as its vapor pressure is remarkably higher than that of other actinides present on the filament (vapor pressures of Am, Pu, U are 5.52, 1.34e-2 and 4.2e-5 Torr respectively at 1800 K). The intensity of Am increases with filament temperature and at 1.78 A, signal corresponding to Pu isotopes started to appear, but with no U signal. The ratio $^{238}\text{Pu}/^{239}\text{Pu}$ was measured at this scenario; subsequently the filament current was increased to 2.2A, to measure $^{240}\text{Pu}/^{239}\text{Pu}$, $^{242}\text{Pu}/^{239}\text{Pu}$ and all the isotopic ratios of U. Am intensity was falling continuously throughout this period, waited for about another 55 minutes to reduce the ^{241}Am intensity to a minimum steady level, then measured $^{241}\text{Pu}/^{239}\text{Pu}$. The spiked mixture was analysed for $^{233}\text{U}/^{238}\text{U}$ and $^{240}\text{Pu}/^{239}\text{Pu}$ directly as they are unaffected with any interfering isotopes. From the above values, concentration of U and Pu were evaluated by IDMS equation.

5B.3 Results and discussion

During the slow steady increase in filament currents, the first spectrum observed was of ^{241}Am , at 1.55 A, as shown in Fig. 5B.1. The intensity of which was found to increase with increase of filament current.

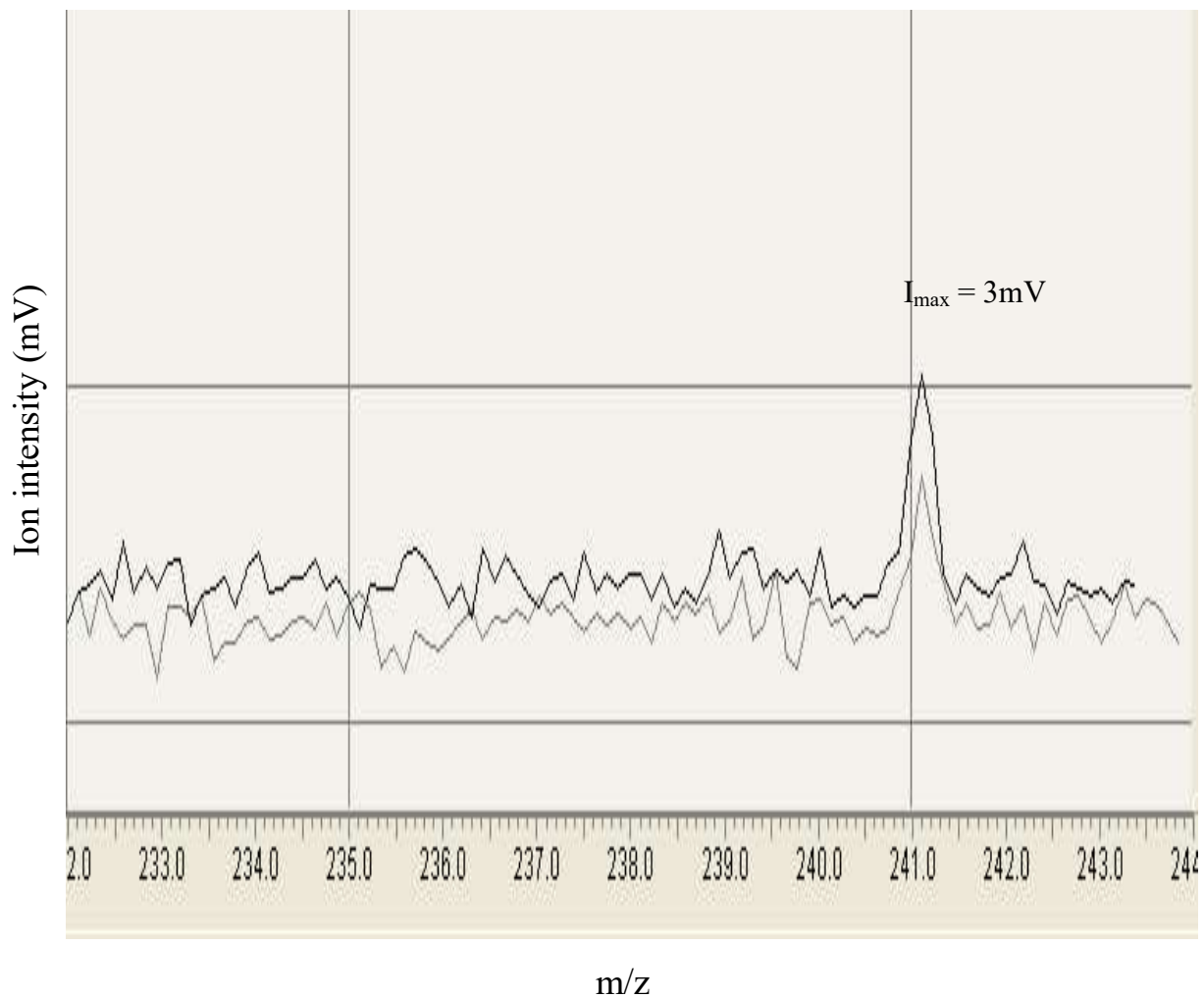


Fig 5B. 1 Mass spectrum of dissolver solution showing only ^{241}Am at sample filament current of 1.55 A.

As the filament current reached 1.78 A, peaks corresponding to Pu isotopes appeared in the spectrum, as seen in Fig 5B. 2. It is to be noticed that no U signal is observed in the spectrum at this stage, hence $^{238}\text{Pu}/^{239}\text{Pu}$ measurements could be made without isobaric ionterference from ^{238}U .

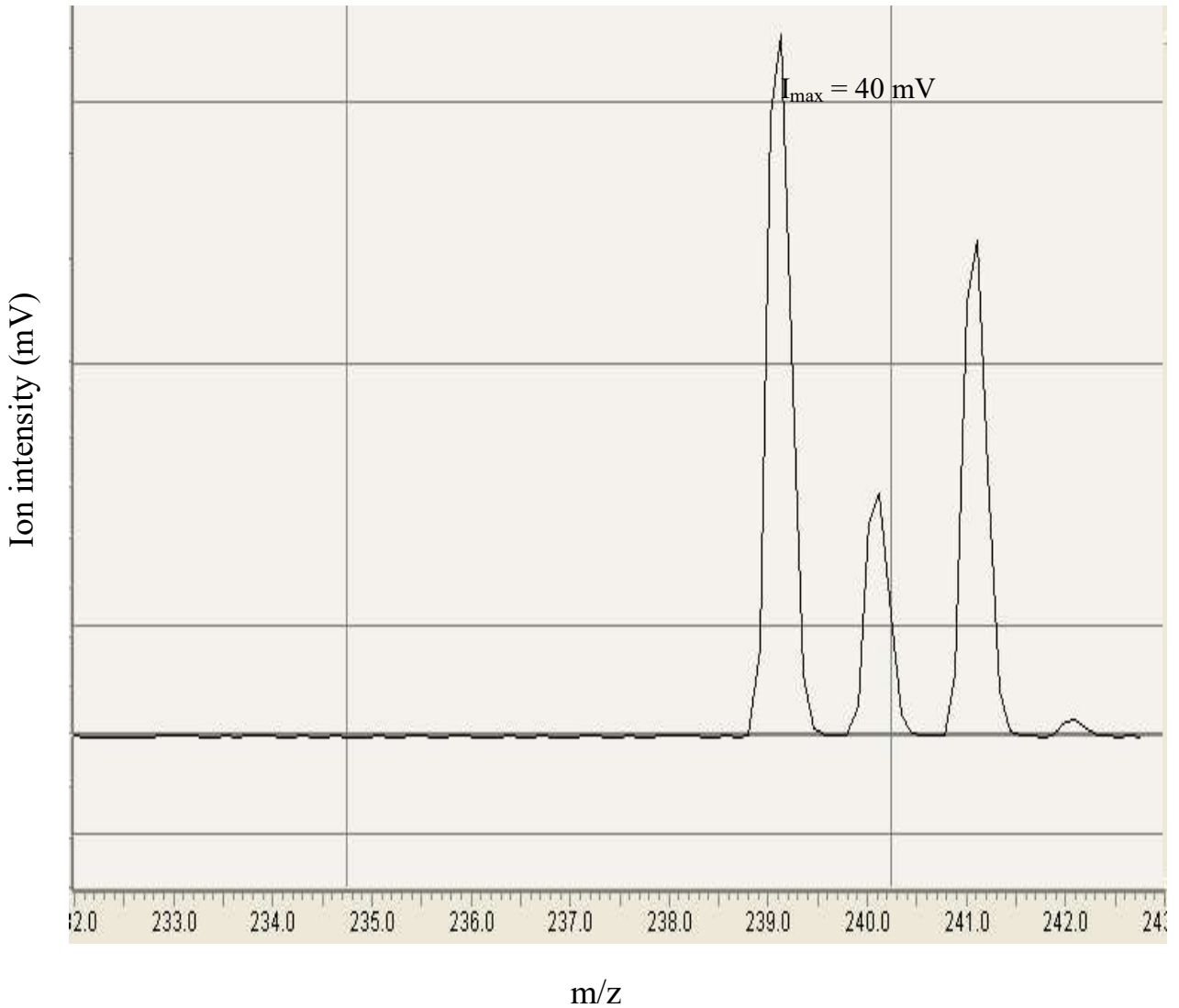


Fig 5B. 2 Mass spectrum of dissolver solution at filament current of 1.78 A, showing Pu and Am.

In order to accelerate the rate of evaporation of Am and to get higher ion intensities for Pu isotopes, the filament current was increased to 2.2 A. The isotopic ratios of $^{240}\text{Pu}/^{239}\text{Pu}$ and $^{242}\text{Pu}/^{239}\text{Pu}$ were measured, followed by isotopic composition of U, at this filament current. The mass spectrum ranging from m/z 232 to 244 obtained at 2.2 A shown in Fig. 5B.3, indicates the presence of U, Pu and Am.

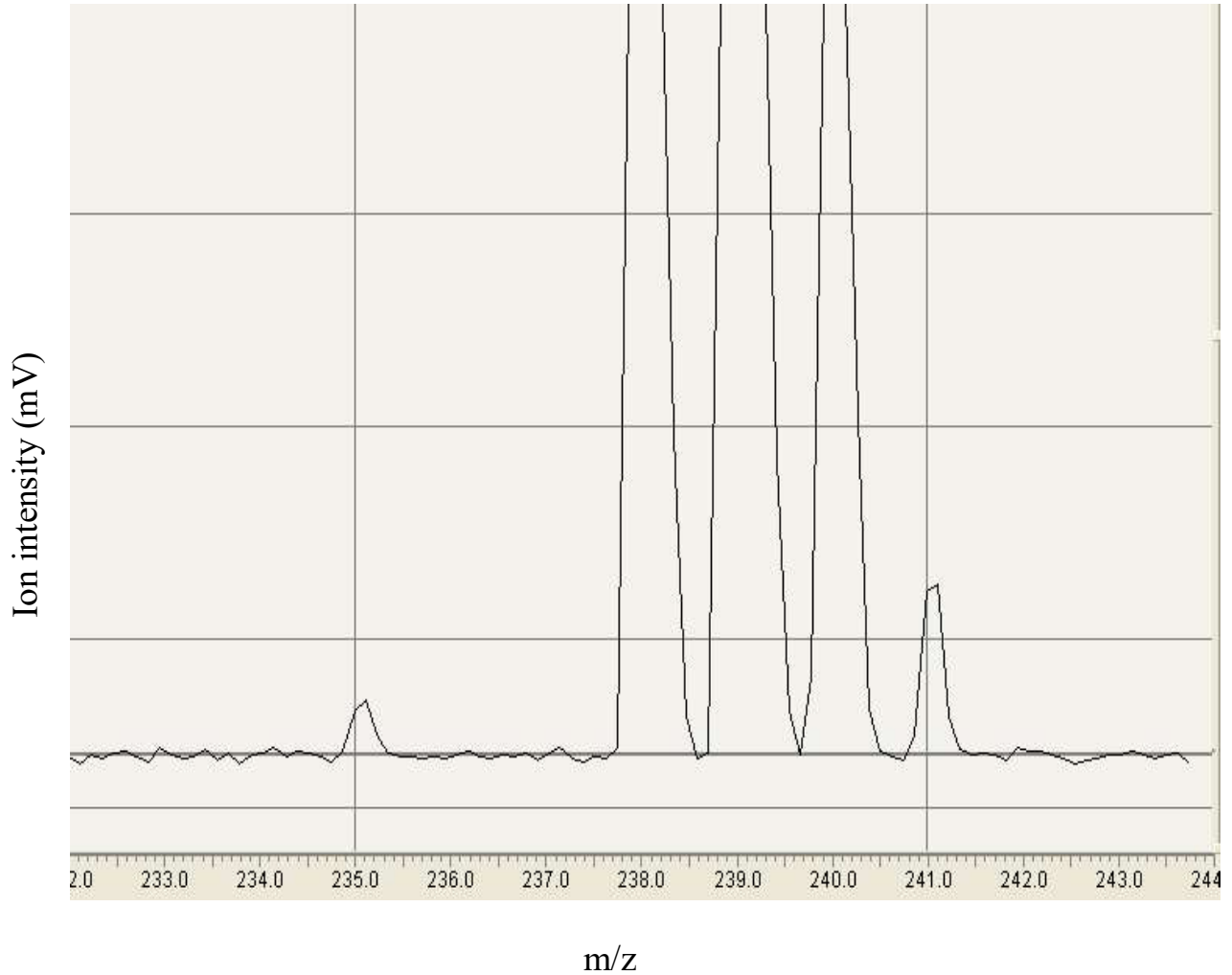


Fig. 5B.3 Mass spectrum of dissolver solution at filament current 5.5/2.2 A, indicating the presence of U, Pu and Am.

The filament was kept at 2.2 A for about an hour to minimize the ^{241}Am contribution to a lowest steady value, and then measured the value of $^{241}\text{Pu}/^{239}\text{Pu}$ so as to have the least isobaric interference from ^{241}Am .

Table 5B. 1 shows the relative abundances of U and Pu measured by the proposed direct loading method compared to that of the reported values based on the conventional method [25]. It is seen that U isotopic composition is comparable with that of reported values, with a marginal deviation in atom fraction of ^{238}U , which is higher than the reported value because of the possible interference from ^{238}Pu (which is 0.06% of total Pu), that reflects slightly in the average atomic weight also.

A mild deviation is seen in atom fraction of ^{238}Pu even though it was measured well before the appearance of U in the spectrum. However, it is to be noted that, the measured intensity is very close to detection limit of the detector, hence could be the possible variation or any trace contribution of ^{238}U was reflected in the values measured. There is noticeable deviation in the abundance of ^{241}Pu because of the contribution of unavoidable residual Am, existing even after prolonged heating.

Using the isotopic composition, atom fractions and average weights, the concentrations of U and Pu were evaluated by IDMS equation. The U/Pu concentration ratio was found to be 0.64 with 4.5% deviation from the reported value of 0.67.

Table 5B.1 Relative abundances of U and Pu isotopes measured by the present direct loading method and by conventional method [25]

Element	Mass No.	Atom fraction observed (by direct loading method)	Atom fraction reported (by conventional method) [25]
U	233	0.0001±0.0001	0.0001±0.0001
	234	0.0002±0.0001	0.0002±0.0001
	235	0.0076±0.0002	0.0075±0.0001
	236	0.0006±0.0002	0.0007±0.0001
	238	0.9917±0.0008	0.9914±0.0006
	Av. At. wt	238.04	238.02
Pu	238	0.0006±0.0001	0.0004±0.0001
	239	0.9020±0.0006	0.9041±0.0003
	240	0.0901±0.0004	0.091±0.0003
	241	0.0045±0.0008	0.0027±0.0003
	242	0.0005±0.0003	0.0004±0.0002
	Av. At. wt	239.14	239.21
Concentration ratio; U/Pu		0.64	0.67

5B. 4 Conclusion

The direct loading method put forwarded for isotopic composition measurements of U and Pu was found applicable for fast analysis of any nuclear fuel (commercial or advanced), without any sample preparation procedure. The method is characterized by very less sample requirement and associated dose, and also lowest production of solid waste and nil production of radioactive liquid waste. Accuracy of the method was found to be comparable with the established analytical tool such as ICP-MS.

References

1. T. Saravanan, K. Arunmuthu, B. B. Lahiri, S. Bagavathiappan, C. N. Venkiteswaran, John Philip, R. Divakar, Jojo Joseph, T. Jayakumar, Dimensional measurements on 112 GWd/t irradiated MOX fuel pins using X-ray radiography, *Ann. Nucl. Energy*, 2015, 83, 8-13.
2. C. N. Venkiteswaran, V. V. Jayaraj, B. K. Ojha, V. Anandaraj, M. Padalakshmi, S. Vinodkumar, V. Karthik, Ran Vijaykumar, A. Vijayaraghavan, R. Divakar, T. Johny, Jojo Joseph, S. Thirunavakkarasu, T. Saravanan, John Philip, B. P. C.Rao, K. V. Kasiviswanathan, T. Jayakumar, Irradiation performance of PFBR MOX fuel after 112 GWd/t burn-up, *J. Nucl. Mater.*, 2014, 449, 31-38.
3. S. Bera, R. Balasubramanian, Arpita Datta, R. Sajimol, S. Nalini, T. S. Lakshmi Narasimhan, M. P. Antony, N. Sivaraman, K. Nagarajan, P. R. Vasudeva Rao, Burn-up measurements on dissolver solution of mixed oxide fuel using HPLC- Mass spectrometric method, *Int. J. Anal. Mass Spec. Chrom.*, 2013, 1, 55-60.
4. ASTM Standards (1974) Standard test method for atom percent fission in Uranium and Plutonium fuels (Neodymium-148 method). E321-69, American Society for Testing Materials, Philadelphia.

5. Standard Test Method for Atom Percent Fission in Uranium Plutonium Fuel (Neodymium-148 method) (1996) Designation, 321-96 Annual of ASTM Standards, 12.02
6. S. K. Aggarwal, D. Alamelu, A novel approach for the determination of ^{238}Pu by thermal ionization mass spectrometry (TIMS) using interfering element correction methodology, *Int. J. Mass Spectr.*, 2005, 241, 83-89.
7. K.V. Suresh Kumar, A. Babu, B. Anandapadmanaban, G. Srinivasan, Twenty five years of operating experience with the Fast Breeder Test Reactor, *Energy Procedia*, 2011, 7, 323-335.
8. R. Sajimol, S. Bera, S. Nalini, N. Sivaraman, M. Joseph, T. Kumar, Preferential Removal of Sm by Evaporation from Nd- Sm Mixture and its Application in Direct Burn-up Determination of Spent Nuclear Fuel, *J Radioanal. Nucl. Chem.*, 2016, 309, 563–573.
9. R. Sajimol, P. Manoravi, S. Bera, M. Joseph, Effect of laser parameters on the measurement of U/Nd ratio using Pulsed Laser Deposition followed by Isotopic Dilution Mass Spectrometry. *Int. J. Mass. Spec.*, 2015, 387, 51–55.
10. K. G. Heumann, *Isotope Dilution Mass Spectrometry in Inorganic Mass Spectrometry*, 1988, Ed. Adams F, Gijbels R, Van Grieken R, John Wiley & Sons, New York, p301-376.
11. Robert Guillaumont, Update on the chemical thermodynamics of Uranium, Neptunium, Plutonium, Americium and Technitium, 2003, Nuclear Energy Agency Organization for Economic Co-operation and Development.
12. N. M. Edelstein, J. D. Navratil, W. W. Schulz, *Americium and Curium Chemistry and Technology*, 1984, D. Reidel Publishing Company, Holland.

13. M. H. Bradbury, R. W. Ohse, High temperature vapor pressure of pure Plutonium, J. Chem. Phys., 1979, 70, 2310-2314.
14. N. D. Erway, O. C. Simpson, The vapour pressure of Americium, J. Chem. Phys., 1950, 18, 953-960.
15. E. G. Rauh, R. J. Thorn, Vapor pressure of Uranium, J. Chem. Phys., 1954, 22, 1414-1418
16. John Roboz, Introduction to Mass Spectrometry- instrumentation and techniques, 1968, John Wiley & Sons, USA, 512-513.
17. Donald L Horrocks, Applications of Liquid Scintillation Counting, 1974, Academic Press, New York.
18. D. Alamelu, S. K. Aggarwal, Determining the age and history of plutonium using isotope correlations and experimentally determined data on isotopic abundances of plutonium and ^{241}Am , J. Radioanal. Nucl. Chem., 2016, 307, 277–284.
19. H. Kanno, Isotopic Fractionation in a Thermal Ion Source, Bulletin of the Chemical Society of Japan, 1971, 44, 1808.
20. E. A. C. Crouch, Atomic Data and Nuclear Data Tables: Fission Product Yields from Neutron Induced Fission, 1977, Academic Press, New York and London.
21. G. Vaidyanathan, Simulation and control studies for FBTR steam water system, Indian J. of Engineering and material science, 2011, 18, 321-328.
22. U. Basak, P.S. Kutty, S. Mishra, S.K. Sharma, K.S. Bhatnagar, R.S. Mehrotra, S. Majumdar and H.S.Kamath, Fabrication of mixed uranium plutonium carbide fuel pellets for FBTR by direct processing of sinter rejects, BARC Newsletter, 2004, Issue No. 249.

23. Arun Kumar, Development, Fabrication and Characterization of Fuels for Indian Fast Reactor Programme, International Conference on Fast Reactors and Related Fuel Cycles: Safe Technologies and Sustainable Scenarios (FR13) , Paris, March 4-7, 2013.
24. C. N. Venkiteswaran, N. Raghu, V. Karthik, A. Vijayaraghavan, V. Anandaraj, T. Ulaganathan, T. Saravanan, V. V. Jayaraj, Shaji Kurien, John Philip, T. Johny, Irradiation Behavior of FBTR Mixed Carbide Fuel at Various Burn-ups, Energy Procedia, 2011, 7, 227-233.
25. R. Balasubramanian, S. Nalini, R. Viswanathan, Proc. ISMAS (2009), Hyderabad, Nov 24-28, 2009, p.377.
26. R. Sajimol, S. Bera, S. Nalini, N. Sivaraman, M. Joseph, T. Kumar, Preferential Removal of Sm by Evaporation from Nd- Sm Mixture and its Application in Direct Burn-up Determination of Spent Nuclear Fuel, J Radioanal. Nucl. Chem., 2016, 309, 563–573.
27. R. Sajimol, S. Bera, N. Sivaraman, M. Joseph, Direct burn-up determination of fast reactor mixed oxide (MOX) fuel by preferential evaporation of interfering elements, J. Radioanal. Nucl. Chem., 2017, 311, 1593–1603.

Laser Ionization Mass Spectrometric Studies of dissolved UC, U-O and Te systems

6.1 Introduction

Laser Ionization Mass Spectrometry (LIMS) finds applications, both in organic and inorganic solid and liquid sample analysis. For organic samples, it is mainly used for identification of molecular masses, with or without the use of a suitable matrix. In the case when a matrix is used, this method is popularly known as Matrix Assisted Laser Desorption and Ionization (MALDI). For inorganic applications, LIMS is not a very useful technique for the quantification of elemental concentrations, because the ionization efficiency is different for different elements from a condensed sample for any given experimental conditions (laser wavelength, fluence etc.). Besides, the ionization efficiency can be different for same element, when it is present in different matrices. However, isotopic quantification is possible for measurement of isotopic ratios, using LIMS [1-3]. The mass spectrometric study discussed in this chapter deals with analysis of inorganic samples of uranium carbide, uranyl nitrate and Te systems, by laser desorption/ionization method.

6.2 UC system

The Fast Breeder Test Reactor (FBTR) located at Kalpakkam uses U, Pu mixed carbide fuel- Mark I ($U_{0.3}Pu_{0.7}C$) and Mark II ($U_{0.45}Pu_{0.55}C$)- as the driver fuel. As a fast reactor fuel, the mixed carbide has many advantages over the oxide fuel, such as high metal atom density, high thermal conductivity, better breeding capacity etc. Further, the centre line temperature and temperature gradient of carbide fuel is lower than that of an oxide fuel due to higher thermal conductivity of the former [4]. In spite of these advantages, the success of

breeder programme depends upon the successful closing of nuclear fuel cycle. The first step of aqueous reprocessing of any nuclear fuel is its dissolution in nitric acid [5]. Reaction of uranium carbide with nitric acid yield uranyl nitrate, soluble organic acids, gaseous products like NO₂, NO and CO₂. Between 50 to 80% of carbide carbon is converted to CO₂, based on the molarity of nitric acid used and the temperature maintained during dissolution. The soluble organic species consist of oxalic acid, benzoic acid, mellitic acid and unidentified compounds which are probably highly substituted aromatic compounds with -COOH and -OH groups [6]. These organic compounds causes formation of emulsion in the solvent extraction steps of PUREX (plutonium uranium redox extraction) process. They also form complexes with U(VI) and Pu(IV) resulting incomplete extraction of these ions [7]. The head-end processes have been extensively investigated by many researchers and several techniques were reported - such as pyrohydrolysis, pyrolytic oxidation, low temperature hydrolysis, electrochemical methods, photochemical methods etc., to destroy the interfering organic compounds, bringing out their merits and demerits [8]. Addition of oxidizing agents like Ag²⁺, Ce⁴⁺, KMnO₄ etc. is a practical approach to the problem, but the precipitate of oxidizing agents may adsorb Pu. The Electro Oxidative Dissolution Technique (EODT) has been reported to destroy oxalic acid completely [9]. Studies on identification of the interfering compounds were reported based on the methods like capillary zone electrolysis [10], conventional redox method [11], electrochemical oxidation [12] etc.

The present study aims at adaptation of a home-built reflectron-time-of flight mass spectrometer (RTOF-MS) coupled to laser desorption /ionization system for the simultaneous identification of organic compounds that are formed on dissolution of UC in nitric acid.

6.2.1. Experimental

Sample preparation

About 50 mg of UC was dissolved in 20 ml of 6 M nitric acid (AR grade) at 50° C for 30 minutes on a hot plate, so that it was concentrated to a thick liquid which was loaded on a stainless steel (SS) holder and kept under IR lamp to evaporate to near dryness and used as the sample for the subsequent analysis.

Instrumentation

A home-built reflectron time of flight mass spectrometer (RTOF-MS) coupled to laser desorption/ionization system with an acceleration voltage of 2500 V was used in this study. Nd-YAG laser with a wave length of 266 nm and pulse width of 8 ns at frequency 1 Hz acted as source for desorption and ionization. The detailed description on instrumentation is given in Chapter 2, section 2B.2. The sample as prepared above was subjected to desorption and ionization by laser beam. Ions thus produced were then subjected to mass analysis. The detection system used was suitable for the mass analysis of positive ions only. Small amount of dilute sodium hydroxide was added to the sample, so that sodium salt of the corresponding ions can also be detected.

6.2.2 Results and discussion

The solution of UC in nitric acid was found to be dark brown in colour. Ferris et al pointed out that the colour was attributed to materials similar to humic acids [6]. The time-of-flight mass spectrum of positive ions present in the solution were recorded as their time of arrival at the detector. The spectra were recorded as intensity (V) versus time of arrival (μ s). The corresponding masses, recorded at a particular time of arrival was evaluated by calibration method. At an acceleration voltage of 2500 V, the spectrum obtained has shown

signals of mass up to 602 amu. A typical mass spectrum obtained for UC dissolved in nitric acid sample is shown in Fig. 6.1; the corresponding masses and the possible compounds/species are listed in Table 6.1.

Masses corresponding to acetic acid and oxalic acid had shown intense peaks at 39.3 and 46.7 μ s respectively, the sodium salt of the latter holds one of the most intense signals in the spectrum at 52.1 μ s. While benzoic acid exhibited a less intense but finite signal at 54.4 μ s, the signal corresponding to mass of phthalic acid was very weak (63.5 μ s). However, the signal for sodium salt of phthalic acid (68.7 μ s) was reasonably intense and finite. Weak signal for corresponding mass of mellitic acid was observed at 92.2 μ s. All the acid species observed in the above study were already reported [6] and we could not observe any new species. The blank spectrum obtained for the above experiment is given in Fig. 6.2 and the corresponding species attributed for blank analysis are given in Table 6.2.

Under identical experimental conditions, when the laser frequency was increased to 10 Hz, the mass spectrum obtained has shown the presence of oxalic acid and benzoic acid in the sample, along with a number of clusters of the type U_xO_y of mass up to 1762 amu, which led us to a detailed investigation on the U-O system.

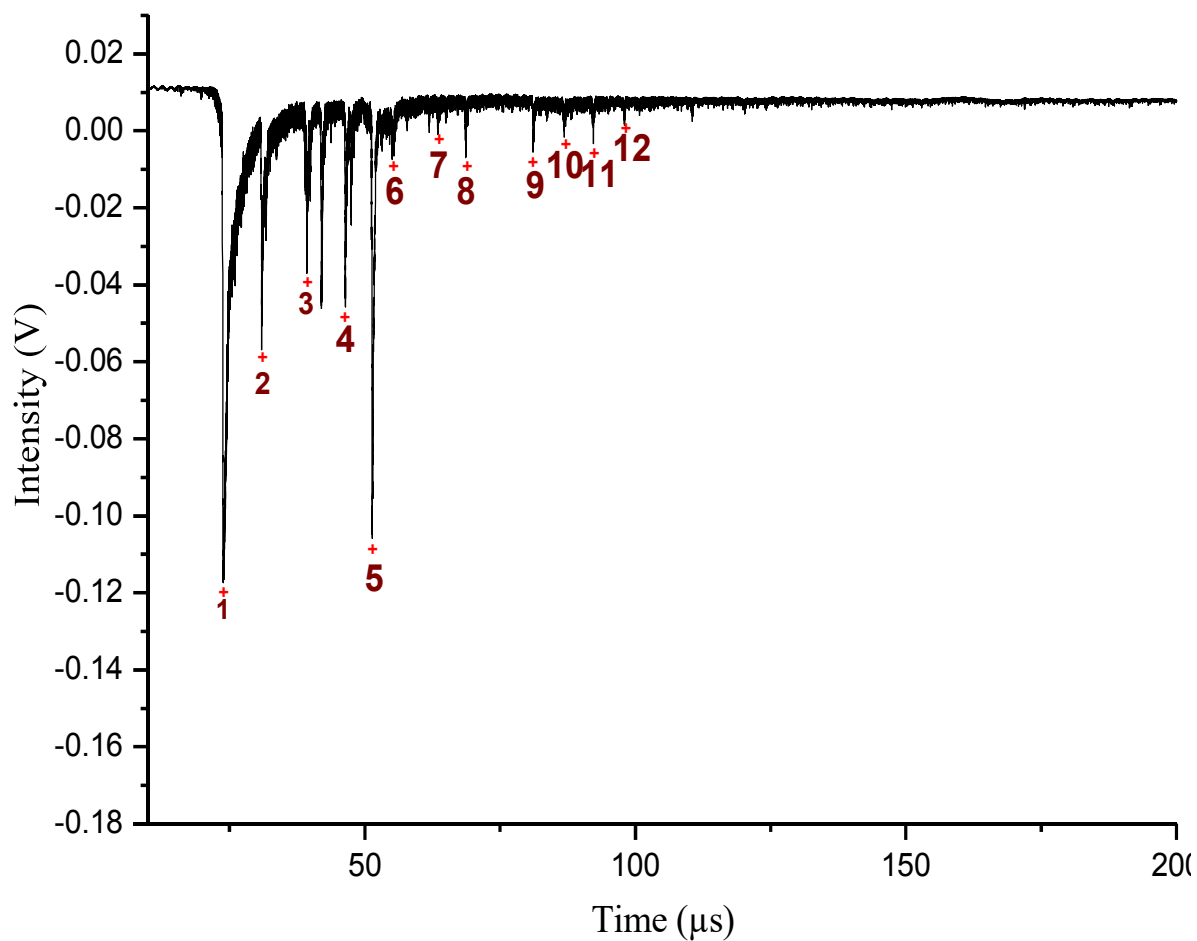


Fig. 6.1 A typical TOF mass spectrum obtained for a sample of UC dissolved in nitric acid when subjected to laser ionization.

Table 6.1 Time-of-arrival, corresponding masses and possible species when UC in nitric acid sample was ionized by laser.

Signal No.	Time (μ s)	Corresponding mass (amu)	Corresponding Compound/species
1	23.8	23.2	Na
2	30.9	38.6	K
3	39.3	61.4	CH ₃ -COOH
4	46.7	88.4	Oxalic acid
5	52.1	110.6	Sodium oxalate
6	54.4	121.4	Benzoic acid
7	63.5	164.6	Phthalic acid
8	68.7	188.8	Sodium phthalate
9	81.1	269.2	UO ₂
10	86.9	305.2	?
11	92.2	342.6	Mellitic acid
12	98.0	386.6	?

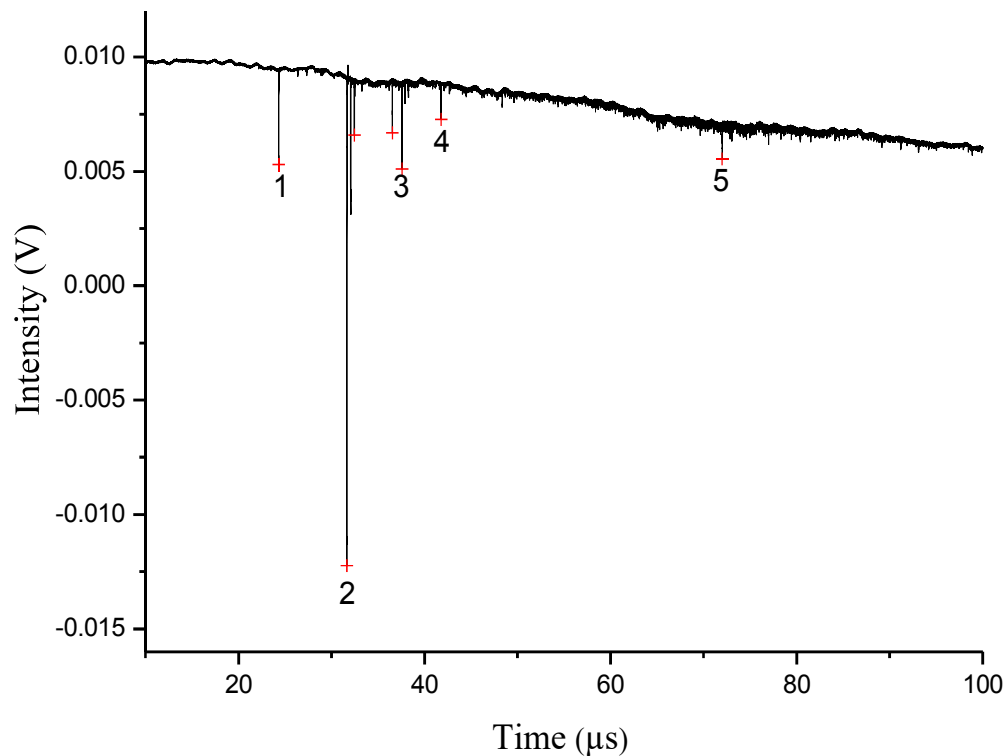


Fig. 6.2 Typical blank time-of-flight spectrum

Table 6.2 Time of arrival and corresponding masses of blank spectrum.

Signal No.	Time (μs)	Corresponding mass (amu)	Compound/ species
1	24.38	22.8	Na
2	31.70	38.8	K
3	37.74	56.8	CH ₃ COCH ₃
4	41.70	67.0	CH ₃ CONa
5	71.99	200	?

6.3. U-O system

Based on the observations of clusters of U and O during the laser desorption/ionization mass spectrometric studies of UC system, an experiment was carried out with uranyl nitrate solution, without the addition of any matrix.

6.3.1 Experimental

The uranyl nitrate solution used was of 1.5 mmol concentration. The sample holder was a 2 mm thick SS disc of about 10 mm diameter. About 10 μ l of the solution was loaded as a spot on the sample holder and dried the sample under IR lamp. A quartz lens with a focal length of 50 cm was used for focusing the laser beam on the sample and the sample was positioned after the focus, forming a spot area on the sample with a diameter of \sim 2 mm. The LIMS experiment was carried out with two different laser fluences, 0.002 J/cm² and 0.03 J/cm², at 10 Hz frequency and 266 nm wavelength.

6.3.2 Results and discussion

Laser Mass spectrometric studies of U-O clusters

Laser Mass Spectrometric (L-MS) studies of uranyl nitrate sample (using a N₂ laser, λ 337 nm) using various organic and inorganic matrices (MALDI) have been reported [13]. In that study, out of twenty two commonly used organic matrices, only 5-chlorosalicylic acid led to generation of clusters of U-O up to mass 1400 amu. Out of eleven inorganic matrices studied, only LiF and LiCl led to clusters of up to a m/z of 570. Clusters of m/z up to 2860 in H₂O and up to 3686 in H₂O/CH₃CN were also reported. In the present study, uranyl nitrate in water was used as the sample and clusters of m/z up to 3686 have been observed, even without addition of any matrix. A typical mass spectrum obtained at low laser fluence (0.002 J/cm²) is shown in Fig. 6.3 and the spectrum corresponding to high

laser fluence (0.03 J/cm^2) is shown in Fig. 6.4. The expanded views of Fig. 6.4 are given in Fig. 6.5 (a) and (b). As can be seen from Fig. 6.3, we could observe clusters up to m/z of 1430 corresponding to the species U_5O_{15} , at low laser fluence.

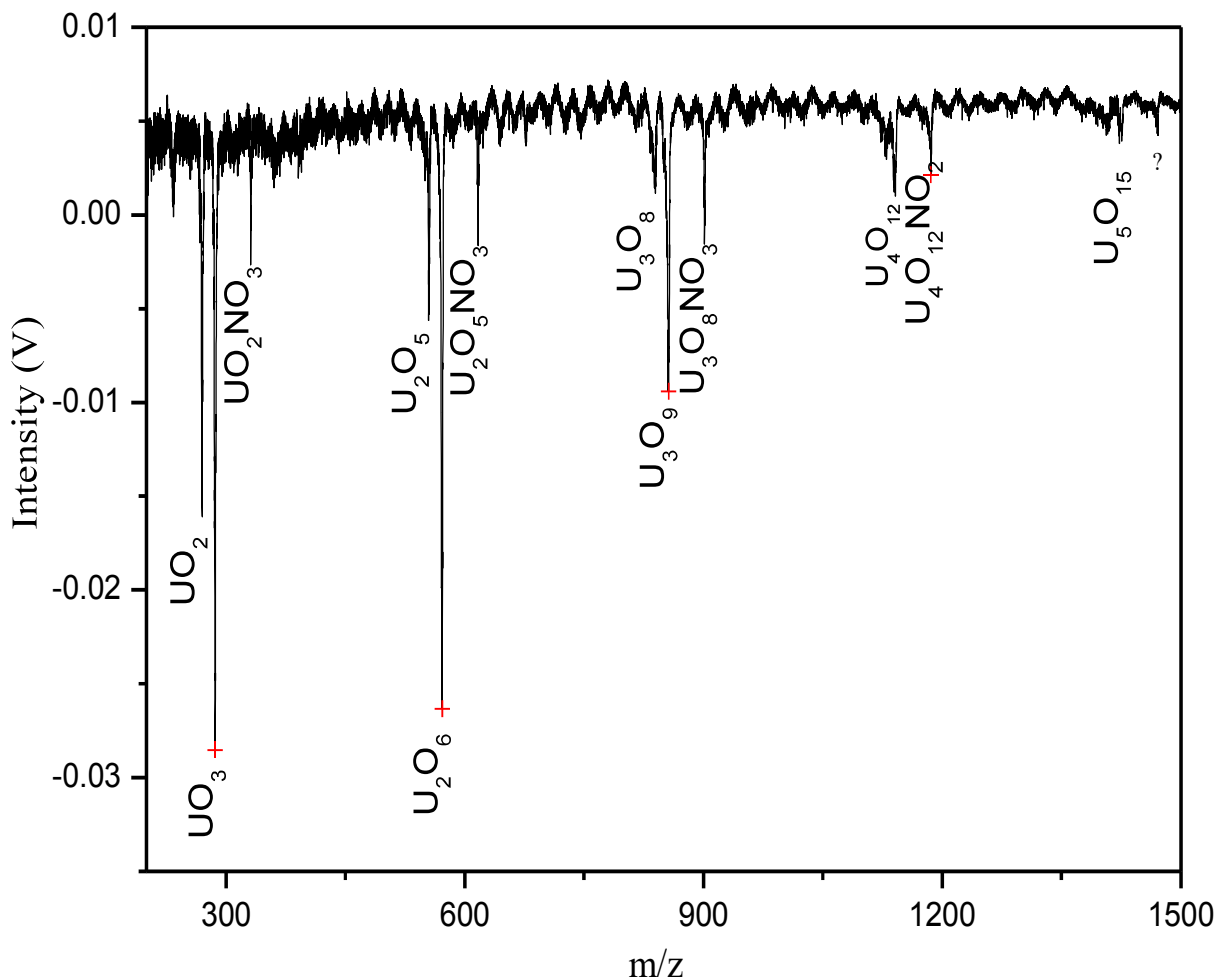
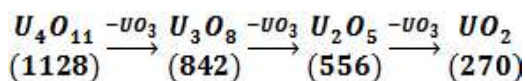
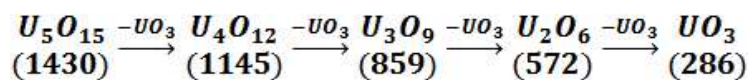


Fig. 6.3 Typical mass spectrum obtained from uranyl nitrate at lower laser fluence of 0.002 J/cm^2 .

The possible series of clusters and the corresponding masses can be expressed as follows.



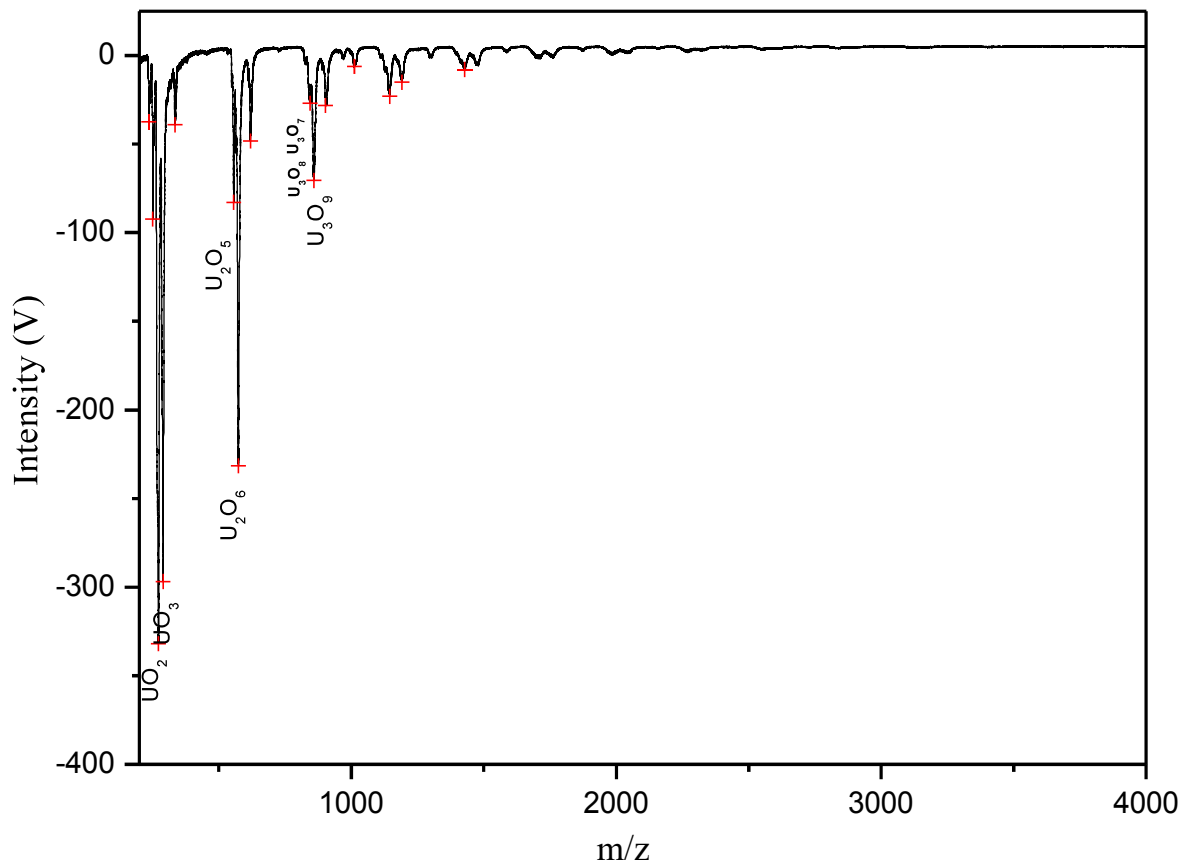


Fig. 6.4 Mass spectra showing higher clusters of U_xO_y at higher laser fluence of 0.03 J/cm^2

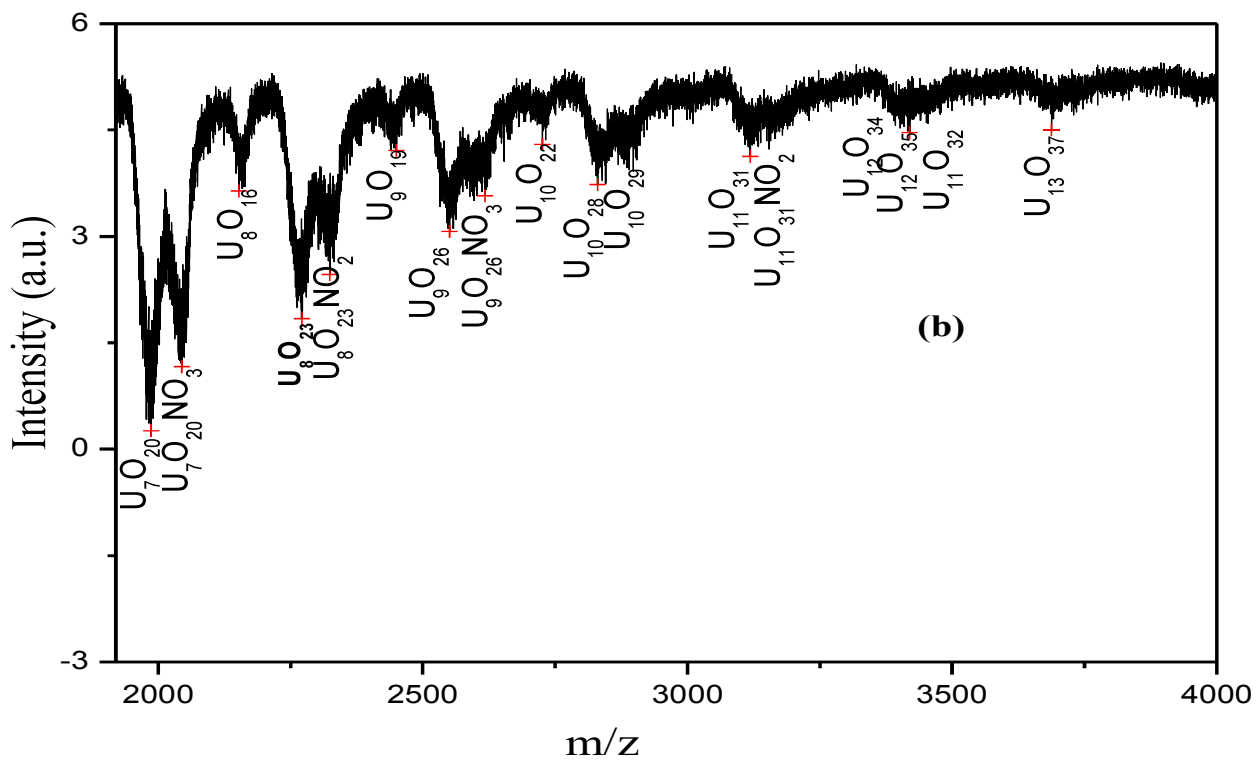
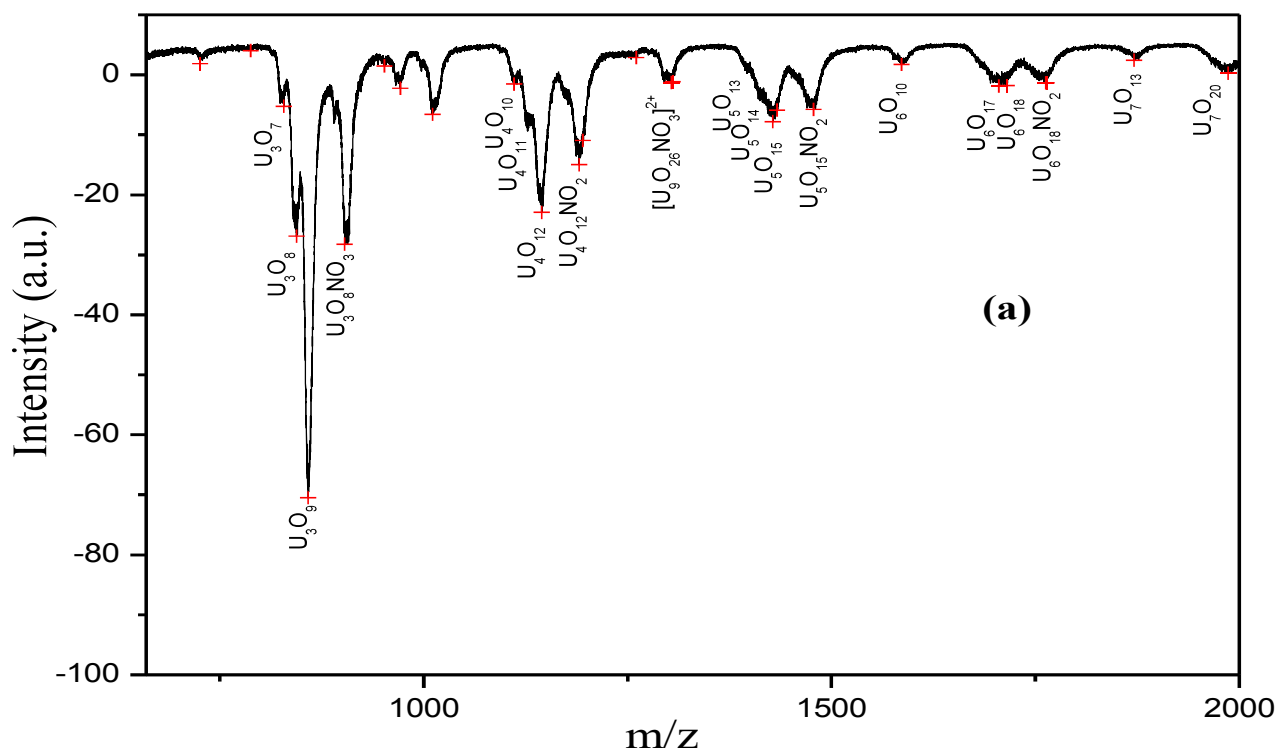
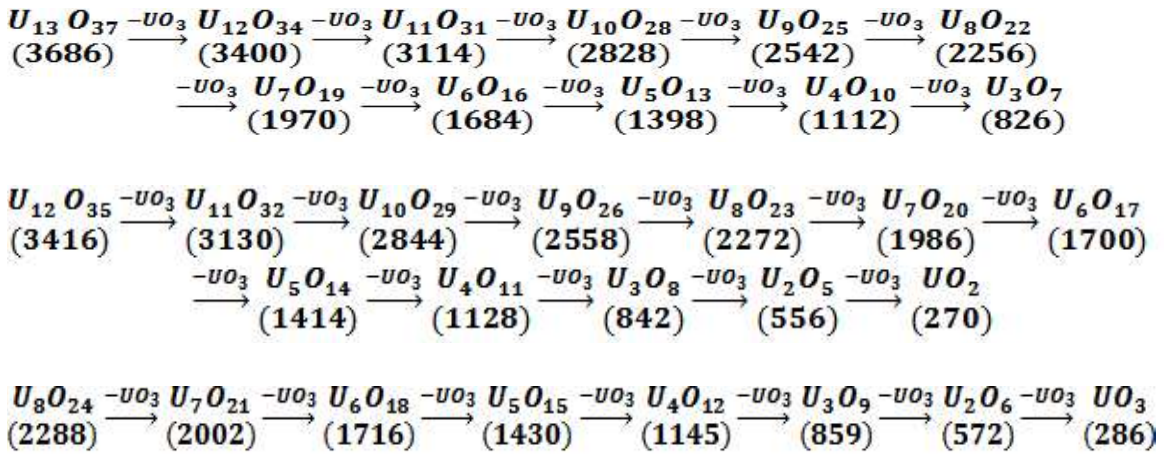


Fig. 6.5 Expanded view of Fig. 6.4 (a)- upto mass 2000 amu; (b) mass range 2000-4000 amu.

For higher laser fluence, the highest mass observed is 3686 corresponding to the species $U_{13}O_{37}$, without the addition of any matrix.

Three possible series identified out of the above two figures (Fig. 6.5 a & b) are given below, similar to the series reported by Guerrero et al [13].



The above observations of higher clusters of U-O system had led us to a study on yet another inorganic system namely Te, on academic interest. It is known that Te can form clusters of the type Te_x .

6.4. Te system

6.4.1 Experimental

Sample

Elemental Te granules supplied by Aldrich Chemicals (99.99% pure) were powdered, made into a slurry using acetone, deposited on SS sample holder in the form of a thin layer and allowed to dry at room temperature.

6.4.2 Results and discussion

Laser Mass Spectrometric studies of Te clusters

Clusters of Te in laser vaporization/ionization have been reported earlier by different groups. Alberty et al reported observation of clusters up to Te_5 by laser ablation using a N_2 laser beam (337 nm) [14]. In that study, Te_2^+ was the most abundant ion, and the intensity of higher clusters were found decreasing with increase in mass. Ban et al reported observation of clusters up to Te_8 by laser vaporization using ruby (693 nm, 800 μs) and Nd-YAG laser (800 μs , 1064 nm and power density about 10^7 W/cm^2) [15], in which they could observe slightly different distributions for neutral species and ions; Te_5 was the most abundant species for both the lasers and Te_2 was the next most abundant for the neutrals. Recently vaporization study of Te using Knudsen effusion mass spectrometry in the temperature region of 590-690 K, has reported the observation of species up to Te_7 , with Te_2 being the major species and contribution of all other species (Te_3 - Te_7 all together) constituting less than 5% [16].

In the present study, we have detected only positive ion species. In the laser vaporization of Te, we could observe clusters up to Te_{28}^+ . The typical mass spectrum obtained is shown in Fig. 6.6. This spectrum was obtained using a 266 nm beam at a fluence of 1 J/cm^2 . For this fluence, we are not able to clearly resolve the mass distribution due to isotopes, as the spread in the kinetic energy results in reduced resolution. However, when the laser fluence is lowered to 0.25 J/cm^2 , we could observe the isotopic distribution and typical spectra obtained for Te_2 and Te_3 are shown in Fig. 6.7 and Fig. 6.8 respectively, along with the calculated intensity distribution using natural abundances of isotopes.

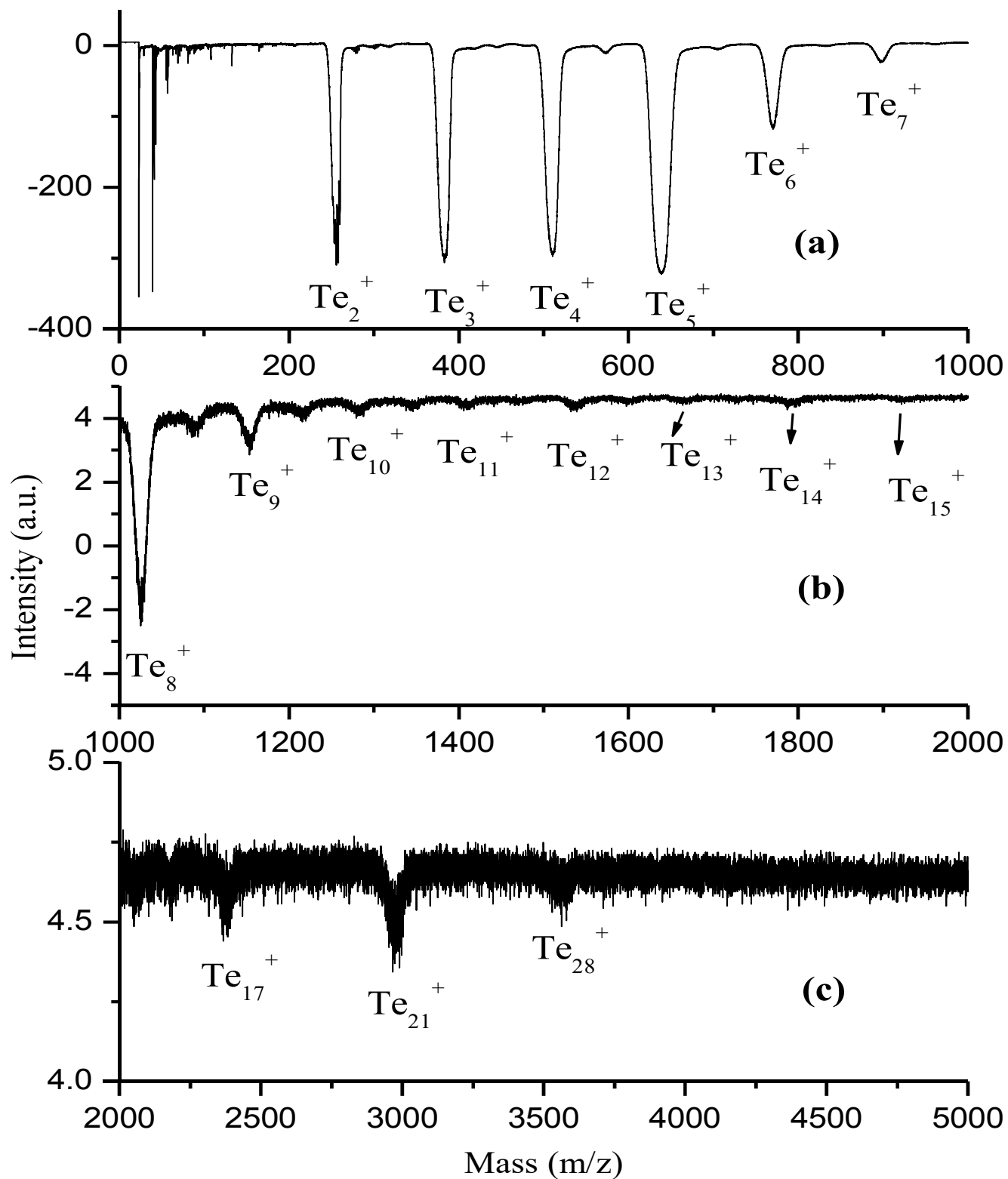


Fig. 6.6 Laser desorption/ionization mass spectrum obtained over elemental Te- (a), (b) and (c) indicate different mass regions.

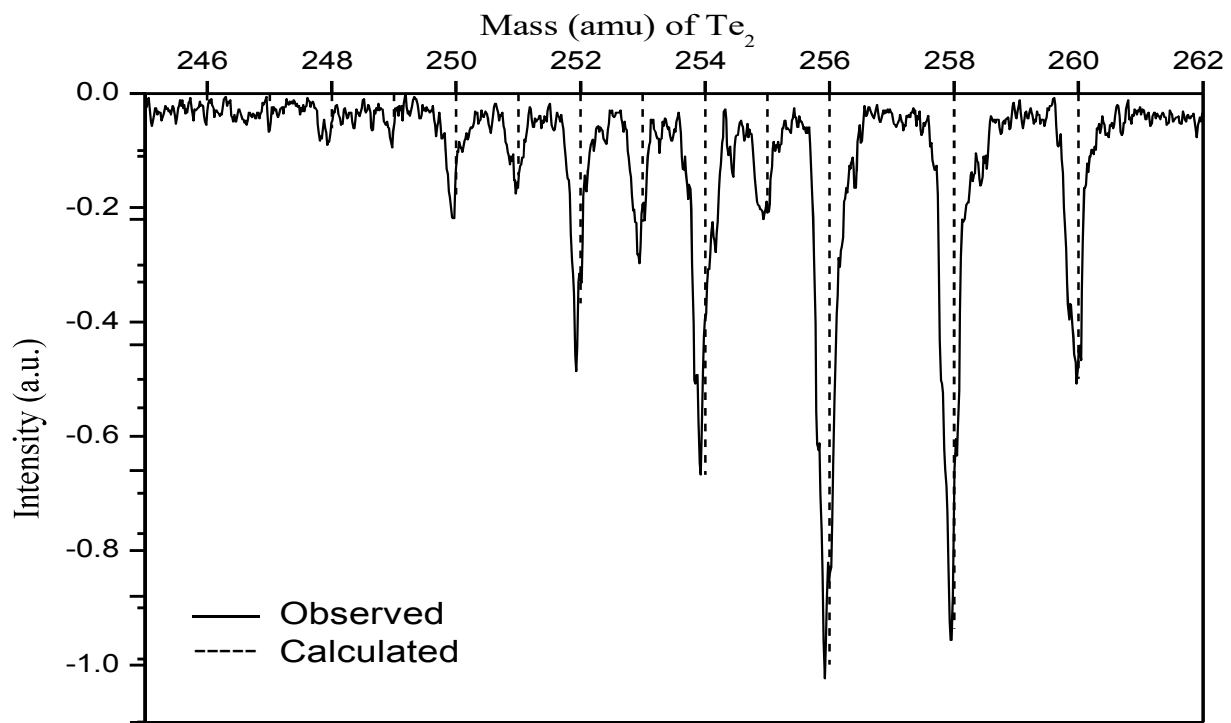


Fig. 6.7 Calculated and observed intensity for Te_2

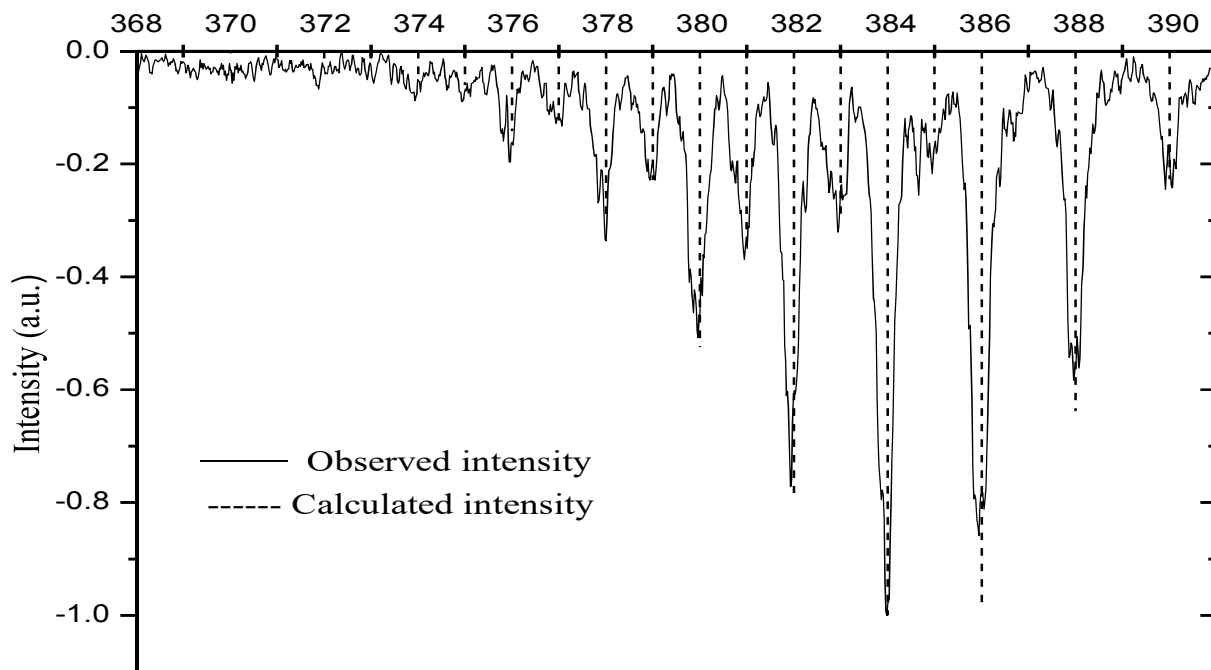


Fig. 6.8 Calculated and observed intensity for Te_3

Effect of wavelength on cluster formation of Te

It was observed that the Te cluster distribution changes depending on the wavelength of the laser used. Typical mass spectra obtained for three wave lengths, namely 1064, 532 and 266 nm are shown in Fig. 6.9, which shows that, for 1064 nm, the most intense cluster is Te_5 . This agrees with the reported observation of Ban et al [15]. However, with 532 nm, Te_2 is the most intense peak, similar to the observation of Alberty et al [14] using laser ablation, and that of Viswanathan et al [16] using Knudsen effusion. For 266 nm, Te_5 is slightly more intense compared to clusters of less number of Te atoms.

For all three wavelengths, beyond Te_5 , the intensity is less and we could observe higher clusters, as high as Te_{28} , using 266 nm, as indicated in Fig. 6.6 (a). To our knowledge, this is the highest cluster size of Te observed over pure phase of Te. The reason for observing higher cluster size with 266 nm compared to higher wavelengths (Te_{15}^+ for 532 nm and Te_9^+ for 1064 nm) could be attributed to the vaporization mechanism. For 266 nm, the absorption coefficient will be higher than those for longer wave lengths, leading to higher surface temperatures. Correspondingly, the vaporization rate as well as the recoil pressure will be high leading to confining the super critical phase for temperatures, well above the suggested critical temperature of 2325 K [17].

Though the above set of experiments on Te was carried out on academic interest, it has implications in the PLD of thin films. The cluster assembled thin films of materials prepared by depositing pre-formed clusters are expected to have different properties instead by atomic or molecular deposition. New magnetic materials with engineered properties can be synthesized by properly choosing the size of cluster and the matrix [18]. Silicon telluride and zinc telluride (SiTe & ZnTe) thin films attracts special interest in semiconductor industry

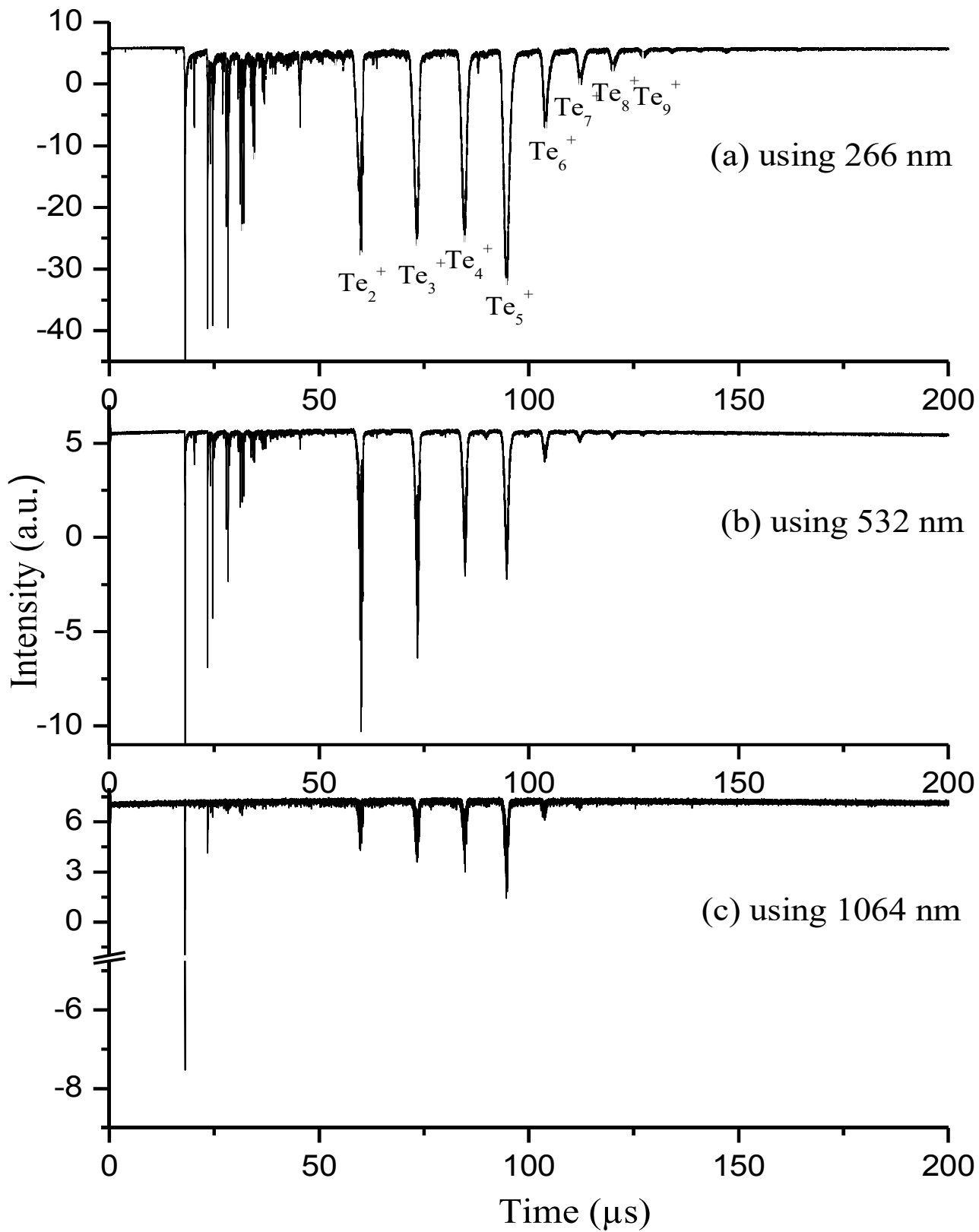


Fig. 6.9 TOF mass spectra obtained over elemental Te using different laser wave lengths.

because of their characteristics such as large energy band gap, low resistivity and photoluminescence properties [18,19]. The present study reveals applicability of the indigenous made LIMS to prepare and characterize such specially featured cluster assembled thin films.

6.5 Conclusion

An in-house developed LIMS facility was used to observe the dissolution products of UC in nitric acid, and the cluster species formed from samples of uranyl nitrate and elemental tellurium through laser desorption/ ionization mass spectrometry. Dissolution products like oxalic acid and benzoic acids could be identified in UC solution. In the case of uranyl nitrate, clusters of mass up to $U_{13}O_{37}$ were observed. With Te, we could observe clusters containing up to 28 atoms of Te (Te_{28}). The present experiments were carried out using an acceleration voltage of 3.86 kV. On increasing the acceleration voltage to higher values, it may be possible to observe clusters of still higher masses due to increased detection efficiency.

References

1. M. Joseph, N. Sivakumar, P. Manoravi, R. Balasubramanian, Determination of boron isotope ratios in boron carbide using laser ionization mass spectrometric method, *Rapid Commu. Mass Spectr.*, 2004, 18, 231-234.
2. M. Joseph, N. Sivakumar, P. Manoravi, R. Balasubramanian, Laser mass spectrometric studies on rare earth doped UO_2 , *Int. J. Mass Spectr.*, 2006, 253, 98–103.
3. P. Manoravi, R. Sajimol, M. Joseph, N. Sivakumar, Laser mass spectrometric studies on measurement of isotope ratio - a comparative study using ps and ns pulsed lasers, *Int. J. Mass spectr.*, 2014, 367, 16–20.

4. P. Rodriguez, Mixed plutonium-uranium carbide fuel in fast breeder test reactor, *Bull. Mater. Sci.*, 1999, 22, 215-220.
5. R. Natarajan, V. Vijayakumar, R. V. Subba Rao, N. K. Pandey, *J. Radioanal. Nucl. Chem.*, 2015, 304, 401-407.
6. L. M. Ferris, M. J. Bradley, Reactions of the uranium carbide with nitric acid, *J. Am. Chem. Soc.*, 1965, 87, 1710-1714.
7. S. K. Nayak, T. G. Srinivasan, P. R. Vasudeva Rao, C. K. Mathews, Photochemical destruction of organic compounds formed during dissolution of uranium carbide in nitric acid, *Sep. Sci. Technol.*, 1988, 23, 1551-1561.
8. A. Palamalai, Thesis, University of Madras, 1987.
9. A. Palamalai, S. K. Rajan, A. Chinnusamy, M. Sampath, P. K. Varghese, T. N. Ravi, V. R. Raman, G. R. Balasubramanian, Development of an electro-oxidative dissolution technique for fast reactor carbide fuels, *Radiochimica Acta*, 1991, 55, 29-35.
10. V. Sladkov, B. Fourest, Simultaneous determination of uranium carbide dissolution products by capillary zone electrophoresis, *J. Chromat. A*, 2009, 12, 2605-2608.
11. K. Ananthasivan, S. Anthonysamy, V. Chandramouli, I. Kaliappan, P. R. Vasudeva Rao, Reprocessing of carbide fuels: Conversion of carbide to nitride as a head end step, *J. Nucl. Mater.*, 1996, 228, 18-23.
12. K. Sini, S. Mishra, F. Lawrence, C. Mallika, S. B. Kognati, Destruction of soluble organics generated during the dissolution of sintered uranium carbide by mediated electrochemical oxidation process, *Radiochimica Acta*, 2011, 99, 23-30.

13. J. S. Guerrero, D. Gajdosova, J. Havel, Uranium oxide clusters by laser desorption ionization during MALDI-TOF MS analysis of uranium(VI), *J. Radio. Nucl. Chem.*, 2001, 249, 139-143.
14. M. Alberty, O. Sedo, J. Havel, Laser ablation synthesis and TOF mass spectrometric identification of tellurium, sulfur and mixed tellurium–sulfur clusters, *Polyhedron*, 2003, 22, 2601-2605.
15. V. S. Ban, B. E. Knox, Mass spectrometric studies of laser-produced vapor species, *J. Chem. Phys.*, 1969, 51, 524-526.
16. R. Viswanathan, R. Balasubramanian, D. Darwin Albert Raj, M. Sai Baba, T. S. Lakshmi Narasimhan, Vaporization studies on elemental tellurium and selenium by Knudsen effusion mass spectrometry, *J. Alloys and Compounds*, 2014, 603, 75-85.
17. Y. P. Varshni, Critical temperatures of elements from their boiling points, *J. Phys. Chem. Liquids: An Inter.*, 2007, 45, 601-607.
18. S. Shanmugan, D. Mutharasu, Optical properties and surface morphology of Zinc Telluride thin films prepared by stacked elemental layer method, *Material Science*, 2012, 18, 1392-1320.
19. D. H. Lowndes, C. M. Rouleau, T. Thundat, G. Duscher, E. A. Kenit, S. Pennycook, Silicon and zinc telluride nano particles prepared by pulsed laser ablation: Size distribution and nano scale structure, Fourth International Conference on Laser Ablation, California, July 21-25, 1997.

Summary and Conclusions

This chapter presents summary of all the studies discussed in the preceding chapters of this thesis. This thesis deals with applicability of mass spectrometry for characterization of nuclear fuel, during the course of passing through the fuel cycle. It mainly addressed the complexities associated with performance evaluation (burn-up) studies of spent nuclear fuel. Conventional burn-up determination procedure starts with dissolution of spent fuel inside a hot cell, which makes the data on radial and axial profile of burn-up irrecoverable. Direct sampling of solid fuel through remote operation and subsequent analysis of the sample would be the most preferred method for burn-up profile analysis, in view of radiation protection by remote handling and minimum sample destruction.

Chapter-2 of this thesis makes a detailed investigation on scope for such a facility, employing laser as the sampling tool. Since the current laser ablation chamber is maintained inactive, the study was carried out with simulated pellets of uranium oxide doped with rare earth elements, having compositions similar to spent fuel pellets of different burn-ups. The experiments revealed that few microgram of sample vaporized and deposited on a substrate is sufficient for the estimation of burn-up, by thermal ionization mass spectrometry. The sampling does not affect integrity of the pellet except the generation of a tiny crater of few micron depth on the surface of pellet. The biggest challenge encountered with the technique was deviation in stoichiometry of the sample vapor compared to that of solid pellet. Optimization studies with lasers of different wave lengths and pulse widths could conclude the laser parameters for near stoichiometric ablation. Experiments with Nd-YAG laser of 8 ns and 100 ps pulse widths and excimer laser of 30 ns pulse width led us to the conclusion that

266 nm, 100 ps laser produces the nearest stoichiometric ablation, with a minimum deviation of ~ 5% in U/Nd value. The magnitude of relative errors in U/Nd values obtained with different laser parameters are summarized in Fig. 7.1.

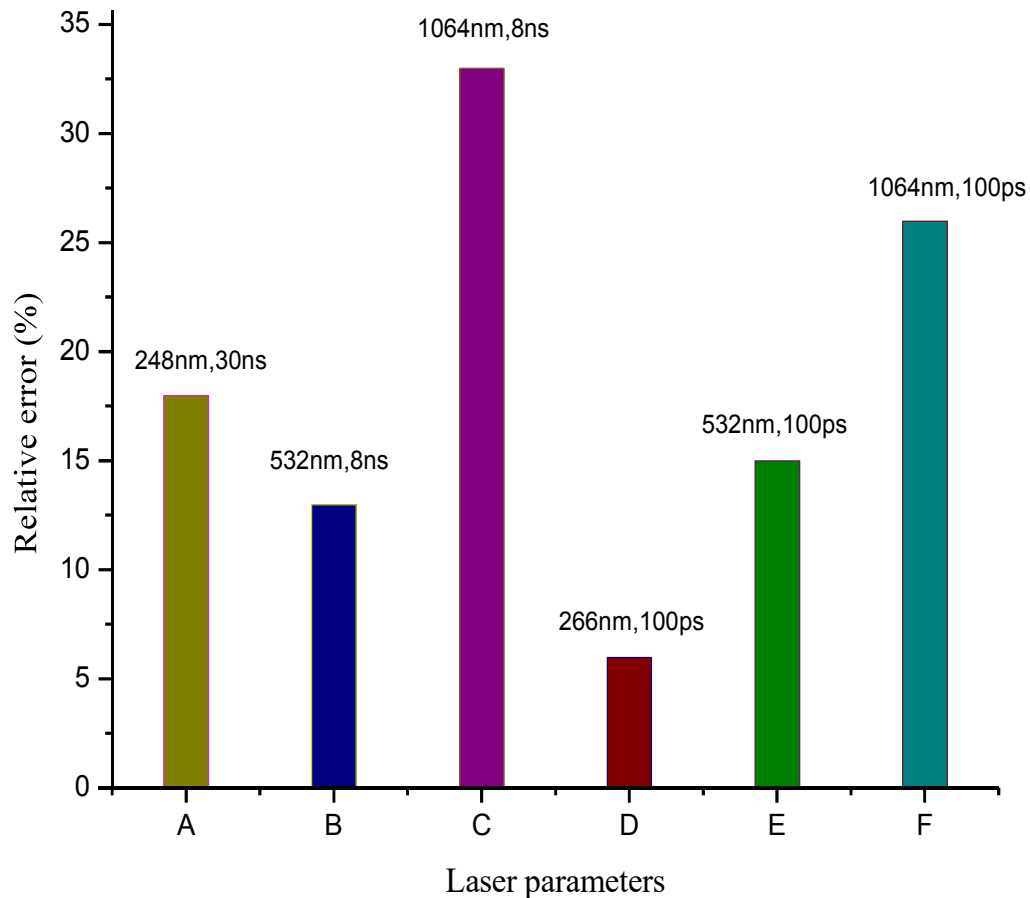


Fig. 7.1 Variation in accuracy of U/Nd values measured, with lasers of different parameters used for PLD.

The observations on ion intensities of U, Nd and Sm isotopes during the course of analysis by TIMS had led to a detailed study on vaporization behavior of Nd- the fission product monitor and Sm- the isobarically interfering element of the former. The study carried out with nitrate mixture of the two elements, by TIMS had concluded the possibility of

elimination of Sm from the mixture, by evaporation for about two hours at filament current 2.25 A, on account of its vapor pressure which is about five order higher than that of Nd. It was also experimentally concluded that the error in isotopic ratios of Nd, originated out of fractionation due to prolonged heating of the sample for the elimination of Sm, is negligible compared to the error caused by isobaric interference. This study had stemmed out the possibility of direct analysis of dissolver solution by loading virgin sample onto the filament for burn-up evaluation, without pre-separation of individual elements. The burn-up evaluated for PHWR spent fuel by the proposed direct loading method was 0.84 at %, against the referral value of 0.82 at %, which was determined by the well established HPLC- ID-TIMS method.

Applicability of the direct loading method for fast reactor fuel was also investigated, where the scenario is more complex due to isobaric interference between U-Pu-Am isotopes, in addition to Nd-Sm interference. The dissolver solution of MOX test fuel assembly irradiated in FBTR for a peak burn- up of ~ 112 GWd/t was directly loaded over Re filament and analyzed by TIMS. A sequential pattern of analysis for different isotopic ratios was put forwarded, considering the interference and vapor pressure factors, by which all the required isotopic ratios could be measured with least influence from interfering isotopes. The burn-up measured with MOX fuel sample is 11.2 at %, against reported value of 10.8 at %. The method was found applicable for advanced fuel like (U, Pu)C irradiated in FBTR also. The most significant contribution of this thesis is the proposal of a simple, time effective method for burn-up evaluation, which requires only sub microgram level of elements of interest in the sample and doesn't involve any sample preparation procedures. Merits of the method include nil production of radioactive liquid waste, reduction in solid

waste generation to one third of that in conventional method and radical reduction in personal exposure to radiation. Burn-up evaluated for thermal and fast reactor spent fuels by direct loading method and conventional method are given in Table 7.1.

Table 7.1 Comparison of burn-up evaluated by the proposed direct loading method and conventional procedure.

Type of fuel (type of reactor)	Burn-up measured by the proposed direct loading method (atom %)	Burn-up measured by conventional method (atom %)	Relative error (%)
Natural U (thermal)	0.84	0.82	2.4
MOX (fast)	11.2	10.8	3.7

This thesis also made an attempt to identify the dissolution products of uranium carbide in nitric acid, by using an in-house developed time-of-flight mass spectrometer. The study could conclude the presence of oxalic acid and benzoic acid in the nitric acid solution of UC. The study opened up another application of the equipment for cluster studies of U-O and Te. The highest cluster of U-O system ($U_{13}O_{37}$) and Te (Te_{28}) could be reported by the study, without the aid of any matrix, which can find applications in the synthesis of cluster assembled thin films and nano clusters.

Scope for future studies

The studies described in this thesis provide scope for extension to-

- i. Laser Ablation- ICP-MS facility for in situ measurement of heavy elements (U & Pu) and burn-up monitor (Nd, La etc.) for direct sampling and online measurement of burn-up of solid spent fuel, by remote operation.
- ii. Determination of radial as well as axial profile of burn-up using the above facility, by making vertical and horizontal movements of the pellet, followed by laser ablation at the point of interest.
- iii. Study on feasibility of adaptation of the direct loading method for routine samples for concentration determination of U and Pu, and for burn-up evaluation, for applications which can bear an error up to 5 %.
- iv. Cluster studies of U-O system using time-of-flight mass spectrometer at higher acceleration voltages (> 5 kV).
- v. Studies on cluster formation behavior of Pu-O system using a glove box adapted time-of-flight mass spectrometer.